The Role of Putative *Tbx1* Target Genes in the Pathogenesis of the 22q11 Deletion Syndrome Phenotype

Catherine Roberts

Thesis submitted in fulfilment of the degree of Doctor of Philosophy

UCL

(Institute of Child Health)

December 2012

DECLARATION

I, Catherine Roberts, confirm that the work presented in this thesis is my own. Where information has been derived from other sources, I confirm that this has been indicated in the thesis.

ABSTRACT

The 22q11 deletion syndrome (22q11DS/DiGeorge Syndrome [DGS]) is a congenital disorder with complex aetiology including cardiovascular, thymic/parathyroid, craniofacial and neuro-behavioural phenotypes. These arise via abnormal development of embryonic structures including the pharyngeal arch/artery apparatus and the secondary heart field. Large (3Mb) hemizygous deletions of 22q11 are found in most human cases. The *TBX1* transcription factor is found within the deleted region. Animal models and non-deleted patient data suggest haploinsufficiency of *TBX1* is the major underlying cause of 22q11DS.

To investigate the role of *Tbx1* in cardiovascular development, putative transcriptional targets were previously identified using microarray. This thesis examines the role of two such targets, the *Cyp26* gene family and *Hes1*. These genes are known to be involved, respectively, in the retinoic acid and Notch-signalling pathways. Both pathways are important in pharyngeal/cardiovascular development. Control of RA homeostasis/dosage is required for normal development and the Cyp26 enzymes metabolise RA to less active forms. Embryonic *Cyp26* genes have altered expression in *Tbx1*$^{-/-}$ mice. This project investigated the effect of chemically blocking Cyp26 function upon pharyngeal/cardiovascular development in the chick. Furthermore, a mutant mouse model was used to establish whether loss of *Cyp26b1* function could result in the 22q11DS phenocopy observed. Finally, epistasis experiments ascertained whether a genetic interaction exists between *Tbx1* and *Cyp26b1*. The transcriptional repressor *Hes1* is required for pharyngeal/cardiovascular development in the mouse. This thesis presents data showing a conserved role for *her6* (zebrafish homologue) in zebrafish pharyngeal development and verification of a *tbx1*/*her6* genetic interaction during pharyngeal development.

Overall, work presented in this thesis provides further evidence that *Tbx1* co-ordinates a number of signalling pathways in pharyngeal/cardiovascular development. This data refines the role of *Tbx1* and RA-regulatory genes in 22q11DS cardiovascular

phenotypes and corroborates the importance of an interaction between *tbx1* and *her6* (*Hes1*) in pharyngeal development.

ACKNOWLEDGEMENTS

I would like to thank my supervisors Pete Scambler and Paul Riley for giving me the opportunity to undertake this PhD, and for all their time and help along the way. A special thank you must go to Pete for allowing me time away from the lab to write up.

I must also thank the Western Labs and UCL Fish Facilty staff for all their hard work, particularly Jenna Haakensteeg. I am very grateful to Prof. Steve Wilson and all the members of his group for giving me injection space and patiently answering many many questions about fish. I am also greatly obliged to Bertrand Vernay for the masterclasses on the confocal and the joys of OPT and to Jen Suntharalingham for all the genotyping.

The members of MMU, both past and present, and particularly the Tbx1 group deserve a massive thank you for contributing to the great collaborative atmosphere and providing so much help, encouragement and laughter along the way.

A particular mention must go to “les filles francaises”, Amelie and Ariane for all their support and all the giggles in the office. I am hugely grateful to Pazzer for somehow finding the time to comment on my thesis. I would also like to thank all my friends both in and out of lab, for quality time, (both with and without wine), which I could not have managed without. In particular, thanks to Kath, Babs, Clazza and Pazzer for doing a lot of listening when times were tough.

Finally, I could not have done this without the constant support and belief of Paul, my parents, Dorothy and Garth, and my brother Alastair, who have always been there for me.

ABBREVIATIONS

22q11CR	22q11 deletion syndrome critical region
22q11DS	22q11 deletion syndrome
aa	amino acid
AAo	ascending aortic arch
AoA	aortic arch
ARSC	aberrant right subclavian artery
ASD	atrial septal defect
ASH2L	(absent, small, or homeotic)-like protein
ATP	adensosine triphosphate
AVC	atrio-ventricular canal
BABB	benzyl alcohol/benzyl benzoate
β-gal	β-galactosidase
BCIP	5-bromo-4-chloro-indolyl-phosphate
bp	base pair
BMP	bone morphogenetic protein
BSA	bovine serum albumin
CAo	cervical aortic arch
CAT	common arterial trunk
CHD	Chromodomain-helicase-DNA-binding protein
CTP	cytidine triphosphate
CYP	cytochrome p450
cDNA	complementary cDNA
C/NCC	cardiac/neural crest cells
dAo	decending aortic arch
DA	dorsal aorta
DAB	3,3-diaminobenzidine tetrahydrochloride
DAPI	4',6-diamidino-2-phenylindole
DORV	double outlet right ventricle
dpf	days post fertilization

DGCR	DiGeorge Syndrome critical region
DGS	DiGeorge Syndrome
DIG	digoxygenin
DMSO	dimethyl sulfoxide
DNA	deoxynucleotide triphosphates
dNTP	deoxyribonucleotide triphosphate
E	embryonic stage mouse
EDTA	ethylene diamine tetra-acetic acid
EGF	epidermal growth factor
EMT	epithelial to mesenchymal transition
ENU	N-ethyl-N-nitrosourea
EST	expressed sequence tag
FACS	fluorescent activated cell sorting
FGF	fibroblast growth factor
FHF	first heart field
FOX	forkhead box
FSC	fluorescein
GFP	green fluorescent protein
GTP	guanosine triphophate
HDAC	histone deactylase complex
Hes	hairy/enhancer of split
HOS	Holt Oram Syndrome
IAA-B	interrupted aortic arch type B
kb	kilobase
l	litre
LA	left atrium
LB	luria bertani
LCR	low copy repeat
loxP	locus of crossover in P1
LV	left ventricle
M	milli

M	molar
MAB	maleic acid buffer
µ	micro
Mb	mega base
MO	morpholino
mRNA	messanger RNA
n	nano
NBT	4-nitro-blue-tetrazoliumchloride
Neo	neomycin
NEXT	Notch extra-cellular domain
NICD	Notch intra-cellular domain
NTMT	NaCl, Tris-HCl, $MgC1_2$, Tween buffer
NTP	ribonucleotide triphosphate
OCT	optimal cutting temperature compound
OFT	outflow tract
OPT	optical projection tomography
PA	pharyngeal arch
PAA	pharyngeal arch artery
PBS	phosphate buffered saline
PBT	phosphate buffered saline + Tween20
PBT_{x100}	phosphate buffered saline+Triton X100
PCR	polymerase chain reaction
PE	pharyngeal endoderm
PFA	paraformaldehyde
PK	proteinase K
PM	pharyngeal mesoderm
PM-VSD	peri-membranous ventricular septal defect
PPE	pharyngeal pouch endoderm
PSE	pharyngeal surface ectoderm
PTA	persistent truncus arteriosus
RA	retinoic acid

RA	right atrium
RAA	right sided arch
RAR	retinoic acid receptor
RE	restriction enzyme
RNA	ribonucleic acid
ROSCA	retro-oesophageal right subclavian artery
RTQ-PCR	real time quantitative PCR
RV	right ventricle
RXR	retinoid X receptor
SAN	sino-atrial node
SDS	sodium dodecyl sulphate
SHF	secondary heart field
SHH	sonic hedgehog
SMAD	small body size/mothers against decapentaplegic
SRF	serum response factor
TGF-β	transforming growth factor-β
TAE	tris-acetate-EDTA
TLB	tail lysis buffer
TLE	Transducin-like-enhancer of split
TESPA	3-aminopropyltriethoysilane
UTP	uracil triphosphate
VCFS	velo-cardio-facial syndrome
VEGF	vascular endothelial growth factor
VSD	ventricular septal defect
WNT	Wingless
X-gal	5-bromo-4-chloro-3-indolyl-β-d-galactosidase

TABLE OF CONTENTS

Table of Figures

List of Tables

CHAPTER 1
Introduction

1.1 22q11 Deletion Syndrome (22q11DS)

22q11DS (also known as DiGeorge Syndrome/VeloCardioFacial Syndrome (DGS/VCFS) is a congenital disease associated with large hemizygous deletions of chromosome 22q11 arising from intrachromosomal recombination between homologous low copy repeat sequences. It is the most common interstitial chromosomal deletion syndrome, occurring at 1 in 4000 live births. The human phenotype is highly variable and includes abnormalities of the aortic arch (AoA) and outflow tract (OFT), such as common arterial trunk (CAT), interruption of the aortic arch between the left common carotid and left subclavian arteries (type B, IAA-B) as well as peri-membranous ventricular septal defects (PM-VSD) and thymic and parathyroid aplasia/hypoplasia resulting in immunodeficiencies. These cardiac and immune system defects lead to a high rate of patient mortality with up to 50% of patients not surviving 12 months after birth. In addition to these problems the 22q11 phenotype can also include craniofacial defects and learning and behavioural anomalies, including an increased predisposition towards developing psychiatric illness, in particular schizophrenia (Fig.1.1) (Arinami, 2006; Conley et al., 1979; Murphy et al., 1999; Scambler, 2000; Wilson et al., 1992). Dental defects including tooth agenesis, hypoplasia and hypomineralization have also been noted (Klingberg et al., 2002; Nordgarden et al., 2011). Rarer defects have also been reported in tissues such as the ear, kidney and skeletal structures (Ryan et al., 1997).

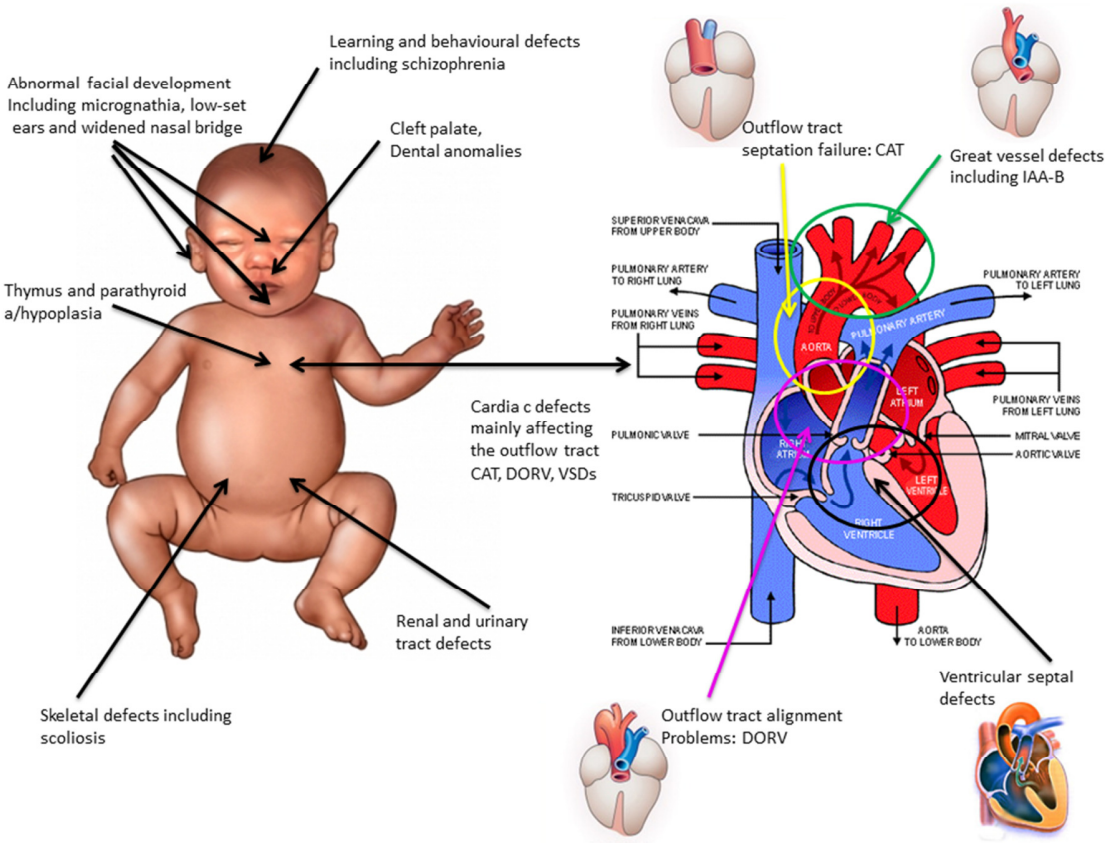

Figure 1.1 The main body systems affected in 22q11DS

Coloured circles indicate the cardiovascular regions where the majority of developmental defects in 22q11DS arise. Green: great vessels, yellow: outflow tract, pink: alignment of great vessels and the ventricular septum, black: ventricular septum. IAA-B, interrupted aortic arch type B, DORV: double outlet right ventricle, CAT: common arterial trunk. Adapted from (Emanuel et al., 1999).

The majority of 22q11DS patients are hemizygous for a large (typically 3Mb) region of chromosome 22q11, with a smaller number (~5%) being deleted for a 1.5Mb region which defines the 22q11DS or DiGeorge Critical Region (22q11CR/DGCR)(Fig.1.2 and 1.8) (Desmaze et al., 1993; Edelmann et al., 1999; Lindsay et al., 2001). These deletions are thought to arise as a result of chromosomal rearrangements mediated by homologous recombination between the four (A-D) 100-400kb conserved low copy repeat (LCR) sequences found on chromosome 22q11. The two largest of these units LCR-A and LCR-D are found at the proximal and distal ends of the common 3Mb deletion, respectively (Edelmann et al., 1999; Scambler, 2010). Patients

are therefore haploinsufficient for the genes contained within the deleted regions. There is no correlation between the size of the 22q11 deletion and the severity of the phenotype and although 90% of patients share the same deletion on 22q11, the observed phenotype is very variable in both the number of tissues/organs affected and the severity of the defects present (Sullivan, 2004).

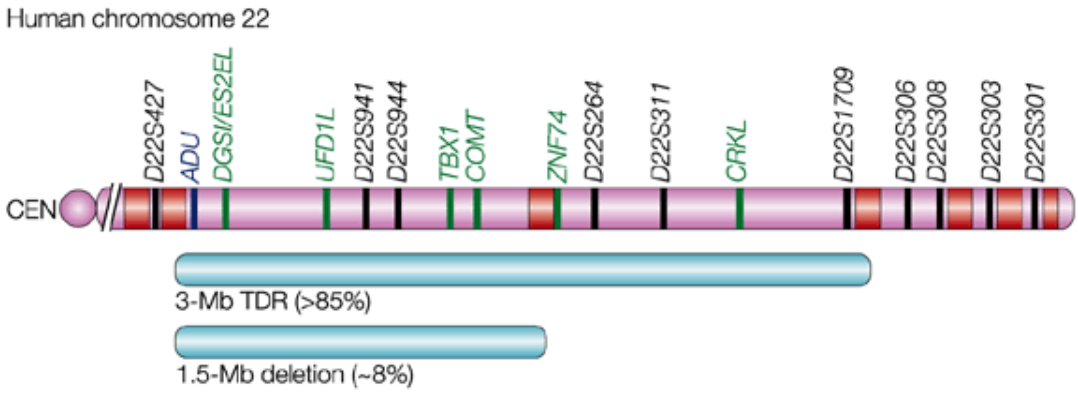

Figure 1.2 The del22q11 region on human chromosome 22

Selected genes are in green and molecular markers in black. Red blocks represent low-copy repeats (LCRs). ADU (blue) is a patient with DiGeorge syndrome and a balanced chromosomal translocation. The common 3 Mb typically deleted region (TDR), which is present in more than 85% of del22q11 patients and the 1.5-Mb (22q11CR) deletion are shown (turquoise). From (Lindsay, 2001).

There are at least thirty genes contained within the 22q11CR (Lindsay, 2001), including the T-box transcription factor *TBX1*. Approximately 10% of 22q11DS cases have no detectable deletion of chromosome 22q11 or 10p13 (Conti et al., 2003; Gong et al., 2001). Screens for point mutations of *TBX1* in such cases have been largely negative so far, as have mutation screens of other deleted genes within the DGCR. However, three Japanese cases of missense and truncation *TBX1* mutations have been described (Yagi et al., 2003) and more recently an inactivating mutation has been reported in a family with VCFS (Paylor et al., 2006) There are also a small number of patients with atypical deletions or translocations which do not disrupt *TBX1* (Rauch et al., 2005). Together, this suggests that multiple genes within the 22q11 deletions, including *TBX1*, could contribute to the patient phenotype (Vitelli et al., 2002b). Besides *TBX1*, animal models and some data from human patients, suggest a role for *CRKL* (Guris et al., 2006; Guris et al., 2001;

Moon et al., 2006), *GNB1L* (Paylor et al., 2006) and *HIC2*. *FGF8* (Abu-Issa et al., 2002; Moon et al., 2006; Vitelli et al., 2002b) and *VEGF* (Stalmans et al., 2003), which map to other chromosomes, may play a modifying role.

1.2 *Tbx1* is a member of the T-box transcription factor family

1.2.1 T-box family characteristics

A number of mouse models for 22q11DS have been created which implicate *Tbx1* in the aetiology of this disease. *Tbx1* is a member of the T-box transcription factor gene family, all of which encode a novel DNA binding motif known as the T-box. Site selection experiments have identified a core binding site sequence TCACACCT which all members of the family examined can bind (Conlon et al., 2001; Ghosh et al., 2001; Wilson and and Conlon, 2002). BRACHURY, the first T-box protein to be identified, binds preferentially to a palindromic arrangement of this consensus sequence, TCACACCTAGGTGTGA (Kispert and and Herrman, 1993). Human TBX1A has also been shown to bind to this palindrome by electrophoretic mobility shift assay (Sinha et al., 2000). As well as acting as a DNA-binding region, the T-box also functions as an interaction domain with other transcription factors, chromatin remodeling complexes and histone-modifying enzymes which play roles in transcriptional control (Boogerd et al., 2009). Seventeen T-box genes organized into five families have been detected in mouse and man and T-box family orthologues are present in most animal species. Most T-box genes appear to be preferentially expressed in progenitor regions, including both early germ layers and the presumptive organs of the developing embryo. These genes are frequently dosage-dependent and can act combinatorially or hierarchically to control a variety of embryological events, often those involving the choice between differentiation versus proliferation and cell fate patterning processes.

T-box proteins can function as either activators, e.g. BRACHYURY (Conlon et al., 1996; Kispert et al., 1995) and TBX5 (Horb and Thomsen, 1999) or repressors e.g. TBX2 (Carreira et al., 1998) and TBX3 (He et al., 1999). TBX1 was thought to be solely an activator (Ataliotis et al., 2005), until recently, when further data suggested that WRPW-

domain protein RIPPLY3 can bind to TBX1 at target promoters, recruiting GROUCHO/TLE/HDAC complexes to repress TBX1 transactivation, in certain contexts (Janesick et al., 2012; Okubo et al., 2011)

The effector domains for these transcriptional activities are frequently found in the C-terminal part of the protein. Most of the homology between family members resides within the T-box, with little or no homology found between the other domains [reviewed (Plageman and Yutzey, 2005; Tada and Smith, 2001; Wilson and and Conlon, 2002)](Fig.1.3). In recent years a number of the T-box family have been found to be heterozygously mutated in a several human congenital diseases. These include: *TBX5* in Holt-Oram Syndrome (HOS) (Basson et al., 1997; Li et al., 1997b), where patients can have ASD's, VSD's, ToF, hypoplastic left heart and conduction defects; *TBX20* in a variety of cardiac defects including septation defects, ToF, valvulogenesis abnormalities and cardiomyopathy (Kirk et al., 2007); *TBX22* is mutated in X-linked cleft palate and hypoglossia (Braybrook et al., 2001) and *TBX3* in Ulnar-Mammary syndrome in which patients suffer malformations of the limb, apocrine glands, genital development and some patients also have VSDs (Bamshad et al., 1997).

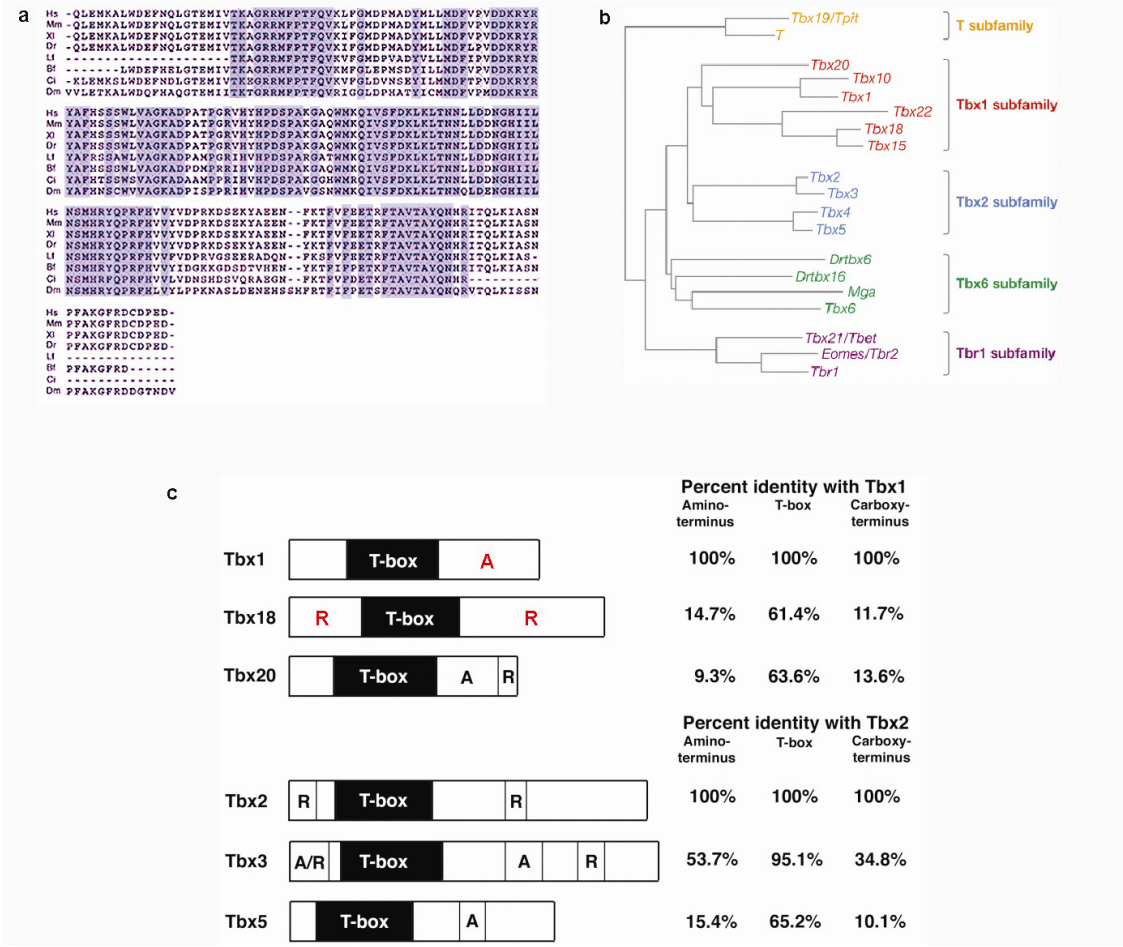

Figure 1.3 Comparison of T-box sequences, phylogenetic tree and structure

a.) Comparison of T-box domains of Tbx1 amino acid sequence from various species. Sequence identity is represented by blue shading and gaps by dashes [from (Ataliotis et al., 2005)]. b.) Schematic phylogenetic tree of T-box vertebrate gene family showing the relationship of genes as grouped into the five subfamilies shown by brackets on the right (from (Naiche et al., 2005). c.) Transcriptional regulatory domains of T-box protein subfamilies expressed in heart development. Conserved T-box domains shown in black. A; transcriptional activation domain R; transcriptional repressor domain (from (Plageman and Yutzey, 2005) A/R indicate activation/repression domains discovered after publication of Plageman and Yutzey. For Tbx1 this data is based on (Ataliotis et al., 2005) and for Tbx18 on (Farin et al., 2007)

1.2.2 T-box genes in cardiac development

Six of the seventeen identified T-box genes are active during mammalian heart development (Greulich et al., 2011) and are expressed and function in a combinatorial fashion in different cardiac progenitor types and compartments. These genes are members of the *Tbx1* subfamily (*Tbx1*, *Tbx18* and *Tbx20*) and the *Tbx2* subfamily (*Tbx2*, *Tbx3* and *Tbx5*)(Fig.1.4).

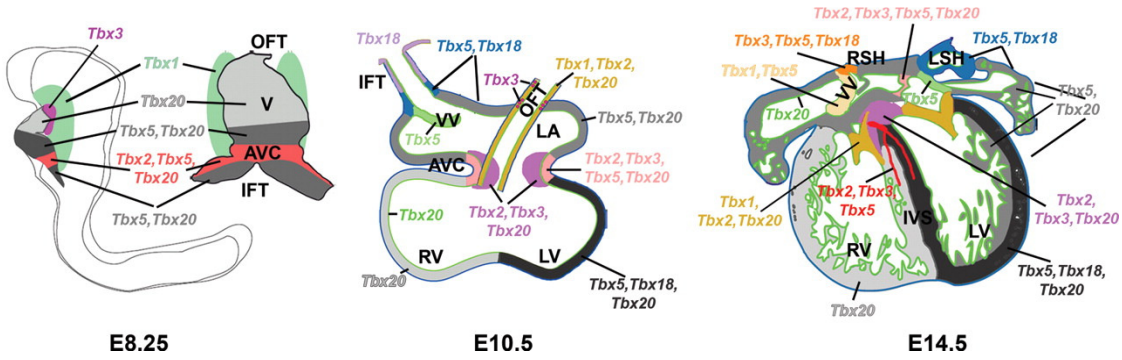

Figure 1.4 Combinatorial expression of *Tbx* genes in the developing heart

Sections through E8.25 (lateral and frontal views), E10.5 and E14.5 (transverse sections). Left and right ventricle (LV, RV), lefta and right atrium (LA, RA) and adjacent non-chamber tissues (inflow tract (IFT), outflow tract (OFT), atrioventricular canal (AVC), sinus venosus (SV), conotruncus (CT), proepicardium (PE), epicardium (EPI), pericardium (PC), left and right sinus horns (LSH, RSH) and venous valves. From (Greulich et al., 2011).

The role of *Tbx1* will be discussed in detail below. Briefly, *Tbx1* is required in the pharyngeal epithelia and mesoderm and secondary heart field (SHF) mesoderm for the normal development of the great vessels of the heart and the proliferation, elongation and septation of the outflow tract (OFT).

Tbx18$^{-/-}$ mice have specific anomalies of the venous return system and the size and boundaries of the sinoatrial node (SAN) are diminished, suggesting *Tbx18* is necessary for the proliferation, differentiation and recruitment of a specific set of precursor cells during the formation of the systemic venous return. Lineage tracing experiments also show *Tbx18*-positive cells contribute to these regions (Christoffels et al., 2006; Wiese et al., 2007). *Tbx20* is necessary for cardiac chamber formation. It is expressed in both the first

(FHF) and second heart fields (SHF) and can be induced in cardiac mesoderm by BMP signalling and repressed by endocardial *Nrg1* (Mandel et al., 2010; Stennard et al., 2003; Stennard et al., 2005). As described above, mutations of *TBX20* cause cardiac disease in man and heterozygous deletions in the mouse cause dilated cardiomyopathy. Homozygote null mice do form a heart tube but fail to undergo the looping and ballooning processes necessary for chamber formation. No expression of chamber-specific genes is seen and *Tbx2* expression is expanded beyond the atrioventricular canal (AVC) (Cai et al., 2005; Singh et al., 2005; Singh et al., 2009; Stennard et al., 2005). An allelic deletion series caused gradually increasing hypoplasia of the OFT and right ventricle implying *Tbx20* also functions in SHF development, possibly acting via activation of *Mef2c* and *Nkx2.5* and repression of *Isl1*(Takeuchi et al., 2005).

Tbx5 also plays an important role in cardiac chamber formation. *Tbx5*$^{-/-}$ mice develop a linear heart tube but FHF-derived components become hypoplastic and heterozygous deletions produce a HOS-like phenotype (Bruneau et al., 2001). Gain-of-function experiments produce looping defects, expansion of left ventricular identity and aberrant ventricular septum (VS) and AVC development (Takeuchi et al., 2003). Together these experiments suggest *Tbx5* is necessary to induce and maintain caudal chamber identity. This activity requires the co-operative binding of *Tbx5* with other factors such as *Gata4* and *Nkx2.5* at the promoters of myocardial down-stream target genes, e.g.the *Nppa* transcription factor. Moreover, later in development *Tbx5* has extra-myocardial functions in chamber septation and development of the conduction system (Garg et al., 2003; Hiroi et al., 2001; Takeuchi and Bruneau, 2009).

Finally, *Tbx2* and *Tbx3* are important for the development of the non-chamber myocardium of AVC (both) and OFT (*Tbx2*). *Tbx2*$^{-/-}$ mice display OFT septation defects and expansion of chamber-specific gene expression into the AVC (Aanhaanen et al., 2009; Christoffels et al., 2004; Harrelson et al., 2004). *Tbx3* mutants also exhibit abnormal OFT development, plus abnormal development of the SAN and AV conduction system (Bakker et al., 2008; Davenport et al., 2003; Hoogaars et al., 2007; Mesbah et al., 2008). Double homozygous mutants exhibit a severe phenotype with early lethality, hypolastic OFT and right ventricle, pericardial oedema and reduced growth overall. Moreover, combination of either deletion with deletions of *Tbx1* produces severe arterial pole defects and hypoplasia

of the pharyngeal region (Mesbah et al., 2011). Gain-of function experiments show *Tbx2* and *3* are necessary and sufficient to prevent chamber myocardium differentiation and the ectopic induction of primitive AVC tissue and pacemakers, respectively (Hoogaars et al., 2007; Shirai et al., 2009). *Tbx2* can also bind to *Nkx2.5* and *Gata4* at the *Nppa*-promoter therefore effectively inhibiting *Tbx5*-mediated transactivation (Habets et al., 2002). Thus *Tbx2* and *3* both act to inhibit chamber formation and promote primitive myocardium and conduction system formation.

1.3 Developmental basis of 22q11DS

The interlinked developmental systems most affected in 22q11DS/animal models of the disease are those of the pharyngeal apparatus and the secondary heart field (SHF). The 22q11DS phenotypic spectrum is attributed to the abnormal development of these tissues, as the structures most frequently affected all arise from these regions during development. The pharyngeal arches (PA) are a transient series of swellings which appear in a time-dependent cranio-caudal fashion, between E8-10.5/11. They have an internal covering of endoderm, forming the pharyngeal pouches (PPE) and externally are covered in ectoderm (PSE). Each arch is comprised of neural crest cell (NCC)-derived mesenchyme, which migrates in from the neuroectoderm. This surrounds the mesodermal core of cells around the endothelial pharyngeal arch arteries (PAA) (Fig.1.5). Each of these cell types gives rise to different derivatives of the head and neck: the PSE gives rise to epidermis; the PPE to endocrine glands such as the thymus, thyroid and parathyroids; the mesodermal core forms the musculature of the head and neck and the endothelium lining the PAA. The neural crest derived mesenchyme differentiates into skeletal and connective tissue. The pharyngeal arch arteries undergo extensive remodelling to form the aortic arch and other vessels of the head and neck (Fig.1.6).

Contributions from two different cell types, external to the outflow tract, have been shown to be critical for its growth, correct alignment and proper septation. These two populations are the cardiac neural crest and the cells of the secondary heart field (SHF).

Cardiac neural crest cells (C/NCC) originate from the neuroepithelium between rhombomere 5 and somite 3 and migrate through the caudal pharyngeal arches into the

outflow tract, where they are important in aorticopulmonary septation (Fig. 1.5 and Fig. 1.6). Many studies have shown that ablation or disruption of CNCC gene patterning gives rise to heart defects very reminiscent of 22q11DS, including abnormal PAA development and remodelling and septation of the outflow tract. CNCC are in close proximity to the SHF during development and are required for its normal development [(Hutson and Kirby, 2007; Keyte and Hutson, 2012; Waldo et al., 2005a) and references there-in](Fig1.5-1.7). The heart is now known to have two sources of myocardial cells, the first or primary heart field (FHF) whose cells form the cardiac crescent and then the primitive heart tube, finally contributing mostly to the left ventricle but also parts of the atria and right ventricle. The second heart field (SHF) consists of mesodermal cells and initially lies dorsal and medial to the cardiac crescent and then is contained within the pharyngeal and splanchnic mesoderm. Normal proliferation of the SHF is required for the growth of the embryonic tube by the addition of cells at the arterial and venous poles from the SHF. These cells contribute to the outflow tract, right ventricle and a large portion of the atrial myocardium (Fig.1.5 and 1.7). They are molecularly delineated by the expression of genes such as *Isl-1*, *Tbx1* and *Fgf10* and complex set of regulatory signals controls the SHF proliferation and differentiation delay during heart tube elongation, including input from the FGF, WNT, HH, BMP and retinoic acid (RA) pathways, (Buckingham et al., 2005; Cai et al., 2003; Kelly and Buckingham, 2002; Kelly et al., 2001; Parisot et al., 2011; Waldo et al., 2005b; Zaffran and Kelly, 2012).

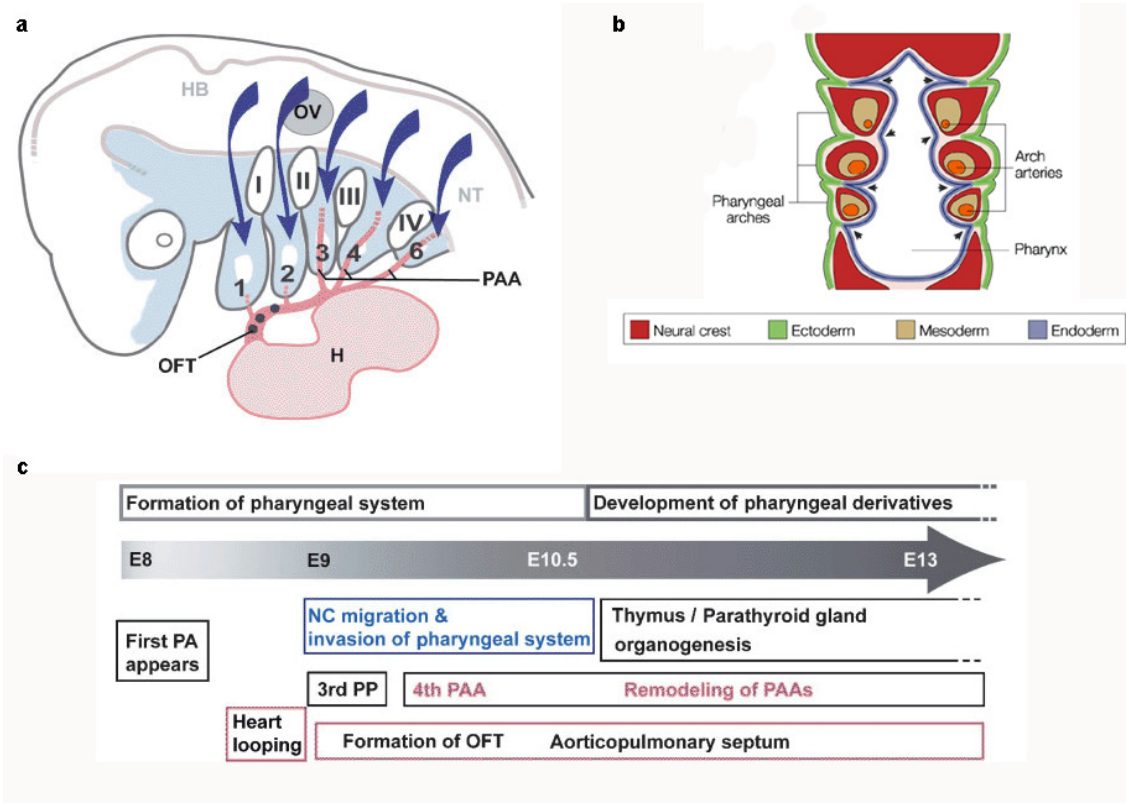

Figure 1.5 Schematic of the pharyngeal apparatus

Transient embryonic swellings of the pharyngeal arches and intervening endodermal pouches. Neural crest arising from the hindbrain fills the pharyngeal arches (dark blue arrows) and enters the forming outflow tract (OFT) of the heart (blue dots). At E10.5 the pharyngeal apparatus consists of pharyngeal arches 1-6 with mesodermal cores (white), pharyngeal pouches (I-IV) and pharyngeal arch arteries (PAA)(from (Wurdak et al., 2005) b.) A coronal diagram showing the relationship of the different tissues comprising the pharyngeal system to each other. Blue; pharyngeal endoderm, red; neural crest, brown; core mesoderm, orange; pharyngeal arch arteries, green; surface ectoderm (from (Lindsay, 2001). c.) Simplified timescale of events during pharyngeal development as divided into two phases; i.) initial formation of pharyngeal arches and pouches from around E8 and ii.) subsequent remodeling and differentiation of pharyngeal derivatives. From (Wurdak et al., 2005).

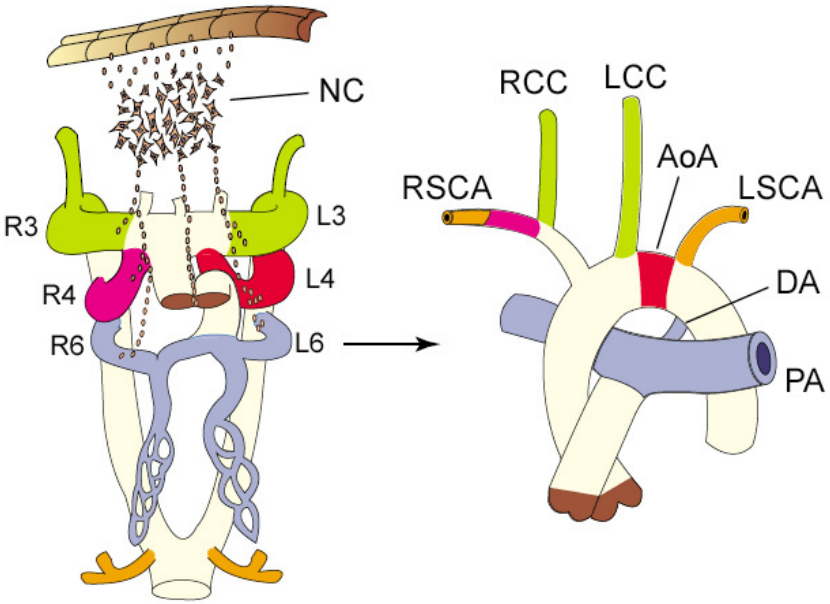

Figure 1.6 Formation of the great vessels of the heart

(A) At E10.5, PAAs 3 (green), 4 (red and purple) and 6 (blue) form as three pairs of symmetrical vessels connecting the heart to the dorsal aorta. Neural crest cells also contribute to the formation of the arch arteries. (B) The origins of great vessels of the mature heart which arise from the aortic arch arteries. Orange vessels represent the seventh intersemgental arteries and their derivatives. Abbreviations: AoA, aortic arch; DA, ductus arteriosus; L, left; LCC, left common carotid; LSCA, left subclavian artery; NC, neural crest; PA, pulmonary artery; R, right; RCC, right common carotid; RSCA, right subclavian artery. Modified from (Yamagishi and Srivastava, 2003).

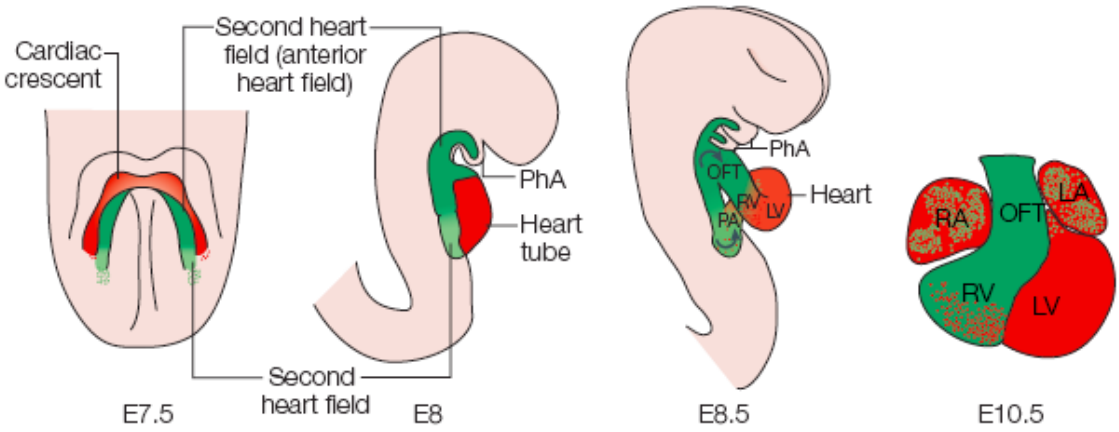

Figure 1.7 Heart fields in the mouse embryo

At E7.5, the first heart field (FHF) (red) is positioned just under the head folds within the cardiac crescent. The second heart field (SHF) (green) is positioned more dorsal and medial to the cardiac crescent. At E8.0, the FHF contributes cells to the primitive heart tube and the SHF is contained within pharyngeal and splanchnic mesoderm. SHF precursors contribute cells to the arterial and venous poles of the elongating heart tube from E8.5 to E10.5. Myocardial cells derived from the FHF give rise to the left ventricle, the atria and part of the right ventricle. The SHF mainly gives rise to the outflow tract, right ventricle and parts of the atria. Abbreviations: PA, primitive atria; PhA, pharyngeal arches; LA, left atrium; LV, left ventricle; OFT, outflow tract; RA, right atrium; RV, right ventricle from (Buckingham et al., 2005).

1.4 Animal models of 22q11DS

Animal models have been crucial to our current understanding of the possible molecular events underlying 22q11DS. A wide variety of mouse mutants from large chromosomal deletions mimicking human disease haploinsufficiency to targeted deletions of individual genes, together with conditional mutants allowing tissue and time specific deletion of certain genes, have all contributed hugely to our knowledge of which genes in the 22q11CR are most likely to contribute to the 22q11DS phenotype and in what manner.

Frog, chick and fish models have also been useful in dissecting elements of 22q11DS. In addition to allowing the candidate 22q11DS genes to be examined in a number of different species these models have a number of advantages not available in mice. In particular they are cheap, large numbers are available in a short space of time and

embryos are very amenable to molecular, drug-based or physical manipulation during development.

1.4.1 Mouse Models of mutant *Tbx1* alleles

1.4.1.1 Large deletions of mouse chromosome 16

Df1/$^{+}$ is a mouse model for a large hemizygous deletion containing at least 30 genes, including *Tbx1*, from the region of mouse chromosome 16, which is syntenic to the most commonly observed 22q11DS-associated deletion of 22q11 (Fig1.8). It has been shown to produce a fully penetrant aplasia or hypoplasia of the 4th aortic arch artery at E10.5, a defect which is associated with deficient contribution of vascular smooth muscle to the forming vessels. This led to characteristic 22q11DS-like aortic arch defects such as IAA-B, right-sided arch and retro-oesophageal or aberrant right subclavian artery (ROSCA/ARSC) at E18.5 (Fig.1-8). Rescue of the *Df1/+* phenotype was accomplished by genetic complementation with P1-derived artificial chromosomes (PACs) or bacterial artificial chromosomes (BACs) containing respectively *Tbx1* or *TBX1*. A second engineered large chromosomal deletion, *Ldgel/*$^{+}$ (Fig1.8), encompassing at least 24 genes from the same region produces a very similar haploinsufficient phenotype (Lindsay et al., 1999; Lindsay et al., 2001; Merscher et al., 2001) (Fig. 1.8). The mutant phenotype is about 25% penetrant at E18.5, but unexpectedly the 4th PAA abnormality is present in all mutant mice at E10.5. It became apparent that most of the 4th PAAs, which are growth impaired and not properly formed at E10.5, do eventually rescue themselves and develop normally. However, 32% of embryos fail to overcome this defect and present with the cardiovascular defects reported at E18.5 (Lindsay and Baldini, 2001).

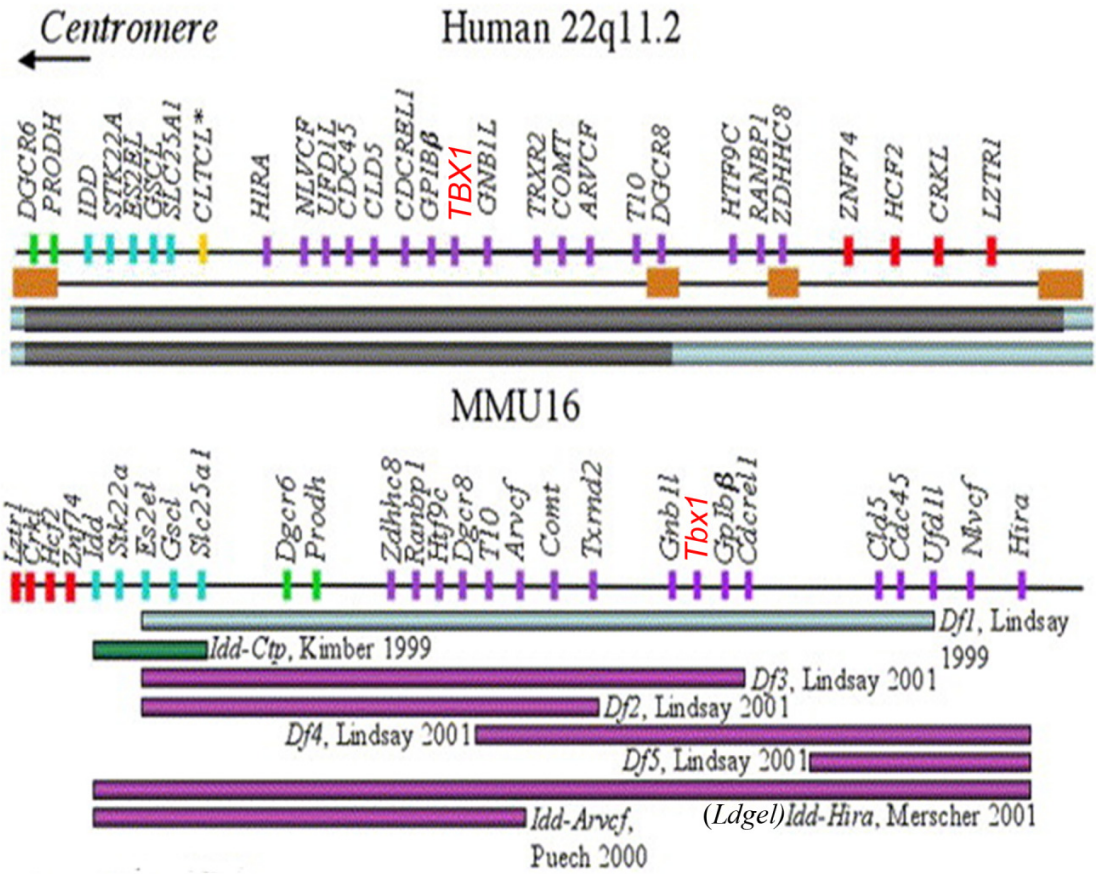

Figure 1.8 Human 22q11.2 and the syntenic mouse genomic region (MMU16)

The large ~3Mb commonly deleted 22q11DS region and the 1.5Mb critical region are shown by grey bars under the human chromosome depiction. Low copy repeat regions are shown as orange bars. Most of the genes are conserved on the syntenic region of mouse chromosome 16 shown below (MMU16) albeit in a different order (shown by matching colours). Primarily, the order of a large block of genes (HIRA-ZDHHC8) is inverted in the mouse genome. Various engineered deletions of mouse chromosome 16 are shown in coloured bars below. Modified from (Paylor and Lindsay, 2006).

1.4.1.2 Conventional null mutations of Tbx1

Homozygous null animals at E18.5 display defects which included the majority of common 22q11DS features arising from the earlier loss of caudal pharyngeal structures. At E10.5 *Tbx1* homozygous null animals have poorly segmented pharyngeal pouch endoderm, a hypo/aplastic pharyngeal arch 2 and complete loss of more caudal arches/

arch arteries (Fig.1-9) and a small outflow tract. The otic vesicle is also reduced in size and head mesenchyme development is abnormal. This early phenotype is closely correlated with the expression of *Tbx1* at E9.5-10.5 in the endoderm pharyngeal pouches, surface ectoderm and the mesodermal core of the pharyngeal arches (PA) surrounding the pharyngeal (or aortic) arch arteries and the outflow tract (Fig.1.9). These earlier defects later result in the failure of septation of the outflow tract, so that all homozygous embryos have a common arterial trunk by E12.5, which remains apparent at E18.5 (Fig.1-9). Failure of the normal remodelling of the pharyngeal tissues also produces hypo/aplasia of the thymus and parathyroid glands. There are also a variety of craniofacial anomalies including cleft palate, skull defects and both external and internal ear malformations. Several different *Tbx1* null mutations recapitulate this phenotype including the $Tbx1^{lacz}$ allele where a *lacZ* reporter gene is inserted into exon 5, (which encodes part of the T-box domain), creating a null allele with a truncated protein, whilst allowing β-galactosidase readout of *Tbx1* expression. $Tbx1^{mcm}$ is a similar null allele, where a tamoxifen inducible-Cre cassette is inserted in the same position. Other null constructs inserted PGK-neo or hygromycin cassettes more 5', just downstream of exon 2 (Jerome and Papaioannou, 2001; Lindsay et al., 2001; Merscher et al., 2001; Xu et al., 2004). Whilst neural crest migration is disrupted in $Tbx1^{-/-}$ embryos, this is believed to be secondary to defects of the PPE and PSE and the signals normally emanating from these structures as Tbx1 is not expressed in NCC (Kochilas et al., 2002; Randall et al., 2009; Vitelli et al., 2002a).

Heterozygous null alleles for *Tbx1* recapitulate the thymic and aortic arch defects of the hemizygous *Df1* chromosomal deletions, also as the result of 4th PAA a/hypoplasia at E10.5 (Fig.1.9) (Lindsay et al., 2001). A similar rate of recovery to that observed in the hemizygous *Df1* chromosomal deletions is also found in *Tbx1* heterozygous embryos.

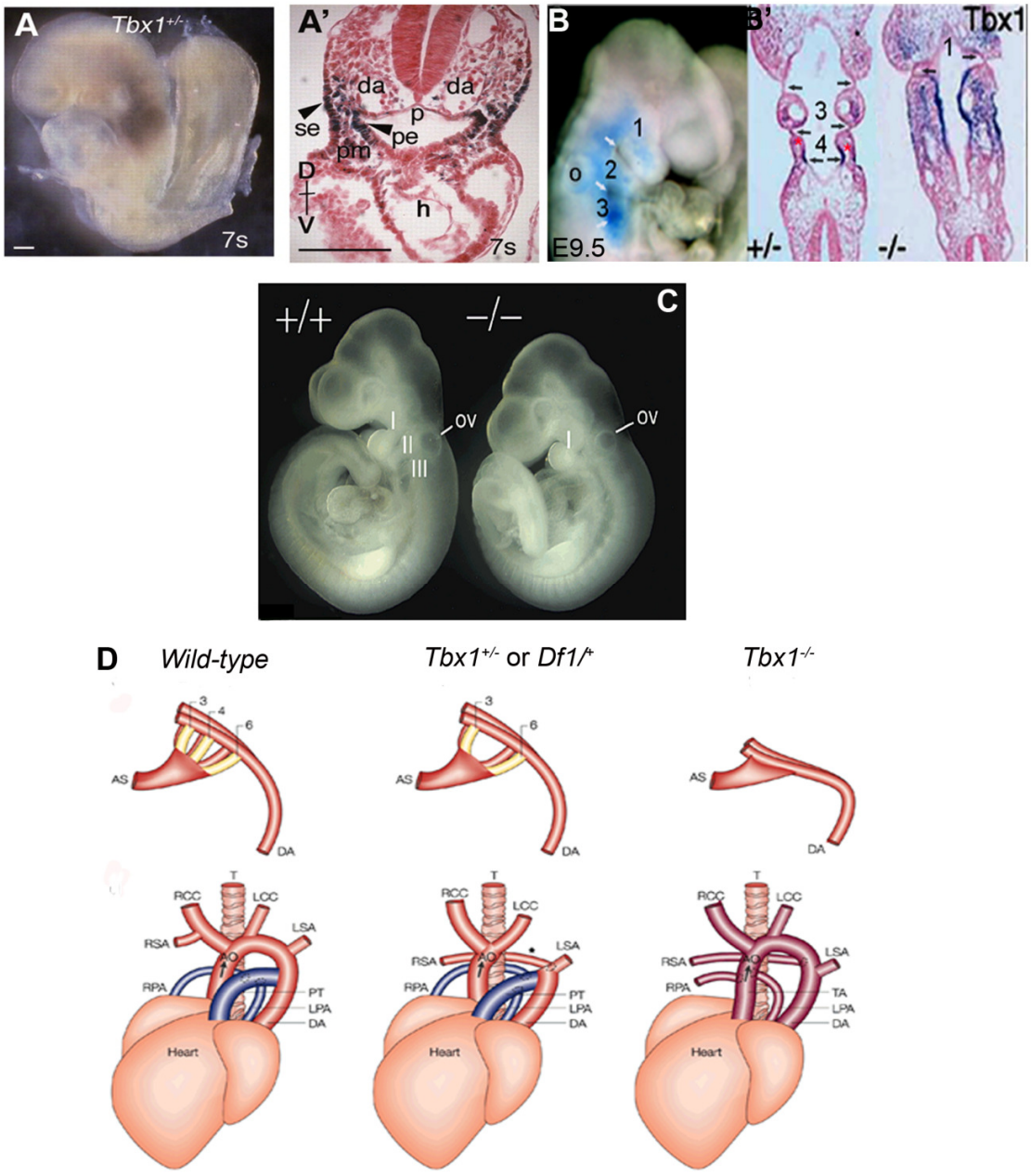

Figure 1.9 *Tbx1* expression and phenotype

LACZ-staining showing *Tbx1* expression pattern in an E8.5 (A.) and E9.5 (B.) heterozygous embryos, with expression in head mesenchyme pharyngeal arches (1-3) and otic vesicle. A' and B'.) Transverse and coronal sections respectively showing expression in pharyngeal ectoderm, endoderm and mesoderm of *Tbx1*$^{+/-}$ and *Tbx1*$^{-/-}$ embryos as indicated. C.) Hypoplasia of caudal pharyngeal arches (I-III) in *Tbx1* null embryos at E9.5.

A'.) da: dorsal aorta, se: surface ectoderm, p: pharynx, pm: pharyngeal mesoderm, pe: pharyngeal endoderm. Numbers in B: pharyngeal arches (pa).White arrows in B; pharyngeal pouch endoderm(ppe). o; otic vesicle. B'.) Numbers indicate pas and black arrows PPE. Note the loss of caudal pharyngeal pouch and arch segmentation in null embryos. * small size of 4th PAA *Tbx1*$^{+/-}$ embryos.

D.) E10.5, *Tbx1*$^{+/-}$ embryos and *Df1/*$^{+}$ embryos have small or absent 4th PAA. In null embryos, there is no development of the pharyngeal apparatus below PA2. PAA3-6 do not form, and the aortic sac (AS) connects directly with the dorsal aorta (DA). d.) At E18.5, *Tbx1*$^{+/-}$ embryos and *Df1*/+ embryos have abnormalities arising from PAA4 derivatives. These include retro-oesophageal right subclavian artery (RoSCA), and an interrupted aortic arch (asterisk). *Tbx1*$^{-/-}$ embryos have persistent truncus arteriosus (PTA or CAT), in which a single vessel exits the heart instead of the normal two, the aorta (AO) and pulmonary trunk (PT). Blue and red vessels indicate pulmonary and aortic arterial flow, respectively. Purple indicates that in the presence of the PTA abnormality, blood from both sides of the heart is mixed. Arrows indicate the direction of blood flow from the heart. (LCC, left common carotid; LPA, left pulmonary artery; LSA, left subclavian artery; RPA, right pulmonary artery; T, trachea; TA, truncus arteriosus (adapted from (Jerome and Papaioannou, 2001; Lindsay, 2001; Zhang et al., 2005).

1.4.2 *Van gogh* (*vgo*) is the *tbx1* null mutant in the zebrafish

The gene for the *van gogh* (*vgo*) zebrafish mutant, which also has 22q11DS-like defects, has been cloned and identified as the zebrafish homologue of *Tbx1* (Kochilas et al., 2003; Piotrowski et al., 2003). Zebrafish TBX1 has a high degree of sequence homology to mouse TBX1, with 98.3% identity within the T-box and 68.5% identity over the whole open reading frame of 460 amino acids (Fig.1-3a). Two different null mutant *tbx1* alleles have been described, *vgo*^{tm208} and *vgo*^{tu285}. In the first, *vgo*^{tm208}, there is an A to T transition, replacing an arginine with a stop codon near the end of the T-box which deletes the entire C-terminus of the protein, including the activation domain. This mutation leads to the loss of an *Alw*N1 restriction site, thus allowing mutant fish to be genotyped by PCR of the region followed by *Alw*N1 digestion. The second mutation, *vgo*^{tu285} introduces a premature stop codon at nucleotide 364 by means of C to T transversion. This deletes 98% of the T-box as well as the C-terminus of the protein (Kochilas et al., 2003; Piotrowski et al., 2003).

Zygotic expression of *tbx1* in the zebrafish is very similar to that of other species including the mouse, chick and frog (Ataliotis et al., 2005; Chapman et al., 1996; Garg et al., 2001; Roberts et al., 2005). At early stages around gastrulation (5.5-6hpf), expression is seen in the hypoblast and presumptive head and lateral plate mesendoderm and pharyngeal endoderm and then also in the cranial paraxial mesoderm. At 18hpf there is expression in the precardiac region of the lateral plate mesoderm, the otic vesicle and pharyngeal arch precursors. By 27hpf this latter expression is localized to the pharyngeal pouch endoderm and arch core mesoderm and arch epithelium. Expression in the pharyngeal tissues is maintained at 48-72h and is also apparent in the outflow tract and otic vesicle (Kochilas et al., 2003; Piotrowski et al., 2003) (Fig.1.10).

The *vgo* mutation was first identified on the Tubingen background from a large scale zebrafish ENU-mutation screen, as causing pharyngeal skeleton and otic vesicle defects (Piotrowski et al., 1996; Whitfield et al., 1996). Later analysis involving ink injections into the aortic arch arteries at 3d.p.f shows that while wild type fish have four PAA, *vgo*/*vgo* mutants only have one (Fig.1-10), a very similar phenotype to that seen at E10.5 in the *Tbx1* null mouse. As in the *Tbx1* mutant mouse, *vgo*/*vgo* fish also fail to form posterior endodermal pouches. This results in thymic a/hypoplasia and in the failure of the neural crest cell populations of individual arches to be separated by endodermal pouch thus allowing the abnormal fusion of neighbouring neural crest streams at 30hpf. By 3dpf, skeletal preparations revealed the neural crest-derived pharyngeal arch cartilages have lost their segmental organization and are fused distally. Cartilage elements are also reduced in size/absent, particularly those derived from the posterior arches (Fig.1.10). Finally, again as in the *Tbx1* null mouse, in *vgo*/*vgo* fish there is loss/disorganization of the muscles of the pharyngeal region which are derived from the non-neural crest mesoderm of the pharyngeal arches (Piotrowski and Nusslein-Volhard, 2000). On the AB* background the phenotype is similar, with embryos dying at 6-7dpf due to cardiac oedema. However, the mandibular (first) arch is always greatly reduced, unlike the Tubingen background where it is rarely affected (Piotrowski et al., 2003).

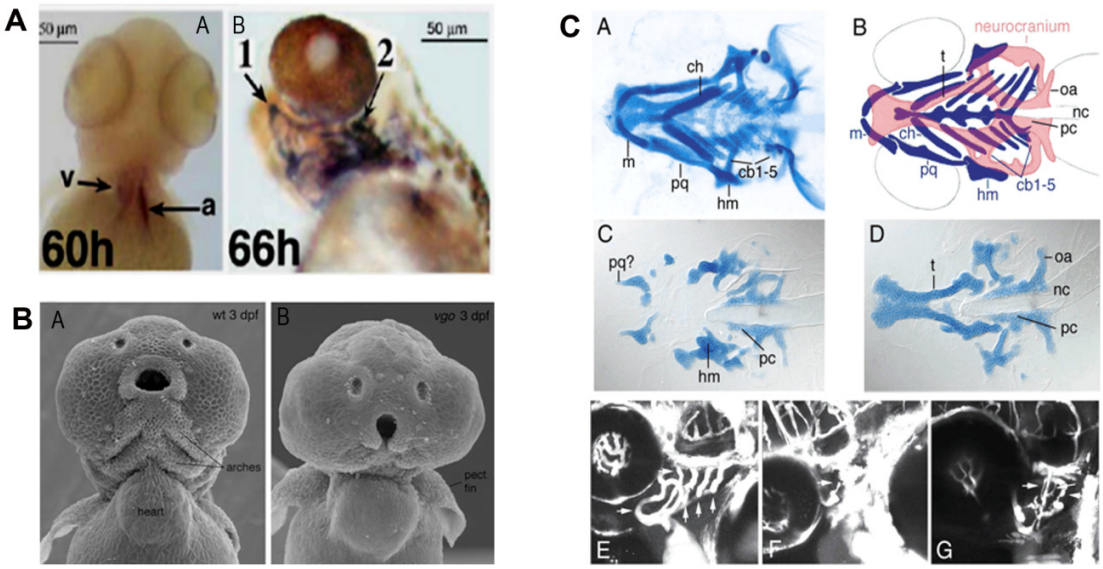

Figure 1.10 The *vgo* zebrafish phenotype

A.) *tbx1* expression in the heart and pharyngeal arches of the zebrafish at A.) 60 h, ventral view: v; ventricle, a; atrium. B.) 66h, pharyngeal arch (numbers) expression. From (Kochilas et al., 2003).

B.) Scanning electron micrograph of wild-type (A.) and *vgo/vgo* (B.) zebrafish at 72hpf. From (Piotrowski and Nusslein-Volhard, 2000).

C.) Craniofacial and aortic arch phenotype in *vgo/vgo* (*tu285* allele, AB* background). (A) Alcian Blue cartilage preparation of a 5 dpf wild-type larva, ventral view. (B) Schematic drawing of the cartilages in A (blue, pharyngeal skeleton; red, neurocranium). (C) Dissected pharyngeal cartilages of a 5 dpf *vgo/vgo* larva. The cartilages in the mandibular (m, pq) and hyoid (ch, hm) arches are drastically reduced and the pharyngeal arches 3-7 (cb1-5) are completely absent. (D) Ventral view of the dissected neurocranium in a *vgo/vgo* larva. The mesodermally derived parachordalia (pc) are malformed and the anterior pole of the notochord (nc) extends almost to the point where the trabeculae (t) fuse. cb1-5, ceratobranchial cartilages 1-5; ch, ceratohyal cartilage; hm, hyomandibula; m, Meckel's cartilage of mandibular arch; nc, notochord; oa, occipital arch; pq, palatoquadrate; pc, parachordalia; t, trabeculae. (E-G) Aortic arches of 2.5 dpf larvae visualized with fluorescent microbeads. (E) Wild-type larva. At this stage, five aortic arches are visible (arrows). (F,G) *vgo/vgo* mutants showing variable reductions of the aortic arches. (F) Only one interrupted aortic arch is present (arrow). (G) Only three aortic arches formed but are much smaller in diameter than wild-type aortic arches (arrows). From (Piotrowski et al., 2003).

Several recent publications have demonstrated that the secondary heart field, as a cell population which is added late, from the pharyngeal mesoderm to the arterial and venous poles elongating the heart tube, is conserved in the zebrafish. These cells express

secondary heart field markers including *Isl1*, which is required for the venous pole contribution, whereas FGF signalling is necessary for the addition of cells to the arterial pole. They give rise to three distinct cardiac lineages; the myocardium, endothelium and smooth muscle of the OFT. Contributions of this cell population are diminished in *tbx1* and *smoothened* mutants leading to a small outflow tract and ventricle (de Pater et al., 2009; Hami et al., 2011; Zhou et al., 2011). Therefore, cardiac development of the zebrafish is more conserved with mammalian models than previously thought. Although they still remain a two-chambered cardiac model (atria and ventricle) and do not undergo PAA remodeling, they provide a useful model for early pharyngeal and cardiac events thanks to their speed of development, ease of visualization and amenability to genetic manipulation.

1.5 Timing, dosage and tissue requirements of *Tbx1* in murine development

Since the original *Tbx1* knock-out papers were published in 2001, a variety of mouse mutants have been employed to further investigate the precise timing and dosage necessary for *Tbx1*, and its role in individual expressing tissues.

1.5.1 Timing requirements of *Tbx1* during development

The tamoxifen-inducible CAGGCre-ER^{TM} mouse line has been used to examine the different time requirements of *Tbx1* for the development of different developmental structures (Fig.1.11). Knocking out *Tbx1* at E7.5 recapitulates the null phenotype including the PAA/aortic arch phenotype, at which time lineage tracing detected a contribution of *Tbx1*-positive cells to the pharyngeal epithelia. The crucial time point for *Tbx1* in OFT development has been determined to be relatively late, between E8.5-9.5, when again there is a strong contribution of *Tbx1*-labelled cells to the OFT. However the PA/PAA phenotype is relatively unaffected later at E8.5. Thymus formation also required *Tbx1* at this time-point, and later at E10.5, showing that *Tbx1* can also be required at more than one time point for the proper development of a tissue. The lineage trace data

correlated progress of segmentation with increasing cranial to caudal contributions of *Tbx1*-positive cells to the pharyngeal endoderm. Elimination of *Tbx1* during pharyngeal segmentation arrested this process and is followed by a decrease in endodermal proliferation (Xu et al., 2005).

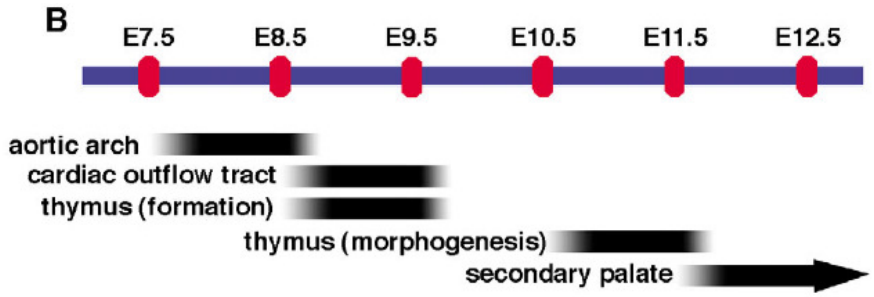

Figure 1.11 Time requirements for *Tbx1* during development
Each pharyngeal structure or process analysed requires *Tbx1* at specific time intervals for normal development. The arrow indicates that the endpoint for *Tbx1*'s role in secondary palate development is unknown. From (Xu et al., 2005)

1.5.2 *Tbx1* dosage gradient affects the observed phenotype

Over and under expression of *Tbx1* in mouse models results in a similar phenotype, indicating that control of *Tbx1* dosage is crucial for development. A series of hypomorphic alleles expressing varying levels of *Tbx1* has revealed differing sensitivities of pharyngeal structures to *Tbx1* (Table 1.1). The thymus and PAA are the most sensitive, with defects apparent even at 70% of wild type levels of *Tbx1* expression. However, outflow tract defects only arise with less than 20% *Tbx1* mRNA. The range of OFT defects was very variable, more closely mimicking that of haploinsufficient 22q11DS-patients. Craniofacial structures such as cleft palate were least sensitive to *Tbx1* dosage, only being present in *Tbx1* null mutants (Zhang and Baldini, 2008).

Table 1.1 *Tbx1* dose-dependent deletion phenotypes

% *Tbx1* genotype / Phenotype	70 *Neo2/+*	53 *Neo/+*	50 *Tbx1+/-*	34 *Neo2/Neo2*	18.5 *Neo2/Neo*	15 *Neo2/-*	4 *Neo/Neo*	0 *Tbx1-/-*
AoA	x 11%	x	x 38%	x 100% (L&R)	x	x	x	x
Thymus hypoplasia	Mild 29%	Mild	Mild 41%	Severe	Aplasia	Aplasia	Aplasia	Aplasia
OFT	-	-	VSD OAo (low)	- ?	VSD DORV ~CAT	~CAT	CAT	CAT
CP	-	-	-	-	-	-	-	x
PA	-	-	-	4th PA hypo	unknown	4th & 6th hypo	No caudal PA	No caudal PA
Lethality	low	low	low	100%	100%	100%	100%	100%

AoA: Aortic arch phenotype including IAA-B and ROSCA/ARSC. OFT: septation and alignment defects, abbreviations as given previously. ? : represents conflicting data: *Tbx1*$^{+/-}$ have a low level of OFT defects but the *Neo2/Neo2* embryos were reported as having none despite less *Tbx1* expression. This might be simply not enough embryos were examined to see a defect. CP: cleft palate, hypo: hypoplasia *Neo* allele: PGKneo cassette inserted into *Tbx1* intron 5. *Neo2*: floxed PGKneo cassette inserted into *Tbx1* intron 5, *Tbx1*: standard null allele. (Lammerts van Bueren, 2008; Lindsay et al., 1999; Xu et al., 2004; Zhang and Baldini, 2008).

Overexpression of *Tbx1* using a BAC transgene produced very similar developmental anomalies to those seen with *Tbx1* null alleles. Hypoplasia of 4th PA/PAA led to characteristic AoA defects including IAA-B. Thymus and parathyroid glands area/hypoplastic and ectopically located in these embryos. Cleft palate and otic defects are also present in *Tbx1* overexpression embryos. These defects can be significantly rescued on the *Tbx1*$^{-/-}$ background (Funke et al., 2001; Liao et al., 2004). In addition, activation of a Cre-dependent *Tbx1* overexpression transgene using a *Tbx1* knock-in Cre, results in VSDs and thymic defects (Vitelli et al., 2009)

1.5.3 Tissue specific effects of *Tbx1* expression

A wide variety of conditional mutants have been used to investigate the role of *Tbx1* in specific tissue types, and have shown that deletion of *Tbx1* in many of its expression domains can recapitulate many of the *Tbx1* null embryonic phenotypes. Deletion of *Tbx1* in the mesoderm with *Mesp1-Cre* has shown that *Tbx1* mesodermal expression is necessary for pharyngeal segmentation, growth and patterning, PAA development, NCC migration, cranial nerve development, OFT growth and septation, thymus and ear development. These embryos also display mesenchymal proliferation defects, possibly secondary to loss of *Fgf8* expression (Xu et al., 2004; Zhang et al., 2006b). *Cre*-mediated mesodermal reactivation of *Tbx1* in hypomorphic $Tbx1^{Neo2/-}$ embryos rescues OFT alignment and septation defects, hypoplasia of PA2, the outer ear and hypoplasia of 3rd and 6th PAA. Therefore, there is a cell-autonomous requirement for mesodermal-*Tbx1* in the development of these structures. However, thymus, 4th PA/ PPE/PAA hypoplasia, and NCC migration defects arenot remedied by this experiment (Zhang et al., 2006b), implying contributions from other *Tbx1*-expressing tissues are required for development of these tissues.

Experiments to determine the role of the PPE have been problematic. Two different approaches gave two different results. In the first, a series of different Cre-drivers, expressed in different combinations of pharyngeal tissues, have established that heterozygous loss of *Tbx1* expression in the pharyngeal epithelia using an *Fgf15-Cre* line (i.e.in the PPE and PSE) is sufficient to confer a 4th PAA hypoplasia phenotype. Results with *Foxg1-Cre* gave similar results, but this driver also appears to be expressed in pharyngeal mesoderm (Zhang et al., 2005). The second set of experiments used the *Foxg1-Cre* on a different genetic background, on which *Tbx1* expression appears to be maintained to some degree in pharyngeal mesoderm, whilst being deleted from PPE and PSE. Null conditional embryos display a hypoplastic unsegmented pharynx, AoA and OFT cardiovascular defects, thymus, parathyroid, otic and craniofacial abnormalities. However, conditional heterozygote deletion of *Tbx*1 yields normal embryos with no PAA defects (Arnold et al., 2006b).

Further work, using conditional deletion of *Tbx1* with *Wnt1- Cre* (NCC) and *AP2α-Cre* (NCC & PSE) recapitulates 4th PAA hypoplasia in conditional heterozygotes. A broad spectrum of 22q11DS-like malformations, including aortic arch defects, thymic hypoplasia, and cleft palate can be seen in in conditional null embryos (Randall et al., 2009). Thus, expression of *Tbx1* in the PSE is necessary for normal pharyngeal development, but the role of the PPE remains unclear, because of the lack of a reliable PPE-specific conditional mouse. Conditional deletion of *Tbx1* with *Tie2-Cre* produces an early post-natal lethality phenotype which has uncovered a requirement for *Tbx1* in endothelial cells during lymphangiogenesis (Chen et al., 2010), but not in PAA development.

As described above, analysis of the differing conditional deletion models is difficult, as a result of disparate expressivity of *Cre*-lines on differing genetic backgrounds and the variation in tamoxifen induction of the *Cre*-alleles, depending upon the protocol used. In addition, different laboratories have investigated particular phenotypes to different degrees, making direct comparisons complicated.

1.6 Regulators of *Tbx1* expression and function

Less is known about the up-stream regulators of *Tbx1* than its down-stream targets. However, the *Tbx1* promoter is known to contain a *Fox* (*forkhead*) binding site which can regulate expression of *Tbx1* in the head mesenchyme and pharyngeal endoderm. This regulatory region is responsive to *Shh* signalling, which is also required for aortic arch development (Washington Smoak et al., 2005). *Shh* is also necessary for *Foxa2* and *c1* expression in the head mesenchyme and pharyngeal endoderm. Both of these genes are required for outflow tract development (Seo and Kume, 2006). Three *Fox* transcription factors could activate transcription of *Tbx1* via the up-stream binding motif, namely *Foxa2*, *Foxc1* and *Foxc2*, suggesting that they are direct regulators of *Tbx1* expression. *Foxa2* and *Tbx1* were also suggested to be in an autoregulatory loop, each being necessary for the others expression in the pharyngeal mesoderm (Hu et al., 2004; Yamagishi, 2003). However, recent experiments whereby the endogenous FOX binding site in the *Shh*-responding enhancer is deleted by gene targeting, have shown that the FOX binding site is

dispensable for *Tbx1* gene expression. The enhancer within which it is located, regulates, to a limited extent, mesodermal expression of *Tbx1*(Zhang and Baldini, 2010).

More recently, inactivation of β-catenin (*Ctnnb1*) signalling in the pharyngeal mesenchyme has been found to generate 22q11-like craniofacial, cardiovascular and thymus defects. Non-cell autonomous NCC differentiation defects led to hypoplastic cranial nerves and apoptosis in the tissue surrounding the PAA increased. *Tbx1* expression increased in these mutants but became extinguished in mutants over-expressing β-catenin. Increased levels of β-catenin signalling also enhance the 4th PAA phenotype in *Tbx1*$^{+/-}$ embryos but reduction of β-catenin expression in the context of either *Tbx1* or *Fgf8* heterozygosity rescues the PAA defects. These results implicate *Wnt- β-catenin* signalling up-stream of *Tbx1*, although whether the regulation is direct or indirect remains to be elucidated (Huh and Ornitz, 2010).

An intriguing report has also proven a role for the histone actetyltransferase MOZ (MYST3/KAT6A) in *Tbx1* regulation. *Moz* null mutants recapitulate the 22q11DS cardiovascular, thymic, craniofacial and palatal defects and the earlier 4th PAA phenotype. *Tbx1* expression is reduced in these mutants. A synergistic rise in frequency and severity of defects is observed in compound heterozygotes and the *Moz* null phenotype can be partially rescued by a *Tbx1* transgene, suggesting epistasis exists between *Tbx1* and *Moz*. The MOZ complex has been shown to occupy the *Tbx1* locus and to promote histone 3 lysine 9 acetylation (H3K9Ac), high levels of which are associated with transcriptional activity. Therefore it would seem that *Moz* drives *Tbx1* expression via H3K9Ac of the locus and is essential for normal development (Voss et al., 2012).

1.7 *Tbx1* target genes

1.7.1 *Tbx1* target genes and proliferation

Tbx1 has been shown to be required for normal proliferation in conjunction with differentiation delay in a number of different tissues. These include the SHF (Xu et al., 2004) and cardiac progenitor cells (Chen et al., 2009), dental epithelium (Cao et al., 2010), basal cortical cells (Meechan et al., 2009), otic mesenchyme and epithelium (Xu et al.,

2007a; Xu et al., 2007b), pharyngeal endoderm (Xu et al., 2005) and pharyngeal and SHF mesoderm (Xu et al., 2004; Zhang et al., 2006b).

1.7.1.1 Tbx1 and FGF signalling in OFT development

Focusing upon the SHF, OFT/SHF hypoplasia is associated with impaired proliferation in *Tbx1* mutants. *Tbx1* appears to use a complex network of mediators to regulate this process. FGF signalling, in particular, seems to play a key role down-stream of *Tbx1* in SHF and in other tissues. *Tbx1* and *Fgf8* are co-expressed in the PPE, PSE and SHF and *Fgf8* is down-regulated in the PPE and SHF of *Tbx1* null embryos (Hu et al., 2004; Park et al., 2006; Vitelli et al., 2002b; Zhang et al., 2006b). *Fgf8* hypomorphs have a very similar phenotype to *Tbx1* homozygotes/22q11DS, including caudal PA/PAA/thymic hypoplasia, and characteristic AoA and OFT defects. Unlike *Tbx1* mutants however, increased apoptosis is observed in these embryos (Abu-Issa et al., 2002; Frank et al., 2002; Meyers et al., 1998). Conditional ablation experiments reveal roles for *Fgf8* in the SHF, PPE and PSE in the production of these 22q11DS-like malformations (Macatee et al., 2003; Park et al., 2006).

In cell culture *Tbx1* can regulate upstream *Fgf8* enhancer elements (Bachiller et al., 2003). Double *Tbx1/Fgf8* heterozygotes display an increased frequency of 4th PAA hypoplasia and later AoA and thymic defects (Vitelli et al., 2002b). Since *Fgf8* PSE expression is unaffected by *Tbx1* deletion, this is unlikely to be the site of interaction (Calmont et al., 2009; Zhang et al., 2005). Deletions of *Fgf8* by different *Tbx1-Cre* drivers also induce varying degrees of OFT alignment and septation defects and 4th PAA anomalies (Brown et al., 2004; Vitelli et al., 2006; Vitelli et al., 2010). However, an *Fgf8* knock-in allele in the *Tbx1* domain did not rescue haploinsufficient *Tbx1* 4th PAA defects, which are in fact enhanced in these embryos. CAT, thymus, ear and palate defects are not rescued in homozygous knock-in embryos either (Vitelli et al., 2006). More recent work in $Tbx1^{Neo2/-}$ embryos, has shown that *Tbx1*-driven *Fgf8* expression in the $Tbx1^{Neo2/-}$ mouse rescues the OFT septation defect by nearly 50%. $Tbx1^{Neo2/-}$ express ~15% of wild-type levels of *Tbx1* and have very similar aortic arch and OFT malformations, with nearly 100% penetrant CAT. Adding FGF8 to cell culture of $Tbx1^{-/-}$ or $Tbx1^{Neo2/-}$ mouse embryo

fibroblasts is sufficient to induce an ERK1/2 phosphorylation response in the latter but not the former. Thus in *Tbx1* nulls there is an loss of the FGF8 tissue response but the presence of a small amount of residual *Tbx1* partially restores this effect (Vitelli et al., 2010). Therefore, different experiments suggest a role for *Fgf8* in mediating *Tbx1* loss-of-function phenotypes in the PAA and OFT. In addition, it appears that complete loss of *Tbx1* impairs the ability of cells to respond to FGF8 signals.

The *Crkl* gene is located in the 22q11-deleted region, and *Crkl*$^{-/-}$ mice recapitulate the 22q11 phenotype (Guris et al., 2001). This family of adaptor proteins transduce tyrosine kinase down-stream signals. FGF8 can phosphorylate tyrosine residues of FGFR1 and 2, which are required for binding to CRKL. CRKL is necessary for FGF8 signalling and *Crkl* and *Fgf8* are in epistasis, as compound mutant mice have increased severity and frequency of PAA, OFT, thymic and craniofacial malformations. This may be mediated via increased NCC apoptosis (Moon et al., 2006; Seo et al., 2009). *Crkl* and *Tbx1* are also found to be in epistasis, and together affect down-stream RA signalling (Guris et al., 2006).

Fgf10 also is involved in arterial pole development. Classic enhancer trap transgene experiments have shown *Fgf10*-positive cells make an important contribution to the pharyngeal mesoderm, SHF and OFT (Kelly et al., 2001). *Fgf10*ias co-expressed with *Tbx1* in the SHF. Expression is reduced in *Tbx1* mutants and *Tbx1* can drive expression of *Fgf10* reporter constructs *in vitro* (Xu et al., 2004). Examination of the *Fgf10-lacZ* transgene in a *Tbx1-/-* background confirmed distal OFT hypoplasia and loss of specific subpopulations of OFT progenitor cells supporting the idea that *Tbx1* regulates the contribution of *Fgf10*-expressing cells to the OFT (Kelly and Papaioannou, 2007). Genetic interaction experiments failed to find any interaction in *Tbx1/Fgf10* double heterozygotes, suggesting redundancy with other *Fgf* genes such as *Fgf8* (Aggarwal et al., 2006) Very recently, a 1.7kb enhancer of *Fgf10* has been identified that is directly regulated by TBX1 in SHF cells. This activation is both necessary and sufficient to direct *Fgf10* expression. NKX2.5 and ISL1 also direct expression of *Fgf10* via this enhancer, playing repressive and activating roles, respectively (Watanabe et al., 2012).

Nkx2.6 has also been identified as a potential target for several *Tbx1* microarray experiments and a homeodomain mutation has been found associated with familial CAT in humans (Heathcote et al., 2005; Liao et al., 2008; van Bueren et al., 2010).

Double null *Six1/Eya1* embryos have been demonstrated to have 22q11DS-like craniofacial and cardiovascular phenotypes and are necessary for cell proliferation and survival in pharyngeal and OFT cells. *Fgf8* expression is reduced in these embryos and *Six1* and *Eya1* bind to and synergistically up-regulate expression of an *Fgf8* enhancer-reporter construct. Increased penetrance and severity of cardiovascular malformation in *Six1/Tbx1* and *Eya1/Tbx1* compound mutants indicates that *Tbx1* is a genetic upstream regulator of these genes, and so can also indirectly regulate *Fgf8* in this fashion (Guo et al., 2011).

1.7.1.2 Other Tbx1 targets in the OFT and other proliferating tissues

Expression of *Wnt5a*, which is necessary for SHF progenitor migration into the OFT, is regulated by *Tbx1*, which binds directly to the *Wnt5a* promoter. There is a genetic interaction between the two genes, with regard to increased frequency of 4th PAA hypoplasia in double heterozygotes. *Wnt5a*$^{-/-}$ embryos exhibit VSDs and incomplete rotation of the great arteries and on a *Tbx1* heterozygous background 59% display the more severe phenotype of CAT. Double homozygote embryos die early in development, but at E9.5 present with OFT and right ventricular hypoplasia. The BAF60A chromatin remodeling complex and histone methyltransferase SETD7 can be recruited to the *Wnt5a* promoter by TBX1 where they are required to alter the chromatin state to facilitate transcription. This complex is also necessary for the transcription of *Fgf8*, *Fgf10* and *Cyp26a1* (Chen et al., 2012a).

Pitx2c is also co-expressed with *Tbx1* in the left SHF, and down-regulated in *Tbx1* null embryos (Nowotschin et al., 2006). Knock-outs of *Pitx2c* have a 22q11DS-like phenotype which includes PAA abnormalities, ventricular septal defects and OFT alignment defects (Kitamura et al., 1999; Liu et al., 2001; Liu et al., 2002). *Tbx1* and *Nkx2.5* have been shown to synergistically activate a *Pitx2* enhancer *in vitro* suggesting

that *Pitx2* is a direct target of *Tbx1* (Nowotschin et al., 2006). Conversely, in the dental epithelium *Tbx1* regulates proliferation by repression of *Pitx2* and thus, its target gene, *p21* , which associated with cell cycle arrest (Cao et al., 2010). This interaction may be the basis for the dental defects observed in 22q11DS patients.

Tbx1$^{-/-}$ mice have a small otic veicle that fails to grow or remodel and does not give rise to the cochlear or vestibular apparatus (Vitelli et al., 2003). Peri-otic mesenchymal *Tbx1* expression is necessary for the development of the cochlea, via an interaction with *Brn4* and possibly altered expression of RA-responsive genes (Braunstein et al., 2009; Braunstein et al., 2008; Monks and Morrow, 2012; Xu et al., 2007a). In the otic epithelium, *Tbx1* expression functions to control a posterior proliferative *Tbx1*-positive domain versus an anterior *Tbx1*-negative neurogenic region. *Tbx1* represses neural fate genes *Neurog1* and *Neurod* and Delta –Notch signalling posteriorly. It is necessary for normal expression of *Otx1* and *Bmp4*, which are required for sensory organ formation. Finally, *Tbx1* positively regulates proliferation in this region of the otic vesicle, which is necessary for its growth (Arnold et al., 2006a; Raft et al., 2004; Xu et al., 2007b).

1.7.1.3 Tbx1 and target protein-protein interactions

A direct protein-protein interaction has been demonstrated between TBX1 and SMAD1 which interferes with SMAD1/4 binding and suppresses BMP4/SMAD1 signalling (Fulcoli et al., 2009). Since a *Bmp/Smad1/Nkx2.5* negative feedback loop can control OFT progenitor specification and proliferation (Prall et al., 2007) TBX1 may also interact with this pathway during SHF development. Consistent with a role for *Tbx1* in suppressing cardiac progenitor cell differentiation *Tbx1* negatively regulated myogenic SHF gene *Mef2c*, via inhibition of its transactivation by *Gata4* (Hinits et al., ; Pane et al., 2012).

BMP-signalling has also been shown to promote OFT myocardial differentiation by SMAD1/5-mediated regulation of miR-17-92 expression. These miRs are required to directly repress the expression of cardiac progenitor genes, including *Tbx1* and *Isl1*, thus promoting myocardial differentiation. Genetic interaction experiments also revealed a

synergistic interaction between the miRs and *Bmp4*, providing in vivo evidence for the roel of this pathway in cardiac development (Wang et al., 2010)

TBX1 and ASH2L (absent, small, or homeotic2-like) are also co-expressed during development. ASH2L is a core component of a histone methyltransferase complex. TBX1 physically interacts with ASH2L, which acts as a co-activator of TBX1 (Stoller et al., 2008). This interaction provides the basis for a potential interaction complex with CHD7 via the recruitment of CHD8 and BAF60C.

TBX1 also binds to serum response stimulating factor (SRF). SRF is a myogenic transcription factor necessary for mesoderm formation and the regulation of muscle differentiation (Arsenian et al., 1998; Wang et al., 2001). *Tbx1* is present in SHF proliferating cells and down-regulated during differentiation. Loss of *Tbx1* causes premature SHF progenitor differentiation, and overexpression reduces differentiation. The physical interaction of TBX1 and SRF reduced SRF levels in vitro in a dose-dependent fashion (Chen et al., 2009).

Ripply3 is co-expressed with *Tbx1* in the PPE and PSE. *Ripply*$^{-/-}$ mice have hypoplastic 3rd and 4th PAA and persistent 2nd PAA, leading to IAA-B, aberrant subclavian arteries and ectopic carotid arteries. Hypoplastic OFT and VSDs are also present. These defects may result from the ectopic expression of *Tbx1* targets, as RIPPLY3 binds to TBX1 at target promoters, such as *Pax9*, where it represses TBX1 target transactivation, probably by recruitment of GROUCH/TLE/HDAC complexes (Okubo et al., 2011).

1.7.1.4 Tbx1 target genes and the pharyngeal surface ectoderm

The pharyngeal surface ectoderm has recently emerged as a signalling centre in which *Tbx1* interactions are important for normal pharyngeal and neural crest cell (NCC) development.

CHD7 haploinsufficiency gives rise to CHARGE (coloboma, heart defects, atresia choannae, retarded growth and development, genital hypoplasia ear anomalies/deafness) Syndrome. CHARGE patients have a significant overlap of cardiac phenotype with 22q11DS and heterozygous *Chd7* genetrap mice present similar 4th PAA defects to *Tbx1*$^{+/-}$ embryos, which give rise to aortic arch defects later in development. Double heterozygotes demonstrated a genetic interaction between these genes by a synergistic rise in IAA-B and bilateral 4th PAA defects. Cre-mediated rescue of the *Chd7* mutant allele by *Wnt1-Cre* (NCC) or *AP2α-Cre* (NCC and PSE) and conditional ablation of *Tbx1* in the PSE revealed the PSE as the site requiring biallelic expression of both genes for normal development (Randall et al., 2009).

More recently, 22q11/*Tbx1* null-like phenotypes have been identified in 40% of homozygous null embryos for the homeobox transcription factor *Gbx2* (Byrd and Meyers, 2005). Synergistic PAA defects have been detected in double heterozygous *Fgf8*$^{+/-}$ */Gbx2*$^{+/-}$ embryos and the frequency of PAA and thymic defects increases in *Gbx2*$^{-/-}$ */Fgf8*$^{+/-}$ embryos. This data supports a genetic interaction between *Gbx2* and *Fgf8*. *Gbx2* is also down-regulated in the PSE of *Tbx1* null embryos at E8.5. Conditional deletion of *Gbx2* using a *Tbx1-Cre* line produces 4th PAA defects and *AP2α-Cre* deletion of *Gbx2* (effectively a PSE-deletion of *Gbx2*) recapitulates the 4th PAA defects observed in *Gbx2* null embryos. These anomalies are correlated with abnormal migration of caudal neural crest (required for normal aortic arch and SHF development) and failure of PAA endothelial cells to form vessels. These defects appear independent of proliferative anomalies and *Fgf8* expression. The *Slit/Robo* pathway, which is implicated in neural crest migration might also be involved, as *Slit2* expression in the PSE of *Gbx2* and *Tbx1* null embryos is reduced, as is the number of *Robo1*-positive migrating NCC cells (Calmont et al., 2009).

1.7.1.5 Tbx1 targets and PAA development.

In addition to the *Tbx1* targets in the PSE which affect PAA development, other down-stream genes are also involved. *Smad7*, which codes for a TGF-B inhibitory

SMAD, is co-expressed with *Tbx1* in the PSE and other pharyngeal tissues. *Smad7* expression is reduced in *Tbx1* null embryos and ChIP showed TBX1 to bind to the *Smad7* promoter during development. *Smad7* genetically interacts with *Tbx1* in an autonomous fashion for PAA remodeling during 4th PAA recovery. This interaction affects development of NCC-derived VSMC coverage of the 4th PAA and ECM deposition.

Mice expressing only the $Vegf^{120/120}$ or $Vegf^{188/188}$ isoforms display 22q11DS-like phenotypes whereas $Vegf^{164/164}$ embryos are normal, suggesting this isoform is important in cardiovascular development. *Tbx1* expression is reduced in $Vegf^{120/120}$ embryos and morpholino knock-down experiments in the zebrafish have shown epistasis between $Vegf^{120}$ and *Tbx1*. A specific *VEGF* sequence variation, has been found to be more common in 22q11DS patients with cardiovascular phenotypes, but the sample size of this study was very small (Stalmans et al., 2003). On the basis of these experiments *Vegf* has been suggested to be a modifier of *Tbx1*.

1.7.1.6 Tbx1 targets and branchiomeric muscle development

Tbx1 is required for the normal activation of *Myf5*, *MyoD*, *Tlx1* and *Fgf10* in the mesodermal core of PA1 and 2. Pre-myogenic cells are present in $Tbx1^{-/-}$ mutants but only activate myogenic regulatory factors sporadically, so the majority of branchiomeric muscles fail to form (Kelly et al., 2004). *Pitx2* is also required for the specification and differentiation of branchiomeric muscle. *Tbx1* expression is unaffected in these mutants, suggesting either it operates upstream of *Pitx2*, as in the SHF, or is in a separate pathway (Dong et al., 2006). BMP, FGF and RA-signalling in the head mesoderm may also play roles in establishing the differential expression of head mesoderm genes including *Pitx2*, *Tbx1* and *MyoR* (Bothe et al., 2011). Pharyngeal mesoderm is known to contribute to both the cranial and cardiac lineages [reviewed in (Grifone and Kelly, 2007; Tzahor E. and Evans S.M., 2011). Microarrays between trunk and pharyngeal mesoderm to identify unique pharyngeal mesoderm markers recently isolated the LIM homeodomain gene *Lhx2*. *Lhx2* is decreased in the pharyngeal mesoderm of *Tbx1* mutants and pharyngeal muscles are completely lacking in *Tbx1/Lhx2* double homozygote nulls. *Mesp1-Cre Lhx2* conditional nulls display OFT alignment defects including VSD and DORV. In addition,

Tbx1/Lhx2 compound heterozygotes display a synergistic VSD malformation. Thus it seems that *Lhx2* and *Tbx1* lie within the same genetic pathway in the pharyngeal mesoderm and contribute to both craniofacial and cardiac mesodermal development (Harel et al., 2012).

1.7.2 Microarray identification of putative *Tbx1* targets

For the purposes of this thesis, potential *Tbx1* targets are broadly defined, and include both direct and indirect interactions. Differential expression of potential targets with varying levels of *Tbx1* in microarray, RTQ-PCR or in situ hybridization experiments could indicate genes which act within the same pathway as *Tbx1*, or, more conservatively, genes which are expressed in a cell lineage important for the development of the structures affected by loss of *Tbx1*. Once disparate expression down-stream of *Tbx1* has been established, further questions can be asked to further refine the interaction with *Tbx1*. These include, whether the target gene has a role in cardiovascular development, and if so, do any aspects of this function relate to the 22q11DS phenotype? If a genetic interaction between *Tbx1* and the target can be demonstrated, this could indicate they are part of the same or convergent pathways and may be important to human 22q11Ds if in epistasis.

Incidentally, the term epistasis has been used to refer to a number of somewhat different phenomena (; Cordell, 2002). Here, the term is used to in a functional/mechanistic sense to refer to the genetic enhancement or suppression of a phenotype in double mutants compared to the expected additive effects of single mutants.

Two separate microarray experiment have been undertaken in this laboratory to identify possible down-stream targets of *Tbx1* (Fig.1-12). In the first experiments, mRNA extracted from the dissected pharyngeal region was compared between wild type and *Tbx1* null embryos (Ivins et al., 2005). In the second microarray, the experiment utilized was optimized using FACS-GAL to identify cell autonomous target genes by comparing cells carrying a *Tbx1-Lacz* knock-in transgene which were isolated by from *Tbx1* heterozygous

and null embryos using a fluorescent β-galactosidase substrate followed by flow-sorting (van Bueren et al., 2010). In both experiments mRNA extracted from tissue samples was hybridized to Affymetrix GeneChips and analysed by GeneSpring software..

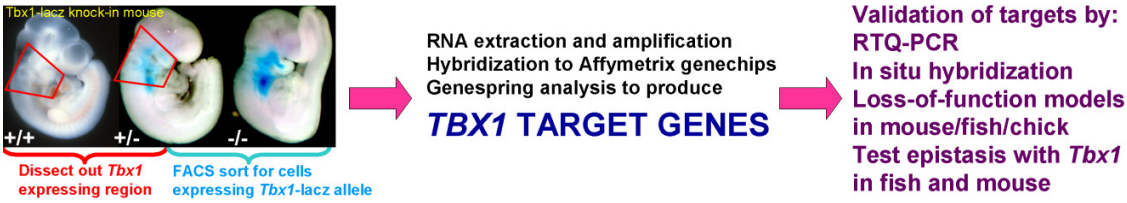

Figure 1.12 Schematic showing the experimental design for identification and validation of potential *Tbx1* target genes

As anticipated a large number of putative target genes were identified from these array experiments. After validation by real-time PCR (RTQ-PCR) and in situ hybridization in wild type and null embryos, some of these genes were investigated at the functional level. These included *Hes1*, a member of the Notch pathway family, and the *Cyp26* family genes, which code for retinoic acid catabolizing enzymes. Other microarrays to identify *Tbx1* targets in otic and SHF development have also isolated these genes, and others, such as *Raldh2*, *Dab2*, *Nkx2.6* and *Pax9*, in common with the microarrays performed in out laboratory (Braunstein et al., 2009; Liao et al., 2008; Monks and Morrow, 2012).

Altered expression for *Hes1* and the *Cyp26* genes in *Tbx1* mutants having been established, the work presented here is aimed at answering some of the more functional questions regarding possible interactions with *Tbx1* as discussed above. An Introduction to the retinoic acid and Notch pathways is given below.

1.8 The retinoic acid pathway

Retinoic acid (RA) is one of the most important signalling molecules in embryogenesis. It has long been known as a signalling molecule required for the normal development of a large number of embryonic tissues including the pharyngeal region and the heart [(Niederreither et al., 1999), reviewed by Mark et al (Mark et al., 2004) and Zile

(Zile, 2004)], the nervous system (Maden et al., 1996; Niederreither et al., 2000; Sockanathan and Jessell, 1998), lung (Malpel et al., 2000), limb (Stratford et al., 1999; Stratford et al., 1996), kidney (Batourina et al., 2001; Mendelsohn et al., 1999) and eye (Wagner et al., 2000). Studies in both mammalian and non-mammalian models have shown that disruption of RA homeostasis via maternal diet or genetic/chemical modification (thus increasing or decreasing RA relative to normal endogenous levels) can result in a phenotype with strong similarities to 22q11DS (Dupe et al., 1999; Ghyselinck et al., 1998; Kastner et al., 1997; Lammer et al., 1985; Lohnes et al., 1994; Matt et al., 2003; Mendelsohn et al., 1994; Mulder et al., 1998; Mulder et al., 2000; Rosa et al., 1986; Wendling et al., 2000), Teratogenic effects in many other tissues were also observed, including craniofacial defects, CNS abnormalities including posteriorization of the hindbrain, caudal truncations, antero-posterior patterning defects and limb defects (Durston et al., 1989; Fantel et al., 1977; Gale et al., 1999; Happle et al., 1984; Iulianella et al., 1999; Kalter, 1960; Kalter and Warkany, 1961; Kistler, 1981; Kochhar and Johnson, 1965; Lammer et al., 1985; Maden et al., 1996; Rosa et al., 1986; Shenefelt, 1972; Summerbell, 1983; White et al., 2000b) .

RA is a lipophilic molecule, manufactured from maternal retinol (vitamin A) in placental species and carotenoids in the yolk of species which are oviparous. It can, theoretically, diffuse across cell membranes, setting up retinoic acid gradients and functioning as a classic morphogen. However, there is also strong evidence that very tight spatiotemporal control of RA synthesis and metabolism via the expression of specific enzymes (RALDHs and CYP26s respectively) is important for normal development. Both these classes of enzyme are expressed in a dynamic and spatially restricted manner during embryogenesis, such that they are often expressed in a complementary, but rarely overlapping fashion (Blentic et al., 2003; Fujii et al., 1997; MacLean et al., 2001; Mic et al., 2000; Niederreither et al., 1999; Reijntjes et al., 2004; Reijntjes et al., 2003; Reijntjes et al., 2005; Schneider et al., 2001; Swindell et al., 1999; Tahayato et al., 2003; Zhao et al., 1996). This Introduction will focus upon the control of RA distribution, its basic mechanism of action within the cell and its function in development.

1.8.1 Retinoic acid metabolic pathways

1.8.1.1 Retinoic acid synthesis

1.8.1.1.1 The role of retinol

In most animals RA is diet derived, as it cannot be synthesized directly, but must be converted from retinol. In mammalian development, embryonic retinol is maternally derived and transferred across the placenta, whereas oviparous species store RA precursors which depending on species include retinol, retinaldehyde and beta-carotin in the egg yolk (Simoes-costa et al., 2008). Circulating retinol is taken up by embryonic retinol binding protein 4 (RBP4) , and this complex the binds to STRA6 (stimulated in retinoic acid 6) and is transported across the plasma membrane in the cell. *Stra6* is expressed in many tissues in the developing embryo, including the epithelia of the pharyngeal arches and facial mesenchyme. Human mutations in *Stra6* proved the only example of congenital disease resulting from retinoid pathway mutations. Patients exhibit a complex phenotype including anophthalmia, lung hypoplasia, mental retardation and craniofacial and heart defects reminiscent of 22q11DS (Pasutto et al., 2007).

1.8.1.1.2 Conversion of retinol to retinaldehyde

Retinol then must be converted by oxidation into the intermediate form of retinaldehyde which is accomplished by two enzyme families, the cytosolic alcohol dehydrogenases (ADHs) and microsomal retinol dehydrogenases (RDHs)(Fig.1.13).

On vitamin A deficient backgrounds varying degrees of postnatal lethality are seen in *Adh1* (40%), *Adh5*, *Adh7*, *Adh1/7* (all 100%) mutants. Excess retinol produces severe

embryonic and post-natal lethality in *Adh1* null mice, alone (Deltour et al., 1999; Molotkov et al., 2002a; Molotkov et al., 2002b; Molotkov et al., 2002c)
Therefore the ADHs may be variously and possibly redundantly involved in RA synthesis and play protective roles against the effects of excess retinol.

Rdh10 is expressed in specific and dynamic fashion in early development, including lateral plate, paraxial and cardiac mesoderm. Null mutations of *Rdh10* gave rise to an RA-deficiency-like phenotype lethal at E13.0. The phenotype was similar to, but milder than that of *Raldh2*$^{-/-}$, and included pharyngeal arch, vascular and cardiac malformations such as CAT, ventricular misalignment and poor trabeculation and atrial septal defects. These defects can be partially rescued by the administration of maternal RA, although cardiac defects remain recalcitrant to this treatment. Maternal retinaldehyde supplementation however, rescues all defects to a greater degree and allows the production of viable and fertile *Rdh10*$^{-/-}$ adult mice (Rhinn et al., 2011; Sandell et al., 2007). *Rdh10* is therefore thought to be the main enzyme involved in embryonic retinol to retinaldehyde conversion.

1.8.1.1.3 Conversion of retinaldehyde to retinoic acid

The final step of the RA synthesis pathway requires the oxidation of retinaldehyde into the active retinoic acid ligand by the retinaldehyde dehydrogenase (RALDH) enzymes (Ang and Duester, 1999; Duester, 1996; Mic et al., 2002)(Fig 1.13). Three of these enzymes are active during development. All three genes are expressed around the developing eye, *Raldh3* is also expressed in the olfactory placodes, whereas *Raldh2* has a wider expression pattern encompassing domains in the head, somatic and splanchnic mesoderm, limb (Li et al., 2000; Mic et al., 2000; Niederreither et al., 1997). Null mutations for *Raldh1* and *Raldh3* suggest these two family members are only necessary for embryonic RA production in a minor fashion as mutants are respectively, viable with mild dorsal retina defects or have choanal atresia (causing respiratory distress and death at birth), shortened ventral retinas and altered forebrain neuronal differentiation (Chatzi et al., 2011; Dupe et al., 2003; Fan et al., 2003; Matt et al., 2005).

In contrast *Raldh2* provides RA to the majority of embryonic tissues, as *Raldh2*$^{-/-}$ embryos die at mid-gestation at E10.5 with a very severe phenotype encompassing failure of axial rotation, a shortened anteroposterior axis and frontonasal process, abnormal somitogenesis, small otocysts, lack of limb buds and a single medial un-looped dilated heart cavity with impaired atrial and sinus venosus formation, posteriorly expanded SHF markers and impaired ventricular cardiomyocyte differentiation. Maternal RA administration is able to rescue much of this phenotype such that embryos survive until E13.5-14.5. (Hochgreb et al., 2003; Niederreither et al., 1999; Niederreither et al., 2000; Niederreither et al., 2001; Niederreither et al., 2002b; Niederreither et al., 2003; Ryckebusch et al., 2008; Vermot et al., 2005). A similar set of malformations has been observed in the zebrafish *raldh2* mutant *neckless* and recapitulated in morpholino knockdowns. This phenotype can also be rescued by the application of exogenous RA (Begemann et al., 2001).

The sensitivity of the the pharyngeal and cardiovascular systems to RA levels has been demonstrated in 'RA-rescued' *Raldh2* null mouse embryos, which reproduce cardiac and thymus defects similar to 22q11DS and *Tbx1* mutant mice, including CAT. Similar phenotypes are also seen in a hypomorphic null allele of *Raldh2* with early abnormalities of PAA1-3 and disorganized migration of the neural crest and later characteristic heart and thymus malformations (Niederreither et al., 2001; Vermot et al., 2003).

Finally, *Cyp1b1* a p450 cytochrome enzyme, has been identified as being capable of converting retinol to retinaldehyde and retinoic acid in the chick, where it has been shown to play a role in neural tube patterning and motor neuron identity during embryological development (Chambers et al., 2007). Whilst mouse null mutations appear normal during embryogenesis (Dragin et al., 2008), human mutations are associated with congenital glaucoma, Peters anomaly (Hollander et al., 2006; Priston et al., 2006) and Axel-Riegers Syndrome (Tumer and Bach-Holm, 2009).

1.8.1.2 Interactions between Tbx1 and Raldh2

Microarray, real-time PCR and in situ hybridization experiments have shown that *Raldh2* is ectopically up-regulated in the splanchnic mesenchyme of *Tbx1*$^{-/-}$ embryos,

displaying an anterior shift of the rostral border of this expression domain in mutants (Guris et al., 2006; Ivins et al., 2005). Compound heterozygotes and homozygotes for *Tbx1* and the *Crkl* adaptor protein exhibit genetic interactions that increase the frequency of 22q11DS-like defects. These embryos also display a similar ectopic anterior shift of *Raldh2,* with a concomitant anterior expansion of expression of RA-responsive genes and a *RARE-lacZ* reporter gene, suggesting increased RA levels in mutant embryos. When a heterozygote *Raldh2* allele is crossed onto the $Tbx1^{+/-}/Crkl^{+/-}$ background a significant decrease in the frequency of thymus hypoplasia can be observed, suggesting that decreased RA levels in these mutant embryos can ameliorate the phenotype (Guris et al., 2006). Furthermore, it has been reported that this ectopic expression can also be seen in $Tbx1^{+/-}$ mutants. As mentioned above, *Tbx1* haploinsufficient mice have a 100% penetrant 4th PAA defect at E10.5, which subsequently recovers, such that only ~30% of remodeled PAA are still abnormal at birth (Lindsay and Baldini, 2001). Double heterozygotes for *Tbx1* and *Raldh2* are found to have a significantly increased rate of recovery from this arterial growth delay at E11.5, possibly as a result of improved differentiation of vascular smooth muscle, although this early recovery is not sufficient for a significant improvement of later aortic arch anomalies (Ryckebusch et al., 2010).

It has been shown that there may be a feedback loop between *Tbx1* and RA in that exogenous retinoic acid can down-regulate *Tbx1* expression in the chick and zebrafish and in pharyngeal mesodermal explants (Roberts et al., 2005; Ryckebusch et al., 2010; Zhang et al., 2006a). However, the effect of RA levels upon *Tbx1* expression may be more complex than simple down-regulation at all stages, as up-regulation of *Tbx1* in *Xenopus* is observed when exogenous RA is applied before stage 18 and is down-regulated if applied at later stages (Janesick et al., 2012). In $Raldh2^{-/-}$ mouse embryos at 8 somites, *Tbx1* is expanded in the pharyngeal/splanchnic mesoderm but reduced in pharyngeal ectoderm and endoderm (Ryckebusch et al., 2008) and RA-bead implantion in the early chick otic placode also up-regulates RA (Bok et al., 2011)

1.8.2 Retinoic acid catabolizing enzymes: the CYP26s

1.8.2.1 CYP26 characteristics

A second important level of control of RA distribution is the expression of the CYP26 metabolizing enzymes (Fig1.13). These are cytochrome P450s enzymes which are part of the microsomal p450 mixed function oxidase system, which is required for the synthesis or degradation of many signalling factors during embryonic development.

CYP26 enzymes hydroxylate RA to more polar metabolites such as 4-hydroxy, 4-oxo and 5, 8 epoxy all-trans RA (Fujii et al., 1997; White et al., 1996; White et al., 2000a). These chemical forms are less biologically active and undergo further glucuronation by UDP –glucuronosyltransferases to 4-O-β-glucuronide and are eventually elimination from the cell (Fig 1.c). All CYP26 enzymes contain several membrane spanning domains and a conserved C'-terminal haem-binding domain which is essential for enzyme function. However, the three CYP26s have only approximately 55% amino acid identity to each-other, although between species each individual CYP26 enzyme is much closely related, with CYP26B1 being the most highly conserved protein (Ross and Zolfaghari, 2011). Knockout mice for *cytochrome p450 oxidoreductase* (*Por*), which is the obligate electron donor for the CYP26 enzymes and necessary for their function, display very severe phenotypes. These included growth retardation, axial rotation defects abnormal head and caudal development, open neural tubes, pharyngeal and cardiovascular defects, which are lethal by E10.5. These embryos exhibit ectopic RA-signalling and can be partially rescued by genetic down-regulation of RA using the *Raldh2* null allele (Otto et al., 2003; Ribes et al., 2007b; Shen et al., 2002), thus displaying the importance of CYP26 function during development.

1.8.2.2 CYP26 function: Activity of polar metabolites versus degradation of RA

It has been suggested that the first polar metabolites may still have biological activity within the embryo and some evidence has been put forward for this idea. All three CYP26-generated RA- metabolites can regulate *Cyp26* expression in the chick and each is capable of rescuing the RA-deficient phenotype of the VAD quail embryo (Reijntjes et al., 2005). Furthermore, 4-oxo-RA causes anteroposterior defects and the induction of *Hoxb4* and *9* in *Xenopus* embryos, and is a high-affinity activating ligand of RARβ (Pijnappel et

al., 1993). In zebrafish 4-oxo-RA produces the same range of development abnormalities as all-trans-RA but at a lower efficiency (Herrmann, 1995). This raises the possibility that some of the effects of CYP26 functional blockade could be the result of reduced metabolite levels, as well as excess RA in the embryo. However, genetic experiments in the mouse suggest that this is not the case, since the majority of *Cp26a1* null embryos on a *Raldh2* heterozygous background survive well past birth. If part of the *Cyp26a1* null phenotype is the result of impaired 4-oxo-RA signalling, then crossing on the *Raldh2* haploinsufficient background should exacerbate the phenotype by decreasing the levels of substrate for the oxidizing enzymes, thus leading to lower levels of 4-oxo-RA. Therefore, it seems that the *Cyp26a1* null phenotype is the result of excess RA in tissues due to the lack of catabolism and not altered levels of metabolites (Niederreither et al., 2002a). Additionally, *Cyp26a1* can rescue excess RA phenotypes, whereas if the CYP26 metabolites were active it might be expected to potentiate the effect of excess RA (Guidato et al., 2003; Hollemann et al., 1998). It may be that in normal development, although the atRA-derived CYP26 metabolites above are biologically active, they are very rapidly conjugated, mainly as glucuronates, and eliminated by excretion before accumulating to levels at which they can exert a biological effect (Reijntjes et al., 2005).

1.8.2.3 Cyp26 expression

The three embryonic *Cyp26* genes are all expressed in regions of the embryo known to require careful RA regulation for normal development, notably in the neural plate and hindbrain, the tailbud, the heart and the pharyngeal tissues, including head and pharyngeal arch mesenchyme, pharyngeal pouch endoderm and neural crest-derived mesenchyme. There is some variation in the expression of each specific gene between vertebrate species, including between chick and mouse embryos. However, the combined domain of expression of all three genes is overall extremely similar between the two species (Blentic et al., 2003; de Roos et al., 1999; Fujii et al., 1997; MacLean et al., 2001; Reijntjes et al., 2004; Reijntjes et al., 2003; Swindell et al., 1999; Tahayato et al., 2003)

1.8.2.4 Targeted disruption of Cyp26 genes reveals discrete embryonic phenotypes

1.8.2.4.1 Cyp26a1 deletion

Targeted disruption of *Cyp26a1* and *Cyp26b1* leads to phenotypes that are similar to application of exogenous RA. Two separate knock-out mice for *Cyp26a1* have been found to have a phenotype which includes posterior truncations and sirenomelia, abnormal development of the posterior gut and urogenital system, homeotic posterior transformations of the vertebrae and hindbrain and cranial nerve patterning defects, and pericardial oedema with looping abnormalities of the heart (Abu-Abed et al., 2001; Sakai et al., 2001). These anomalies are accompanied by an increase in RA signalling which has been linked to the mispatterning of the brain and vertebrae and caudal truncation associated with down-regulation of *Brachyury* and *Wnt3a* (Iulianella et al., 1999; Takada et al., 1994; Wilkinson et al., 1990; Yamaguchi et al., 1999; Yoshikawa et al., 1997). Similar phenotypes are also observed in the zebrafish *cyp26a1* null mutant, *giraffe* (Emoto et al., 2005).

Cyp26c1 knockouts alone seem to have no discernible embryological defects. This may be due to functional redundancy with *Cyp26a1* with which it is expressed in an overlapping pattern and is found on the same chromosome (Tahayato et al., 2003). Double homozygous mutants for *Cyp26a1/c1* display a more severe RA embryopathy phenotype than either mutant alone, with lethality by E11.0. This includes CNS patterning abnormalities, a reduced size of the head, eye, frontonasal region and an open neural tube between the fore and hindbrain, hypoplastic PA1 and 2 and abnormal NCC migration. The NCC defects can be rescued in the context of a *Raldh2*$^{-/-}$ genetic background, thus suggesting that CYP26s have a protective role against inappropriate RA exposure during development. Studies which support this idea show that *Cyp26a1*$^{+/-}$ embryos undergo anterior truncations of the head and abnormal vascularization, when exposed to maternally administered subteratogenic doses of RA that do not result in defects in wild-type embryos (Ribes et al., 2007a). Caudal truncation malformations appear to be mediated by inappropriate activation of *Rarg* (retinoic acid receptor gamma). Loss of *Rarg* confers resistance to the caudal abnormalities induced by teratogenic RA doses (Iulianella et al., 1999; Lohnes et al., 1993) and rescues *Cyp26a1*$^{-/-}$ caudal regression/lethality in 50% of

embryos. In the wild-type state it seems *Cyp26a1* function is to protect against the effects of excess environmental RA, particularly since RA can induce *Cyp26a1* expression via RARE sites in its promoter (Abu-Abed et al., 1998; Iulianella et al., 1999; Loudig et al., 2005; White et al., 1996), although this system is not sufficient to degrade teratogenic doses of exogenous RA.

1.8.2.4.2 Cyp26b1 deletion

Cyp26b1 null mutants have been reported to have severe meromelia-like limb defects with oligodactyly, micronathia and lethality immediately after birth as a result of respiratory distress. Abnormal limbs undergo increased apoptosis and become proximilized and ectopic distal RARE-lacZ expression was observed. The apoptotic defect appeared to be mediated via *Rarg* but not the proximo-distal patterning anomalies (Dranse et al., 2011; Pennimpede et al., 2010b; Probst et al., 2011; Yashiro et al., 2004).

Two *cyp26b1* mutants in the zebrafish, *stocksteif* and *dolphin* exhibit a reduction in midline cartilage of the neurocranium and pharyngeal arches and severe over-ossification of the axial skeleton and craniofacial bones leading to fusion of the vertebrae, which can be phenocopied in mouse embryos by treatment with CYP26 inhibitor R115866 (Laue et al., 2008; Spoorendonk et al., 2008). Neural crest markers appear unaffected in contrast to reports using a *Cyp26b1* morpholino (MO) (Reijntjes et al., 2007) in which cranial nerve patterning and *Dlx2* expression in the neural crest is down-regulated, suggesting either the mutants may be hypomorphic or the MO is producing non-specific effects. Craniofacial defects are also reported in the mouse. *Cyp26b1* null embryos have a 100% penetrant cleftpalate defect, arising from reduced proliferation in the bend region of the palatal shelves (MacLean et al., 2009; Okano et al., 2012). Craniofacial ossification is reported to be reduced, along with severe abnormalities in the craniofacial skeleton where many bones are missing or deformed with abnormal fusions. Similar malformations are observed in the trachea, larynx, auditory system and dental development. Molecular markers reveal hindbrain patterning to be relatively normal but disturbance of caudal neural crest migration and cranial nerve patterning is present (MacLean et al., 2009).

Other experiments suggest that in males, *Cyp26b1* also acts as a meiosis inhibiting factor by protecting the germ cells against RA-signalling until the appropriate time point and is also required for the survival of the germ cells (MacLean et al., 2007; Niederreither and Dolle, 2008; Pennimpede et al., 2010a) and references there-in.

1.8.2.4.3 Deletion of all three Cyp26 genes

In mutant mice lacking all three *Cyp26* genes, *Nodal* expression is ectopically activated in the entire epiblast during gastrulation, via an RARE in the *Nodal* auto-regulatory enhancer. This ectopic activation results body axis duplication in approximately half the embryos and severe patterning defects in the brain in the remaining embryos, similar to those seen in *Cyp26a1/c1* null embryos. About 25% of these *Cyp26a1/c1*$^{-/-}$ embryos also displayed duplication of the primitive streak whereas *Cyp26a1/b1*$^{-/-}$ mutants did not, suggesting *Cyp26a1* extra-embryonic expression is the main *Cyp26* gene in early development, acting non-cell autonomously to keep the epiblast RA-free. However, since *Cyp26a1* mutants have no gastrulation defects, the other two genes must be able to compensate for its loss. Increased dietary RA was able to increase the frequency of severe phenotypes in triple and double homozygous mutants. These defects could be induced by very high levels of added RA in wild-type diets. This suggests mutant phenotypic variation may be due to varying maternal RA levels and again highlights the importance of CYP26s in development, as under normal conditions the embryo should be protected against levels of variation of dietary maternal RA (Uehara et al., 2009). Expression of CYP26 in a cell depletes it completely of RA (Chithalen et al., 2002; Iulianella et al., 1999), so current theories suggest that that the major role of the CYP26s during development is to act in a protective gate-keeping role to limit cellular exposure to RA, rather than to produce a morphogenetic gradient of RA (Niederreither and Dolle, 2008; Pennimpede et al., 2010a; Rhinn and Dolle, 2012).

1.8.3 Gene regulation by RA

Once RA has been generated in the cell by the synthesizing pathway it binds cellular retinoic acid binding protein 2 and is transported into the nucleus and delivered to the retinoic acid receptors (RARs) (Hoover et al., 2008; Rhinn and Dolle, 2012)(Fig 1.13). The three conserved RARs (α, β and γ) are members of the nuclear receptor superfamily and bind RA in partnership with one of their three the retinoid X receptor (RXRα, β and γ) heterodimer binding partners. The activity of RAR-RXR heterodimers is probably mediated via binding of all-trans-RA to the RAR partner (Kastner et al., 1997; Mic et al., 2003). Different heterodimer combinations can transduce the RA signal in many tissues (Dolle, 2009) and usually at least two receptors must be deleted in concert to ascertain any developmental defects. Compound receptor mutations which produce abnormalities of the outflow tract similar to 22q11DS include various compound mutants of *RARα/β*, *RARα/γ* and *RARβ/γ* , compound mutants of RXRα with any of the RARs and *RXRα* mutants alone (Ghyselinck et al., 1998; Lohnes et al., 1994; Lohnes et al., 1993; Mendelsohn et al., 1994; Wendling et al., 2001) and reviewed (Mark et al., 2009).

In the absence of ligand the RAR/RXR heterodimers bind to specific motifs within the promoters of target genes, known as retinoic acid response elements (RAREs), and recruit co-repressor complexes which make the DNA unavailable for transcription. When RA binds to the RAR, a conformational change is initiated in the RAR-ligand binding domain, which results in the co-repressor complexes being released. Transactivating complexes are recruited instead, leading to the induction of chromatin remodelling and the activation of the transcriptional machinery (Fig1.13)(Niederreither and Dolle, 2008; Rhinn and Dolle, 2012).

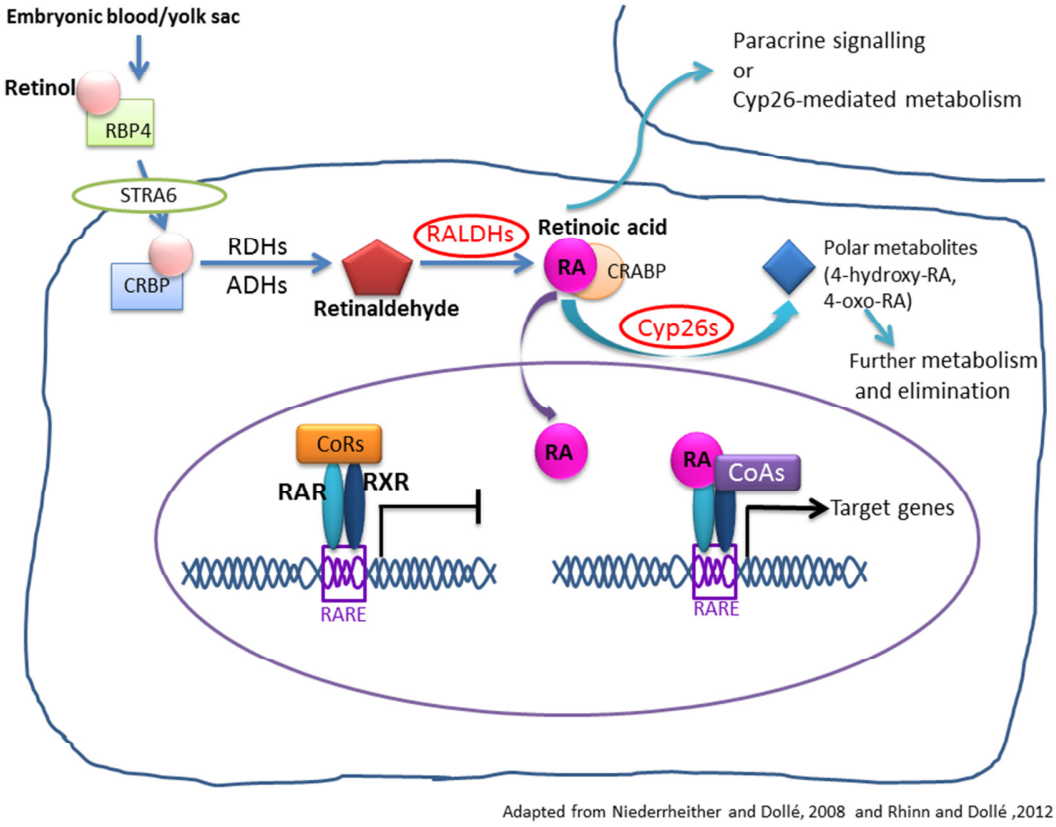

Figure 1.13 The retinoic acid signalling pathway

Circulating retinol bound to retinol binding protein 4 (RBP4) enters the cell via membrane transporter STRA6, where it binds to cellular retinol binding protein (CRBP) and is converted to retinaldehyde by the alcohol/retinol (ADH/RDH) dehydrogenase enzymes. The retinaldehyde dehydrogenase enzymes (RALDHs) oxidize retinaldehyde to retinoic acid (RA). Bound to cellular retinoic acid binding protein 2 (CRABP2) RA is translocated into the nucleus where it binds to the retinoic acid receptor (RAR) partner of the RAR/RXR (retinoid X receptor) heterodimer. The RAR/RXR moiety is bound to the target DNA at the conserved retinoic acid response element (RARE) motif. Upon binding of RA conformational changes release co-repressor complexes (CoRs) and recruit transactivating complexes (CoAs) in their place leading to transcription of target genes. In cells expressing the CYP26 RA-metabolizing enzymes instead of nuclear translocation, RA is hydroxylated to less biologically active polar metabolites which are further processed and eventually eliminated from the cell.

1.9 The Notch pathway

The Notch pathway is one of the classical signalling pathways operating in developmental biology, stem cell biology and cancer biology and is highly evolutionarily conserved. It affects a diverse range of cell types and is, in general, concerned with cell fate decisions, maintenance of progenitor cells, and the regulation of cellular proliferation, apoptosis, differentiation. Well known areas in which Notch signaling plays a major role during development include, neurogenesis, somitogenesis, haematopoiesis, angiogenesis, development of the visceral organs, sensory organ development, limb development and cardiovascular development. The focus of this Introduction will be upon the core Notch pathway, the role of Notch signalling in the cardiovascular system and its down-stream target genes of the *Hes* and *Hey* gene families.

1.9.1 Modes of Notch action

One of the Notch pathways' major operational mechanisms is lateral inhibition, which controls a binary cell fate choice. Using this system, two cells, initially equivalent in terms of levels of Notch receptor/ligand expression, can be directed into two different cell fates. Basically, over time a small stochastic difference in some element of the signaling pathway occurs and is then magnified by a feedback loop, where Notch signaling activates transcription of down-stream targets, such as the bHLH *Enhancer of Split* gene family, which act as transcriptional repressors. Notch receptor and ligand expression levels also alter in response to these changes. Eventually, one cell with up-regulated ligand and down-regulated receptor becomes the signal-sending cell and the other, which up-regulates the receptor and down-regulates the ligand, acquires the signal-receiving cell fate [(Fortini, 2009) and references therein]. This mechanism to generate binary cell fate has been implicated in many tissue types including inner ear hair cell production (Chrysostomou et al., 2012; Lanford et al., 1999), Clara versus clilated cell differentiation in the lung (Morimoto et al., 2010), , intestinal cells secretory cells (Stamataki et al., 2011), and tip-cell formation in mammalian angiogenesis (Hellstrom et al., 2007b; Siekmann and Lawson, 2007), amongst others.

Notch signalling is also used in many types of inductive signaling between initially different cell types, including astrocyte differentiation (Tanigaki et al., 2001), cone cell patterning in the fly retina (Lai and Rubin, 2001), avian somite boundary formation (Sato et al., 2002) and cardiac ecto-mesenchymal transition (EMT) (Timmerman et al., 2004). Many of the features of this inductive signaling are similar to those of the lateral inhibition mechanism, including the pathway being briefly active in both cells initially before altered transcription of the Notch receptors/ligands and Notch target genes which eventually enhance the unilateral direction of signalling between the two cell types.

1.9.2 The core Notch canonical pathway

The core canonical pathway of Notch signalling (Fig.1.14) is very simple. It consists of those elements required to transmit the signal from the cell surface to the nucleus, where a transcriptional read-out is produced, plus a further set of components which are not signal-conducting themselves but are essential to allow signal conveyance. Notch receptors consist of single pass transmembrane proteins, which undergo furin-mediated processing in the Golgi apparatus of the signal-receiving cell and are converted into heterodimers, the two halves of which remain linked by covalent bonds. Receptor molecules consist of an extracellular domain of 29-36 EGF-like repeats, LIN-12-Notch repeats at the plasma membrane and large intracellular domains (NICD). Notch ligands, produced by the signal sending cell, similarly have 6-16 EGF-like repeats in their extracellular domains and canonical ligands are defined by the presence of N-terminal DSL (Delta-Serrate-Lag) motifs which are required for binding in conjunction with the EGF-like regions.

Notch signalling consists of a direct extracellular interaction between Notch transmembrane ligands expressed at the surface of one cell and Notch transmembrane receptors found at the plasma membrane of neighbouring cells. This binding initiates extracellular proteolytic cleavage by ADAMS-proteases leading to the removal of the extra-cellular portion of the Notch receptor by lysosomal degradation. The remaining extra-cellular part of the Notch receptor (Notch extra-cellular truncated domain, NEXT) also undergoes proteolytic cleavage during endocytosis, mediated by ADAM-secretases

and γ-secretase-containing complexes, leading to the release of the Notch intra-cellular domain (NICD). It is thought that the mechanical forces generated during endocytosis of both the receptor and the ligand in the signal-receiving and sending cells respectively, are required to induce the conformational change, which reveals the hidden cleavage sites. Each activated Notch receptor produces one NICD, during which process it is irreversibly cleaved and ultimately destroyed, meaning there is little signal amplification in the core Notch pathway. The NICD contains two nuclear localization signals, seven ankyrin repeats, an RBPJκ binding domain and a proline/serine rich PEST domain which allows it to be quickly targeted for ubiquitination and degradation once released from the transactivation complex.

Once the NICD is translocated to the nucleus it binds to the DNA-binding protein CSL converting it from a repressive function into a transactivator. The CSL family consists of C-promoter binding factor 1 (CBF1) also known as recombination binding signal for binding protein for immunoglobulin kappa J region (RBPJ-κ) or kappa-binding factor 2 (KBF2) in mammals, Suppressor of Hairless (SuH) in *Drosophila* and Longevity-assurance gene-1 (LAG-1) in *C. elegans*. Together with the co-activator, MAML (Mastermind-like), the NICD/RBPJ-κ complex can then activate the transcription of Notch target genes, which include the beta-helix-loop-helix (bHLH) *Enhancer of Split/Hairy* repressor genes in *Drosophila* and their mammalian homologues the *Hes/Hey* gene family (Andersson et al., 2011; Borggrefe and Liefke, 2012; Fortini, 2009; Wang, 2011).

Given the lack of amplification in this system it seems likely that signalling input and output are balanced in the Notch pathway and that initial signal strength is important in creating the necessary cellular and tissue outcome. In accordance with this idea, *Notch* signalling is very dosage sensitive, with both reduction and over-expression of *Notch1* in *Drosophila* causing abnormal development of the eye and sensory structures. Heterozygous mutations of *Dll4* in the mouse also lead embryonic lethality due to arterial vascular anomalies, respectively (Gale et al., 2004; Krebs et al., 2004). In human disease, haploinsufficiency of *NOTCH-1* causes aortic valve disease (Garg et al., 2005) and similar defects are seen in heterozygous RBPJκ mutant mice when fed a high cholesterol diet (Nus et al., 2011). Alagille syndrome (liver, heart, eye and vertebral abnormalities) is

associated with haploinsufficiency of both *NOTCH-2* and *JAG1* in man and mouse (Li et al., 1997a; McCright et al., 2002; McDaniell et al., 2006; Oda et al., 1997; Vrijens et al., 2006). Dominant mutations in *NOTCH3* result in the hereditary vascular disease CADASIL (Cerebral Autosomal Dominant Arteriopathy with Subcortical Infarcts and Leukoencephalopathy) which affects for angiogenesis and vascular smooth muscle within the brain (Fouillade et al., 2012; Louvi and Artavanis-Tsakonas, 2012) Finally, it has recently been shown that haploinsufficiency of *MESP2* and *HES7* give rise to congenital scoliosis in humans and this is also true of deletion of one allele of *Hes7*, *Notch1* and *Dll1*, although not *Mesp2* in the mouse. Incidence of vertebral defects in all four of these genes in the mouse can be increased by mild hypoxia which induces a temporary downregulation of FGF and WNT signaling in the pre-somitic mesoderm (PSM) and also disrupts cyclical Notch signaling, ultimately disrupting somitogenesis (Sparrow et al., 2012), indicating the importance of cross-pathway signalling and gene-environmental factor interaction in Notch-related genetic disease.

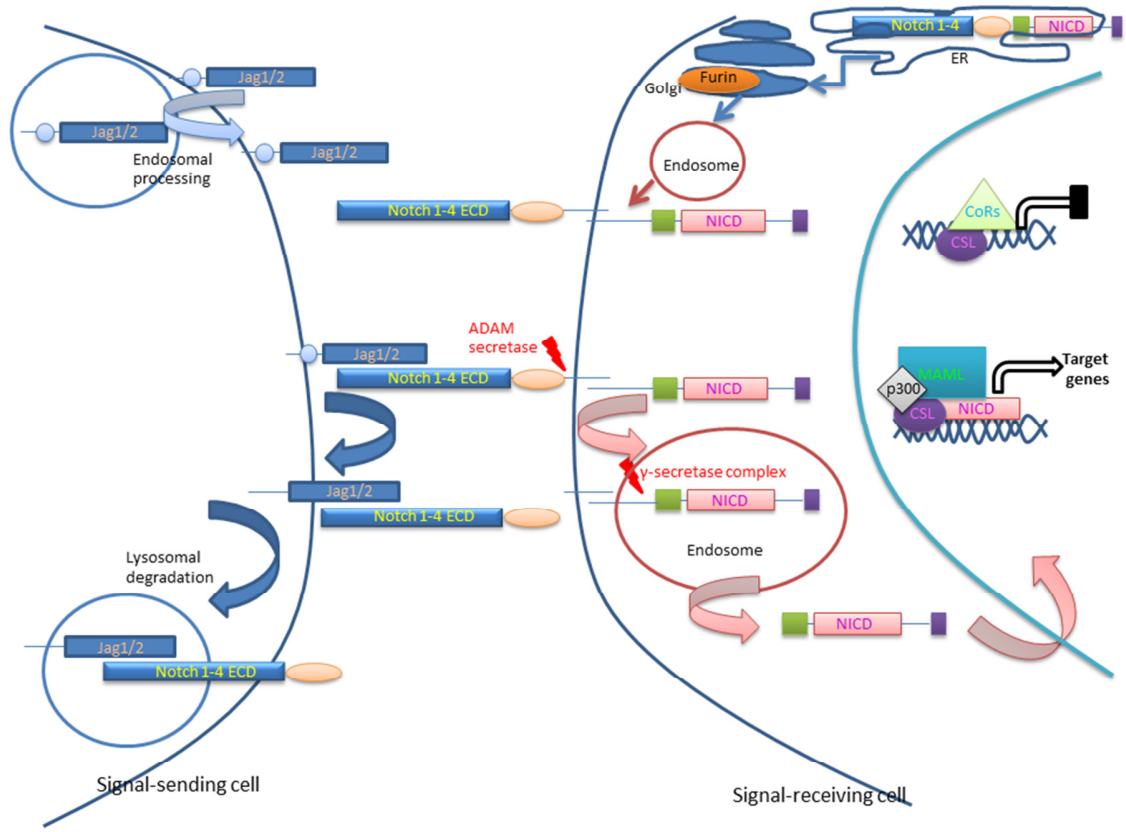

Figure 1.14 Schematic of the core Notch pathway signaling network.

Notch receptor is synthesized in the ER as a single transmembrane receptor which is Furin-processed into a heterodimeric form which is expressed on the surface of the signal receiving cell. In the signal sending cell Notch ligand (here shown as Jag 1 or 2 but also including Dll1, 3 and 4) undergoes endosomal processing and is also expressed on the cell surface. Receptor and ligand binding mediated by the EGF-like domain of both molecules takes place and is followed by two proteolytic cleavages of the receptor and endocytic internalization of both the receptor and ligand. This releases the NICD cleaved product which translocates to the nucleus and forms part of a transactivation complex which drives expression of target genes which are repressed in the absence of the NICD. ER: endoplasmic reticulum, ECD: extracellular domain, NICD: Notch intracellular domain, CSL; CBF1/Su(H)/LAG-1 DNA- binding protein, p300 and MAML: activating co-factors, CoRs: repressive co-factors.

1.9.3 Additional regulation of the core Notch pathway.

Layers of complexity can be added to this straight-forward core signaling system, via several different mechanisms, modulating the signaling pathway to allow very specific

spatiotemporal regulation of Notch signaling. For example, in mammals there are four different Notch receptors (*Notch 1-4*) and five canonical DSL ligands (*Jagged* (*Jag*)*1* and *2* and Delta-like (*Dll*) *-1*, *-3* and *-4*). The differential expression of these various ligands and receptors generates a complex network, although currently there is no strong evidence for particular receptor-ligand combinations producing a specific transcriptional response. A growing number of accessory molecules have been identified, which whilst not strictly necessary for Notch signaling can influence many different stages of the core signaling mechanism and thus generate further signal diversity.

These modulatory functions currently comprise processes such as proteolysis, glycosylation, phosphorylation, ubiquitination and subsequent degradation and recycling of Notch receptor/ligand components. Post-translational modifications of the NICD, endodocytic and endosomal trafficking regulation also play a role. The asymmetric division of other *Notch*-regulatory factors such as *Numb/Numb-like* between daughter cells, epigenetic modifications at target promoters, activity of microRNAs and cis-inhibition by ligands expressed on the same cell as the Notch receptor are also important in modulating the Notch pathway. Non-canonical activation of the Notch pathway and/or target genes and cross-talk with other developmental signalling cascades such as the Wnt/β-catenin, TGFβ, VEGF and hypoxia-response pathways add yet another layer of control [reviewed in (Andersen et al., 2012; Andersson et al., 2011; Blanco and Gerhardt, 2012; Borggrefe and Liefke, 2012; Fortini, 2009; Wang, 2011)].

1.9.4 The Notch pathway in cardiovascular development.

The Notch pathway has been demonstrated to be essential for a number of cardiovascular functions, which can be broadly grouped into roles in the development of the atrioventricular canal and conduction system, normal development of the cardiac neural crest and outflow tract and great vessels, functions in the cardiac cushions necessary for aortic valve development and Notch signaling is also important for cardiac repair.

1.9.4.1 Notch signalling in pharyngeal and outflow tract development

Components of the Notch pathway are expressed in a combinatorial and dynamic fashion within cardiovascular tissues during development, with different combination of ligands and receptors plus the NICD and *Hes/Hey* Notch-pathway effectors being expressed in the same or adjacent tissues. Primary sites of expression which affect cardiovascular development include the endocardium, myocardium, OFT mesenchyme and endocardium, inflow and outflow tract, cardiac neural crest, pharyngeal arch artery endothelium, pharyngeal arch mesenchyme, vascular smooth muscle, the epicardium and sub-epicardial mesenchyme [reviewed in (de la Pompa and Epstein, 2012)].

A number of different mouse models have shown the importance of *Notch* signaling in various tissues which contribute to the normal development of the outflow tract. *Pax3-Cre* or *Wnt1-Cre* driven expression of dominant-negative MAML (DNMAML) in NCC produces a phenotype similar to Tetralogy of Fallot, with pulmonary stenosis, VSDs and great vessel defects consistent with abnormal persistence or regression of PAA 3-6, with those defects relating to the 6th PAA such as an absent ductus arteriosus, being the most common. Neural crest migration and proliferation are normal but differentiation into vascular smooth muscle in PAA and *in vitro* explants is diminished (High et al., 2007).

Similar experiments performed by driving DNMAL or *Jag1*$^{flox/flox}$ expression in the SHF with *Islet1-Cre* or *Mef2c-Cre,* produce outflow tract and aortic arch malformations including CAT and DORV. This inhibition of Notch signaling in the SHF gives rise to abnormal patterning and hypoplasia of the caudal PA/PAA with impaired cardiac neural crest migration into the OFT cushions. Thus Notch signaling via *Jag1* is essential in SHF derivatives for normal OFT and pharyngeal development. Overall, gene expression in mutant hearts and pharyngeal explant cultures explant experiments suggest *Notch* signalling controls EMT in the OFT endothelium by controlling the expression of *Fgf8* and *Bmp4* expression in the adjacent OFT myocardium (High, 2009).

OFT valve development is also affected in these mutants. A combination of reduced NCC contribution, excess of extracellular matrix deposition, and reduced apoptosis within the maturing valve leaflets produces dysfunctional bicuspid aortic valves

with aortic insufficiency. Thus, Notch function in the SHF is required for valve development, possibly by mediated interactions between neural crest and endocardium-derived mesenchymal cells (Jain et al., 2011).

NOTCH1 nonsense and missense mutations are also associated bicuspid aortic valve (BAoV) disease (Garg et al., 2005) which is the commonest cardiac malformation of the adult population at 1.4%. It can be found in isolation or in conjunction with other left-sided abnormalities, VSDs and atrial defects and has been observed in 22q11DS patients. BAoV becomes linked to high morbidity/mortality as aging leads to complications arising from calcification, dilation or dissection of the abnormal valve. Modelling the missense mutations *in vitro* determined that these mutations produced impaired EMT via reduced expression of *Notch* pathway targets *HEY2* and *HEYL* and genes which are inducers of EMT and SNAIL 1 and *2* (Riley et al., 2011). *NOTCH1* mutations may also potentiate the calcification of the aortic valves as *in vivo* and *in vitro* experiments have shown *Notch* and *Hey1* and *2* repressed *Bmp2* and *Runx2*, leading to activation of osteogenic markers and the formation of calcified deposits (Garg et al., 2005; Nigam and Srivastava, 2009; Nus et al., 2011). Mouse models have also shown that *Gata5* and *Nos3* mutants also exhibit BAoV. Notch signalling is affected downstream of *Gata5*, which also directly regulates *Nos3* expression (Laforest et al., 2011; Lee et al., 2000). In the AVC, Notch signalling has also been shown to regulate NOS3 function and NO-receptor expression, which are required for endothelial-mesenchymal transition during valve development (Chang et al., 2011).

Alagille syndrome is an autosomal dominant syndrome with a variably expressive and penetrant phenotype that affects the liver, kidney, skeleton,cardiac and craniofacial development. The severity of the cardiac phenotype can range from mild pulmonary stenosis to Tetralogy of Fallot (ToF). Haploinsufficiency via mutations of *JAG1* and *NOTCH2* is the major underlying cause of AGLS and a subset non-syndromic ToF is also associated with mutations in *JAG1* and *NOTCH1* (Li et al., 1997a; Oda et al., 1997), reviewed and references there-in (MacGrogan et al., 2011; Penton et al., 2012).

In mice, compound heterozygotes of a *Jag1*-null allele and a *Notch2* hypomorphic allele were found to reproduce many of the human phenotypes (McCright et al., 2002). Conditional deletion of *Jag1* or *Notch1* in the endothelial lineage using a *VE-cadherin-Cre* driver led to mutant phenotypes which closely resembled those of AGLS, including VSDs, overiding aorta, coronary artery defects, atrioventricular and semilunar valve abnormalities and right ventricular hypertrophy. These phenotypes are found to be the result of deficient EMT during endocardial cushion formation earlier in development. Adult animals have also been discovered to have calcified valves associated with abnormal ECM modeling which contain ectopic bone and cartilage nodules (Hofmann et al., 2012). Use of a Tie-2 endothelial driver recapitulated the Jag1 null phenotype with embryonic lethal cardiovascular failure and striking vascular smooth muscle defects (High et al., 2008). Smooth muscle-specific deletion of *Jag1* using *SM22a-Cre* yields a post-natal lethal phenotype caused by patent ductus arteriosus (a 6th PAA derivative), attributed to abnormal arterial smooth muscle differentiation (Feng et al., 2010). Deletion of *Jag1* in the cranial neural crest and mesoderm also recapitulates the midline hypoplasia and craniosynostosis features of ALGS, respectively (Humphreys et al., 2012; Yen et al., 2010).

Known down-stream targets of canonical Notch signaling such as *Hes1* and the *Hey* genes are also required for normal development of tissues contributing to the development of the cardiovascular system, including the cardiac neural crest, secondary heart field and vascular smooth muscle of the OFT (Rochais et al., 2009a; van Bueren et al., 2010)

1.9.4.2 Notch and the development of the atrioventricular canal and trabeculation

The atrioventricular canal (AVC) is located between the prospective atrial and ventricular myocardium. Normal AVC development is important for the development of the mitral and tricuspid valves and the conduction system. This requires the maintenance of a primitive 'non-chamber' myocardium in the AVC territory, which is achieved by *Bmp2* activation of *Tbx2/3* expression, which represses the formation of chamber-type myocardium (Christoffels et al., 2004; Ma et al., 2005). Although ectopic NICD

expression can induce *Hey*1 which represses *Bmp2* and *Tbx2*, *Notch*-receptors are not normally expressed in AVC myocardium. AVC myocardial *Bmp2* is required for *Tgfb2*, *Notch1*, *Snail1*, *Snail2*, and *Twist1* expression in valve-forming regions. Endocardial *Notch1* is required for *Tgfb2* expression, which activates *Snail1* and *Snail2*, and represses *Bmp2* in the endocardium via HEY proteins. Myocardial BMP2 and endocardial NOTCH1 signals converge in AVC endocardium to promote complete EMT. This is reflected in NOTCH activation of *Snail1* expression and BMP2-mediated SNAIL1 nuclear stabilization, via GSK3B inhibition, thus leading to maintenance of mesenchymal gene sets (de la Pompa and Epstein, 2012; Luna-Zurita et al., 2010; Rutenberg et al., 2006; Watanabe et al., 2006). AVC specification is also important for the development of the conduction system from non-chamber myocardium. Normal conduction of electrical impulses can only travel between the atria and ventricles via the slow conduction of the AV node, due to the presence of the insulating annulus fibrosus. However, ectopic NICD expression in the myocardium causes mice to develop a ventricular pre-excitation phenotype reminiscent of Wolff-Parkinson-White (WPW) syndrome where additional muscular connections allow ectopic transmission of electrical impulses between the chambers, potentially producing fatal arrhythmias (Aanhaanen et al., 2011; Rentschler et al., 2011).

Notch signalling has been shown to play a role in ventricular trabeculation, as embryos with a full or endocardial-specific deletion of *Notch1/RBPJκ* or ectopic mesodermal NICD expression have abnormal myocardial and endocardial ttrabeculation(Grego-Bessa et al., 2007; Watanabe et al., 2006), as do over-expression *Notch2* mutants, with ectopic myocardial expression (Yang et al., 2012). *Bmp10* and *Nrg1* were implicated as down-stream targets, required for proliferation of trabecular myocardium and cardiomyocyte differentiation respectively (de la Pompa and Epstein, 2012; Grego-Bessa et al., 2007; Watanabe et al., 2006; Yang et al., 2012)

1.9.4.3 Notch in angiogenesis

Both VEGF-A and Notch signalling are required during sprouting angiogenesis, the process by which existing endothelial networks expand. Endothelial cells within the existing vessels adopt specialized phenotypes known as tip and stalk cells to accomplish this process. Notch and VEGF families are involved in directing the identity of tip versus stalk cells. Angiogenesis is triggered by hypoxic conditions which lead to the release of VEGF-A. VEGF-A signalling is both necessary and sufficient to induce tip cells, and also forms a gradient along which acts as a guide to the developing vascular network, in that sprouting tip cells are induced by and migrate towards higher VEGF-A concentrations (Gerhardt et al., 2003; Hellstrom et al., 2007a; Leslie et al., 2007). However, tip cells do not form directly next to each other, instead displaying a characteristic spaced branching and sprouting. Altogether, the many studies upon VEGF-Notch regulation of angiogenic sprouting support a model in which VEGFR signalling quantitatively regulates *Dll4* levels, thus determines the ability of a cell to adopt a tip or stalk cell fate. A cell which receives more Notch signalling during this process will become a stalk cell as it is prevented from becoming a tip cell by lateral inhibition (reviewed in (Blanco and Gerhardt, 2012).

1.9.5 The *Hes/Hey* gene family: transcriptional targets of Notch Signalling

1.9.5.1 Hes/Hey functional characteristics

The *Hes* and *Hey* (also known as *Hesr*, *Hes-related* genes) gene families are primary targets of the Delta-Notch signaling pathway. They are the mammalian homologues of the *Drosophila* genes *hairy* and *Enhancer of split* (*E(spl*), which function as pair-rule genes in the segmental development of the fly embryo.

All HES/HEY proteins contain three functional domains: the basic helix-loop-helix (bHLH) domain for DNA binding consists of the basic domain for DNA interaction adjoining two amphipathic α helices separated by a loop that serves as a dimerization region with other bHLH proteins; the Orange domain which contains two further α-helices and regulates the selection of bHLH heterodimer partners and finally; the C-terminal WRPW region for HES proteins (or functionally related YRPW/YXXW motif for HEY

proteins), which confers transcriptional repressive activity and acts as a polyubiquination signal (Fig 1.15A). HEY proteins also contain a final small conserved C-terminal motif TE(I/V)GAF of unknown function. HES/HEY factors mainly function as transcriptional repressors, and use at least two different mechanisms to enact this function upon their target genes; namely, active and passive repression. During active repression (Fig.1.15B), HES factors form either homodimers or heterodimers with other bHLH repressors, such as the HEY1 and HEY2 proteins. These dimers bind to target DNA at class C (CACG(C/A)G) or N box (CACNAG) sequences in the target promoters. HEY proteins preferentially bind another target DNA sequence, known as an E-box (CANNTG), which is also recognized by HES1 and HES6. Active repression of the target gene is then dependent upon the WRPW domain which interacts with co-repressors of the Groucho-Related/Transducin-Like E(Spl)(TLE) family which in turn recruit histone-deacetylase (HDAC) complexes and other co-repressor molecules such as members of the SIN3 family, eventually leading to chromatin inactivation. The HEY-YPRW motif cannot interact with TLE co-repressors, but instead directly interacts with other co-repressors such as N-COR and MSIN3A which can then indirectly recruit HDAC1. Both HES1 and HEY can also recruit the co-repressing histone deactelyase SIRT1.

Passive repression involves HES factors dimerizing with bHLH activating factors such as MASH1 and E47 (mammalian homologues of the Drosophila proneural achaete-scute complex). These factors also bind E box sequences when unattached to HES proteins, but once bound to them the resulting heterodimers can no longer bind to the E box, leading to passive repression of the bHLH activator protein (Fig.15C [(Fischer and Gessler, 2007; Kageyama et al., 2007) and references therein].

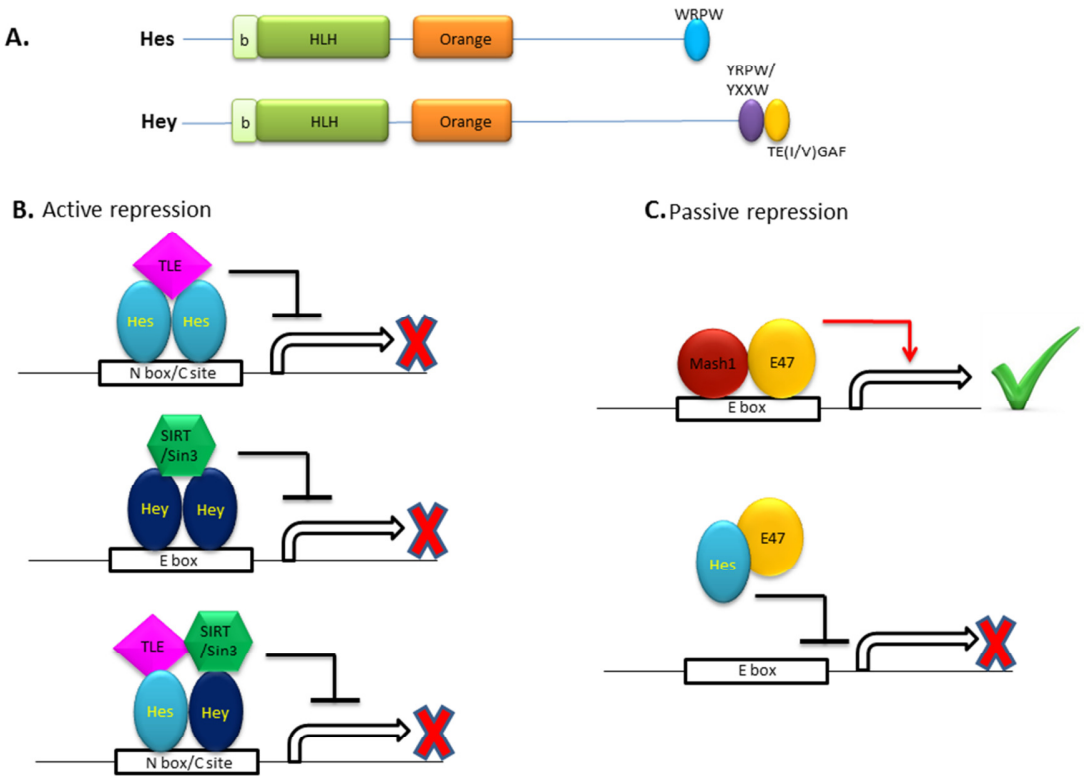

Figure 1.15 Structure and function of HES/HEY factors

(A) The conserved domains of HES and HEY factors. The basic (b) (light green), HLH (dark green), Orange (orange) and WRPW (bright blue) or YRPW (purple) and TE(I/V)GAF (yellow) domains (B) Active repression: HES homodimers (bright blue), HEY homodimers (dark blue) or HES/HEY heterodimers (bright blue/dark blue) factors bind to the N box/class C site or E box motifs within target promoters and actively repress transcription by interacting with co-repressors, such as TLE or SIRT/Sin3 familiy co-repressors. (C) Passive repression: bHLH activators such as MASH1 and E47 form heterodimers that bind to the E box and activate transcription in the absence of HES factors which otherwise form non-DNA binding heterodimers with bHLH activators such as E47 and inhibit transcriptional activation. Adapted from (Fischer and Gessler, 2007; Kageyama et al., 2007).

1.9.5.2 Hes1 is a molecular oscillator

Hes1 is also a molecular oscillator in a number of cell types including fibroblasts, myoblast and neuroblasts. Its expression oscillates with a periodicity of 2 hours and is cell autonomous, depending upon a short-lived period of negative autoregulation. This

oscillation has been linked to a number of possible biological processes. These include a biological clock role during somitogenesis (Pasini et al., 2004), promotion of ES cell multipotency and direction of differentiation depending upon *Hes1* levels within the cell regard (Kobayashi et al., 2009) and a possible role in initiation of lateral inhibition (Kageyama et al., 2008b). Sustained, non-oscillatory *Hes1* expression may also be linked to CNS boundary formation as opposed to the oscillating *Hes1* expression in proliferative neural progenitor compartments within the CNS [(Baek et al., 2006; Hirata et al., 2001; Shimojo et al., 2008), reviewed in (Kageyama et al., 2008a; Kageyama et al., 2010)].

1.9.6 Developmental roles of *Hes/Hey* genes

There are seven members of the mammalian *Hes* family and three *Hey* genes. As a result of genome duplication, in the zebrafish up to nineteen *her* homologues have been reported. All three mammalian *Hey* genes are regulated by canonical Notch signaling, as are *Hes1*, *Hes3*, *Hes5* and *Hes7* (Androutsellis-Theotokis et al., 2006; Bessho et al., 2001; Jarriault et al., 1995; Ohtsuka et al., 1999).

1.9.6.1 Hes1 in development

Hes1 (Sasai et al., 1992) is the most well studied member of the *Hes* gene family and can act as part of Notch dependent and independent pathways in a variety of functions. These include maintenance of progenitor cells in the nervous system, eye, pituitary, thymus and pancreas and intestine by repressing pro-differentation genes (Crosnier et al., 2006; Hatakeyama et al., 2004; Jensen et al., 2000; Lee et al., 2005; Raetzman et al., 2007; Tomita et al., 1999). *Hes1* is also important in the regulation of boundary formation between the mid and hindbrain by a combination of prevention of neuronal differentiation and suppression of proliferation (Baek et al., 2006). The control of binary cell fate decisions in the nervous system, pituitary gland, biliary system, pancreas and gut is also determined by *Hes1* (Bjerknes et al., 2012; Broom et al., 2012; Fukuda et al., 2006; Hatakeyama et al., 2004; Hirata et al., 2001; Ishibashi et al., 1995; Jensen et al.,

2000; Kita et al., 2007; Ohtsuka et al., 2001; Raetzman et al., 2007; Sumazaki et al., 2004; Wendorff et al., 2010; Zheng et al., 2000).

Recently, further roles for *Hes1* have come to light suggesting *Hes1* activity affecting the neural crest lineage is important for a number of processes. Lineage tracing with a *Wnt1-Cre:R26R* allele has shown a strong contribution of neural crest cells to the superior cervical sympathetic ganglion (SCG), the carotid body and the walls of the common carotid arteries and aortic arch. In *Hes1* null mice the SCG is severely hypoplastic. In some cases the common carotid artery and carotid body derived from PA/A3 did not form, and when present was mislocated and hypoplastic (Kameda et al., 2012). *Hes1*$^{-/-}$ embryos also display severe craniofacial defects in tissues requiring a neural crest contribution for their normal development, including a shortened mandible and maxilla, calvarial agenesis, a malformed anterior cranial base and impaired palate and tongue growth (Akimoto et al., 2010). In *Hes1/Hes5* double mutant mice, in addition to a severe CNS phenotype, the peripheral nervous system is also affected, with severe disorganization of the cranial (and spinal) nerve systems: (Hatakeyama et al., 2006).

Splotch mutant mice, which lack functional *Pax3* exhibit various neural crest-based developmental defects, including reduced migration, melanocyte differentiation defects, 22q11DS-like cardiovascular malformations and premature neurogenesis. Up-regulated p21 and reduced proliferation of stem cell populations have also been observed. PAX3 has been shown to directly regulate the *Hes1* promoter and *Hes1* neural crest expression is reduced in *Sp/Sp* embryos. Furthermore, loss of *Pax3* induces miR expression, leading to repression of histone demethylase KDM6B, which is required for the demethylation of H3K27me2/3. This, in turn, up-regulates H3K27me2 methylation of the *Hes1* promoter in *Sp/Sp* embryos leading to decreased expression of *Hes1*. Thus both these non-Notch- mediated interactions at the *Hes1* promoter may be important for normal development.

Other Notch-independent signaling mechanisms shown to regulate *Hes1* include *Shh* acting via binding of GLI2 to the *Hes1* promoter and Ras/ERK mediated FGF-signaling (Ingram et al., 2007; Nakayama et al., 2008; Wall et al., 2005; Wall et al., 2009). Finally, a role for *Hes1* in cardiac development has also been elucidated: *Hes1* mutant mice have been shown to have outflow tract alignment defects and VSDs, associated with

a shortened outflow tract, decrease secondary heart field proliferation and a reduction in the number of migrating cardiac neural crest cells (Rochais et al., 2009a). 22q11DS-like great vessel and thymic defects have also been identified as a consequence of a/hypoplasia of the 3rd-6th PAA earlier in development, where vascular smooth muscle is absent and proliferation in the signalling centre of the pharyngeal ectoderm decreased (van Bueren et al., 2010).

1.9.6.2 Hey genes in development

Hey 2 is expressed in both endocardium and myocardium. Heart defects similar to Tetralogy of Fallot were also observed *Hey2*$^{-/-}$ embryos, with varying degrees of penetrance, depending upon the genetic background (Donovan et al., 2002; Gessler et al., 2002; Kokubo et al., 2004; Sakata et al., 2002; Xiang et al., 2006). *Hey2* is also necessary in the ventricular myocardium for normal smooth muscle recruitment to coronary arteries and for vein identity (Watanabe et al., 2010). Loss-of function of *Hey2* down-stream of Notch signaling in the zebrafish results in blockage of the aorta, similar to coarctation, and is required for the specification arterial versus venous fate (Lawson et al., 2001; Zhong et al., 2000; Zhong et al., 2001). In the mouse, loss of *Hey1* alone has little phenotype, but when combined with loss of *Hey2* results in an early embryonic lethality due to severe defects of vascular remodeling and widespread haemorrhage (Fischer et al., 2004), a phenotype very similar to those observed in *Notch1* and *Jag1* knockout mice (Krebs et al., 2000; Xue et al., 1999). In addition, abnormalities of cardiac cushion formation and septation have been observed in double mutants (Kokubo et al., 2005). Combination of *Hey1* loss-of-function alleles with the same for *HeyL*, leads to a similar phenotype as seen in *Hey2* nulls, including defective EMT whereby the number and invasiveness of mesenchymal cells population the cardiac cushion jelly is reduced, plus dysplastic aortic and pulmonary trunk valves and peri-membranous VSDs (Fischer et al., 2007). The similar phenotypes observed between the different knockouts suggest a level of redundancy/compensation between the *Hey* genes. Given that their common site of expression is the endocardium, this tissue may be key to many of the developmental anomalies observed in the mutant mice.

At the molecular level, it has been determined that the *Hey* genes are required in prospective chamber regions to repress a *Bmp2/Tbx2* pathway in the myocardium, where *Bmp2* has been shown to lie upstream of *Tbx2* in the AVC myocardium. Expression of both genes is necessary for normal AVC development and the repression of chamber-specific genes (Christoffels et al., 2004; Harrelson et al., 2004; Ma et al., 2005), thus delineating the extent of the AVC and the conduction and valve-forming region in the heart. Mis-expression of *Hey1* and *Hey2* in the presumptive AVC of the chick or the mouse repressed *Bmp2* and *Tbx2* expression in this region, leading to loss/reduction of AVC specification. Moreover, deletion of *Hey2* in the embryonic heart led to an expansion of *Bmp2* expression in the ventricular myocardium. In addition, overexpression of *Tbx2* can down-regulate *Hey1* and *2* in the chamber territories, suggesting the presence of a negative feed-back loop between *Hey* genes, *Bmp2* and *Tbx2* to specify chamber versus AVC identity (Kokubo et al., 2007; Luna-Zurita et al., 2010; Rutenberg et al., 2006)[reviewed in (de la Pompa and Epstein, 2012; MacGrogan et al., 2011; Wiese et al., 2010)].

1.10 Aims and overview

Tbx1 plays a crucial role in cardiovascular development, mediated by a wide array of down-stream target genes. Microarray studies identified two further possible interacting pathways, both of which are already known to also be essential for cardiovascular development. These were *Hes1*, the bHLH transcription factor, a down-stream effector of the Notch and the Cyp26 retinoic acid-metabolizing enzymes, which are crucial in controlling the function of the RA pathway.

The aim of the work presented here was to investigate to what extent these pathways may contribute to the phenotype of *Tbx1* mutant mice, and in particular the cardiovascular defects observed. To this end the function of these genes in cardiovascular development was investigated in several animal models, including the chick, mouse and zebrafish, using a variety of experimental approaches. These included chemical, genetic and morpholino knockdown. Furthermore, using genetic and morpholino knock-down and rescue experiments, the question of whether genetic interaction or modifying effects exist between *Tbx1* and these two potential target genes was explored.

CHAPTER 2
Materials and Methods

2.1 Animal models

2.1.1 Ethical statement

All work involving the animal models presented in this thesis was performed under the aegis of the relevant Home Office project and personal licences as required by the Animals (Scientific Procedures) Act 1986. In accordance with this act appropriate anaesthetic/analgesic measures were administered where required at all times.

2.1.2 Mouse strains

All animals were maintained on the inbred background C57Bl6 to potentiate any heart defect phenotypes. All strains obtained from outside this laboratory were either re-derived onto this background or underwent successive rounds of breeding until the C57Bl6 background was at least 96.125%.

2.1.2.1 The Tbx1^{mcm} allele

The *Tbx1*^{mcm} line was kindly provided by our collaborator Dr Antonio Baldini (Xu et al., 2004). The *Tbx*^{mcm} allele is a knock-in of a Tamoxifen inducible Cre construct, IRES-mcm (MerCreMer) and the PGK neo cassette into exon 5 at an insertion site from which full *Tbx1* expression has been previously recapitulated using a lacz knock-in loss-of-function allele (Lindsay et al., 2001). Exon 5 encodes part of the *Tbx1* DNA-binding domain so in the absence of tamoxifen this construct functions as a loss-of-function deletion allele. In the presence of tamoxifen, Cre recombinase is activated and if the line has been crossed to a suitable reporter such as R26R, a read-out of *Tbx1* expression is available (Fig2.1).

2.1.2.2 The Cyp26b1 deleted allele

The *Cyp26b1* knockout line was obtained from the lab of Prof. Hiroshi Hamada via our collaborator Dr. Kenta Yashiro. *Cyp26b1* is a knockout line in exons 3 to 6, which encode the heme-binding, steroid-binding, and oxygen-binding domains of CYP26B1 are removed resulting in a loss-of function allele. Heterozygous mice are viable and fertile. *Cyp26*$^{-/-}$ embryos have previously been reported to suffer from extreme meromelia by midgestation and die immediately after birth due to respiratory distress (Yashiro et al., 2004).

2.1.3 Mouse breeding, maintenance and embryo production

For each breeding colony animals of breeding age were maintained as monogamous pairs, producing six litters per pair before replacement. General husbandry procedures were performed by Institute of Child Health animal facility staff. Animals surplus to requirement were culled using a Schedule 1 method. For timed matings to produce embryos of a specific age, stud males were maintained in their own cages on a standard 12h light cycle and mated with female mice overnight. Females were examined for the appearance of a vaginal plug the following morning. To track embryo age if plugs was observed the animals were designated as being 0.5 days post-coitum (d.p.c) at midday and were maintained separately until the day of required age of embryo was reached.

2.1.4 Basic mouse embryo dissection

At the relevant developmental stage, pregnant maternal animals were sacrificed by a Schedule 1 method. The uterus containing the embryos was roughly dissected out into ice cold PBS. The deciduas containing the embryos were removed from the uterus in fresh PBS and the embryos carefully dissected free of the decidual material using watchmakers forceps. Embryos were transferred to fresh PBS for fine dissection of the extra-embryonic membranes. Either the yolk sac or a small embryonic tissue sample was taken from each embryo and rinsed several times in PBS, then placed in an individual labelled eppendorf.

These samples were stored at -20°C or directly processed for genotyping of embryos. Embryos were then either fixed in 4% paraformaldehyde (4% PF) for histology/in situ hybridization/antibody staining o processed as appropriate for other experimental procedures.

2.1.4 Mouse genotyping

2.1.4.1 Tissue collection for genotyping

Litters of offspring were ear-punched between 10-15 days old to provide identification and DNA for genotyping**.** Tissue samples were either processed directly or stored at -20°C. Jenifer Suntharalingham performed much of the routine genotyping.

2.1.4.2 Tissue digestion and genomic DNA extraction for genotyping of adult mice and E9.5+ embryos

Adult ear punch tissue, tail tips and embryonic tissue or yolk sac samples were digested in 100µg/ml proteinase K (PK) in tail lysis buffer (TLB) (100mM Tris pH8.5, 0.5M EDTA, 10% SDS, 5M NaCl) overnight at 55°C. The volume of PK/TLB used depended upon the amount of tissue to be digested: for adult samples and embryonic samples from E9.5 to E18.5 typically 200-400µl of lysis solution would be added. After digestion an equivalent volume of isopropanol was added and shaken thoroughly until the DNA was seen to precipitate. The spans were then centrifuged for 30 minutes at 1400rpm. The supernatant was decanted and the DNA left to air dry, then resuspended in the same volume of TE solution (10mM Tris-HCl, 1mM EDTA, pH8) or distilled water (dH2O) as used in the original digestion. The resuspended DNA was then used directly in genotyping PCR reactions. A separate protocol for genotyping embryonic samples younger the E9.5 is described below.

2.1.4.3 Tissue digestion and genomic DNA extraction for genotyping of embryos younger than E9.5

Yolk sacs or small tissue sample from embryos younger than E9.5 were digested in 50µl of 100µg/ml PK/TLB overnight at 55ºC. Five microliters of the lysate was removed, diluted 1:10 with dH_2O and heated at 95ºC for 5 minutes before being used in the genotyping PCR. The remaining 45µl of lysate was mixed with an equal volume of isopropanol to precipitate the DNA. Samples were centrifuged at 1400rpm for 30 minutes, washed in 70% ethanol, re-centrifuged for 15 minutes, then washed in 100% ethanol and re-centrifuged again for 15 minutes. The supernantant was decanted and the pellet air-dried and resuspended in 50µl of dH_2O and then used in the genotyping PCR.

2.1.4.4 PCR amplification

Genotyping PCR reactions were normally set-up using a Bioline Taq kit (Invitrogen) mastermix (all reaction reagents save the DNA) or the illustra™ PuReTaq™ Ready-To-Go™ PCR beads (GE Healthcare). The mastermix reagents were usually combined as in Table 2.1 below, and multiplied up to make the volume required. The volume of water added was altered if necessary to account for variations in thethe other reagents. To reduce contamination the mastermix and pipettes previously cleaned in 70% EtOH were UV cross-linked before use. Generally reactions were performed in 25µl volumes with 22µl of mastermix and 3µl of genomic DNA. The mastermix was pipetted out first into PCR tube stripettes and the DNA added afterwards. A blank negative control containing water rather than DNA was always carried out to check for the presence of contaminating DNA and where possible a positive control sample was also run. Sequences for primers used in the genotyping PCRs and the programme used for amplification are given in Table 2.2 below.

Where the PuReTaq Ready-To-Go beads were used, the mastermix consisted solely of the primer sequences in the same volume and concentrations as previously (ie 1µl of 10µM stock of each primer per 25µl reaction) plus the volume of ddH_2O required to make the reaction up to 25µl after the addition of the genomic DNA. After the PCR

reaction was complete 5µl of loading buffer was added and 5-25µl of each reaction sample run on a 1.5% agarose gel. The gel was then UV-imaged and photographed as described previously. The results were attributed to the correct animal and those of unwanted genotypes were then culled by a Schedule 1 method and the others used for further breeding and embryo production.

Table 2.1 Standard PCR reaction set-up

Reagent and stock concentration	1x reaction (µl)
Ammonia (NH_4) buffer (10x)	2.5
$MgCl_2$ (50mM)	0.75
dNTPs (10mM each)	0.5
Forward primer(s) (10µM)	1.0
Reverse primer(s) (10µM)	1.0
Taq enzyme	0.15
Genomic DNA	3.0 (variable)
ddH_2O to 25µl	15.35 (variable)

Table 2.2 Mouse genotyping primers and conditions

PCR type	Strain used to genotype	Genotyping PCR Primer sequences	PCR conditions	PCR product size
Cyp26b1	*Cyp26b1*	Cyp26b1-puro 5'-AGCAGCCTCTGTTCCACATAC-3' Cyp26b1-3 5'-AAGTGCTTCAATCTGCAAGCC-3' Cyp26b1-55 5'-CTACAGCATTAGAATCCCAGC-3'	95°C 2min x1 95°C 30s 62°C 30s x30 72°C 30s 72°C 8min x1	WT: 660bp *Cyp26b1* 320bp
Tbx1^{mcm}	*Tbx1^{mcm}*	2 Primer Tbx1^{mcm} PCR Tbx1^{mcm} Forward: 5'-GCTCCACTTCAGCACATTCC-3' Tbx1^{mcm} Reverse: 5'-CATAAGCCAGAGAAGGGTCG-3'	94°C 3min x1 94°C 30s 60°C 30s x30 72°C 30s 72°C 5min x1	WT: no band *Tbx1^{mcm}*: ~400bp
Standard Cre	*Tbx1^{mcm}*	Standard 2 primer Cre PCR Cre Forward: 5'-TGGAAAATGCTTCTGTCCGTT TGC-3' Cre Reverse: 5'-AACGAACCTGGTCGAAATCAGTG-3'	94°C 3min x1 94°C 30s 60°C 30s x30 72°C 30s 72°C 7min x1	WT no band *Cre*: 300-350bp

2.1.5 Zebrafish lines

One mutant, one wild-type and four transgenic zebrafish lines were used for the work reported in this thesis (Table 2.3). Lines were maintained at the fish facility in the Department of Anatomy, UCL according to normal aquarium practices comprised the *tbx1* null mutation *vgo*^{tm208}, the transgenic lines *Tg(fli-1:gfp)* and *Tg (sox10:gfp)* and wild-type fish. Adult fish were maintained and bred on the Tübingen genetic background under standard husbandry conditions (Brand et al., 1995). *Tg(hsp70:gal4)* and *Tg(UAS:myc-notch1a-intra)* [*Tg(UAS:nicd)*] crosses were kindly provided by Prof. Julian Lewis and the CRUK fish facility at the London Research Institute .

Table 2.3 Zebrafish mutant and transgenic lines

Gene	Strain/allele	Construct type	Reference
tbx1	*van gogh: vgo*^{tm208}	Null point mutation in the DNA-binding T-box domain	(Kochilas et al., 2003) (Piotrowski et al., 2003)
fli-1	*Tg(fli1a:gfp)*	Transgenic driving gfp expression in the *fli-1* expression domain; neural crest and endothelial cells	(Roman et al., 2002)
sox10	*Tg (sox10:gfp)*	Transgenic driving gfp expression in the *sox-10* expression domain; neural crest cells	(Dutton et al., 2008)
gal4	*Tg(hsp70:gal4)*	Transgenic with heat-shock inducible expression of the *gal4* activation domain.	(Scheer et al., 2002; Scheer and Campos-Ortega, 1999)
Notch-1a	*Tg(UAS:myc-notch1a-intra)*	Transgenic with upstream activating sequence (UAS) driving expression of *notch1a* intracellular domain when bound by gal4.	(Scheer et al., 2001; Scheer et al., 2002)

2.1.6 Zebrafish breeding, maintenance and embryo production

Mixed adult male and female wild type fish were maintained in large tanks on a standard light cycle and fed at least twice daily. Collection trays were placed in the tanks the night before a lay was required. One to four cell embryos were collected half hourly and rinsed in aquarium water before undergoing experimental procedures and/or further incubation. Embryos were normally incubated in 100mm petri-dishes of aquarium water plus a small amount of methylene blue at 28.5ºC until the required developmental stage was reached, with maximum stage collected being 3 to 4 days post fertilization (dpf). In some cases incubation took place at 18°C or 32°C to delay or speed up development for logistical reasons.

2.1.7 Basic zebrafish embryo dissection

The protective chorionic membrane was dissected away from embryos at early stages prior to hatching from the chorion using watchmakers forceps. Anaesthetic Tricaine (3-amino benzoic acidethyester) solution (Sigma) (4mg/ml solution, pH7.0 with 1M Tris-HCl pH9.0) was added 1:25 to aquarium water and the embryos left for 15 minutes before fixation in 4% paraformaldehyde or other experimental procedures were performed.

2.1.8 Zebrafish genotyping

2.1.8.1 Fin clipping for genotyping

Individual fish were placed in small breeding tank filled with a 16% working Tricaine solution until they were unable to maintain equilibrium in the water, indicating that anaesthesia had been successful. They were quickly removed from the tank with a plastic spoon and placed upon a piece of Parafilm on a petri-dish lid. A small portion (2-5mm) of the caudal tail fin was amputated using a clean scalpel or razor blade. The fish were then immediately returned to individual small breeding tanks filled with aquarium

water. Fish were maintained in individual tanks while the genotyping PCR was carried out. Fish of the required genotypes were then maintained in communal tanks. Unwanted fish were culled by terminal anaesthesia.

2.1.8.2 Tissue digestion and DNA extraction for adult fish

Fin samples were digested in 50µl volumes of 200µg/ml Proteinase K (Sigma) in fish lysis buffer (10mM Tris-Cl pH 8.2, 10mM EDTA, 200mM NaCl, 0.5% SDS) overnight at 55°C. The enzyme was inactivated at 95°C for 10 minutes and the genomic DNA precipitated by adding an equal volume of cold isopropanol which was mixed by inverting the tubes. The DNA was centrifuged down at 13,000rpm for 30 minutes then the isopropanol was removed and the DNA air-dried. The DNA was resuspended in 200µl of TE diluted 1:10 with dH_2O and then cleaned by phenol-chloroform precipitation. One hundred microliters each of Tris-buffered phenol (Invitrogen) pH8.0 and chloroform: iso-amyl alcohol (49:1 $CHCl_3$:IAA) were added and vortexed. The resulting suspension was then centrifuged for 5 minutes at 13,000rpm at 4°C. The upper layer (aquatic phase) was placed in a new tube and the DNA precipitated by the addition and mixing of $1/10^{th}$ the volume of 3M NaOAc (pH5.2) plus 2.5 volumes of cold 100% ETOH followed by incubation at -20°C for 30 minutes to overnight. The DNA was pelleted by centrifugation at maximum speed for 20 minutes (4°C). The supernatant was discarded and the pellet air-dried until all the ethanol had evaporated, after which it was resuspended in 20µl warm dH_2O.

2.1.8.3 Hotshot DNA extraction from zebrafish embryos

Either whole embryos post-experimental use or tails dissected prior to experimentation were washed with PBS and placed in individual eppendorf tubes. Fifty microliters of 50mM NaOH was added to each sample and all samples were heated at 95° C for 10 minutes until the embryos became noticeably friable. Samples were then cooled at 4°C and 5ul (1/10 volume) of 1M Tris-HCl pH 8 added to each one before being

centrifuged at 7500rpm for 10minutes. The supernatant was then used for genotyping PCR.

2.1.8.4 PCR amplification for vgo^{tm208} genotyping

PCR reactions for the *vgo^{tm208}* allele were performed using either PuReTaq Ready-To-Go PCR beads or the Bioline Taq mastermix(see 2.1.4.4.). The only change in the mastermix was an increased in the amount of Taq enzyme added from 0.15µl per reaction to 0.3µl/reaction. Again 3µl of genomic DNA and 22µl of mastermix was used per reaction. Primer sequences and conditions are in Table 2.3 below(Piotrowski et al., 2003). Five microliters of the reaction was run out on a 1% agarose gel to check that a 373bp band had been amplified. The remaining reaction volume was reserved for the RE digestion required to give the final genotype.

2.1.8.5 Restriction fragment digestion for vgo^{tm208}genotyping

The *vgo^{tm208}* null mutant allele consists of an A to T transition. This base change mutation leads to the loss of an *AlwN1* restriction site, allowing genotyping by *AlwN1* restriction enzyme digestion of the PCR product. The PCR product was digested (5-20µl) in a 50µl volume reaction, comprising the PCR DNA, 5µl NEB buffer 4(10x), 2.5µl *AlwN1*enzyme (NEB) with the final volume made up to 50µl with dH_2O. Digestion took place overnight at 37°C and the digest was run on a 1.5% agarose gel. Wild type fin or embryo DNA produced a 200bp band, in null *vgo$^{tm208/tm208}$* mutant embryos a band of 373bp was present and in *vgo$^{tm208/+}$* heterozygote fin or embryo DNA gave a band of both sizes (Piotrowski et al., 2003).

2.1.8.6 PCR amplification for genotyping other zebrafish transgenic lines

HotShot DNA extraction was performed on embryonic offspring of the *Tg(hsp70:gal4)* x *Tg(UAS:myc-notch1a-intra)* cross. PCR was performed for gal4 and

notch1a-intra using previously published primers and PCR conditions (Scheer et al., 2002) as given in Table 2.4 below.

Table 2.4 Zebrafish genotyping PCR primers and conditions

PCR type	Strain used to genotype	Genotyping PCR Primer sequences	PCR conditions	PCR product size
vgo^{tm208}	*vgo*^{tm208}	Forward primer 5′-GCTCTGGAGTGAACTTGATTACC TG-3′ Reverse primer 5′-AACGGTCAAGTAGGCCTGTAGCA C-3′.	94°C 3min x1 94°C 30s 59°C 30s } x30 72°C 30s 72°C 7min x1	373bp
gal4	*Tg(hsp70:gal4)*	Hsp70: 5′-CGGGCATTTACTTTATGTTGC-3′ gal4: 5′-CATCATTAGCGTCGGTGAG-3′	94°C 5min x1 94°C 30s 56°C 30s } x34 72°C 30s 72°C 7min x1	950bp
notch1a-intra	*Tg(UAS:myc-notch1a-intra)*	UAS:5′-CATCGCGTCTCAGCCTCAC-3′ *notch1a:intra:* 5′-CGGAATCGTTTATTGGTGTCG-3′	94°C 5min x1 94°C 30s 58°C 30s } x34 72°C 30s 72°C 7min x1	450bp

2.1.9 Chicken embryo production

Fertilized hens eggs (White Leghorn) were obtained from Henry Stewart & Co. Ltd. UK on a weekly basis. Eggs were stored in cool conditions until required. Incubation took place in a humidified incubator at 38°C for the necessary length of time for the required stage of development. All developmental stages in this thesis are quoted according to the Hamburger and Hamilton (HH) staging system (Hamburger and Hamilton, 1951).

2.1.9.1 Basic chick embryo dissection

If not incubated vertically, embryos were left in this position to rotate. The top of the egg shell was then broken with large forceps and dissected away and the albumen surrounding the yolk tipped gently away and discarded, until just the yolk plus embryo was left in the base of the shell. Excess shell above the yolk surface was peeled away with forceps. Using small dissection scissors a square around in the embryo was cut in the vitelline membrane. This membrane plus attached embryo was then picked up with watchmakers forceps or a small spatula and transferred to a petridish of ice-cold PBS and the vitelline membrane and other extra-embryonic membranes and any remaining yolk removed before either fixation in 4% paraformaldehyde or other experimental processing.

2.2 Experimental embryo manipulation

2.2.1 Chick embryo R115866 treatment

Fertilized hens' eggs (White Leghorn, Henry Stewart & Co. Ltd. UK) were incubated in a humidified incubator at 38°C until stages 10 or 14 (E2 and E3) were reached. R115866, a chemical inhibitor of Cyp26 enzyme function was kindly donated by Janssen Pharmeceutica. Roughly 2.5-5ml of albumen was removed via needle and syringe before window was cut in the shell each egg and either 2µl of 5mg/ml R115866 in ethanol (high dose) or a lower dose (0.5µl of 5mg/ml R115866/EtOH or less) added *in ovo*. In control embryos an equivalent volume of ethanol alone was added. Fifty microliters of 100x antibiotic/antimycotic solution (Sigma) was added and the eggs were resealed with cellotape. High dose embryos were then cultured a further 24 or 48h and low dose embryos were cultured to E8-10, after which they were dissected as in 2.1.9.1 for further experimental processing.

2.2.2 Ink injection

This technique allows the visualization of formation and patency of the pharyngeal arch arteries and, after remodelling, the great vessels. Indian ink was diluted 50:50 with sterile PBS and loaded into a pulled glass microneedle, which was attached to a mouth injector. To visualize the PAA, E9.5-10.5 mouse embryos and stage 14+ chick dissected embryos were pinned out on their sides in PBS in Sylgaard dishes. Ink was injected into the paa via the outflow tract. At later embryonic stages (E15.5+ in the mouse and E8 in the chick), after paa remodelling, embryos were pinned out with the ventral surface uppermost. The ribcage was removed and the body cavity flooded with PBS. Where not enough blood remained in the great vessels to visualize their layout clearly, ink was again injected via the aorta to fill the great vessels. Embryos could be ink injected immediately after dissection, prior to fixation, but more usually they were first fixed in 4% PFA/PBT beforehand and rinsed in PBS before the ink injection took place.

2.2.3 Zebrafish injection experiments

Microinjection needles were calibrated using a graticule (Graticules Ltd, 1.0x 0.01mm) and 1-4nl of morpholino or mRNA was injected per embryo, depending upon concentration.

2.2.3.1 Morpholino knock-down

Morpholinos (MOs) were ordered from GeneTools, USA and made up to 1mM stock concentrations using ddH_2O. Sequences ordered are given in Table 2.4. Morpholino injections were performed on 1-4 cell embryos collected half-hourly. All morpholinos used had been previously validated and published (see Table 2.5). Further dilutions as appropriate for injection also used ddH_2O. Initial injections to determine the morphant phenotype were made in the 750-500µM range and the concentration titrated down until a consistent pharyngeal arch phenotype was present at 3dpf without excessive death.

Table 2.5 Morpholino sequences

Gene	MO sequence	Reference
tbx1 (translation blocking)	5'-GATGTCTCCAATAGATAATGTGTC G-3'	(Stalmans et al., 2003)
tbx1 mismatch	5'-GATCTCTGCAATACATAATCTCTC-3'	GeneTools, USA http://www.genetools.com/
her6 (translation blocking)	5'-TATCGGCAGGCATCTTCTCTGGGAA-3'	(Pasini et al., 2004)
her6 mismatch	5'- TATCCGCAGCCATGTTCTGTCGGAA-3'	GeneTools, USA http://www.genetools.com/
Human β-*globin* (standard control)	5'-CCTCTTACCTCAGTTACAATTTATA-3'	GeneTools, USA http://www.genetools.com/
p53	5'-GCGCCATTGCTTTGCAAGAATTG-3'	GeneTools, USA http://www.genetools.com/ (Robu et al., 2007b)

2.2.3.2 mRNA rescue and over-expression: injection of capped MRNA transcripts

Capped mRNA is similar to most eukaryotic mRNA in that it has 7-methyl guanosine cap structure at the 5' end, which protects against premature degradation. To copy this feature in the mRNA injected in the 1-cell embryo we used the mMESSAGE mMACHINE High Yield Capped RNA transcription kit from Ambion Template DNA plasmids were linearized at the 3' end to allow transcription of sense mRNA from the 5' RNA polymerase (see table 2.6), with the RE enzyme reaction being set up with 10µg DNA in 50-100µl. The digested DNA was ethanol precipitated with 0.1volume NaOAc and 2.5 volumes ethanol.

The capped transcription reaction was assembled according to the mMESSAGE mMACHINE kit protocol. Each reaction contained 1µg linearized template DNA, 1x NTP/CAP (from stock 2x NTP/CAP: ATP, CTP, UTP 10mM, 2mM GTP, 8mM cap analogue in SP6 kits or 15mM ATP, CTP, UTP, 3mM GTP, 12mM cap analogue in T3 and T7 kits), 1x reaction buffer (from 10x stock) and 2µl enzyme mix. The reagents were mixed thoroughly, then briefly spun down and incubated for 2h at 37°C. The mRNA was then precipitated by the addition of 30µl each Nuclease-free water and LiCl Precipitation Solution. After mixing well the precipitation took place at -20°C for at least 30 minutes, more usually overnight. The mRNA was pelleted by centrifugation at 14,000rpm for 15

minutes, then the supernatant removed and the pellet washed with 1ml of 70% ethanol, followed by re-centrifigation. The ethanol was removed and the pellet air-dried and then resuspended in nuclease-free water and quantitated using the Nanodrop.

Table 2.6 mRNA template constructs

Gene	Plasmid	Linearizing RE	Polymerase	Source
XTbx1	β-UT	EcoR1	T3	(Ataliotis et al., 2005)
her6	pCS2	Not1	SP6	(Pasini et al., 2004)

2.2.3.3 Zebrafish embryo heat-shock protocol

Tg(hsp70:gal4) x *Tg(UAS:nicd)* were mated overnight and the resulting embryos injected with 750µM *tbx1* at the 1-4 cell stage the following morning, as above. To avoid gastrulation defects embryos were cultured 5-6hpf until they reached 50-60% epiboly. Heat-shock activation of *UAS:nicd* was then carried out at 38ºC for 30 min, after which embryos were incubated as normal at 28.5°C until 72hpf.

2.3 Molecular Biology techniques

2.3.1 Real Time Quantitative PCR (RTQ-PCR)

During RTQ-PCR the progress of the PCR is monitored as it occurs and he data collected throughout the reaction process rather than at the end of the PCR. Reactions are characterized by the time-point at which the amplified target is first detected i.e a fixed level of fluorescence (Ct value) rather than the amount of target accumulated after a fixed number of cycles. RTQ-PCR was used to quantitate RNA levels according to the 2-step method.

2.3.1.1 RNA extraction

Zebrafish embyos were dissected out of the chorion and the yolk sac removed. Tissues from embryos undergoing the same experimental treatment were pooled, snap frozen in liquid nitrogen and stored at -80°C. RNA was extracted from the tissue samples using the Qiagen RNeasy Micro Kit. After thawing the tissue was disrupted and homogenized in 350µl Buffer RLT (proprietary composition containing high levels of guanidine isothiocycanate) supplemented with a final concentration of 0.04M dithiothreitol. One volume of 70% ethanol was added to the lysate and mixed by pipetting. The sample plus any precipitate was immediately transferred onto an RNeasy MinElute spin column in a 2ml collection tube. Spin columns centrifuged for 15 seconds at ≥ 8000 x *g*. The flow-through was discarded and columns washed by adding 350µl Buffer RW1 (stringent washing buffer of proprietary composition which contains guanidine salt and ethanol) and centrifuged as before. The DNase I stock solution was made by adding 550µl ddH2O to the lyophilized DNase I supplied. This was then diluted in Buffer RDD (proprietary composition; provides efficient on column DNA digestion) with 10µl DNase I solution added to 70µl Buffer RDD, mixed by inversion and the final 80µl added directly to the spin column membrane. The digestion was allowed to proceed for 15 minutes at RT, after which 350 µl of wash buffer RW1 was added to the column which was centrifuges for 15 seconds at ≥ 8000 x *g*. Four volumes of ethanol was added to Buffer RPE (proprietary composition). Five hundred microliters of the resulting solution was added to each column and centrifuged as before to remove salt traces. The flow-through was discarded and a further wash of 500µl of 80% ethanol added to the spin column. This was centrifuged for 2 minutes at ≥8000 x g. Columns were re-centrifuged open for 5 minutes at 13000 rpm to dry the column membrane. Fourteen microlitres of RNase-free water was added to the centre of each column membrane to elute the RNA, which was collected by centrifugation at 13000rpm for 1 minute.

2.3.1.2 cDNA reverse transcription

First strand cDNA was made using the SuperScript II Reverse Transcriptase kit (Invitrogen).The SuperScript II Reverse Transcriptase is engineered version of MMLV (Moloney Murine Leukaemia Virus) reverse transcriptase with reduced RNase H activity and increased thermal stability. Each reaction consisted of 1µl random primers (100ng) (500µg/ml), 1µg total RNA, 1µl dNTP mix (10mM each) made up to 12µl with ddH_2O. After mixing the reaction was heated to 65°C for 5 minutes and then quickly chilled on ice. After a brief centrifugation to collect the contents of the tube the following was added to each reaction: 4µl of 5x First Strand Buffer, 2µl 0.1M DTT. After gentle mixing the reactions were incubated for 2 minutes at RT before 1µl (200 units) of SuperScript II Reverse Transcriptase was added and mixed by gentle pipetting. The reactions were then incubated at RT for 10 minutes before the reaction was stopped by heat inactivation at 70°C for 15 minutes.

2.3.1.3 Real Time PCR reactions

The PCR reactions were run in MicroAmp^{TM} 96-well ABI Optical Reaction Plates (Applied BioSystems). Each plate contained triplicates for each experimental sample amplified with target gene primers (*her6*) and with house-keeping control primers (*gapdh*) for normalization. All primers used had been previously published (primer sequences and references are given in Table 2.7). On the same plate duplicates for each set of primer pairs were run for serial dilutions (1- $1x10^{-4}$) of pooled cDNA (1µl from all samples) to produce a standard curve to assess the relative efficiencies of the different PCR reactions. It was assumed for the purposes of calculating reaction amounts that 1µg of RNA entered into the reverse transcription reaction resulted in 1µg of cDNA being made per 20µl reaction. The cDNA was diluted to 3.2ng/µl so that 5µl per RTQ-PCR would give 16ng cDNA per reaction. Each 25 µl RT-PCR reaction contained 12.5µl Quantitect SYBR Green master mix (Qiagen), 0.4µl each of 25µM forward and reverse RTQ-PCR primers, 5µl of 3.2ng/µl cDNA as above and 6.7µl of ddH_2O. The SYBR Green dye binds to double-stranded DNA products, allowing detection of the PCR products as they

accumulate during the PCR cycles. A master mix of all the reagents except the cDNA was made, in a volume depending upon the number of samples to be run. Twenty microliters of master mix was added per reaction plus 5µl of cDNA. The pipette tip was changed between every pipetting action to minimize variation resulting from pipetting error.

Table 2.7 RT-PCR primers

Gene	Primer sequences	Reference
her6	F: 5'-CGTTAATCTTGGATGCTCTG-3' R: 5'-CTTCACATGTGGACAGGAAC-3'	(Bertrand et al., 2010)
gapdh	F: 5'-GTGTAGGCGTGGACTGTGGT-'3 R: 5'-TGGGAGTCAACCAGGACAAATA-'3	(Pei et al., 2008)

The RT-PCR reactions were run on an ABI Fast Real Time PCR system 7900HT machine (Applied BioSystems) using standard run conditions. These comprised 15 minutes at 95°C, 40 cycles of 15s at 94°C, 30s at 60°C, 30s 72°C, at which point fluorescent measurements were taken. A dissociation stage was added and these curves used to analyse product specificity, as they highlight the melting temperatures of the products and the presence of primer dimers. Expression values were determined from the data collected by the SDS2.2.1 software in Microsoft ExCel according to the procedure detailed in "Chapter3 : Relative Standard Curve method for Quantification" from the Applied BioSystems "Real Time PCR Systems Chemistry Guide". Briefly standard curves were constructed from the pooled cDNA dilutions for the *her6* and *gapdh* amplifications and used to determine the relative efficiencies of the two PCR reactions. Since the efficiencies were not always <0.1 the relative standard curve method of quantitation was generally used. The equations generated for the slope and intercept of the standard curves were used with the Ct values of experimental samples to generate the average input amount for both sets of primers. The amount of *her6* was then normalized against the *gapdh* values. One sample was designated as the calibrator to determine fold-changes between the samples. Standard deviation and the co-efficient of variation were calculated for all samples and a t-test performed using the GraphPad QuickCalcs

(http://www.graphpad.com/quickcalcs/ttest1.cfm) software to assess the statistical significance of any difference in sample mean values.

2.3.2 DNA preparation

2.3.2.1 LB plates

LB-Agar gel was made with 1% Bacto-tryptone, 0.5% NaCl, 0.5% yeast extract and 1.5% agar/ dH_2O and autoclaved. After cooling to 50º, 100µg/ml of the relevant selection antibiotic (for which the transformed plasmid should confer resistance if present in the bacterial cell) was addedand the gel was poured into 100mm petri-dishes under a biohazard air-flow safety hood and allowed to set. If the plasmid allowed lacz colour selection 50µl of 50mg/ml X-gal solution and 100µl of 0.1M IPTG (isopropyl β-D-1-thiogalactopyranoside) could be spread over the surface of the set plate and allowed to dry before plating the bacterial transformation.

2.3.2.2 Bacterial heat- shock transformations.

One hundred microlitre aliquots of competent bacterial cells (DH5α, Invitrogen) in eppendorf tubes were thawed on ice and 1-5ng of the plasmid DNA to be transformed added to the thawed cells. The bacteria plus DNA tubes were left on ice for 30 minutes and then heat-shocked by placing them directly into a 42º water bath for 45 seconds before returning them immediately onto ice for 5 minutes. One millitre of LB (Luria Bertani) broth (1% Bacto-tryptone, 0.5% NaCl, 0.5% yeast extract/ dH_2O) without antibiotic was added to each tube and the tubes incubated in a heated shaker at 37ºC, 250-300 rpm for 1hour. The bacterial cells were then plated out under a biohazard airflow safety hood 50-300µl on LB-agar plates. After drying, the plates were incubated at 37ºC overnight.

Alternatively, if JM101 bacterial cells were used, 1µl of DNA was added to a 20µl aliquot, on ice for 30 seconds. The transformation was heat-shocked at 42ºC for 45 seconds and replaced on ice for 2 minutes. Eighty microliters of SOC (0.5% yeast extract, 2% Tryptone, 10mM NaCl, 2.5mMKCl, 10mM $MgSO_4$, 20mM glucose (added after

autoclaving) or LB media without antibiotic was added and the whole cultured at 37ºC for 1h without shaking. The whole 100µl transformation was plated onto LB-agar antibiotic plates and grown overnight at 37ºC as previously.

2.3.2.3 Bacterial culture and glycerol stocks

Individual colonies from bacterial transformations were picked from agar plates and added to 10mls of LB broth plus antibiotic in 20ml or larger Sterilin vials. The vials were incubated shaking (250-300 rpm) overnight at 37ºC. After extraction DNA and restriction enzyme digest to confirm the presence of a single transformed specific plasmid glycerols stocks were made for long term storage. Using cryotubes (Nunc), 0.5mls of the overnight culture was thoroughly mixed with sterile glycerol and then stored at -70ºC.

To re-culture the plasmid containing bacteria from glycerols, they were thawed, and a sample taken with a bacterial loop, and drawn out sequentially over the surface of an LB agar plus antibiotic plate. After drying the plate was cultured overnight. Single colonies were then picked from the plate and cultured as described above.

2.3.2.4 DNA extraction and purification protocols

Plasmid DNA was extracted from bacterial cultures of various volumes, and thus varying amounts, depending upon the required application. The Quiagen Plasmid Mini, Midi or Maxi kit and protocols (Quiagen Plasmid Purification Handbook) were used depending on the amount of DNA required. These kits use an anion-exchange resin to which plasmid DNA is bound, washed and eluted in a purified form.

2.3.2.5 DNA extraction: Qiaprep Spin Miniprep Protocol

. This protocol is designed for the purification of up to 20µg of DNA. Ten ml overnight cultures from individual colonies were grown as previously. 1-3mls of the culture was pelleted by centrifugation at 13,000rpm and resuspended homogeneously in 250µl of buffer P1 (50mM Tris-HCl pH8, 10mM EDTA, 100µg/ml RNAse A). An equal

volume of lysis buffer P2 (200mM NaOH, 1% SDS [v/v]) was added to the bacterial cell suspension and mixed gently by inversion until the solution was viscous and slightly clear. This lysis reaction was not allowed to continue for more than 5 minutes. Three hundred and fifty microliters of buffer N3 (proprietary composition) was added and the mixed by inversion immediately, resulting in a cloudy solution from precipitation of bacterial proteins. This solution was centrifuges at 13,000rpm for 10 minutes. The post-centrifugation supernatant was applied to the Qiaprep column in a 2-ml collection tube and then centrifuged again at 13,000rpm for 30-60 seconds. The flow-through was discarded and the columns washed with 0.5ml buffer PB (Proprietary composition containing high concentrations of guanidine hydrochloride and isopropanol) and centrifuged as before for 30-60 seconds. Flow-through was discarded and the columns were then washed again with 0.75mls buffer PE (proprietary composition) and again centrifugesd at 13,000 rpm for 30-60 seconds. After throwing away the flow-through the columns were re-centrifuged for another 60 seconds to remove any residual wash buffer. Columns were then placed in clean 1.5ml eppendorf tubes and 50µl of elution buffer EB (10mM Tris-HCl pH8.5) or dH_2O added to the centre of each column. Columns were incubated for 1 minute at RT before the DNA was eluted by 13,000rpm centrifugation for 1 minute. DNA concentration and quality was then ascertained by Nandrop quantification.

2.3.2.6 DNA extraction: Qiagen plasmid purification for midi and maxipreps

Midi and maxi-preps allow the extraction and purification of up to 100 or 500µg of plasmid DNA. For midi-preps of high copy plasmids 25mls of bacterial culture was grown in LB+antibiotic media, and for maxi-preps 100 mls, all cultured in larger volume containers to aid bacterial growth. The bacterial culture was pelleted by centrifugation at 6000 x g in 25 and 100ml volumes for midi and maxi-preps respectively. The supernatant was discarded and the pellet homogeneously re-suspended in buffer P1 (50mM Tris-HCl pH8, 10mM EDTA, 100µg/ml RNAse A). Lysis buffer P2 (200mM NaOH, 1% SDS (v/v) was added in 4ml or 10ml volumes respectively for midi and maxi-preps, mixed thoroughly by inversion and incubated at RT or 5 minutes. The same respective volumes of neutralization buffer P3 (3M KOAc pH5.5) were then added, mixed by inversion and

the tubes left on ice for 15 or 20 minutes volumes respectively for midi and maxi-preps. The bacterial lysate was cleared by centrifugation. Midi and maxi-preps were spun at ≥ 20, 000 x g for 30 minutes at 4ºC. The midi/maxi-prep supernatant was then further cleared of bacterial lysate by passing it through sterile glass wool in a 50ml sterile plastic syringe. Midi/maxi Quiagen-tip colums were equilibrated with 4 or 10mls of buffer QBT (750mM NaCl, 50mM MOPS pH7.0, 15% isopropanol [v/v], 01.15% TritonX-100 [v/v]) and allowed to empty by gravity flow. The plasmid-containing supernantant was applied to the column and entered the DNA-binding resin by gravity flow. The resin-bound DNA was washed with 2 x 10 or 30 mls buffer QC (1M NaCl, 50mM MOPS pH7.0, 15% isopropanol [v/v]) respectively for midi and maxi-preps, again by gravity flow. The DNA was eluted into clean 15ml (midi) or 50ml (maxi) vessels using 5 or 15mls buffer QF (1.25M NaCl, 50mM Tris-HCL pH8.5, 15% isopropanol [v/v]). The plasmid DNA was precipitated by adding 3.5 0r 10.5 mls of RT isopropanol to the midi/maxi elutants respectively. After mixing by inversion the DNA was centrifuged down at ≥15, 000 x g for 30 minutes at 4ºC. The supernatant was carefully decanted and the pellet washed with 2 or 10mls of 70% ethanol and re-centrifuged for 15 minutes at ≥15, 000 x g. The supernatant was carefully removed and the DNA pellet air-dried for 5-10 minutes before being resuspended in a suitable volume of TE buffer or ddH_2O.

2.3.2.7 DNA digestion by restriction enzymes (RE).

For transformations three individual colonies were picked for each plasmid and cultured overnight. Miniprep digests to check plasmid identity, orientation and insertion sites were performed in 20µl reactions consisting of 0.5-1µg of DNA, 2µl of RE buffer, 1µl of each required restriction enzyme, made up to the final volume with dH_2O. Digests were incubated at 37ºC for 1h or overnight and then run out and visualized on an electrophoresis agarose gel. For larger quantities of DNA, e.g. linearization of 10-20µg of plasmids for RNA transcription, the reaction volume was increased to to 100µl and the volume of the reaction components scaled up accordingly, with 10µl RE buffer and 3µl of RE used per reaction. The digest was incubated for 3h-overnight. In all reactions where there was the possibility of star activity from the RE used 100µg/ml of BSA was added to

the reaction. The linearized DNA digest was incubated with 50µg/ml Proteinase K at 37°C for 30 minutes. The DNA was then purified by two 1:1 (volume:volume) phenol chloroform extractions. An equal volume of both of Tris-buffered phenol (source) pH8.0 and chloroform: iso-amyl alcohol (49:1 $CHCl_3$:IAA) and vortexed. The resulting suspension was then centrifuged for 5 minutes at 13,000rpm at 4°C. The upper layer (aquatic phase) was placed in a new tube and the phenol chloroform extraction repeated. The DNA precipitated by the addition and mixing of $1/10^{th}$ the volume of 3M NaOAc (pH5.2) plus 2.5 volumes of cold 100% ETOH followed by incubation at -20°C for 30 minutes to overnight. The DNA was pelleted by centrifugation at maximum speed for 20 minutes (4°C). The supernatant was discarded and the pellet air-dried after which it was resuspended in ddH_2O and used in RNA transcription reactions.

2.3.2.8 Agarose gel electrophoresis

Agarose gels were made in the range of 1-4% depending on the size of the nucleotide fragments to be visualized. Smaller fragments require higher percentage gels to be clearly separated. Miniprep digests and RNA transcriptions were usually run on a 1% gel and PCR products on a 1.5 or 2% gel. The required amount of agarose for the percentage and volume of the gel was dissolved in 1x Tris-acetate-EDTA buffer (40mM Trizma base, 20mM glacial acetic acid, 1mM EDTA, pH8) and 0.5µg/ml ethidium bromide added before pouring into the gel plate. 10 x loading buffer (20% Ficoll, 0.1M EDTA, 1% SDS, 0.25% bromophenol blue or Orange G dye) was added 1: 5 (v/v) to the nucleotide samples. DNA size marker ladder appropriate for the sample (1Kb or 100bp DNA ladder, Invitrogen) was also run. The gel was loaded and electrophoresed in 1xTAE buffer at 60-120V until the nucleotide fragments were sufficiently separated. DNA was visualized under UV illumination.

2.3.2.9 Nanodrop ND 1000

The amount and quality of DNA and RNA nucleotides were ascertained using two different methods. The Nanodrop ND 1000 machine(ThermoScientific) and software

allows electronic quantification of the overall amount of nucleotide present to picogramme quantities and provides a graphical readout of nucleotide quality determined by absorbance at λ260 and λ 280. The machine was initialized with 1µl dH_2O, a blank reading taken using 1-2µl solvent only, then 1-2µl of each sample loaded and measured.

2.3.3 In situ hybridization

In situ hybridization is a widely used technique which allows the localization, both spatially and temporally of mRNA transcripts for a specific gene in cells, tissue section or embryo/organ whole-mounts. Linearized DNA plasmid template containing part or all of this gene sequence is transcribed using the RNA polymerases T7, T3 or SP6 to produce an "antisense" transcript of complementary sequence to the mRNA of interest. The transcription reaction contains uracil nucleotide bases typically tagged with either digoxigenin (DIG) or fluorescein (FSC) molecules, thus labelling the antisense probe. Hybridization of this tagged RNA probe at high temperature to the tissue of interest allows it to bind to the target mRNA where it can be subsequently detected by antibodies against the digoxigenin or fluorescein epitopes and then visualized by a colour precipitation reaction or fluorescent labels.

2.3.3.1 Labelled RNA probe preparation

Plasmids consisting of appropriate vectors, i.e containing RNA polymerase sites at either end of a multiple cloning site (MCS), with template DNA for the gene of interest cloned into the MCS were obtained from a variety of commercial and academic sources (see Table 2.8 for details). After mini-prep purification plasmid DNA was checked by RE digestion to verify the identity and insertion sites of the target DNA in the MCS. Subsequently, DNA for use as transcription templates was purified using the Quiagen midi or maxi-prep protocols. DNA was linearized by the relevant RE digest to allow transcription of antisense and sense mRNA. Following linearization, the DNA was incubated with Proteinase K and purified by phenol:chloroform extraction and ethanol precipitation.

The purified linearized plasmid was then used in transcription reactions to produce DIG or FSC-labelled probes. Transcription reactions comprised 1µg linearized DNA, 1x transcription buffer (5x stock buffer, Promega), 0.66mM nucleotide mix (stock: 10mM ATG, 10mM CTP, 10mM GTP, 6.5mM UTP, 3.5mM digoxigen-11-UTP), 1x DTT (10x stock, Promega), 40U RNAsin (ribonuclease inhibitor, 40U/µl, Promega), 40U T7, T3 or SP6 RNA polymerase (20U/µl stock, Promega) made up to a final volume of 30µl with ddH_2O. The reactions were incubated at 37°C for 2 hours and then precipitated by the addition of 100µl TE, 10µl 4M LiCl and 300µl ethanol at -20°C overnight. The transcribed RNA was pelleted by centrifugation at 14,000rpm for 30 minutes, the supernatant discarded and the pellet washed with 70% ethanol and recentrifuged at maximum speed for 15 minutes. The ethanol wash was discarded and the RNA air dried before being resuspended in ddH_2O. Alternatively the transcription reaction was cleared of unincorporated nucleotides by passing through a illustra ProbeQuant G-50 Micro Column (GE Healthcare). Columns were centrifuged at 735 x g for 1 minute. The transcription reaction was made up to 50µl with ddH_2O and loaded onto the column and spun at 735 x g for 2 minutes. In both cases a few microliters of the reaction was then run on a 1% agarose gel and quantified in the Nanodrop to assess quality and amount of the transcribed RNA probe.

Table 2.8 List of DNA templates used to make labelled RNA probes

Species	Gene	Insert	Vector	Linearizing RE	Probe transcription	Source
Chick	*Fgf8*	400bp	unknown	antisense *EcoRI* sense *XhoI*	antisense T7 sense T3	Francis-West Lab, KCL
	Hoxb1	2kb	pPS-SK	antisense *Xba1*	antisense T7	Maden Lab, KCL (Gale et al., 1996)
	Pax9	825bp	pBS II KS+	antisense *EcoR1* sense *Not1*	antisense T7 sense T3	GeneService
	Raldh2	1.5kb	pGEM-TEasy	antisense *SacII*	antisense SP6	Dr.S Reijntes Maden Lab, KCL
	Sox10	?	pBS-SKII	antisense *EcoRV*	antisense T3	Scotting Lab (Cheng et al., 2000)

	Tbx1	373bp T-box domain	pGEM -TEasy	antisense *PstI* sense *NcoI*	antisense SP6 sense T7	In house (Roberts et al., 2005)
	Mef2c	1600bp	pBS	antisense *HindIII*	antisense T3	Riley lab, UCL (Edmondson et al., 1994)
	Isl1	497bp	?	antisense *XhoI*	antisense T3	Evans lab, UCSD (Cai et al., 2003)
Zebrafish	*fli-1*	3kb	?	antisense *XbaI*	antisense T3	Wilson Lab, UCL (Brown et al., 2000)
	her6	6kb	pBS-SK	antisense Hind III	antisense T7	Dr.A.Pasini Wilkinson Lab, NIMR (Pasini et al., 2001)
	tbx1	2374bp	pExpress-1	antisense *EcorI* sense *Not1*	antisense SP6 sense T7	GeneService
	myoD	1.65kb	pBS	antisense *BamHI*	antisense T7	Tada lab, UCL (Weinberg et al., 1996)
	pax9a	1330bp	pGEM-5zf	antisense *PvuII*	antisense T7	Graham,Lab KCL (Nornes et al., 1996)
	crestin	No DNA template information. In situs performed with supplied *crestin*-DIG antisense RNA probe				Dr. D Jenkins, ICH,UCL
	tie1	2kb	pBS-SK	antisense *EcoRI*	antisense T7	Dr.A.Ciau-Uitz Weatherall Institute, Oxford.(Lyons et al., 1998)
	tie2	800bp	pBS	antisense *XhoI*	antisense T3	Dr.A.Ciau-Uitz Weatherall Institute, Oxford.(Lyons et al., 1998)

pBS: pBluescript

2.3.3.2 Standard single in situ hybridization protocol for mouse and chick embryos

The in situ protocol used was based upon those published previously (Streit et al., 1998; Wilkinson D, 1992). Dissected embryos were fixed in 4% paraformaldehyde for 1h to overnight depending on developmental stage and transferred through a methanol series to 100% methanol. Following rehydration through a methanol series they were washed 2x 10 minutes in PBS/0.1% Tween (PBT) digested by 10µg/ml proteinase K in PBT for 30 minutes and then rinsed briefly in PBT. Embryos were re-fixed in 4% paraformaldehyde/0.1% glutaraldehyde/PBT for 20-30 minutes after which, they were rinsed in hybridization solution (50% formamide, 1.3xSSC pH5.3, 5mM EDTA, 50µg/ml yeast RNA, 0.002% Tween 20, 0.5% CHAPS, 100µg/ml heparin), then incubated in fresh hybridization solution for at least 2h-overnight at 68-70ºC. Following this prehybridization step, DIG- or FSC-labeled RNA antisense probes were denatured for 5 minutes at 95°C and cooled immediately on ice before being added to hybridization solution at 0.2-1µg/ml. Hybridization took place over night at 62°C for 150-250 nucleotide (nt) length probes, 65°C for 250-400nt probes and at 68-70°C for probes of length greater than 400 nucleotides. Where FSC-labelled probes were used all following steps were performed in the dark by wrapping containers in foil.

Post-hybridization, the probe was removed and embryos rinsed twice with pre-warmed hybridization solution at the same temperature as the hybridization reaction. The following washes and incubations were carried out on rotating platforms where possible. Post-hybridization washes consisted of three 30 minute washes with pre-warmed hybridization solution finishing with 20 minutes in pre-heated 1:1 hybridization solution: TBST (25mM Tris-HCl pH7.5, 8mg/ml NaCl, 0.2mg/ml KCl, 11mg/ml Tween20). Embryos were rinsed three times in TBST and then washed 3 x 30 minutes in TBST at RT. They were then incubated in blocking solution (10% sheep serum, 1% BSA in PBT) for 3h. The blocking solution was removed and replaced with anti-digoxigenin-AP (alkaline phosphatase) or anti-fluoroscein-AP antibody (Roche) diluted 1:2000 in block, overnight at 4°C. Three rinses in TBST followed by three 30 minute washes in TBST were performed. Embryos were then equilibrated in NTMT buffer (0.5M NaCl, 0.1M Tris-HCl pH 9.5, 0.05M $MgCl_2$, 1% Tween-20) for 2x 10 minutes. They were then

incubated in the dark (foil-wrapped) in a colour substrate solution made from NBT/BCIP (nitro blue tetrazolium chloride/5-Bromo-4-chloro-3-indolyl phosphate toluidine tablets (0.4mg/ml NBT, 0.19mg/ml BCIP, 0.1M Tris-HCl pH9.5) (Roche) until the desired end point. Embryos were then washed in TBST and fixed in 4% paraformaldehyde.

2.3.3.3 Standard single in situ hybridization protocols for zebrafish embryos

Standard in situ hybridization was carried out using a protocol closely based upon that of (Xu et al., 1994). Dechorionated embryos were fixed in 4% paraformaldehyde for 1h to overnight depending on developmental stage and transferred through a methanol series to 100% methanol. Following rehydration through a methanol series they were washed 2x 10 minutes in PBS/0.1% Tween (PBT) and then digested in varying concentrations of proteinase K/PBT for varying lengths of time depending upon developmental stage (see Table 2.9).

Table 2.9 Proteinase K incubation times and concentrations for zebrafish

Developmental stage	PK concentration (10mg/ml stock=1000x)	Incubation time
Up to tailbud	No PK	N/A
2-10ss	10µg/ml (1x)	In and out
10-15ss	10µg/ml (1x)	4 min
16-26ss	10µg/ml (1x)	5 min
24hpf	10µg/ml (1x)	20 min
30hpf	10µg/ml (1x)	30 min
36-48hpf	10µg/ml (1x)	1h
2.5 dpf	15µg/ml (1.5x)	1h
3dpf	20µg/ml (2x)	1h

After two rinses in PBT embryos were re-fixed for 20min in 4% paraformaldehyde. They were then incubated in pre-hybridization solution (PHS) (50% formamide, 5xSSC, 0.1% Tween 20, adjusted to pH6 with citric acid) for at least 2h-overnight at 65ºC after which embryos could be stored at -20°C if desired. Following prehybridization, prehybridization DIG- or FSC-labeled RNA antisense probes were denatured for 5 minutes at 95°C and cooled immediately on ice before being added to

hybridization solution (PHS plus 50µg/ml heparin and 20µg/ml yeast RNA). Hybridization took place for at least overnight at 65ºC. Where FSC-labelled probes were used all following steps were performed in the dark by wrapping containers in foil.

The following washes and incubations were carried out on rotating platforms where possible. Post-hybridization washes were performed at 65ºC also and comprised 5 minutes of PHS, 5 minutes of 25% PHS/75% 2xSSC, 10 minutes 2xSSC and 3x 30 minutes of 0.2xSSC. Embryos were equilibrated in 2 washes of maleic acid buffer (MAB; 150mM NaCl, 100mM maleic acid) and then blocked in 2% Blocking Agent(Roche)/MAB for 2-3h at room temperature. Antibody incubation took place overnight in 1:6000 dilution anti-digoxigenin-AP antibody (Roche) in block at 4°C. Embryos were washed 6x 15 minutes in maleic acid buffer and then rinsed twice in 0.1M Tris-HCl pH9.5/0.1% Tween-20. They were then incubated in the dark (foil-wrapped) in a colour substrate solution made from NBT/BCIP (nitro blue tetrazolium chloride/5-Bromo-4-chloro-3-indolyl phosphate toluidine tablets (0.4mg/ml NBT, 0.19mg/ml BCIP, 0.1M Tris-HCl pH9.5) (Roche) until the desired end point. Embryos were then washed 3x in PBS/0.1% Tween 20(PBT) and fixed in 4% paraformaldehyde.

2.3.3.4 Standard double in situ hybridization in zebrafish embryos

Dissection, fixation and prehybridization of embryos was identical to the single in situ protocol in section 2.3.5.3 above. However, two antisense RNA probes were prepared, one labelled with digoxigenin-11-UTP and the other with fluorescein-12-UTP. Usually the weaker probe was labelled with DIG and the stronger with FSC. Both probes were added to the hybridization mix together at 0.2-1µg/ml each. Overnight hybridization and post-hybridization washes were carried out as before, Blocking and anti-DIG-AP antibody detection of the weaker, DIG-labelled probe, subsequent washed and NBT/BCIP colour reaction was executed as normal. After the PBT washes, embryos were refixed in 4% paraformaldehyde for 1h. They were then washed 3x 5 minutes and incubated in PBS at 65°C for 1h to inactivate the first antibody.

Following this embryos were re-equilibrated in MAB and blocked as previously. The second probe fluorescein-labelled probe was then detected overnight at 4°C with anti-

fluoroscein-AP antibody (Roche) diluted in 1:6000 in blocking buffer. Post-antibody MAB washes were the same as the original protocol. Embryos were then rinsed twice in 0.1M Tris-HCl pH8.2 and incubated in a Fast Red (Invitrogen) colour substrate solution prepared from tablets (0.25mg/ml napthol substrate, 1mg/ml fast red chromogen, 0.2mg/ml levamisole, 0.1M Tris-HCl pH 8.2). As formerly, the colour reaction was terminated at the appropriate point by washing in PBT and embryos were fixed in 4% paraformaldehyde.

2.3.3.5 Fluorescent double in situ hybridization in zebrafish embryos

The protocol used for double fluorescent in situ in zebrafish was essentially that published by the Holley lab (Brend and Holley, 2009b). Embryos were de-chorionated as previously and fixed overnight in 4% paraformaldehyde at 4°C. Embryos were given 2 times 5 minute washes in PBS and taken through a methanol series to 100% methanol. This was replaced with fresh methanol after one hour and embryos placed at -20°C for 1h or overnight. Embryos were then rehydrated back through a methanol/PBT series at RT and washed for 2 times 5 minutes before re-fixation in 4% paraformaldehyde/PBS for 20 minutes. Following the fixation step the samples were washed again in PBT twice for 5 minutes and digested in 5µg/ml proteinase K/PBT for 5-12 minutes depending upon developmental stage, with younger embryos being digested for less time (see Table 2.10)

Table 2.10 Proteinase K digestion times for double fluorescent in situ in zebrafish

Developmental stage	PK digestion time (5µg/ml) (minutes)
Up to 10ss	5
10-15ss	6
15-26ss	7
24hpf	8
30hpf	10
36hpf	12

After PK digestion embryos were briefly rinsed in PBT, then washed for 5 minutes in PBT. A second fixation in 4% paraformaldehyde/PBS for 20 minutes was carried out and the embryos again washed twice for 5 minutes each in PBT. Embryos were

incubated at 65°C in pre-hybridization (HYB-) solution (50% formamide, 5xSSC, 0.1% Tween-20) for 5 minutes, then pre-hybridized 2h-overnight in hybridization (HYB+) solution (HYB- solution plus 5mg/ml yeast RNA, 50µg/ml heparin).

Subsequently, this solution was replaced with HYB+ solution containing 0.2-1µg/ml each of the separate DIG- and FSC- labeled probes and incubated overnight at 65°C. For best results the exact concentration of probe was determined previously by determining the concentration which gave a robust result by colour substrate in situ hybridization after 30-45m minutes of development. From the hybridization step onwards the embryos were kept in the dark by wrapping containers in foil.

The following washes and incubations were carried out on rotating platforms where possible. All post-hybridization washes were carried out at 65°C and comprised 2 times 30 minutes in 50% formamide, 2xSSC, 15 minutes in 2xSSC and one times 30 minutes in 0.2xSSC. After these washes embryos were blocked for at least 2h in 2% Blocking Agent (Roche) in MAB before incubation with the anti-fluorescein-peroxidase (POD) antibody (Roche) diluted 1:500 with blocking buffer for at least 4h-overnight at 4°C. Excess antibody solution was washed out with four 20 minute MAB washes followed by two 5 minute PBS washes.

The fluorescein-labelled probe was detected using a tyramide amplification signal kit (TSA^{TM}PLUS Fluorescence, PerkinElmer). The tyramide reagent was diluted 1:20 in the amplification diluent buffer and the embryos incubated in it for 45-60 minutes. Embryos were then washed three times 10 minutes in PBS and subsequently incubated in 1% H_2O_2/PBS for 30 minutes, followed by three times 10 minute washes in PBS before being blocked again for at least 2h in blocking reagent as previously. The anti-DIG-POD antibody (Roche) to detect the second DIG-labelled probe was diluted 1:500 in blocking buffer and embryos incubated in this, 4h to overnight at 4°C. Post antibody washes again comprised four times 20 minute MAB washes before two 5 minute PBS washes. Tyramide signal amplification was performed using the PerkinElmer TSA^{TM}PLUS Cy3 kit at the same dilutions as before, again for 45-60 minutes. Three PBT washes of 10 minutes each were carried out and then the embryos were counterstained in 1% DAPI before two final 10 minute PBT washes. They were then stored in Vectashield mounting medium (Vector Labs) at 4°C before being flat-mounted.

2.3.3.6 Fluorescent in situ hybridization plus antibody staining in zebrafish embryos

Tg(fli-1:gfp) or *Tg(sox10:gfp)* were incubated to the required stages as previously. Fluorescent in situ hybridization with a *tbx1* probe visualized with TSA-Cy3 was performed as before, except that both the pre-hybridization and hybridization incubations were performed at the lower temperature of 55°C. After the TSA reaction embryos were washed 3 x 10 minutes in PBT and blocked for at least 1h at RT in blocking buffer. They were then incubated overnight at 4°C in rabbit anti-gfp antibody (AbCam) diluted 1:500 with blocking buffer. Embryos were washed 6x 15 minutes in PBT at RT before being incubated overnight at 4°C in the secondary antibody, anti-rabbit IgG Alexafluor 488, diluted 1:100 in blocking buffer. Embryos were again washed 6 x 15 minutes in PBT and then stained in 1% DAPI before two final 10 minute PBT washes, after which they were stored in Vectashield mounting medium at 4°C before being flat-mounted.

2.4 Antibody staining

2.4.1 Whole-mount antibody staining in zebrafish

Embryos were fixed for at least 1h in 4% paraformaldehyde/PBT, then washed 2x 10 minutes in $PBTx_{0.25}$ (0.25% Triton 100 in PBS). Permeabilization of the embryos was performed by incubation in 20µg/ml Proteinase K solution in PBS at room temperature for 5 minutes for 24hpf embryos, 15 minutes for 48-52hpf embryos and 25 minutes for 72hpf embryos. Embryos were then briefly rinsed in PBS before being re-fixed in 4% paraformaldehyde/PBT for 20 minutes. Two 5 minute washes of PBTx were performed and then the embryos were blocked in 5% sheep serum in PBTx for at least 1h at RT before being incubated in primary antibody diluted in 2% sheep serum in PBTx overnight at 4°C. Please see Table 2.11 below for primary antibody details and concentrations. The following day embryos were washed 6 x 15 minutes in $PBTx_{0.25}$ before a further overnight incubation in the dark at 4°C in an AlexaFluor 568 or 488-tagged secondary antibody diluted 1:100 with 2% sheep serum in PBTx. The following day embryos were washed 6 x 15 minutes in PBTx, counterstained in 1% DAPI where required, washed

again in PBTx for 2 x 10 minutes before being mounted in Vectashield mounting medium (without DAPI) for fluorescence and confocal microscopy

Table 2.11 Antibodies used for embryo staining

Primary antibody	Working dilution	Source	Secondary antibody	Working dilution	Source
Anti- zebrafish DM-Grasp(Zn8) mouse IgG hybridoma concentrate	1:10	Developmental Studies Hybridoma Bank	Anti-mouse IgG AlexaFluor-568	1:100	Life Technologies
Anti-GFP chicken polyclonal IgG	1:50	AbCam	Anti-chicken IgG AlexaFluor 488	1:100	Life Technologies
Anti-Phospho-Histone H3 (Ser 10)-R:sc 8656-R (rabbit polyclonal IgG)	1:500	Santa Cruz Biotechnology	Anti-rabbit IgG AlexaFluor 488	1:100	Life Technologies
Anti-smooth mucle actin	1:800	Sigma	Anti-mouse IgG-HRP	1:200	Sigma

2.4.2 Vascular smooth muscle staining on wax sections

Embryo sections were de-waxed, rehydrated through and alcohol/PBS series and washed in PBS, then blocked at 4°C in 1% BSA, 10% sheep serum in PBT (PBS, 1% Tween 20). They were then incubated in primary antibody overnight at 4°, washed 5 x 10 min washes in PBT and incubated in secondary antibody overnight at 4°.The embryos were then again washed 5 x 10 min in PBT (see table2.10 for antibody specifics). Antibody staining was visualized by developing in 0.5mg/ml DAB (3,3,5,5, diaminobenzidine tetrahdrochloride) in 0.1M Tris HCl pH 7.5 (1x 10mg tablet[Sigma] in 20ml 0.1M Tris) with 0.003% hydrogen peroxide until the required staining level was

reached. Slides were then rinsed in running tap water 10-20 minutes and then rinsed 2 x dH_2O before being mounted in Aquamount (Raymond Lamb).

2.4.3 Cryo-embedding and sectioning

Cryo-embedding and sectioning was used to prepare sections for antibody staining for mouse and chick and to provide sections from zebrafish on which double in situ hybridization visualized with a colour precipitation enzymatic reaction had been performed. In those specimens where one of the colour substrates (Fast Red) was soluble in organic solvents wax sections could not be prepared without loss of staining so embryos were cryo-embedded and sectioned instead after the post-staining fixation step.

Embryos were dissected out as before and rinsed with PBS, then fixed for up to 2h with 4% paraformaldehyde in PBS, followed by 2 x 10 minute washes in PBS. They were then transferred to 30% sucrose solution at 4°C overnight or until equilibration was observed by specimens sinking to the bottom of the container. Embryos were then incubated in 50:50 30% sucrose: OCT (Optimal Cutting Temperature compound) embedding matrix (Raymond Lamb) for 30 minutes. They were then embedded in OCT plastic moulds either over dry ice or transferred directly to the -80°C freezer. Embryo blocks were trimmed and mounted on metal chucks. The embryo block was sectioned on a Leica CM-3050-S cryostat in 5-15µm slices as required, and each section collected upon TESPA-coated superfrost (VWR) glass slides or positively charged Superfrost-Plus (VWR) slides kept at RT. Once on the slides, the sections were stored at -20°C until processed further.

In situ double-stained embryos were cryo-sectioning because of the solubility of Fast Red in organic solvents. After sectioning the slides were brought to room temperature and washed through changes of PBS until the OCT embedding material dissolved. They were then mounted with coverslips in Aquamount and photographed.

2.4.4 Whole mount TUNEL staining for apoptosis in zebrafish

Zebrafish embryos were processed in whole-mount for apoptosis staining using the DeadEnd™ Fluorometric TUNEL System (Promega) which measures the fragmented DNA of apoptotic cells by catalytically incorporating fluorescein-12-dUTP at 3´-OH DNA ends using the Terminal Deoxynucleotidyl Transferase, Embryos were fixed in 4% PFA/PBT after dissection and then transferred to 100% methanol and stored at -20°C before being used in the protocol. Embryos were washed 2 x 5-10 minutes in $PBTx_{1.0}$ (PBS/1% Triton 100) and then permeabilized in 10µg/ml Proteinase K/ $PBTx_{1.0}$ (PK provided in the kit, diluted in 100mM Tris-HCl pH 8.0/50mM EDTA) for 20 minutes. After re-fixation in 4% PFA/PBT embryos were rinsed twice in PBS and transferred to Equilibration Buffer from the kit (200mM potassium cacodylate pH 6.6, 25mM Tris-HCl pH 6.6, 0.2mM DTT, 0.25mg/ml BSA, 2.5mM cobalt chloride) for 30 minutes at RT. The dTdT reaction mix was prepared on ice in dark eppendorf tubes and consisted of 270µl Equilibration Buffer, 30µl nucleotide mix (50µM fluorescein-12-dUTP, 100µM dATP, 10mM Tris-HCl pH 7.6, 1mM EDTA) and 6µl 30U/µl rdTd (Terminal Deoxynucleotidyl Transferase, Recombinant) enzyme. After the equilibration step, the embryos were incubated in the reaction mix overnight at 37°C in the dark. The reaction was then terminated by 2 x 10 minutes washes in 2x SSC provided in the kit. Embryos were then washed 2 x 10 minutes in $PBTx_{1.0,}$ stained with 1% DAPI for 20-30 minutes and then given 4 x 5 minute final washes in $PBTx_{1.0.}$ Embryos were stored in Vectashield mounting medium at 4°C, before flat-mounting.

2.5 Histology

2.5.1 TESPA-coating glass slides

Superfrost (VWR) glass slides were placed in slide racks and cleaned by dipping in a solution of 10% HCl/70% ethanol followed by rinsing in dH2O and then 95% ethanol. Slides were dried in a hot oven and allowed to cool. They were then dipped in 2% TESPA

(3-aminopropyltrethoxysilane [Sigma]) diluted in acetone for 10 seconds per rack. Slides were then washed in two changes of acetone and finally in dH2O and dried at 37°C.

2.5.2 Wax embedding and sectioning

Embryos were dissected out in PBS and fixed overnight in 4% paraformaldehyde. Embryos which had previously been processed for in situ hybridization or whole mount antibody staining with permanent colour substrates were post-fixed for 1h in 4% PF. Embryos were then incubated for at least 30 minutes or longer depending on stage in the following solutions; twice in 0.83% NaCl at 4°C, twice in 1:1 0.83%Nacl:ethanol at 4°C, twice in 70% ethanol at 4°C, 85% ethanol RT, 95% ethanol RT, twice in 100% ethanol and twice in Histoclear. This was followed with 20 minutes incubation in 1:1 paraffin wax (ThemoScientific/RaymondLamb): Histoclear at 60° and embryos were then incubated in wax alone for 3 x 20 minutes at 60°C. Embryos were then transferred into plastic moulds of appropriate size filled with molten wax and orientated with a warm needle before the block was allowed to set. All incubation times were increased for embryos larger than 7mm in length/E12.5 or equivalent. Before sectioning the blocks were removed from the moulds, excess wax trimmed away and the block mounted by melting one face of the wax block onto a wooden or metal chuck in the correct orientation for the section plane required. After setting the chuck was positioned in an rotary (Ankit Scientific) microtome and ribbons of 5-15µm cut using a disposable microtome blade (Accu-Edge). The ribbons of wax sections were floated out upon a bath of distilled water at 50-60°C to remove creases and the sections collected upon either TESPA-coated superfrost (VWR) glass slides (see section xxx above) or positively charged Superfrost-Plus (VWR) slides. The slides were either air-dried for 48h or dried at 37°C overnight and stored dessicated at 4°C, before further processing for haemotoxylin-eosin staining or, in the case of whole-mounts in situ stained embryos, counter-staining with eosin.

2.5.3 Haemotoxylin-eosin staining

Wax-embedded slides were de-waxed by incubation in two changes of Histoclear for 1-5minutes. Sections were then rehydrated through an ethanol series: 2x 5 minutes in 100% EtOH and 5 minutes each in 95%, 85%, 70% ethanol/dH_2O. They were then rinsed dH2O and transferred to Gills' #3 haemotoxylin solution for 15 seconds-3 minutes depending on the tissue and intensity of staining required and then washed in running tap water to remove excess stain. Two further rinses in dH2O were performed before eosin-staining for 5-10 minutes in 0.5% aqueous eosin. Two times 5 minute washes followed and the slides left to air dry completely or dehydrated through and alcohol series before mounting in DPX.

For eosin counter-staining of purple NBT/BCIP-stained whole-mount in situ sections the same protocol as above was followed up to the first dH2O wash, after which the haemotoxylin staining step and washing with running tap water was omitted and the slides processed directly for eosin staining as in the protocol above.

2.5.4 Alcian Blue staining

Zebrafish embryos (72hpf) were fixed in 4% paraformaldehyde and bleached in 10% hydrogen peroxide/PBS for 1 hour. Embryos were washed in PBS and incubated in 0.1% Alcian Blue (Sigma UK) in acidic alcohol (70% EtOH/10% HCl) overnight. Embryos were then washed in acidic alcohol to remove excess stain, transferred to PBS for 2 x 10 minutes before equilibrating in 80-100% glycerol. They were then photographed as described below .

2.6 Microscopy

2.6.1 Specimen preparation

2.6.1.1 Flat-mounting whole-mount zebrafish embryos

Zebrafish to be flat-mounted were equilibrated in glycerol overnight if non-fluorescently stained and in Vectashield if labelled fluorescently. They were then placed in a drop of glycerol or Vectashield on the lid of a 35mm petridish and the yolk sac dissected away with fine glass needles. Embryos were then transferred to a fresh drop of mounting medium on a new lid. The remaining yolk cells were removed from the embryos by repeatedly dragging them away from the main drop using the fine glass needles so that remaining yolk cells were scraped away by friction with the plastic lid and/or by gently scraping away yolk cells from the embryonic tissue. Embryos older than 48h were dissected further, removing the eyes, brain and neural tube so that the pharyngeal arch regions could be flat-mounted without excess tissue. During this process embryos were repeatedly transferred to fresh drops of mounting media as necessary. Once the embryos were clean a drop of mounting media was placed at one end of a Superfrost (VWR) glass microscope slide and 5-7 embryos relocated into it close to the edge of the media droplet closest to the rest of the glass slide. Each embryo was gently dragged out of the drop by fine glass needles as far along the length of the slide as possible so that the anterior-posterior axis extended along the length of the slide. A no. 1.5 thickness 22 x 50 cm glass coverslip as placed angled within the drop of mounting media so that roughly one third to half the mounting media was between the coverslip and the embryos. The coverslip was then gently lowered to cover the embryos, pushing the mounting media along to cover the embryos. The coverslip was then gently pressed down, thus flattening the embryos onto the slide. The excess mounting media was gently wiped away and the coverslip fixed in position with nail varnish. The slides were then stored at 4°C in the dark until they were photographed.

2.6.1.2 Cavity slide mounting whole-mount zebrafish embryos

Some embryos were mounted in cavity slides rather than being flat-mounted. Zebrafish to be flat-mounted were equilibrated in glycerol overnight if non-fluorescently stained and in Vectashield if labelled fluorescently. Five-ten embryos were transferred to a fresh drop of mounting media placed in the well of a 1.2-1.5 mm glass cavity microslide and the cavity filled to the top with mounting media. The embryos were orientated as required and a No.1.5 thickness 22 x 22 cm glass coverslip gradually lowered in an angled fashion to cover the cavity and the embryos. The excess mounting media was gently wiped away and the coverslip fixed in position with nail varnish. The slides were then stored at 4°C in the dark until they were photographed.

2.6.1.3 Mounting embryo sections for photography

Sections to be photographed in white light bright field were mounted in Aquamount or DPX depending on whether they were still aqueous or dehydrated at that stage using No. 1.5 thickness 50 x22 cm or 60 x22 cm glass coverslips. Fluorescently labelled sections for fluorescence or confocal microscopy were mounted in Vectashield mounting medium with the same coverslips as before.

2.6.2 Standard light and fluorescence microscopy/photography

Whole embryo photography in bright field and fluorescence was performed upon a Zeiss Stereo Lumar V.12 microscope with an AxioCam HRc camera and AxioVisio 4.8 software. Higher power bright field and fluorescence photography was performed on the Zeiss Apotome AxioImager.Z1 microscope with an AxioCam MRm camera and Axiovision 4.8 software or a Zeiss Axioplan 2 microscope with an AxioCam HRc camera and AxioVisionLE software. Further analysis/processing of images was performed using Image J and Fiji software and Adobe Photoshop CS5.

2.6.3 Confocal laser scanning microscopy

For confocal imaging green fluorescent protein transgenic zebrafish lines *Tg(fli-1:gfp)* and *Tg(sox10:gfp)* and embryos processed for fluorescent in situ hybridization or those stained with fluorescently-tagged antibodies were experimentally processed as as described previousl.. Stained embryos were examined by epifluorescence on an inverted LSM710 confocal system mounted on an AxioObserver Z1 microscope (Carl Zeiss Ltd, United Kingdom). The images were captured with a LD LCI Plan-Apochromat 25x/NA 0.8 water immersion DIC objective (Carl Zeiss Ltd, United Kingdom). The Alexa Fluor 488 and Alexa Fluor 568 dyes were sequentially excited with a 488 nm Argon laser and a 561 nm diode. The emitted light detection range was automatically setup by the Smart setup module of the ZEN2009 software to avoid bleed-through between emission spectra and the absence of bleed-through was controlled using single labeled controls (Carl Zeiss Ltd, United Kingdom). The pinhole aperture was set to create a 3.4 µm thick optical section and z-stack images were acquired with 1.7-2.2 µm spacing between optical slices. The images files were exported into ImageJ (Rasband, 1997-2009, http://rsb.info.nih.gov/ij/) or Fiji (Schindelin et al., 2012) where they were processed for publication. 3D reconstructions were produced with the ImageJ 3D Viewer plug-in written by Benjamin Schmid (http://rsb.info.nih.gov/ij/plugins/3d-viewer/).

2.6.4 Optical Projection Tomography (OPT)

Optical Projection Tomography (OPT) is a microscopy technique that produces high resolution section and 3D images of fluorescent and non-fluorescent biological specimens up to 15mm thick. Resolution varies with the size and type of specimen but resolution sufficient (2µm) to identify single cells is easily possible. OPT is especially helpful for providing the 3D shape of a structure or set of structures and for tracing the complete distribution of a signal through an entire specimen. It is therefore particularly useful for high-throughput anatomy and phenotyping, mapping gene expression and localization of labelled cells within a tissue. For a review see (Quintana and Sharpe, 2011).

The approach pioneered for OPT (Sharpe et al., 2002) suspends the specimen in an index-matching liquid (BABB, 1:2 benzyl alcohol: benzyl benzoate) thus reducing light scattering and the heterogeneities of refractive index throughout the specimen. This allows light of various wavelengths to pass through the rotating specimen in roughly straight lines and optical images are captured that approximate projections and the back-projection algorithm can generate relatively high-resolution images. All specimen preparation and scanning procedures described below were as found in the Bioptonics Microscopy OPT Scanner 3001M User manual V1.12.4 (MRC Technologies).

2.6.4.1 Embryo dissection for OPT

Tissue blocks up to the size of E15.5 day embryos can be successfully processed for OPT. However, a better resolution of section is achieved using somewhat smaller specimens. Accordingly, fixed E15.5 mouse embryos were rinsed in PBS and the great vessels were dissected and photographed as described. After photographing the heart and great vessels in situ within the embryo, the great vessels were cut at a high cervical level in the region of the clavicle, and the heart and lungs with attached great vessels scooped out to the body cavity. The lower portion of the lungs was usually removed to allow clear 3D imaging of the ventricles and as much remaining blood was pushed out of the heart as possible to facilitate clear OPT imaging. Embryos were washed overnight in PBS before being embedded in agarose.

2.6.4.2 Agarose embedding of embryo tissues for OPT imaging

Forty millilitres per specimen of 1% Ultrapure low melting point agarose (Invitrogen) gel was made in dH_2O and filtered through Whatman 113V filter paper. The agarose was then cooled to 34°C and maintained at this temperature in an incubator. Once this temperature was reached a 50 x 25 mm petri dish was placed on a cold plate or ice and filled to the brim with agarose. The specimen was briefly blotted of excess PBS and the transferred into the agarose. Using blunted glass pipettes, the specimen was orientated with the long axis horizontal along the bottom of the dish and gently maintained in the

centre of the dish in terms of diameter and depth until the agarose below cooled and set. Once the whole petri dish of agarose had set it was wrapped in cling-film and stored at 4°C for 2h-overnight to become firm.

2.6.4.3 Trimming the agarose block for OPT imaging

A microtome blade was used to produce a rectangular block of agarose with the specimen in the centre. The block was then aligned on the trimming template provided in the Biptonics Microscopy OPT Scanner 3001M User manual V1.12.4. Normally the specimen was orientated with the long axis along the blue vertical line. When reconstruction is of the scan is performed the transverse orientation will be along the long axis. When cutting the short axis edge to be attached to the mount at least 5mm distance was maintained between the specimen and the end of the block The rest of the block was then trimmed along the edges to reduce the size until it is slightly larger than the magnetic mount. The block was then centred on a circle the same diameter as the mount and trimmed into an octagonal shape, tapering slightly out from the top to the base. The agarose block was then placed in a small glass bottle and covered with 100% methanol and incubated at RT overnight to dehydrate the specimen. The methanol was then changed the following day and left for several hours before being changed again, until on gentle swirling no water could be seen immiscible with the methanol. At this point the methanol was replaced with BABB solution (1:2 benzyl alcohol: benzyl benzoate [Sigma]) and left to clear overnight, in the dark, with bottle lids off to allow the methanol residue to evaporate. The final number of changes of BABB and total length of incubation was dependent on specimen and block size, but at least one (or more) further changes of BABB were performed, until the specimen was fully cleared. Before scanning each specimen was centred on a magnetic metal mount and attached using superglue.

2.6.4.4 OPT Scanning

All scanning processes were performed on a Bioptonics Microscopy OPT Scanner 3001M according to the procedures described in the Bioptonics Microscopy OPT Scanner

3001M User manual V1.12.4 using the Bioptonics Microscopy OPT Scanner 3001M software. The scanner was calibrated using the alignment pin attached to the magmetic rotation stage and the 2-point alignment measurement, at maximum and minuimum magnification.to ensure the misalignment pixel value was less than +/-64 pixels for standard resolution scans and less than +/-128 pixels for high resolution scans.

The cleared sample to be scanned was then mounted upon a magnetic mount using superglue (Permabond 200, Sigma) with the centre of the specimen directly over the centre of the mount and the long axis vertical. The magnetic mount plus specimen was placed in the centre of the magnetic rotation stage and lowered into the BABB-filled quartz cell. Using white light (100%) the magnification and vertical position of the sample was set. The exposure to view the specimen was usually in the 15-30ms range. The rotational alignment of the specimen was performed, as the specimen must be rotating about the centre of its axis for reconstruction of the scan data to be successful. For the simple anatomical reconstruction reported in this thesis, only fluorescent imaging for anatomy on one of the UV light channels was required. Accordingly, once the initial settings were fixed the UV lamp was turned on and the Texas Red channel selected as this provides improved penetration into the specimen. The specimen was focussed using at least two separate rotation positions. The exposure time per rotation was set making sure that the exposure was at the highest intensity possible. The specimen was then raised from the quartz chamber and the relevant flat field correction (dark field) acquired. This allows background artefacts to be removed from the image. The specimen was replaced in the quartz cell and the UV channels to be used to scan selected and rotation values set at 0.9° for standard resolution scans and 0.45° for high resolution scans, before the scan was initiated. No averaging was used in these scans. Once the scan was finished, the data was loaded into the DataViewer software to see the original projection images. The 3D projection of the specimen was rotated through 360° and its position relative to a drawn horizontal and vertical line checked in the first and last image. If the position of the images was the same in both the data was then processed for reconstruction.

2.6.4.5 OPT Reconstruction

The scan dataset was loaded into the NRecon software allowing 3D image projection. The top and bottom parameters of the region to be reconstructed were set. The post-alignment (misalignment compensation) projection and value were examined. Where the value was greater than +/- 5 then the two shadow images were aligned manually until they were at a value of less than +/- 5. The fine-tuning facility was then used to further refine the selection of the post alignment value. A line was drawn through the region of interest in the 3D image projection and this one section was then processed with different values. Typically seven different trials were conducted at paramenter steps of 0.5 and the value giving the best image chosen. This was then repeated for a different section to ensure the post alignment value used gave the best image throughout the specimen. Ring artefact reduction was generally set at 4 and defect pixel masking at 50%.

The output was usually set as a Tiff 16-bit format and the output histogram grey level settings altered if required. Once a destination file was chosen, the data could be added to the batch for reconstruction. After all files to be reconstructed had been scanned and processed and added to the batch the reconstruction process was started.

Once the files had been reconstructed the data was examined by loading them into the Fijii or ImageJ analysis programmes.

2.7 Statistics

Statistical tests were performed on all data where relevant to establish whether observed differences between sample groups were statistically significant. Statistical significance was assumed where $P \leq 0.05$. In general t-tests were performed for data with continuous variables and chi-squared, contingency tables or Fishers' Exact Test were used for data with discreet variables as appropriate. Various online calculating tools were used from GraphPad QuickCalcs (http://www.graphpad.com/quickcalcs/ttest1.cfm), VassarStats: Website for Statistical Computation (http://vassarstats.net/) and Simple Interactive Statistical Analysis (SISA). (http://www.quantitativeskills.com/sisa/statistics/

fishrhlp.htm).

CHAPTER 3

Knock-down of Cyp26 function in the chick phenocopies 22q11 deletion syndrome and the Tbx1 null mouse

3.1 Introduction

Previously, to begin to identify possible down-stream transcriptional targets for TBX1 two different microarray experiments were performed. These arrays are described in the Chapter 1.7.3, and designated Array1 and Array2. Briefly, in Array1 mRNA extracted from the dissected pharyngeal region was compared between wild type and functional *Tbx1* null embryos (*Df1:Tbx1*$^{-/-}$) (Ivins et al., 2005). In Array2 the experiment was optimized by using FACS-GAL to identify cell autonomous target genes. Comparison was made between cells carrying a *Tbx1-lacz* knock-in transgene which were isolated by from *Tbx1* heterozygous and functional null embryos(as above), using a fluorescent β-galactosidase substrate followed by flow-sorting (van Bueren et al., 2010).

Members of the Cyp26 retinoic acid catabolizing enzyme family were identified as being down-regulated in both these microarray screens and indeed a similar, later study, using mesoderm-specific deletion of *Tbx1* to examine otic development also identified *Cyp26a1* and *Cyp 26c1* as potential *Tbx1* targets (Braunstein et al., 2009). As already described in detail in Chapter 1.8, retinoic acid distribution is carefully controlled during embryogenesis by the combined action of synthesizing enzymes (Ang and Duester, 1999; Duester, 1996; Mic et al., 2002) and catabolic enzymes of the Cyp26 family, which are cytochrome P450s that convert RA to more polar metabolites such as 4-hydroxy, 4-oxo and 5, 8 epoxy all-trans RA(Fujii et al., 1997; White et al., 1996; White et al., 2000a). The metabolites are less biologically active than RA, thus Cyp26 expression prevents RA signalling during embryogenesis, protecting those tissues sensitive to RA from inappropriate exposure and allowing careful control of RA expression within the developing embryo. Both these classes of enzyme are expressed in a dynamic and spatially restricted manner during embryogenesis, such that they are often expressed in a

complementary, but rarely overlapping fashion (Blentic et al., 2003; Fujii et al., 1997; MacLean et al., 2001; Mic et al., 2000; Niederreither et al., 1997; Reijntjes et al., 2004; Reijntjes et al., 2003; Reijntjes et al., 2005; Schneider et al., 2001; Swindell et al., 1999; Tahayato et al., 2003; Zhao et al., 1996).

3.1.1 *Cyp26* gene expression is down-regulated in *Tbx1* null mice in two microarray screens and by RTQ-PCR

Cyp26a1, was identified as a potential *Tbx1* target from both Array 1 and Array 2 Affymetrix microarray screen comparing wild type and null *Tbx1* mouse embryo pharyngeal arches at E9.5. RTQ-PCR showed *Cyp26a1* to be down-regulated 2.7-fold in E9.5 *Tbx1* functional null embryos (compound heterozygotes $Df1^{/+};Tbx1^{lacz/lacz}$) embryos relative to wild type at E9.5 (Table1). Array2 using the flow-sorted $Tbx1^{+/lacz}$ and cell populations also identified *Cyp26a1* as a potential *Tbx1* target gene. RTQ-PCR on RNA extracted from $Tbx1^{+/lacz}$ and $Df1:Tbx1^{lacz/lacz}$ cell populations demonstrated *Cyp26a1* levels in *Tbx1* null cells to be 1.67-fold reduced assessed against *Tbx1* heterozygous cells (Table 1) (Lammerts van Bueren, 2008).

The other two Cyp26 family members, *Cyp26b1* and *c1* were not present upon the Affymetrix chips used in the microarray screens which isolated *Cyp26a1* as a putative *Tbx1* target. However, RTQ-PCR on both types of RNA samples showed that *Cyp26b1* was down-regulated in $Df1^{/+};Tbx1^{lacz/lacz}$ E9.5 mouse embryos 1.6-fold in Array 1and 2-fold in Array 2 (Table 3.1)(Lammerts van Bueren, 2008). Finally, *Cyp26c1* was reduced 2.6-fold in Array 1 (Table 3.1)(Roberts et al., 2006). However, *Cyp26c1* was not identified as a potential *Tbx1* target from the microarray on isolated *Tbx1*-positive cells, suggesting that the loss on *Cyp26c1* expression in *Tbx1* null embryos was more likely to be non-cell autonomous.

Table 3.1 Real-time quantitative PCR results for *Cyp26* genes

Gene	from Array 1	from Array 2
Cyp26a1	0.360 ± 0.01	0.6 ± 0.1
Cyp26b1	0.610 ± 0.09	0.5 ± 0.025
Cyp26c1	0.383 ± 0.22	

Relative expression levels of Cyp26 genes compared to wild type (value=1.0) by RTQ-PCR. From Array 1: RTQ-PCR on RNA extracted from dissected pharyngeal region of E9.5 *Tbx1* functional null embryos (compound heterozygotes, *Df1:Tbx1*$^{-/-}$) embryos as compared to wild type at E9.5 carried out on the Cepheid SmartCycler or ABI 7000 (corrected for GADPH expression, mean of at least three separate experiments, ± standard deviation). This work was carried out by Dr Sarah Ivins (Ivins et al., 2005). From Array 2: RTQ-PCR on RNA extracted from *Tbx1*$^{+/lacz}$ and *Df1*$^{/+}$*;Tbx1*$^{lacz/lacz}$) FACS-Gal-sorted pooled cell populations carried out on the ABI PRISM 7000 Sequence Detection System (corrected for GADPH expression, mean of at least three separate experiments, ± standard deviation). These experiments were performed by Dr. Kelly Lammerts van Bueren (Lammerts van Bueren, 2008; van Bueren et al., 2010)

3.1.2 *Cyp26* genes are co-expressed with *Tbx1* in wild-type embryos

Cyp26 and *Tbx1* expression domains have been described broadly in the Introduction. According to published expression patterns between E9.5 and 10.5, *Cyp26a1* is co-expressed with *Tbx1* in the otic vesicle, peri-otic mesenchyme and in head/pharyngeal mesenchyme and first pharyngeal arch epithelium (Chapman et al., 1996; de Roos et al., 1999; Fujii et al., 1997; MacLean et al., 2001; Merscher et al., 2001; Vitelli et al., 2002a). Previously reported data for *Cyp26b1* suggests there is overlapping expression with *Tbx1* in the pharyngeal ectoderm and endoderm from E9.0 (MacLean et al., 2001; Zhang et al., 2005). *Cyp26c1* expression correlates with many *Tbx1* expression domains, including head and pharyngeal mesenchyme and the endoderm, ectoderm and mesodermal core of PA1 and 2 from E8-9.5. However, by E10.5 *Cyp26c1* expression is restricted to a small region of expression ventral to the pontine flexure and the ventral part of the maxilla (Tahayato et al., 2003).

3.1.3 Altered *Cyp26* expression domains in *Tbx1* null mutant mice.

In *Tbx1*$^{-/-}$ embryos at E10.5 expression of *Cyp26a1* in the pharyngeal region was found to be considerably decreased by in situ hybridization compared to stage-matched wild type embryos, confirming the microarray and PCR results (Fig.3.1A.) (Guris et al., 2006; Ivins et al., 2005; Roberts et al., 2006). Transverse sections showed that the areas of reduced expression were peri-otic/pharyngeal mesenchyme, including neural crest cells for cranial ganglia V, VII/VIII and IX/X (Fig.1B., 1C.). *Cyp26a1* was unaffected in the tailbud region which does not normally express *Tbx1* (not shown).

As with *Cyp26a1*, expression of *Cyp26b1* was altered in *Tbx1*$^{-/-}$ embryos. Whole-mount in situs showed reduced expression in the pharyngeal arches of *E9.5 Tbx1* mutant embryos, whereas hindbrain expression appeared unaffected (Fig.3.1D.). More specifically, coronal sections showed a loss of *Cyp26b1* expression from the caudal portion of the pharyngeal endoderm and an anterior shift in the ectodermal expression in the mutants (Fig.3.1E.). The alteration in *Cyp26b1* expression in the mutants therefore appeared more complex than simple down-regulation in the absence of *mTbx1*.

In situ hybridization for *Cyp26c1* in *Tbx1* null embryos revealed dramatic expression changes. In addition to a complete loss of expression in the peri-otic mesenchyme (including neural-crest derived mesenchyme), otic vesicle, lateral epibranchial placodes and caudal pharyngeal endoderm there was an expanded domain of expressing cells in the first arch mesenchyme (Fig.3.1F-I). Expression in the hindbrain and maxillo-mandibular cleft was unchanged. Thus, as for *Cyp26a1*, altered *Cyp26c1* expression was seen in both *Tbx1* and non-*Tbx1*-expressing tissues, whereas changed expression of *Cyp26b1* was only observed in *Tbx1*-positive tissues, implying a non-cell autonomous role for *Tbx1* in the control of *Cyp26a1* and *c1* but not *b1*.

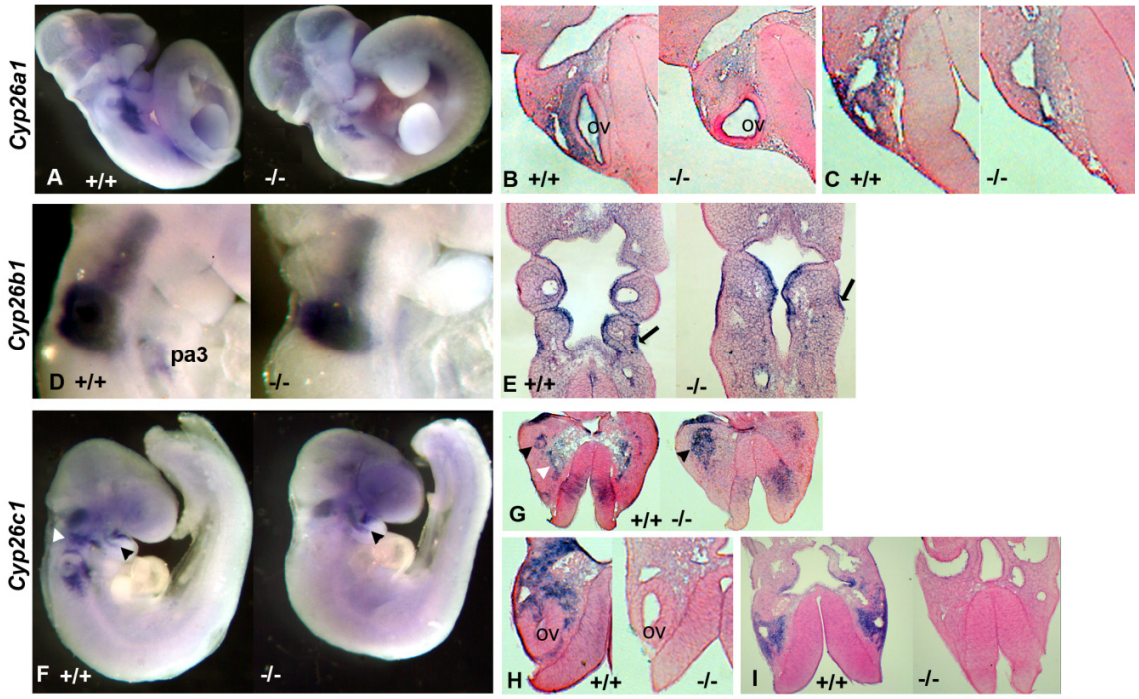

Figure 3.1 In situ hybridization results showing down-regulated/altered expression of *Cyp26a1*, *b1* and *c1* in *Tbx1* null embryos compared to wild type at E9.5.

A, D, F; whole mount in situ for *Cyp26a1*, *bl* and *c1* respectively. (B) and (C) Transverse sections show reduced expression of *Cyp26a1* in facio-acoustic and glossopharyngeal-vagal neural crest cells respectively. (D,E) Reduction of *Cyp26b1* expression in the caudal pharyngeal endoderm of Tbx1-/- E9.5 embryos is accompanied by an anterior shift in ectodermal expression (arrows in E, coronal sections). (F-I) *Cyp26c*1 expression in E9.5 in *Tbx1*$^{-/-}$ and wild type embryos. Black arrowheads in F and G (transverse sections) indicate the region of first arch mesenchymal expression which is expanded in the mutants, white arrowheads (G) indicate epibranchial placode expression which is lost in the mutants. (H, I) Transverse sections show loss of staining in peri- and post-otic mesenchyme as well as in otic vesicle and pharyngeal endoderm in *Tbx1*$^{-/-}$ embryos PA2, PA3; second and third pharyngeal arch, pe; pharyngeal endoderm, p; pharynx, ov; otic vesicle. From (Roberts et al., 2006). These experiments were performed by Dr Sarah Ivins.

3.1.4 R115866, an inhibitor of Cyp26 enzyme function

The initial discovery of significantly altered expression of all three *Cyp26* genes in conjunction with the ectopic shift in *Raldh2* expression and increased RARE-lacZ reporter activity in *Tbx1*$^{-/-}$ embryos (Guris et al., 2006; Ivins et al., 2005) suggested dysregulation of RA control pathways in *Tbx1* null mice. This led to the hypothesis that *Cyp26* family

knockdown might recapitulate some aspects of 22q11DS. Rather than initially taking a single or multiple allele loss-of function approach in the mouse, which would likely be expensive and time-consuming, the experimental direction chosen harnessed the ease of application of chemical agents in the chick embryo, using a chemical inhibitor of Cyp26 enzyme function, R115866. R115866 (B)-N-[2-ethyl-1-(1H-1,2,4-triazol-1-yl)butyl]phenyl]-2-benzothiazolamine) was originally designed with a view to enhancing RA treatment of skin cancers. It has previously been identified as a potent and selective inhibitor of Cyp26 retinoic acid metabolism (Stoppie et al., 2000). In vitro, it has been shown to be a nanomolar inhibitor of Cyp26-dependent RA conversion (IC_{50} =4nm). While no compound is totally specific, the selectivity for Cyp26 in particular is evidenced by trivial inhibition of other Cyp-dependent synthesis of estradiol and testosterone (micromolar concentrations of R115866 are required to inhibit Cyp19, Cyp 17, Cyp 2c11, Cyp3a and Cyp2a1). In vivo, oral administration of R115866 to adult rats resulted in raised levels of RA in plasma, skin, fat, kidney and testis. R115866 also reproduces known retinoidal effects including vaginal keritanization, induction of epidermal hyperplasia and epidermal transformation and up-regulation of *Cyp26* mRNA expression in rat liver. These effects can all be reversed by administration of retinoic acid receptor antagonists suggesting that R115866 inhibition of Cyp26 results in an increased availability of endogenous RA (Stoppie et al., 2000).

Using the chick as model system permitted titration of the developmental effects of different concentrations of R115866 and because the compound can be added at any point in development also circumnavigated any gastrulation phenotypes by treating embryos at stages roughly equivalent to E8 in the mouse. In addition, knock-down of all Cyp26 function circumvented issues of redundancy.

3.2 Results

3.2.1 Loss of pharyngeal arches in R115866 treated chick embryos phenocopies the *Tbx1* null mouse mutant

Embryos treated with a high dose of R115866 at stage 10 or 14 and cultured for a further 24-48 hours displayed a variety of externally visible defects including decreased head mesenchyme, smaller otic vesicles and loss of pharyngeal arches (PA), loss of anterior tissues such as the forebrain and heart defects such as abnormal looping and pericardial oedema (Fig.2). Many of these defects are phenocopied in *Tbx1* null mice and embryos treated with excess RA. Severity varied from embryo to embryo, with some displaying all these phenotypic characteristics, whereas others were normal apart from the loss of caudal pharyngeal arches. In common with the *Tbx1* null mouse the caudal arches were the more severely affected; most embryos retained pharyngeal arch 1 and a rudimentary arch 2 was sometimes visible but pharyngeal arches 3 and 4 were rarely seen in treated embryos (Fig.3.2A. and B.). Analysis of histological sections of these embryos also reflected the phenotypic range. The majority of embryos had at least some form of pharyngeal arch 1 and the accompanying pharyngeal arch artery 1 (Fig.3.2B3., B4., B8-10.), although in the most severe embryos no other pharyngeal arches could be distinguished (Fig.3.2B5.). In slightly less severe embryos, hypoplastic remnants of pharyngeal arches 2 and sometimes 3 were also visible, but the segmentation of the pharyngeal pouch endoderm was essentially lost (Fig.3.2B3., B4., B8-10) as compared to controls (Fig.3.2B1., B2., B6., B7.). Asymmetry in the formation of the bilaterally paired pharyngeal tissues was also sometimes apparent (Fig.3.2B4., B8-10.). Embryos with the very mildest phenotypes did occasionally form more caudal pharyngeal arches 3 and 4, but these were hypoplastic, abnormally shaped and contained extremely small non-patent pharyngeal arch arteries (Fig.3.6).

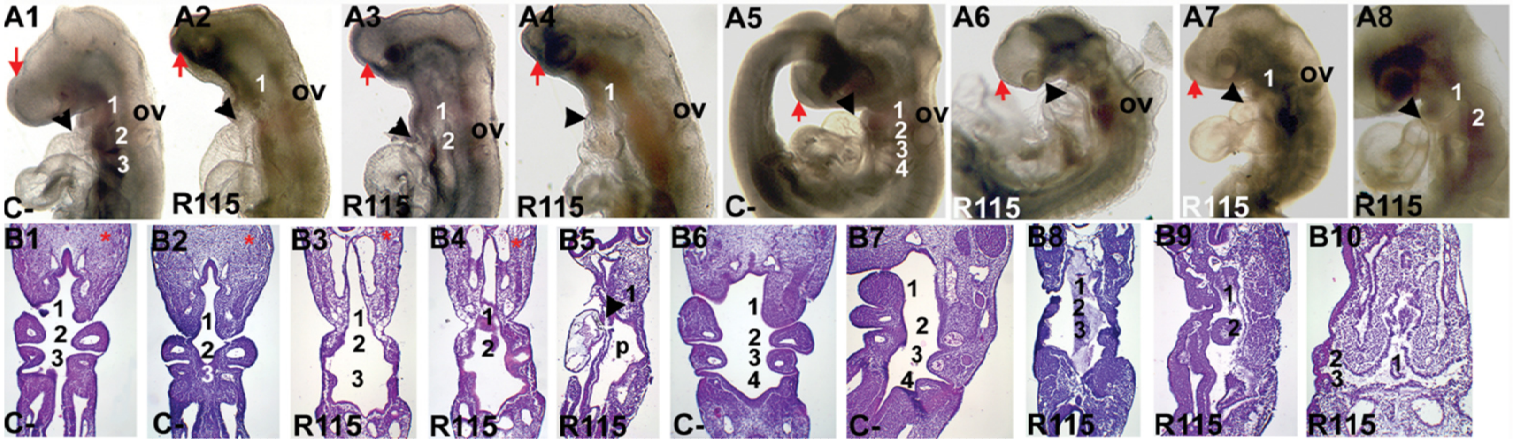

Figure 3.2 Abnormal head and pharyngeal development in R115866-treated embryos

Phenotype of stage 10 chicken embryos treated in ovo with a high dose of R115866 and cultured for either 24 hours (A1-A4) or 48 hours (A5-A8) further. In all panels control embryos are labelled C- and R115866-treated embryos with R115. (A1-A8) R115866-treated embryos have impaired caudal pharyngeal arch development, small otic vesicles (ov), shorter straighter outflow tracts and reduced tissue anterior to the eye (red arrows) (A2-A4, A6-A8). Numbers identify the appropriate pharyngeal arch, black arrowheads point to the outflow tract of the heart. (B1-B8) Coronal sections through embryos treated at stage 10 and cultured for 24hours (B1-B5) or 48 hours (B6-B10).

3.2.2 Abnormalities of neuroepithelial tissues in R115866 treated embryos

Other tissues affected by R115866 treatment included the otic vesicle which showed an overall size reduction in many cases and was narrower in others (Fig.3.3A1.-A4. and Fig.3.4C3.-C6.). Neuroepithelial development was also affected; abnormal folding of the neuroepithelium was seen, more commonly rostral to the spinal cord and failure of neural tube closure was also observed (Fig.3.3A4.-A7.). More caudally the pseudostratified columnar epithelial nature of the neural tube was disrupted by what appeared to ectopic tissue of a mesenchymal nature which caused breaks in the integrity of the neural tube (Fig.3.3A8.,A 9. and Fig.3.4C3.).

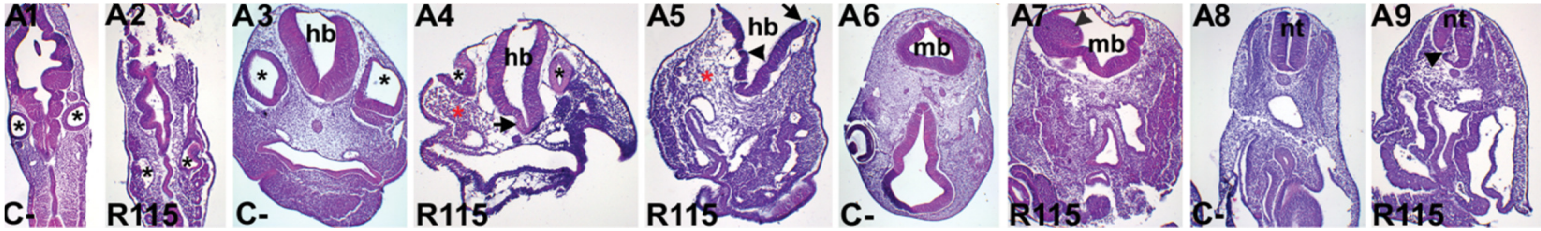

Figure 3.3 Abnormal development of the CNS and sensory organs in R115866-treated embryos

(A1-A9) Neuroepithelial phenotypes 24 hours after treatment. Coronal sections at the level of the hindbrain show small misshapen otic vesicles (*) in R115866 embryos (A2) compared to controls (A1). (A3-A9) Transverse sections also show this otic vesicle (*) phenotype (A4) as well as misshapen neural tubes (arrow in A4 and arrowhead in A5 and A7) and failure of the neural tube to close (arrow in A5). Head mesenchyme (red *) is also reduced. More caudally neural tube pseudostratified epithelial morphology breaks down and ectopic mesenchymal cells cause breaks in the integrity of the neural tube (arrowhead A9). Hb; hindbrain, mb; midbrain, nt; neural tube

3.2.3 Altered early cardiac development in R115866 treated embryos

Cardiac development in treated embryos was compromised; twenty-four hours after treatment, affected embryos appeared to have much shorter and straighter outflow tracts than in controls, with the distal OFT being particularly affected (Fig.3.2A1.-A8., Fig. 3.4A1.-A10.). Cardiac looping was reduced in these treated embryos as a consequence (Fig.3.A1.-A10., Fig.3.4C1.-C6.) and there appeared to be reduced ballooning of the ventricular chambers. The inner curvature of these hearts reflected this, appearing deeper and more perpendicular than in controls twenty-four hours after R115866 treatment (Fig.3.4B1.-B4.).Forty-eight hours after treatment the inner curvature appeared smaller in treated embryos than in controls (Fig.3.4B5., B6.). The myocardial trabeculation of the ventricular chambers also seemed to extend more cranially in some of these embryos (Fig.3.4B5., B6.). It was also noted that the caudal movement of the OFT was altered, with the OFT often remaining much more cranial and exiting the body just below pharyngeal arch 1, probably as a consequence of the loss of caudal pharyngeal structures (Fig.3.2.A1.-A8., Fig.3.4D1.-D5.). Territory encompassing the secondary heart field including the splanchnic mesoderm underlying the caudal pharynx was also dysmorphic, appearing to be thinner and more disorganized in R115866 embryos. The distinctive pseudostratified columnar morphology, described by Waldo and colleagues (Waldo et al., 2005b), as part of the secondary heart field which is continuous with the splanchnic mesoderm and outflow tract myocardium, was not identifiable, with cells having a more general mesenchymal appearance (Fig.3.4E1., E2.)

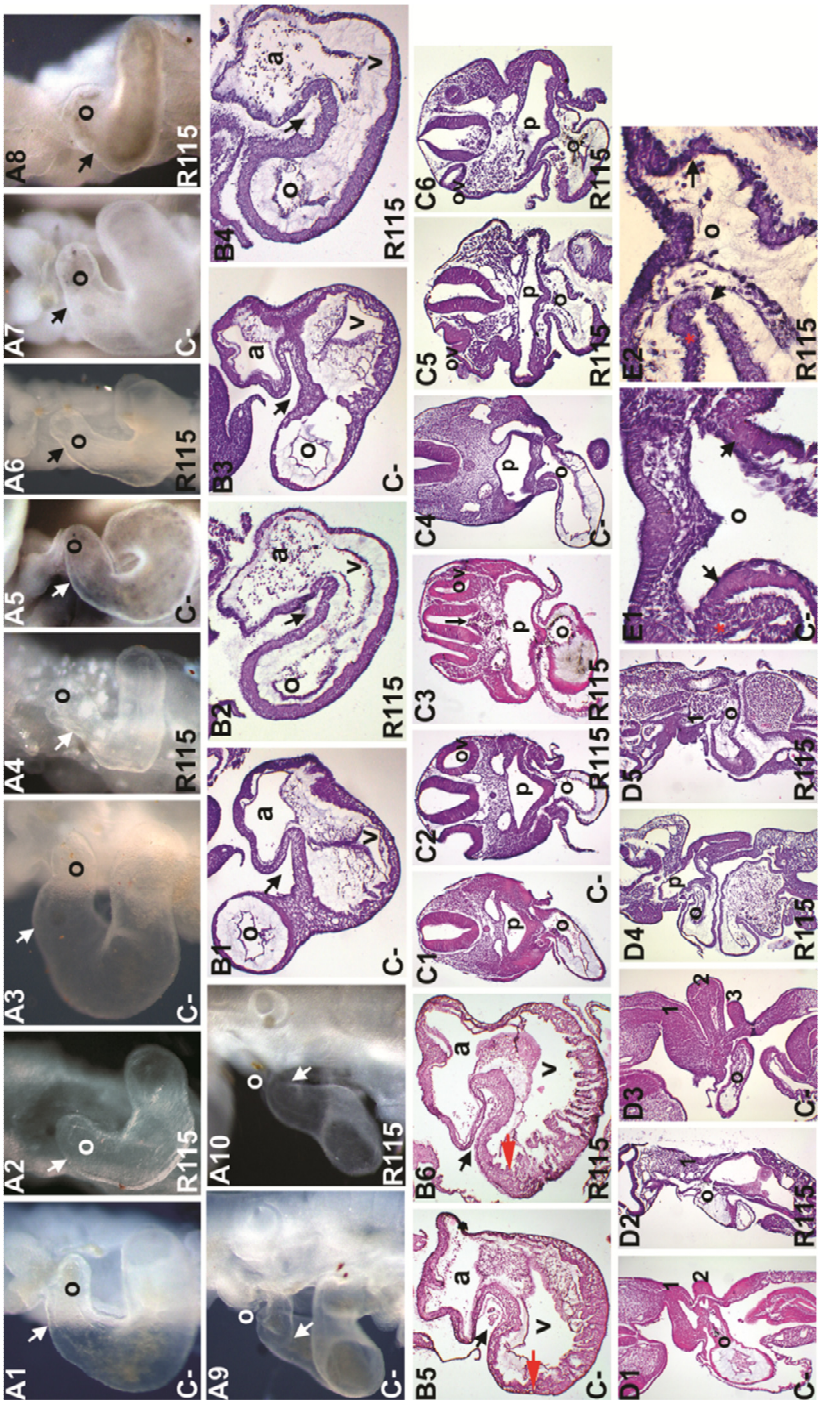

Figure 3.4 Abnormal cardiac development in R115866 treated embryos

(A1-A8) Ventral views of the outflow tract and hearts from embryos treated at stage 10 and cultured for 24 hours (A1-A6) or 48 hours (A7, A8). (A9, A10) Side-views of the outflow tract and heart 24 hours after treatment. In R115866-treated hearts the outflow tract (o) is shorter and straighter than in controls and rightward looping is reduced (arrows A1-8). Arrows in A9 and A10 indicated reduced length of distal outflow tract.(B1-B6) Transverse sections through the heart,

showing alterations in inner curvature and chamber differentiation 24 hours (B1-B4) and 48 hours (B5, B6) after treatment. The inner curvature (arrows) of treated hearts appeared deeper and more perpendicular than controls after 24 hours culture, possibly due to reduced ballooning of the ventricular chamber (v). After 48 hours of culture the inner curvature of treated embryos was much reduced in size and myocardial trabeculation extended higher in the ventricle of R115866 embryos than in controls (compare position of red arrows in B5 and B6).a; atrial chamber, o; outflow tract.(C1-C6) Transverse sections through the aortic sac/distal outflow tract 24 hours (C1-C3) and 48hours (C4-C6) after treatment, showing the shorter straighter outflow tract (o) with reduced rightward looping in R115066 embryos (C2, C3, C5, C6) compared to controls (C1, C4).Arrowhead in C3 indicates ectopic mesenchymal cells within the floorplate. The otic vesicles in R115866 embryos are often abnormally small and misshapen (C3, C5 and C6) and were visible only in R115866 sections at the level of the outflow tract because of the abnormally anterior position of the outflow tract resulting from the loss of caudal pharyngeal arch arteries. (D1-D5) Coronal sections through the outflow tract and pharyngeal arches. Control embryos 24 hours (D1) and 48 hours after culture (D3) show the pharyngeal arch arteries emptying into the aortic sac/outflow tract (o) at the level of pharyngeal arch artery 2 and 3 respectively. In time matched R115866 embryos the outflow tract joins body at the level of pharyngeal arch artery 1 as caudal pharyngeal arches fail to form (D2, D4, D5). (E1, E2) High power photographs of the secondary heart field 24 hours after treatment. The splanchnic mesoderm (red *) is thinner and less organized and the pseudostratified columnar epithelial layer morphology (arrows) was not apparent in R115866 embryos (E2) compared to controls (E1).

3.2.4 R115866 prevents caudal pharyngeal arch artery formation

In *Tbx1* null mice the pharyngeal arch arteries (PAA) posterior to PAA1 are not formed. Embryos were given either R115866 in ethanol or the equivalent volume of ethanol alone at st10 *in ovo* and cultured for a further 24-48 hours to stages 14-18, when they were injected with Indian ink to visualize the pharyngeal arch arteries. The results are presented in Table 3.2. Two-thirds of control embryos examined had clearly formed patent pharyngeal arch arteries 2, 3 and 4 (n=25/40) (Fig.3.5E.). A further third of control embryos which appeared slightly younger had well-formed patent PAA 2 and 3 alone (n=12/40) (Fig.3.5A.). Many of the R115866-treated embryos (n=40) exhibited elements of RA teratogenesis as well as disruption/loss of pharyngeal arch formation (n=33/40). In 45% of these embryos (n=15/33) ink injections and sections showed that no PAA formation had taken place. In a further 18% (n=6/33) formation of PAA1 had been

attempted on at least one side of the embryo and in the remaining 36% of embryos PAA1 formation was seen after ink injection (n=12/33) (Fig3.5B.-D., F.). However, 17.5% of all R115866-treated embryos (n=7/40) had a much milder phenotype and did not display any sign of general RA teratogenicity; these embryos retained some form of PA1 but had missing pharyngeal arches caudal to PA1 (Fig.3.5C., G.). All of these embryos had also failed to form caudal pharyngeal arch arteries; 86% (n=6/7) had formed PAA1 alone and one embryo had formed PAA2 on one side in addition to PAA1 (Fig.3.5H.). The phenotype of these embryos was reminiscent of *Tbx1* null mice which also form only PAA1 normally. Using Fishers exact probability test results showed that pharyngeal arch artery abnormalities resulting from R115866 treatment when compared to controls were statistically significant at $P<3x10^{-8}$

Table 3.2. Pharyngeal arch arteries fail to form in R115866-treated embryos.

R115 treatment	$5x\ 10^{-7}$M (high dose)		Et0H C-
RA teratogenicity	yes	no	no
PAA1-4 L+R	0	0	25
PAA 1-3 L+R	0	0	12
No PAA	15	0	0
PAA1 L/ R only	6	0	0
PAA1 L+R	12	6	0
PAA1 L+R, PAA2 L/R	0	1	0
Total	33	7	0
Total /treatment	40		37

Pharyngeal arch artery patency in st 14-18 chick embryos after 24-48h culture with a high dose R115866 in ethanol compared with control embryos given ethanol alone. PAA:pharyngeal arch artery, L:left side of embryo, R:right side of embryo. RA teratogenicity means that embryos had other developmental defects in addition to those affecting the pharyngeal arch system; in particular rostral or caudal truncation or an oedemic heart.

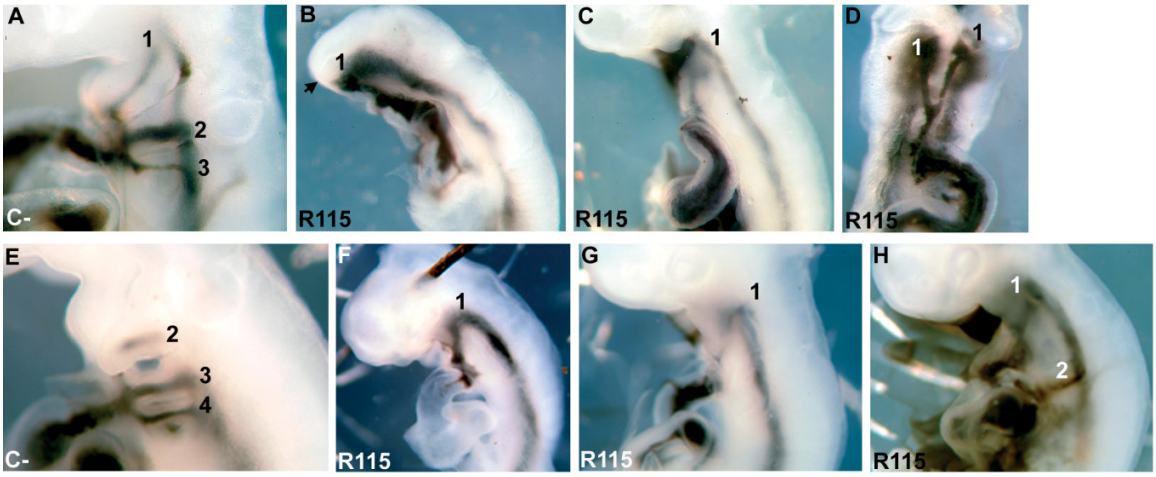

Figure 3.5 Pharyngeal arch arteries are lost/reduced in size and patency in R115866-treated embryos.

(A-H) Ink injections into the pharyngeal arch arteries (PAA) to show patency. Twenty-four hours after R115866 treatment at stage 10 control embryos (A) have patent PAA1-3 and after forty-eight hours patent PAA1-4 (E). R115866 embryos generally only have a patent PAA 1 (B,C side view; D ventral view). Forty-eight hours after treatment PAA 4 is patent in controls (E) whereas only PAA1 (F,G) and sometimes PAA2 (H) remain patent in R115866-treated embryos

3.2.5 Loss of vascular smooth muscle in PAA and OFT of R115866-treated embryos

Vascular smooth muscle (VSM) has been shown to be lacking in the 4th pharyngeal arch arteries of *Tbx1* heterozygous embryos in which they are reduced in size and patency (Lindsay and Baldini, 2001). *Tbx1* null mice fail to form arch structures including PAA below PA2. The majority of R115866 –treated chick embryos also failed to form caudal arch structures including patent pharyngeal arch arteries as described above. Those embryos which were less affected by R115866 were examined for the presence of VSM by immunohistochemistry for smooth muscle α-actin (SMA) to see if the loss of VSM could be contributing to the loss of pharyngeal arch arteries in these embryos. Treated embryos with the least affected pharyngeal phenotype were selected for staining. Some of these embryos had attempted to form hypoplastic abnormally shaped pharyngeal arches 3 and 4. However, even in these less affected embryos arch artery size was reduced compared to controls. Staining for smooth muscle actin revealed that expression around the pharyngeal arch arteries and the carotid arteries was reduced relative to untreated

embryos, although expression remained high in the dorsal aorta. The number of SMA-positive cells surrounding the arch arteries appeared reduced as compared to controls. Lack of these cells probably contributes to the small pharyngeal arch artery phenotype observed in R115866-treated embryos (Fig.3.6A.-F.). The secondary heart field has been shown to express αSMA22 and to contribute cells to the vascular smooth muscle the base of the great vessels as well as OFT myocardium (Waldo et al., 2005b). This region was examined in R115866-treated embryos, and again diminished numbers of αSMA22-positive cells were found (Fig.3.6G.-I.). These cells could either be SHF cells or possibly αSMA22 neural crest-derived cells which also contribute to the smooth muscle of the arterial pole (Waldo et al., 2005a; Waldo et al., 2005b). Secondary heart field markers *Islet-1* and *Mef2c* were also widely down-regulated in R115866-treated embryos, with loss of expression including that of the pharyngeal mesoderm and outflow tract (Fig.3.6J-M.).

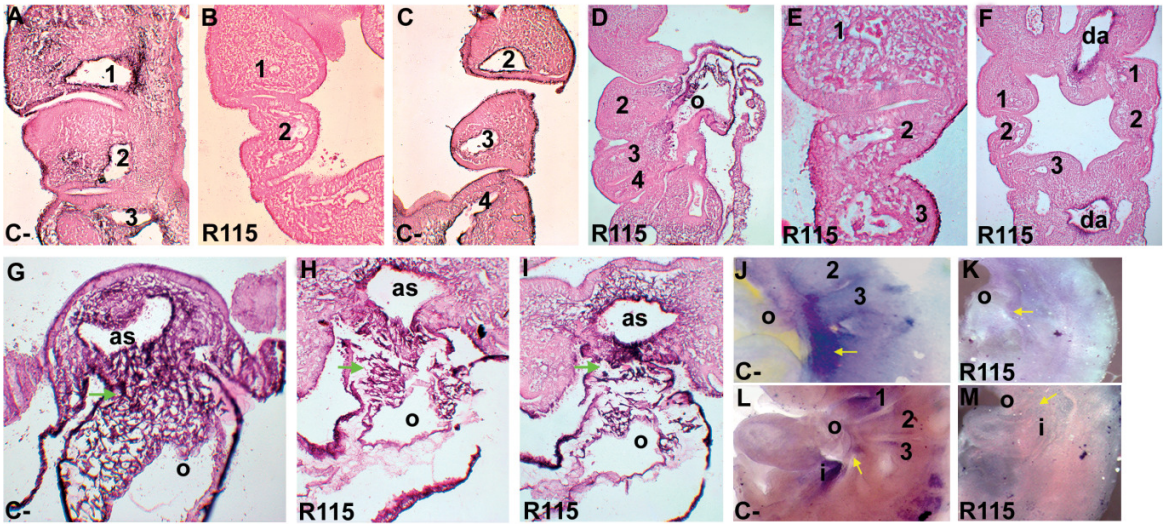

Figure 3.6 Abnormal vascular smooth muscle staining in R115866-treated embryos.

(A-I) Coronal sections stained for smooth muscle actin as a marker of vascular smooth muscle cells. Strong staining in these cells lining the pharyngeal arch arteries was seen in control embryos at 24(A) and 48 (C) hours after treatment. Arch arteries were frequently small and non-patent with very few smooth muscle actin-positive cells present at both 24 (B) and 48 (D-F) hours after treatment. In contrast, strong smooth muscle actin staining was visible in the dorsal aorta (F). The secondary heart field and the outflow tract myocardium and is positive for smooth muscle actin staining (G). Sections through this region revealed many fewer positive cells both in the outflow tract and around the aortic sac(green arrows) (H, I). Secondary heart field markers *Islet-1* (J, K) and *Mef2c* (L, M) were also down-regulated in R115-treated embryos (K, M) compared to controls

(J,L). Yellow arrows indicate ventral pharyngeal mesoderm. Numbers indicate the appropriate pharyngeal arch artery, as; aortic sac, i; inflow tract, o; outflow tract, da; dorsal aorta.

3.2.6 Low dose R115866 produces common arterial trunk and aberrant aortic arch artery patterning in chick embryos.

3.2.6.1 Great Vessel remodelling defects in R115866-treated embryos

Embryos given lower doses of R115866 could be cultured for much longer than high dose embryos which generally died by E5 at the latest. The external development of the heart and great vessels was examined by ink injection at E8+. Seventeen of thirty-two surviving R115866-treated embryos (53%) exhibited abnormalities in development of the cardiac outflow tract and/or PAA derivatives. Five embryos (29%) had a small brachiocephalic artery (BCA) compared to controls. Four of those affected had a reduced right BCA and one had a reduced left BCA. In some of the embryos with a small right BCA the branch point of the right subclavian artery (RSCA) appeared to be lower than normal (Fig.3.7A1.-A5.). Defects in alignment of the great vessels, and outflow tract and/or ventricular size/shape were seen in the majority of these 17 embryos. 15 of 17 embryos with cardiac anomalies were otherwise normal on external observation. In two embryos with heart defects craniofacial malformations were also seen. Similarly, in a *Tbx1* allelic series the pharyngeal arch artery and outflow tract derivatives are more dose-sensitive than craniofacial tissues (Hu et al., 2004). None of the 64 control embryos examined appeared to have cardiac or other anomalies on external inspection. All 17 R115866-treated embryos with vascular defects were sectioned. Poor section quality led to the exclusion of two of these from further analysis.

3.2.6.2 Peri-membranous ventricular septal defects in R115866-treated embryos

One of the 15 R115866-treated hearts had normal morphology, but the remaining 14 hearts all displayed ventricular septal defects (VSD) of varying type; 11 of these had a peri-membranous and doubly committed juxtarterial VSD, a type classically associated

with 22q11 deletion syndrome patients (McCarthy et al., 2000) and references therein) and also seen in mice carrying *Tbx1* mutant alleles (Jerome and Papaioannou, 2001; Lindsay et al., 1999; Lindsay et al., 2001; Merscher et al., 2001). This type of VSD extends onto the membranous portion of the ventricular septum. There is also failure of the formation of the subpulmonary infundibulum with which it would normally fuse and consequently the VSD is related to both of the valves of the aorta and pulmonary trunk which form the roof of the defect (Fig.3.7C1.-C5.). In three embryos reduced size of one of the brachiocephalic arteries was seen in conjunction with the VSD (Fig.3.7B1.-B3.).

3.2.6.3 Common arterial trunk and double outlet right ventricle in R115866-treated embryos

Three embryos were more severely affected, in that they all exhibited common arterial trunk (CAT), in which there is failure of septation of the outflow tract not only below the level of the arterial valves (PM-VSD) but also at the level of the valves and above so that there is a common valve and arterial trunk (Fig.3.7D1.-D5.). This defect is also a feature of 22q11 deletion syndrome and the *Tbx1* homozygous null mouse (Conley et al., 1979; Jerome and Papaioannou, 2001; Lindsay et al., 1999; Lindsay et al., 2001; Merscher et al., 2001; Wilson et al., 1992). One of these embryos had a brachiocephalic artery of reduced size and another exhibited abnormal craniofacial development. Two embryos with PM-VSD were also found to have double outlet right ventricle (DORV), in which both the aorta and pulmonary trunk exit from the morphologically right ventricle. In these cases with the great arteries were in the normal spiral relationship to each other (Fig.3.7E2.). Three of 14 embryos had morphologically distinct septal defects; one embryo had a subaortic VSD, where the VSD is more closely related to the aortic valve than the pulmonary valve. This embryo also had a double outlet right ventricle, this time with the great arteries in an abnormal parallel arrangement relative to each other (Fig.3.7E4.). DORV, an outflow tract alignment defect, is thought to be the result of insufficient looping and rotation and remodeling of the inner curvature of the heart (Gittenberger-de-Groot et al., 2005) and is also found in 22q11DS patients and *Tbx1* mice

null for a hypomorphic allele which transcribes a low level of *Tbx1* (estimated to be about 25%) of normal levels (Hu et al., 2004; Xu et al., 2004)

3.2.6.4 Atrioventricular septal defects in R115866-treated embryos

Two embryos had an atrioventricular septal defect with failure of fusion of the atrioventricular cushions and both also had a common arterial trunk i.e. failure of OFT cushion fusion (Fig.3.7F1., F2.). In both of these embryos the positioning of the heart was not normal with one embryo having ectopia cordis. This embryo also had a thin ventricular wall with disorganized myocardium and an abnormal ventricular shape. The atrial wall was also thicker than normal and disorganized.

3.2.6.5 Low level of endogenous defects in control hearts

Of the nine control hearts also sectioned, seven were normal and two abnormal. Using Fishers exact probability test indicated the incidence of cardiovascular defects resulting from R115866 treatment versus ethanol carrier was statistically significantly greater with a P value of 0.00075. These data are summarized in Table 3.3.

Table 3.3 22q11-deletion syndrome-like heart phenotypes in R115866-treated embryos

Phenotype	R115866-treated embryos	Control embryos
Normal	1	7
PM-VSD only	3	1
PM-VSD+small BCA	3	0
PM-VSD+ CAT	2	1
PM-VSD+ small BCA+CAT	1	0
PM-VSD+DORV	2	0
Subaortic VSD+DORV	1	0
AVSD+CAT	2	0
Total	15*	9*

Comparison of heart phenotypes at E8 in chick embryos treated with a low dose of R115866 in ethanol at st10 with controls given an equivalent dose of ethanol alone. PM-VSD=perimembranous ventricular septal defect, small BCA= small size of brachiocephalic artery, cat=common arterial trunk, DORV=double outlet right ventricle, subaortic VSD=subaortic ventricular septal defect and AVSD= atrioventricular septal defect. * $P<0.0008$ statistically significant using Fishers exact probability test.

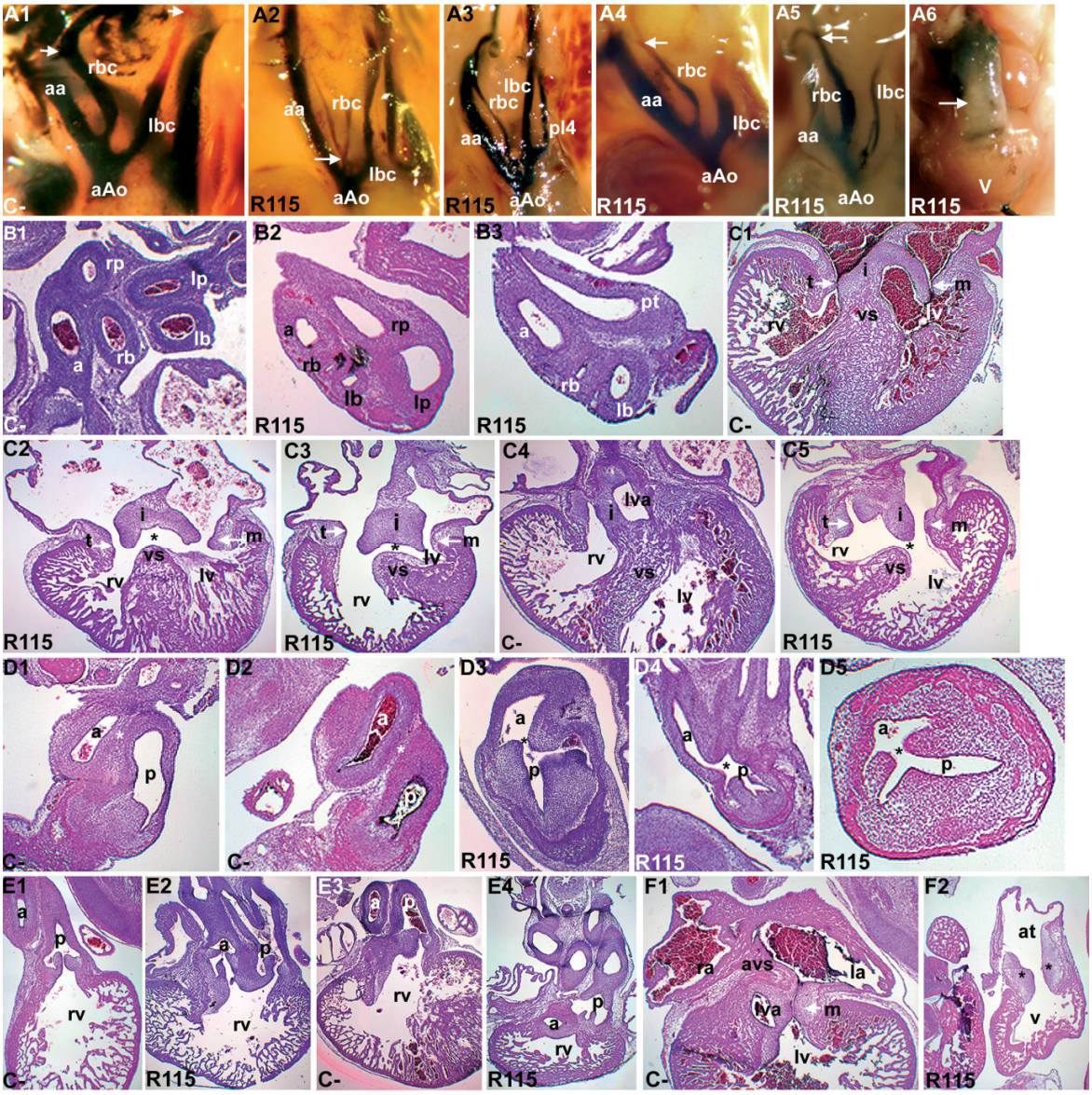

Figure 3.7 Low doses of R115866 produce 22q11 deletion syndrome-like heart phenotypes at E8+.

(A1-A6) Ink injections showing great vessel abnormalities in R115866 treated embryos. The right brachiocephalic artery (rbc) arising from the aortic arch (aa) can be reduced in size (A2-A4) compared to controls (A1) as can be the left brachiocephalic artery (lbc) (A5). The branch point of the right subclavian artery (white arrow) off the right brachiocephalic artery was also low in some cases (A2) and a persistent left fourth arch artery was also seen (A3). aAo; ascending aorta. (A6) External appearance of a heart with common arterial trunk. White arrow indicates no clear separation of the aorta and pulmonary trunk. v; ventricles. (B1-B3) Transverse sections through the great vessels showing reduced size of both the right (B2, B3) and left (B3) brachiocephalic arteries compared to controls (B1). (C1-C5) Transverse sections through the ventricular septum

(vs) and inferior atrioventricular cushions (i) showing perimembranous doubly committed juxtarterial ventricular septal defects (*) in R115866-treated embryos (C2, C3, C5) as compared to controls (C1, C4). (D1-D5) Sections showing the failure of formation of the aorticopulmonary septum (*) which forms normally in controls (D1, D2) resulting in common arterial trunk in R115866 embryos (D3-D5). (E1-E4) sections showing mal-alignment of the great vessels with their respective ventricles. The aorta and pulmonary trunk both exit from the right ventricle(rv) (double outlet right ventricle) in R115966 embryos(E2, E4) whereas only the pulmonary trunk does so in normal controls (E1, E3).Control embryo (F1) and developmentally delayed abnormal embryo (F2) with an atrioventricular(AV) septal defect due to failure of formation of AV septal structures and fusion of AV cushions (*). a;aorta, at; atrial chamber, avs; atrioventricular septum, p; pulmonary trunk, lva; left ventricular aortic outlet, m; mitral valve, la; left atrium, lv;left ventricle, ra; right atrium, rv; right ventricle, t;tricuspid valve, v; ventricular chamber.

3.2.7 Molecular markers reveal altered gene expression and morphogenesis in the pharyngeal endoderm and modified expression of RA-responsive genes

To examine whether blocking Cyp26 function was raising endogenous RA levels as anticipated the expression of a number of genes suggested either to be targets of *Tbx1*, RA, or in some cases both was examined. Embryos in which Cyp26 function had been blocked by a high dose of R115866 at st10 and followed with 24-48h culture were used for these experiments.

3.2.7.1 Pax9: a pharyngeal endoderm marker in R115866-treated embryos

In the *Tbx1*$^{-/-}$ mouse one of the major tissues affected is the pharyngeal endoderm. A number of genes normally expressed in this tissue are down-regulated in the *Tbx1* null embryos. One of these is *Pax9*, a molecular marker for the endoderm of the pharyngeal pouches (Ivins et al., 2005). *In situ* hybridization in the chick revealed that the organization of these structures was badly disrupted by Cyp26 inhibition. As in *Tbx1*$^{-/-}$ embryos the caudal pouches were the worst affected. Expression of *Pax9* in the endoderm was apparent at the expected anterior-posterior level, albeit sometimes at reduced levels, but the organization of the endoderm into the segmented regular loops of the pouches was almost entirely lost. A structure approximating to pouch 1 was often apparent and in some

embryos there was an attempt to form pharyngeal pouch 2. However, in the majority of embryos the organization of the pharyngeal pouches was non-existent posterior to pouch 1 in a fashion reminiscent of *Tbx1* null embryos at equivalent developmental stages (Fig.3.8A1.-A11.). However, *Pax9* expression was maintained in the endoderm in the absence of pharyngeal pouch segmentation (Fig3.8A1-A11.), suggesting that Cyp26 function as an RA sink is more important for the segmentation of pouch endoderm than induction or maintenance.

3.2.7.2 Fgf8: a pharyngeal endoderm marker and Tbx1 target in R115866-treated embryos

Tbx1 is known to be able to regulate the expression of *Fgf8* and $Tbx1^{+/-}$:$Fgf8^{+/-}$ mouse embryos have a higher penetrance of cardiac defects than $Tbx1^{+/-}$ mutants alone (Hu et al., 2004; Vitelli et al., 2002b). In the pharyngeal tissues the results with *Fgf8* were similar to those seen with *Pax9*. In some more severely affected embryos, pharyngeal expression was nearly completely lost although expression in the forebrain and midbrain/hindbrain boundary was maintained (Fig.3.8B.3). However, in others expression in the pharyngeal endoderm was present in pouches 1 and 2 but lost more caudally, and those pouches still expressing *Fgf8* seemed dysmorphic (Fig.3.8B1., B2. And B4., B5.). Thus it seems that in some R115866-treated embryos, not only was endodermal pouch segmentation affected, but endodermal marker expression was also lost. Additionally, in many of these embryos the expression domain in the branchial groove ectoderm was appreciably closer to the most anterior pharyngeal endoderm expression, suggesting loss of tissue in pharyngeal arch 1 (Fig.3.8B1.-B5.).

3.2.7.3 Tbx1 is itself down-regulated in R115866-treated embryos

Tbx1 itself provides a good marker for non-neural crest pharyngeal tissues and has also been shown to be reduced in the presence of exogenous RA (Roberts et al., 2005; Zhang et al., 2006a). In most R115866-treated embryos both the spatial domain and intensity of *Tbx1* expression was reduced in both pharyngeal endoderm and mesoderm, the

secondary heart field and the otic vesicle and the remaining expression reflected the disorganization and abnormal development of the pharyngeal region in R115866 embryos (Fig.3.8C1., C2.).

3.2.7.4 Alteration of Raldh2 expression in R115866-treated embryos

The expression of the RA-synthesizing enzyme *Raldh2* in R115866-treated embryos was also examined. *Raldh2* is altered in the *Tbx1*$^{-/-}$ mouse such that there is an apparent rostral shift of expression in the splanchnic mesoderm. Expression in a small patch of mesenchymal cells between the forebrain and dorsal aorta just rostral to pharyngeal arch 1 is also up-regulated (Guris et al., 2006; Ivins et al., 2005). In the Cyp26-blocked chick embryos the strong expansion of expression in the small patch of mesenchymal cells rostral to pa1 seen in *Tbx1*$^{-/-}$ mice was observed in over half R115866-treated chick embryos (n=5/9). In these embryos there was also an anterior extension of expression in the ventral mesoderm, ectopic expression was also observed in pharyngeal arch 1 and in some cases it seemed that overall expression was also up-regulated (Fig.3.8D1.-D4.).

3.2.7.5 Abnormal expression of Sox10 and cranial ganglia patterning in R115866-treated embryos

Sox10 was used as a marker for migrating neural crest and cranial ganglia in R115866 embryos (Cheng et al., 2000). Results showed diminished intensity of *Sox10* staining and a reduction in the number of positive migrating neural crest cells (Fig.3.8E1.-E3.). Abnormal patterning of the cranial ganglia as observed in *Tbx1* mutant mice was also seen with the trigeminal ganglion (X) being greatly reduced in size as were the facioacoustic (VII/VIII) and glossopharyngeal (IX) ganglia. Aberrant neuronal pathfinding was also observed (Fig.3.8E4., E5.).

3.2.7.6 Retinoic acid levels are altered in R115866-treated embryos

Hoxb1 is a retinoic acid-responsive gene normally expressed in endoderm and mesoderm caudal to pharyngeal pouch 3/4 depending on the age of the embryo. Treatment with RA induces ectopic anterior *Hoxb1* expression in both tissues (Bel-Vialar et al., 2000) and this ectopic rostral *Hoxb1* expression was also seen in *Tbx1*$^{-/-}$ embryos (Guris et al., 2006). Very similar rostralectopic shifts of expression to a level just below pharyngeal arch 1 were present in the pharyngeal endoderm and mesoderm of R115866-treated chick embryos supporting the interpretation of a rise in the levels of RA in this region (Fig3.8F1., F2.).

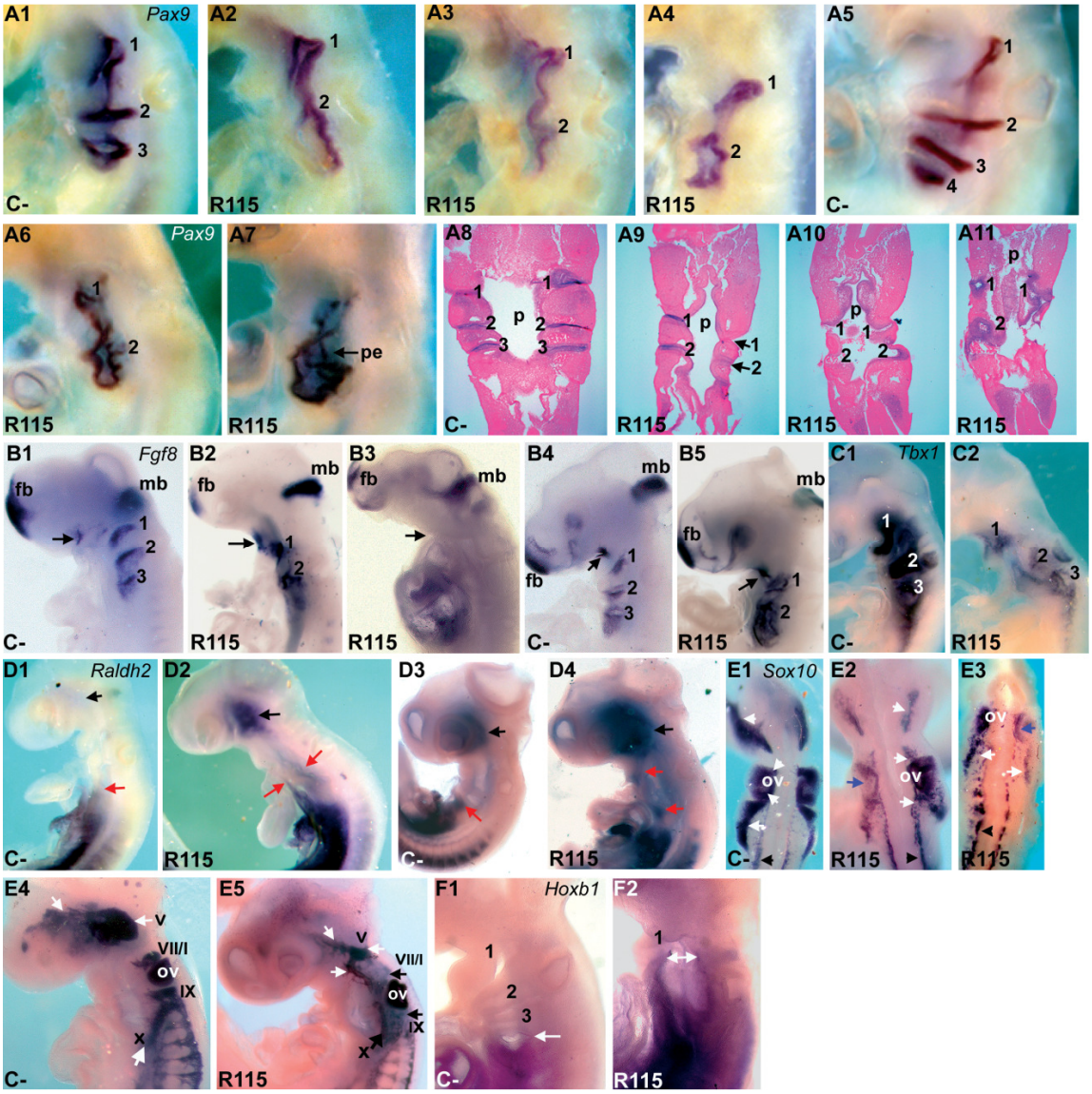

Figure 3.8 Altered molecular markers in high dose R115866-treated embryos.

(A1-A7) In normal embryos *Pax9* delineated endoderm of pharyngeal pouches 1-3(A1) or 1-4 (A5) 24 and 48 hours respectively after treatment. In R115866 embryos *Pax*9 was expressed throughout the pharyngeal pouch endoderm however, the morphology of pouches caudal to pouches 1/2 was very abnormal at both 24 (A2-A4) and 48 (A6, A7) hours after treatment. *Pax9* transcripts were also sometimes detected at lower levels in R11566 embryos than in controls (A2, A3). (A8-A11) Coronal sections through *Pax9* confirm variable disorganization of pharyngeal pouch morphology. (A8) Control embryo with *Pax9* expression in normally segmented pharyngeal pouches 1-3. (A9) R115866 embryo with unilaterally normal pouches 1 and 2. On the contralateral side pharyngeal arches and arch arteries 1 and 2 are very small and pouch segmentation and *Pax9* expression is reduced. Pharyngeal pouch 3 segmentation is lost bilaterally. (A10, A11) R115866 with more severely dysmorphic pharyngeal pouch segmentation; In both embryos only

pouches 1 and 2 are distinguished and lack bilateral symmetry of pharyngeal pouches. Numbers indicate the appropriate pharyngeal pouch, p; pharynx, pe; pharyngeal endoderm. (B1-B5) *Fgf8* pharyngeal expression similarly suggests dysmorphogenesis of the pharyngeal pouches 24 (B1, B2) and 48 (B3-B5) hours after treatment. *Fgf8* expression in the pharyngeal pouch endoderm and branchial groove ectoderm (arrows) is abnormal; no expression caudal to pouch 3 is apparent and pouches 1 and 2 have an abnormal shape and often appear to be closer together as does the branchial groove expression to pouch 1 (B2 and B5). In some embryos pharyngeal expression was lost altogether although expression domains in the forebrain (fb) and at the midbrain/hindbrain(mb) boundary were maintained (B3). (C1, C2) In situ hybridization for *Tbx1* showed that normal strong expression in pharyngeal arch mesoderm, secondary heart field, pharyngeal pouch endoderm and otic vesicle (C1) was greatly reduced in R115866 embryos. (D1-D4) *Raldh2* transcripts in R115866 embryos are also dysregulated at both 24 (D1, D2) and 48 (D3, D4) hours after culture. A normally weak expression domain in the head mesenchyme next to the eye (black arrows) (D1, D3) is greatly up-regulated in R115866-treated embryos (D2, D4). Ectopic up-regulated expression can be seen in the ventral mesoderm (red arrows) of R115866-treated embryos (D2, D4) compared to controls(D1, D3). (E1-E5) *Sox10* expression in migrating neural crest (white arrows) 24 hours after treatment (E1-E3) and in neural-crest derived cranial ganglia 48 hours after treatment (E4, E5). Expression is also seen in the otic vesicle (ov). Numbers of *Sox10*-positive migrating cranial neural crest cells are greatly diminished in R115866 embryos (E2, E3) compared to controls (E1). Trunk neural crest (black arrowheads, E1-E3) seems relatively unaffected. Otic vesicle staining can also be diminished (blue arrows, E2, E3). Cranial ganglia patterning is disrupted in R115866 embryos (E5) compared to controls (E4). The trigeminal (V, white arrows) ganglion is greatly reduced in size, is shifted caudally and has aberrant neuronal pathfinding. The facioacoustic (VII/I and glossopharyngeal (IX) and vagal(X) ganglia appear to be missing almost entirely (black arrows, E5). (F1, F2) Control and R115866-treated embryo hybridized for *Hoxb1* 24 hours after treatment. *Hoxb1* is normally restricted to the endoderm and mesoderm caudal to pharyngeal pouch 4 in controls. In R115866 embryos this expression is ectopically expanded to just below pharyngeal pouch 1 (white arrows in F1 and F2).

3.3 Discussion

3.3.1 Results summary

All three embryonic *Cyp26* genes have been shown previously to have reduced/altered expression patterns in the *Tbx1*$^{-/-}$ mouse. The data presented above demonstrated that when the activity of the Cyp26 enzymes was inhibited *in vivo* in the

chick embryo using R115866, a potent and selective inhibitor of Cyp26 enzyme function (Stoppie et al., 2000), many of the phenotypes associated with the *Tbx1* null mouse and 22q11DSwere reproduced. The R115866 phenocopy includes the loss of caudal pharyngeal arches and arch arteries and the specific heart defects common in 22q11 patients, including CAT and DORV in association with perimembranous and doubly committed juxtarterial VSDs. This data suggests a functional link between altered expression of the *Cyp26* genes with secondary disruption of the RA regulatory pathway and the 22q11DS/ *Tbx1* null phenotype.

3.3.2 Are increased RA levels in *Tbx1* mutants mediated by both altered *Cyp26* and *Raldh2* levels?

The discovery of three embryonic Cyp26 RA-metabolizing genes as potential *Tbx1* targets raised the possibility that part of the *Tbx1* phenotype may be mediated by a rise in levels of retinoic acid local to *Tbx1*-expressing domains due to the loss of RA-metabolizing capacity, particularly as there are strong phenotypic similarities between the effects produced by excess RA and those seen with *Tbx1* null mutations. As previously reported in independent studies (Guris et al., 2006; Ivins et al., 2005) mouse *retinaldehyde dehydrogenase 2* (*Raldh2*), the enzyme responsible for synthesizing the majority of embryonic RA also appears to have an ectopic anterior shift of expression in the splanchnic/ventral pharyngeal mesoderm and to be upregulated in the head mesenchyme of *Tbx1* nulls. This suggests a possible up-regulation of RA synthesis in addition to down-regulation of RA-metabolizing *Cyp26* genes which would further alter local RA levels. Evidence in favour of this theory was provided by *RARE-LacZ* reporter transgenic mice. Colourimetric assays of β-galactosidase demonstrated that the boundary of expression of the RARE-reporter construct is shifted anteriorly in the pharyngeal endoderm and head mesenchyme of *Tbx1* homozygous null embryos (Guris et al., 2006). The authors of this study suggested that loss of *Tbx1* alters *Raldh2* with altered *Cyp26a1* and *b1* expression occurring as a subsequent event. In situ hybridization studies have reported a similar cranial expansion of *Tbx1* expression in the lateral mesoderm at E8.0. Since no phenotypic variation was evident between *Tbx1* null and control embryos at this stage these authors

suggest *Tbx1* directly regulates *Raldh2*. Furthermore they also hypothesize that since RA regulates *Cyp26a1* expression and T-box consensus binding sites have been identified proximal to the first exon of *Raldh2* (Liao et al., 2008), altered *Cyp26* expression in *Tbx1* nulls is the result of a negative feedback loop caused by increased RA synthesis from ectopic/up-regulated *Raldh2* (Ryckebusch et al., 2010). However, whilst this is an attractively simple hypothesis there are existing data which suggest a more complex mechanism. Firstly, the data presented here suggests that Cyp26 inhibition (albeit likely to a greater extent than that seen in *Tbx1* nulls) is sufficient to cause a similar anterior shift in *Raldh2* expression as seen in *Tbx1* nulls and a 22q11DS phenocopy. Secondly, depending upon the system used, retinoic acid has been shown to regulate not only the expression of all three *Cyp26* genes but also *Raldh1* and *Raldh2* (Dobbs-McAuliffe et al., 2004; Hu et al., 2008; Loudig et al., 2005; Niederreither et al., 1997; Reijntjes et al., 2003; Reijntjes et al., 2005; Tanibe et al., 2008; Xi and Yang, 2008; Yamamoto et al., 2000). Although the *Raldh* response to RA appears more variable than that of the Cyp26s', the fact that it can be regulated by RA means it is less useful as a criterion to assign a regulatory hierarchy in the *Tbx1* mouse. Thirdly, corroborating evidence for the idea that *Cyp26* alteration in *Tbx1* nulls is not simply the secondary effect of excess RA levels due to up-regulated *Raldh2* signalling comes from comparison of the effect of RA upon *Cyp26* expression with the effect of null alleles of *Tbx1*. In the mouse oral administration of RA to pregnant mice at E8.5 and E9.0 which were then examined at E9.5 abolished or greatly reduced *Cyp26a1* expression in the caudal neural plate, tailbud mesoderm and hindgut. In the same embryos *Cyp26a1* expression was greatly up-regulated and expanded in anterior expression domains such as the cervical neural crest mesenchyme destined to form the cranial ganglia and the otic vesicle (Fujii et al., 1997). However, in the *Tbx1*$^{-/-}$ mouse *Cyp26a1* expression was considerably down-regulated in these anterior tissues, particularly in the cranial ganglia neural crest cells. In the chick, grafts of RA-soaked beads also up-regulated *Cyp26a1* expression in this cervical mesenchyme. For *Cyp26b1* no published data is available on the effect of RA application in the mouse but in the chick RA-bead grafts up-regulated expression in anterior and posterior tissues (Reijntjes et al., 2005). Retinoic acid also induced *Cyp26b1* expression in three human cell culture lines (White et al., 2000a). This is in contrast to the down-regulation of expression in caudal pharyngeal endoderm in

combination with an anterior shift of ectodermal expression from PA3 to PA2 seen in *Tbx1*$^{-/-}$ embryos. Only with *Cyp26c1* does the result of excess RA partially match the changes in expression seen in *Tbx1*$^{-/-}$ embryos with loss of expression in cervical mesenchyme in both these embryos and E8.5 mouse and chick embryos exposed to exogenous RA (Reijntjes et al., 2005; Sirbu et al., 2005). However, even here there was an expansion of *Cyp26c1* positive cells in first arch mesenchyme in *Tbx1*$^{-/-}$ embryos which was not observed in RA-treated embryos. Obviously, variation between species, experimental approach and timing of RA application could all contribute to these differences, but they are still sufficient for a cautious approach to the idea of *Cyp26* altered expression being due only to the secondary effect of raised RA levels in *Tbx1* null mice. Finally, whilst consensus T-box binding sites have been found in *Raldh2* control sequences (Ryckebusch et al., 2010), bioinformatic surveys of the *Cyp26* genes performed using a consensus sequence matrix weighted towards *Tbx1* binding (P. Ataliotis pers. comm.) has identified similar sites in the putative promoter regions of the *Cyp26* genes. It therefore seems apparent that ectopic/up-regulated expression of *Raldh2* and down-regulated/ectopic expression of *Cyp26*s both contribute to the *Tbx1* null phenotype but the precise hierarchy of interaction between *Tbx1*, *Raldh2*, the *Cyp26* family and RA signalling remains unclear, requiring promoter binding studies to be properly dissected.

3.3.3 The *Raldh2* and *Cyp26* genes may not represent the only RA pathway members altered in *Tbx1* mice

Retinoic acid rescue of a *Raldh2* $^{-/-}$ *RARE-LacZ* reporter mouse at early stages, followed by a period of RA clearance, reveals sites of RA production which do not correspond to the expression pattern for *Raldh1* and *3*, thus raising the possibility that novel RA sources exist in the embryo in addition to *Raldh1-3* (Mic et al., 2002). *Cyp1b1* has been identified as one such alternative RA source. It is a p450 cytochrome family member but contributes to RA synthesis via production of all-trans-retinal and all-trans-retinoic acid from the precursor all-trans retinol but does not have an RA-metabolizing capability. It is expressed in a number of tissues during development, including the pharyngeal endoderm and this expression domain along with some but not all others

appears dependent on RA signaling. *Cyp1b1* has been shown to able to pattern motor neurons, antagonize the formation of the epibranchial placodes and to contribute to anterior-posterior patterning of the hindbrain in the chick (Chambers et al., 2007). *Cyp1b1* is also down-regulated in Array 2. Several other genes from the retinoic acid synthesis/degradation pathway were also found to be down-regulated in this array (Lammerts van Bueren, 2008) including: *Rbp4* (a circulating retinol carrier protein which transports retinol to target tissues)(Goodman and Blaner, 1984); transthyretin (*Ttr*) (*Rbp4*-associated serum protein preventing retinol degradation)(Malpeli G. et al., 1996); *Adh1*(important in oxidation of retinol to retinaldehyde)(Duester et al., 2003)); *Crabp2* (binds atRA intracellularly, solubilizing and protecting it in the cytoplasm and is associated with nuclear import and delivery of RA to RARs) (Budhu and Noy, 2002) and several members of the RA-RAR/RXR binding activated transcription pre-initiation complex including Pol II subunits and TBP (TATA binding protein)-associated factors (TAFs)(Rhinn and Dolle, 2012). It therefore seems that a careful analysis of the expression patterns of all these different genes and the retinoic acid receptor genes in *Raldh2* and *Cyp26* knockout mice might contribute useful data towards resolving what appears to be a complex hierarchy of interactions between *Tbx1*, *Raldh2*, the *Cyp26* genes, RA levels and the RA-receptor genes. This is likely to be an extremely intricate set of feedback loops given that many of the genes involved, including *Tbx1* itself are RA-responsive.

3.3.4 Could the Cyp26 loss-of-function phenotype be caused by the observed down-regulation of *Tbx1*

The finding that *Tbx1* itself is down-regulated in high dose R115866-treated embryos raises the question of to what extent the morphological phenotype is due directly to blockade of RA catabolism versus an indirect affect caused by reduced *Tbx1* levels. Whilst the lower levels of *Tbx1* expression due to the rise in RA levels may make a small secondary contribution to the observed phenotypes of R115866 embryos this is much more likely to be directly attributable to loss of Cyp26 function for several reasons. Firstly, *Tbx1* expression is only partially repressed and yet the phenotype seen is as severe,

or worse than that seen in the *Tbx1* null mouse which expresses no *Tbx1* at all. Secondly, we have observed a clear phenotype in embryos 16 hours after R115866 treatment (data not shown). For this to be mostly due to RA-mediated *Tbx1* repression the drug would have to act to raise RA levels sufficient to repress *Tbx1*. The reduced levels of *Tbx1* would then have to affect downstream transcription and translation to produce a phenotype within 16 hours. Given that RA repression of *Tbx1* requires 12 hours to become apparent (Roberts et al., 2005) this seems unlikely. Finally, we have shown that embryos treated with low doses of R115866 have significant defects of the cardiovascular system later in development, which are very similar to those seen in *Tbx1* mutant mice and 22q11DS patients. In situ hybridization of low dose embryos with probes for *Tbx1* at earlier stages revealed no difference in expression between control and treated embryos making it very improbable that this phenotype is due to diminished *Tbx1* but rather is due to the inactivation of Cyp26 function.

3.3.5 Could altered metabolite ratios contribute to the Cyp26 knock-down phenotype?

Cyp26 genes metabolize atRA (alltrans RA) to more polar metabolites, including 4-oxo-RA, 4-OH-RA and 5,6-epoxy-RA. These metabolites have usually been deemed to be relatively biologically inert. Nevertheless, several reports in the literature suggest that all three, but particularly 4-oxo-RA may exert a biological effect. As described in Chapter 1.8.2.1. all three of these metabolites have been shown to bind to RARβ, regulate the expression of RA-inducible genes and rescue or induce RA deficient/excess phenotypes respectively in vertebrate embryos (Baron et al., 2005; Gaemers et al., 1996; Herrmann, 1995; Reijntjes et al., 2005). This raises the possibility that some of the effects of Cyp26 functional blockade could be the result of reduced metabolite levels as well as excess RA in the embryo. However, since in genetic experiments in the mouse (also described in section 1.8.2.1) a *Raldh2*$^{+/-}$ allele can rescue *Cyp26a1*$^{-/-}$ embryonic lethality (Niederreither et al., 2002a) and exogenous excess RA phenotypes can be rescued by expression of *Cyp26a1* (Guidato et al., 2003; Hollemann et al., 1998) it seems much more likely that Cyp26s function by removing bioactive RA from sensitive tissues than via any metabolite

activity. Therefore it is far more probable that the R115866-induced phenotype is the result of excess RA than loss of Cyp26 metabolite function.

3.3.6 Non/cell autonomous function of *Tbx1* upon *Cyp26* expression?

One question which arises is whether the influence of *Tbx1* upon *Cyp26* expression is cell-autonomous, or non-cell autonomous. In some tissues *Tbx1* and the *Cyp26* genes are co-expressed e.g. *Cyp26b1* in pharyngeal endoderm and ectoderm suggesting a possible cell autonomous effect. The results from Array 2 described above (section 3.1 and 3.1.1 cells found down regulation of *Cyp26b1* in $Tbx1^{-/-}$ cells compared to $Tbx1^{+/-}$ cells, adding further support for a cell autonomous effect. However, in other cell types a non-cell autonomous effect must be taking place; for example the strong expression of *Cyp26c1* in cervical neural crest is down regulated in *Tbx1* null embryos even though *Tbx1* is not expressed in neural crest.

3.3.7 Is RA metabolism required for normal PAA formation?

R115866 blockade of Cyp26 function in the chick embryo phenocopies both the *Tbx1* null mouse and 22q11DS to a substantial degree. When a high dose is given, pharyngeal development is severely dysmorphic. In the majority of embryos, pharyngeal arches caudal to arch 2 failed to form, as did the characteristic bulges of the endodermal pharyngeal pouches. In 63% of these embryos only pharyngeal arch artery 1, with an occasional pharyngeal arch artery 2, was patent and in the remainder did not form a fully patent PAA1. Additionally the otic vesicle was often hypoplastic. These features have all been described as characteristic of the $Tbx1^{-/-}$ null mouse at E10.5 (Jerome and Papaioannou, 2001; Lindsay et al., 2001) and in conjunction with our data it is tempting to speculate that RA catabolism maybe required for pharyngeal arch artery formation. Further support for the role of Cyp26 enzymes in vascular development including PAA development comes from several other studies. Cytochrome P450 oxidoreductase (*Por*) acts as essential electron donor to all cytochrome P450 enzymes. *Por* null mouse mutants exhibit severe inhibition of vasculogenesis (amongst other defects) including loss of all

PAA (Otto et al., 2003; Shen et al., 2002), which can be rescued by reducing RA levels by crossing onto a *Raldh2*$^{+/-}$ background (Ribes et al., 2007b). *Cyp26b1* has also been reported as being expressed in vascular smooth muscle and endothelial cells and a specific *Cyp26b1* splice variant has been isolated from these cells. Silencing of *Cyp26b1* expression via siRNA knock-down or R115866 treatment increased atRA-mediated signalling and resulted in decreased cellular proliferation (Elmabsout et al., 2012; Ocaya et al., 2011). Thus it seems the Cyp26 enzymes may play an important role in PAA vascular development, downstream of *Tbx1* signalling. In addition, it has been shown RA receptor function is independently required in pharyngeal mesoderm, where it promotes the assembly of endothelial precursors into nascent pharyngeal arch arteries during vasculogenesis (Li et al., 2012). By controlling levels of available free ligand for receptor-binding, Cyp26 enzymes could indirectly play a role in this process.

The severe phenotype observed where not even PAA1 formed is more extreme than normally observed in *Tbx1* mutant mice. This could be the result of Cyp26 functional abrogation in all Cyp26 expression domains, not just those which co-express *Tbx1* as these phenotypes are somewhat akin to those of the *Por*$^{-/-}$ mouse and multiple *Cyp26* gene knockout mice (Shen et al., 2002; Uehara et al., 2009). Additionally, there is evidence that RA is required for endothelial cell proliferation and vascular remodelling at late gastrulation/early somiogenesis stages of mouse development (Bohnsack et al., 2004; Lai et al., 2003). Owing to the mode of R115866 application it is possible that the exact concentrations embryos were exposed to for specific lengths of time/during particular time windows varied from embryo to embryo, thus producing this phenotypic variation.

3.3.8 Cardiovascular tissues are more sensitive to R115866 than other embryonic regions

In these R115866-treated embryos, early heart development was also compromised with a hypoplastic outflow tract, reduced looping and inner curvature remodelling. Lower doses of R115866, which allowed embryos to survive longer produced severe outflow tract abnormalities of a type classically associated with 22q11DS and also seen in a variety of *Tbx1* mutant mice (Hu et al., 2004; Jerome and Papaioannou,

2001; Lindsay et al., 2001; Xu et al., 2004; Xu et al., 2005). These include common arterial trunk, double-outlet right ventricle and doubly committed juxtarterial VSD, which is very closely related to CAT and frequently observed in 22q11DS (McCarthy et al., 2000). Interestingly, at these lower doses the cardiovascular system appeared to be more sensitive to loss of Cyp26 function and the concomitant increase in RA than craniofacial regions with very few embryos displaying additional abnormal phenotypes to the heart defects observed. This is also true of *Tbx1* knockout mice, where in an allelic series, the aortic arch and cardiovascular system was affected at *Tbx1* dosages where craniofacial systems remained normal (Hu et al., 2004). Additionally, in *Raldh2* null embryos 'rescued' by maternal RA administration all phenotypes except for those of the cardiovascular system were ameliorated by the provision of exogenous RA(Niederreither et al., 2001; Niederreither et al., 2003). This variation in sensitivity in different tissues to RA dosage is also a likely explanation for the fact that at low doses of R115866, which produced classic DGS-like cardiac abnormalities, no thymic defects were observed, although the pharyngeal endoderm, which gives rise to the thymus, was severely abnormal in high dose embryos.

3.3.8 Early SHF defects in R115866-treated embryos may contribute to later OFT anomalies

The early heart defects seen are consistent with the type of outflow tract abnormalities detected at later stages; both OFT hypoplasia and abnormal looping and remodelling are associated with a spectrum of defects including CAT, DORV and the type of VSDs seen here (Gittenberger-de-Groot et al., 2005; Kirby, 2002; Rothenberg and Fisher, 2003; Towbin et al., 2000). Contributions from two different cell types, external to the outflow tract, have been shown to be critical for its growth, correct alignment and proper septation. These two populations are the cardiac neural crest and the cells of the secondary heart field (SHF). The SHF consists of pharyngeal and splanchnic mesoderm cells and is molecularly delineated by the expression of genes such as *Isl-1*, *Tbx1* and *Fgf10* (Cai et al., 2003; Kelly and Buckingham, 2002) and references therein). Comparison of the expression of *Cyp26* genes with *Tbx1* in mouse and chick reveals

possibly overlapping domains of expression in the SHF with *Cyp26a1* and *b1* at E8.25-8.5 in the mouse and *Cyp26b1* at stages 11-16 in the chick (Fujii et al., 1997; MacLean et al., 2001; Reijntjes et al., 2003). Using *Tbx1* as a marker of the SHF in R115866-treated embryos revealed diffuse staining across a reduced area rather than the normal strong expression. Loss of expression of other SHF markers *Isl-1* and *Mef2c* was also seen. Histological sections revealed substantial dysmorphogenesis in this region, suggesting that the SHF domain was not as extensive nor as well organized as in controls and/or did not express molecular markers normally. *Tbx1* appears to have a cell proliferative role in regulating the addition of cells of the SHF to the developing heart as revealed by the OFT hypoplasia of *Tbx1* homozygote mutant embryos at E9.5 which later leads to the severe OFT defects such as CAT and DORV at E18.5 in these embryos (Chen et al., 2009; Jerome and Papaioannou, 2001; Lindsay et al., 2001; Xu et al., 2004; Xu et al., 2005; Zhang et al., 2006b). Sections revealed fewer SMA22-positive vascular smooth muscle cells in the proximal OFT. This could be the result of a reduced contribution from the secondary heart field to the smooth muscle of the arterial pole (Waldo et al., 2005b) possibly via reduced proliferation. Overall, the development of the secondary heart field and OFT was disturbed in R115866-treated embryos likely contributing to the later cardiovascular phenotypes observed.

3.3.9 A role for abnormal neural crest development in the R115866 phenotype?

Both *Cyp26a1* and *c1* are expressed in pharyngeal mesenchyme, which is mostly neural crest derived and expression in this domain of both genes is lost in *Tbx1* null mice. Altered *Cyp26* expression in the neural crest or in pharyngeal tissues with which the crest interacts may also contribute to the 22q11-like heart phenotype observed after R115866-treatment. Altered gene expression in neural crest cells has been shown to produce 22q11-like heart defects including CAT, interrupted aortic arch type B, DORV in numerous mouse models [reviewed (Stoller and Epstein, 2005)]. In the chick, neural crest ablation is well-documented to produce similar phenotypes including CAT, DORV, VSD and Tetralogy of Fallot (Kirby et al., 1985; Nishibatake et al., 1987; Waldo et al., 2005a; Waldo et al., 2005b; Ward et al., 2005; Yelbuz et al., 2002). In both species neural crest

has been shown to contribute to the aorticopulmonary septum and OFT cushions and subpulmonary infundibulum during normal septation and alignment of the OFT and ventricles (Jiang et al., 2000; Waldo et al., 1998; Webb et al., 2003). It has been shown that ablation of the neural crest produces a shortened and straighter OFT which inhibits subsequent looping, explaining the malalignment heart phenotypes produced by neural crest ablation (Yelbuz et al., 2002). Neural crest ablation has a significant affect upon the SHF, preventing SHF cells destined to become OFT myocardium from entering the OFT, although SHF-derived vascular smooth muscle cells are unaffected (Waldo et al., 2005a; Waldo et al., 2005b). A number of similar phenotypes to those of neural-crest ablation were observed in the R115866-treated embryos including shorter straighter outflow tract, reduced looping and reduced caudal movement of the OFT, suggesting that the neural crest interaction with the SHF is abnormal. The smooth muscle layer required to maintain the integrity of the pharyngeal arch arteries is also neural crest derived. SMA22 staining is greatly reduced in surviving pharyngeal arch arteries suggesting an aberrant neural crest contribution to this cell population.

Sox10 expression showed a reduced number of positive migrating neural crest cells in Cyp26-inhibited embryos, variable transcript levels compared to controls and changed migration pathways relative to controls. Cranial ganglia patterning was also anomalous, with ganglia often missing, shifted in position or fused with other ganglia. Similar abnormal developmentof the neural-crest derived cranial ganglia was also seen as in *Tbx1* mutant embryos, in particular the hypoplasticity of cranial nerves IX and X which innervate the caudal pharyngeal arches (Vitelli et al., 2002a). Abnormal migration of the caudal neural crest streams has also been observed in a *Cyp26b1* null mouse, whilst hindbrain gene expression remained normal (MacLean et al., 2009). Severe neural crest migratory defects, particularly affecting the neural crest of the fore and midbrain were also observed in double *Cyp26a1*$^{-/-}$ *Cyp26/c1*$^{-/-}$ embryos.

Finally, anteriorly shifted expression of the pharyngeal surface ectoderm (PSE) *Cyp26b1* domain was observed in *Tbx1* null mutants. Recent publications have demonstrated the importance of the expression of *Tbx1* and interactors *Chd7* (Randall et al., 2009) and *Gbx2* (Calmont et al., 2009) within the pharyngeal ectoderm for the proper migration of the neural crest in *Tbx1* mutant mice and subsequent PAA and cardiovascular

development. This raises the possibility that the shift in *Cyp26b1* PSE expression could contribute to the aberrant neural crest behaviour seen in *Tbx1* null embryos and inhibition of Cyp26b1 function in this domain might also possibly also influence the R115866 phenotype. On this note, the Cyp26 enzymes are also expressed in pharyngeal endoderm and *Cyp26b1*and *c1* at least are down-regulated in the pharyngeal endoderm in *Tbx1* null embryos. Extensive publications indicate that proper patterning of the pharyngeal endoderm is required for normal pharyngeal neural crest development (Couly et al., 2002; Crump et al., 2004; David et al., 2002; Graham, 2008; Mulder et al., 1998; Piotrowski and Nusslein-Volhard, 2000; Rizzoti and Lovell-Badge, 2007; Sato et al., 2011; Tucker and Lumsden, 2004; Wendling et al., 2000), suggesting endodermal defects in R115866 embryos could also contribute to the neural crest phenotype.

3.3.10 The role of *Tbx1* and *Cyp26* expression in pharyngeal mesoderm and endoderm

Finally, as well as the proper contribution from the neural crest and secondary heart field, normal patterning and development of both the pharyngeal endoderm and craniofacial mesoderm (Tirosh-Finkel et al., 2006) are required for normal heart development. Both *Foxg1-Cre* and *Mesp1-Cre* driven *Tbx1* conditional knockouts have a hypoplastic OFT at E10.5, hypoplastic pharynx lacking normal endodermal pouch formation and patterning at E11.5, abnormal craniofacial development, absent thymus and parathyroid glands and a characteristic cardiovascular defect of CAT with VSD (Arnold et al., 2006b; Zhang et al., 2005; Zhang et al., 2006b).

Cyp26b1 and *c1* are expressed in the pharyngeal endoderm and in *Tbx1*$^{-/-}$ mice expression of both genes is down-regulated in the pharyngeal endoderm at E9.5. *Cyp26c1* has also been shown to have an expanded domain of core mesoderm expression in PA1. In R115866-treated embryos normal pouch segmented morphogenesis was lost within the pharyngeal endoderm as in the *Tbx1* null mouse. Diminished *Fgf8* expression was observed in some embryos, which is also a feature of *Tbx1*$^{-/-}$ embryos, where *Fgf8* is an important downstream target and is known to be required for normal pharyngeal and cardiovascular development.

Retinoic acid signalling involving the pharyngeal endoderm has long been known to be important for pharyngeal pouch development. Loss of RAR signalling induces agenesis of PP3 and 4 (Li et al., 2012; Mulder et al., 1998; Wendling et al., 2000), and fusion of PP1 and 2 (Matt et al., 2003). RA signalling has also been shown to be required for endodermal pouch morphogenesis but not specification (Kopinke et al., 2006), which is similar to the phenotype seen in R115866-treated embryos. The RA signalling gradient has been posited to be important for endodermal organ specification along the antero-posterior axis, with RA acting as a caudalizing agent along the pharyngeal endoderm to co-ordinate the position of endodermally derived organs such as the thyroid and pancreas (Bayha et al., 2009). Mildly abnormal thymus development has been observed in *Cyp26b1*$^{-/-}$ embryos and *Cyp26a1* plays a critical role within gut anterior endoderm in defining the area over which RA can induce pancreatic cell fate (Kinkel et al., 2009), leading to speculation they may play a similar role in the pharyngeal endoderm.

It is not clear to what extent the mesenchymal dysregulation of *Cyp26a1* and *c1* observed is within mesodermal versus neural crest derivatives, but certainly altered levels of both genes are observed in these tissues in *Tbx1* null embryos. Mesodermal specific knock-out of *Tbx1* reproduced the *Tbx1* null phenotype and reactivation of mesodermal *Tbx1* expression rescued much of the null phenotype including OFT defects, but not thymic defects, 4th arch/artery hypoplasia or neural crest/cranial nerve defects (Zhang et al., 2006b). Recently, RA signalling within the mesoderm, but not the endoderm has been shown to result in a caudal PAA agenesis/hypoplasia due to the failure of endothelial cells to coalesce and form blood vessels (Li et al., 2012) but a specific role for the Cyp26 enzymes in pharyngeal mesoderm has not yet been reported.

Foxg1-Cre and *Mesp1* conditional *Tbx1* mutants and R115866 treated embryos have many developmental anomalies in common. It would be interesting to examine the expression of the *Cyp26* genes in the *Mesp1*and *Foxg1-Cre Tbx1* conditional mice to see what parts of the *Cyp26* expression changes are attributable to the loss of *Tbx1* in the pharyngeal mesoderm versus endoderm.

3.3.11 Contribution of individual Cyp26s to the R115866 phenotype

R115866 blockade of Cyp26 enzyme function phenocopies 22q11DS and the *Tbx1* null mouse with loss of pharyngeal segmentation, hypoplasia of pharyngeal arch arteries, hypoplasia and reduced OFT looping and characteristic great vessel and OFT alignment defects. Similar small otic vesicles are also observed. Additionally, the R115866-treated embryos have CNS defects not seen in the *Tbx1* mouse probably resulting from knock-down of Cyp26 function in tissues such as the hindbrain where *Tbx1* is not expressed. Homozygous null mutants for cytochrome P450 reductase, the essential electron donor for all Cyp26s, have a severe embryonic lethal phenotype which includes loss of the pharyngeal arches, defective vasculogenesis and somitogenesis, heart oedema and acute anterior and caudal truncation (Otto et al., 2003; Ribes et al., 2007b; Shen et al., 2002). Triple knock-out mouse embryos for all the *Cyp26*s are embryonic lethal. In 44% of embryos duplicated axes were found, which are the result of uncleared maternal RA inducing ectopic Nodal signalling in the epiblast during gastrulation. Double *Cyp26a1/c1*$^{-/-}$ mutants displayed these defects in 26% of embryos, but they were not seen in *Cyp26a1/b1*$^{-/-}$ embryos (Uehara et al., 2009). *Cyp26a1/c1* null embryos without gastrulation defects display severe CNS patterning and neural crest migration defects, some axial duplications, exencephaly and vertebral transformations plus hypoplastic head and pharyngeal arches 1 and 2 in addition to the defects seen with *Cyp26a1* alone (pericardial oedema, abnormal heart looping and caudal truncation) (Abu-Abed et al., 2001; Sakai et al., 2001; Uehara et al., 2007). There are similarities in this phenotype with the R115866-treated embryos, particularly the reduced size of the head and pharyngeal arches, but not the pharyngeal arch artery defects or specific great vessel and OFT alignment defects. Caudal truncation was also infrequently observed in the chick model. *Cyp26b1*$^{-/-}$ mice have severe limb defects, small external ears and micrognathia (Yashiro et al., 2004). A recent paper analysing a different *Cyp26b1* knock-out allele documented craniofacial abnormalities, including cleft palate, reduced or absent incisor development, micrognathia and absent posterior nasopharynx (MacLean et al., 2009). Certainly, young, high dose R115866 embryos had abnormal craniofacial development including micrognathia and small otic vesicles. R115866 embryos were not investigated for limb

bud patterning abnormalities in high dose younger embryos, and no striking limb phenotype was noticed in older lower dose embryos.

Some variation between the phenotypes described for the R115866-treated embryos and mouse knock-outs are to be expected; these could be ascribed to possible species differences or differences in experimental approach. For example, although R115866 is an effective inhibitor of Cyp26 function it will not be as effective or long-lasting as a genetic knock-out, plus two different concentrations were used to avoid excess toxicity later in development. Additionally, R115866 was only added at stage10 of development rather than being functionally abrogated from conception. However, the cardiovascular defects seen in the R115866 embryos were very striking and it was surprising these had not been documented in mouse *Cyp26* knock-outs. It seemed likely that either they were hidden by early lethality as seen in some of the compound mutants or had not been investigated fully in the single mutant reports. Alternatively, the other Cyp26 genes may have compensatory roles in these mutants.

3.4 Future Directions

3.4.1 Further investigation of the R115866 cardiovascular phenotype in the mouse

Some mid-gestational lethality and oedema has been reported for the *Cyp26b1* null mouse mutants (Yashiro et al., 2004) that was not fully explained by the reported phenotype. A more detailed investigation of the cardiovascular system in these animals might reveal whether loss of *Cyp26b1* can contribute to the cardiovascular phenotypes seen with chemical blockade of Cyp26 function in the chick.

Another approach might be to explore a conditional knock-out of all three *Cyp26* genes post-gastrulation using an inducible CAGGS-Cre system to avoid the early lethality and to determine if loss of function of all three Cyp26 enzymes is necessary to produce the 22q11DS-like phenotype detailed in this chapter.

If it was found that *Cyp26b1* mutant mice had a similar cardiovascular phenotype to Tbx1 mutants then cross-breeding studies could be undertaken to begin to explore

whether *Tbx1* and *Cyp26b1* lie within the same genetic pathway during development of these tissues

3.4.2 Exploration of any hindbrain phenotype in R115866-treated embryos

Cyp26b1 mutants are reported to have normal patterning in the hindbrain. However, differences in molecular markers such as *Krox20*, *Hoxb1* and *Epha2*, *Otx2*, *Meis1* and *Fgf8* are observed in *Cyp26a1* and *Cyp26a1/c1* nulls, consistent with the expansion of the hindbrain at the expense of the fore and midbrain. Patterning of *Fgf8* at the midbrain-hindbrain junction appeared normal in R115866-treated embryos at 24-48h (st14-24) but a more detailed investigation with additional markers, at younger stages could be carried out, in part to investigate whether any of the neural crest and cranial nerve defects observed could be attributed to abnormal hindbrain patterning. Additionally, expression of the *Cyp26* genes might be examined in R115866 embryos to see if any feedback mechanisms led to any redundant activation of *Cyp26* gene expression as a consequence of loss of Cyp26 function.

3.4.3. Proliferation and Apoptosis in R115866-treated embryos

Proliferation and apoptosis was not investigated in this study, an oversight that should be remedied given the well-documented role of *Tbx1* in proliferation of a number of different tissues in the mouse including the otic epithelium (Xu et al., 2007b), periotic mesoderm (Xu et al., 2007a), hair follicles (Chen et al., 2012b), dental epithelium (Cao et al., 2010; Catón et al., 2009), palatal mesenchyme (Funato et al., 2012) pharyngeal/cardiac mesoderm including splanchnic and secondary heart field mesoderm (Ai et al., 2006; Chen et al., 2009; Liao et al., 2008; Xu et al., 2004; Zhang et al., 2006b), and pharyngeal endoderm (Xu et al., 2005). Less is known regarding the Cyp26s in this area, but a few publications indicate they can act to stimulate or decrease proliferation in different systems (Elmabsout et al., 2012; Kipp et al., 2011; Ocaya et al., 2011; Ocaya et al., 2007). Furthermore certain reports suggest Cyp26s may be protective against apoptosis in the developing gonad and may act as a ‘meoisis-inhibiting’ factor in these cells [reviewed in

(Rhinn and Dolle, 2012)]. Immunohistochemistry for phosphohistone H3, BrdU studies, Tunel staining or immunohistochemistry for members of the apoptotic pathway such as the caspases could all be used to document the effect of R115866 blockade upon cellular proliferation or apoptosis in the pharyngeal and cardiovascular tissues.

CHAPTER 4

Cyp26b1$^{-/-}$ mice display heart defects characteristic of 22q11DS and Tbx1 mutant mice

4.1 Introduction

As discussed in the previous chapter, experiments that abrogate Cyp26 enzyme function phenocopy the pharyngeal, thymic and cardiovascular defects observed in 22q11DS and its animal models. Expression of all three genes is altered in *Tbx1* null mice as described in Chapter 3. Individual *Cyp26* knock-out models have not been reported as having these defects so far, suggesting either this is a previously undiscovered phenotype or that knock-down of all three Cyp26 enzymes is required for these abnormalities to manifest.

Cyp26b1$^{-/-}$ embryos have been described as suffering from early neonatal lethality (Yashiro et al., 2004) leading to the possibility that these embryos are suffering from developmental defects other than limb anomalies. To answer this question it was decided to further investigate these animals and a *Cyp26b1* null allele line was obtained from Prof. Hiroshi Hamada, and the offspring of heterozygous crosses examined for cardiovascular defects.

4.2 Results

4.2.1 Oedema and haemorrhage in *Cyp26b1* null embryos

Embryos from heterozygote crosses were examined at E15.5, after the pharyngeal arch arteries have remodeled into the mature configuration of the great vessels and ventricular and aortic/pulmonary trunk septation should be complete. Embryos of all genotypes were recovered in Mendelian ratios at this stage of development (Table 4.1)

Wild type and *Cyp26b1*$^{+/-}$ embryos were externally indistinguishable at this stage, whereas *Cyp26b1* null mutants were easily recognized by the previously reported meromelia of fore and hind limbs (Yashiro et al., 2004)(Fig.4.1E.-H.), as compared to normal limb outgrowth in wild type and heterozygote embryos (Fig.4.1A.-D.). Small external ear pinnae and micrognathia as described previously were also observed in *Cyp26b1* nulls, with the micrognathia phenotype being 100% penetrant (n=14/14)(MacLean et al., 2009; Yashiro et al., 2004) (Fig.4.1A.-F., H.). Minor variations in size were observed in embryos of all genotypes. The midline fusion of the ribs and sternum failed to occur in some *Cyp26b1*$^{-/-}$ embryos (2/14, 14%) (Fig.4.1J.), in accordance with the role of *Cyp26b1* in skeletogenesis, chondrogenesis, osteogenesis and ossification (Dranse et al., 2011; Laue et al., 2008; MacLean et al., 2009; Spoorendonk et al., 2008; Yashiro et al., 2004). It was also determined that embryos displayed cleft palate. Some embryos were dead by this stage, appearing white and without beating hearts (3/14, 21%) (Fig.4.1H.) and others had begun to reabsorb, presumably these embryos died at earlier stages (1/14, 7%) (Fig.4.1K.). Obvious oedema in the head and body was present in 29% (4/14) of *Cyp26b1* null embryos at E15.5 (Fig.4.1F. and G.). Most strikingly, when embryos were first dissected, before they fully bled out, a high degree of haemorrhage and associated reduction of blood vessel patterning over the whole embryo was noticeable in 79% (11/14) of *Cyp26b1*$^{-/-}$ embryos (Fig.4.1A.-H). This phenotype was already present at E12.5 (Fig.4.1L.) and could contribute to the embryonic lethality seen at E15.5. However, the majority of null embryos survive past E15.5 so other factors must be contributing to the reported neonatal lethality.

Table 4.1 Table of genotypes recovered at E15.5 from *Cyp26b1*$^{+/-}$ crosses

	Wild-Type	*Cyp26b1*$^{+/-}$	*Cyp26b1*$^{-/-}$
Observed frequency	19	29	14
Expected frequency	15.5	31	15.5

P>0.05 from a chi-squared analysis, therefore genotype ratios are recovered as expected in a 1:2:1 Mendelian frequency for wild-type: heterozygous: null *Cyp26b1* genotypes. n=62.

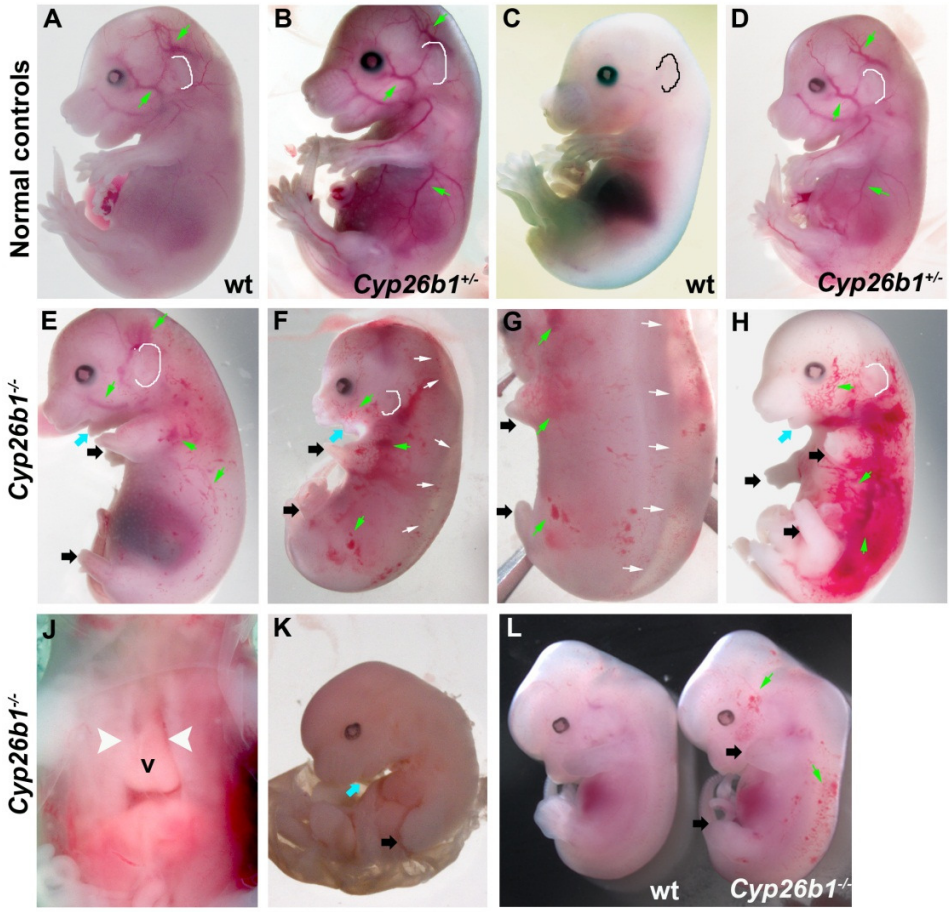

Figure 4.1 Externally observed defects in *Cyp26b1*$^{-/-}$ embryos at E15.5

A.-D.). Control embryos at E15.5, wild-type (A.,C.) and *Cyp26b1*$^{+/-}$ (B., D.). embryos. E-K.). Examples of *Cyp26b1*$^{-/-}$ embryos at E15.5. The embryo in K.) is reabsorbing. L.) Wild-type and *Cyp26b1*$^{-/-}$ embryos at E12.5. External ear pinnae are outlined in white or black. Small green arrows: blood vessels in controls and sites of haemorrhage in mutant, small white arrows: oedema. large black arrows: meromelic limbs, large turquoise arrows: micrognathia and white arrowheads: failure of midline closure, wt: wild type.

4.2.2 Cardiovascular defects in *Cyp26b1* null mutant mice

The thoracic cavity of E15.5 embryos from *Cyp26b1*$^{+/-}$ crosses was opened and the arrangement of the great vessels examined. Optical projection tomography (OPT) was also performed to confirm these finding. Wild-type embryos had a normally sized and positioned thymus at the midline over the aortic arch (Fig.4.2A., Fig.4.3A.). The pharyngeal arch arteries had remodelled into a normal aortic arch with the right

brachiocephalic (RBC), right subclavian (RSC), right common carotid (RCC), left common carotid (LCC) and left subclavian (LSC) arteries arising from it (Fig.4.2F., Fig4.3D.). The majority of heterozygous embryos were also normal. However 6/29 appeared to have one thymus lobe slightly reduced in size (21%). In contrast, all *Cyp26b1* null embryos exhibited a defect of thymic and/or great vessel development, reminiscent of those characteristic of 22q11DS and *Tbx1* null mouse mutants (Table 4.2, P<0.0001). Thymus defects of varying severity were found at 100% penetrance. This range of anomalies included one lobe of the thymus being smaller than the other (Fig4.2B.), both thymic lobes being reduced in size (Fig4.2C.), reduced size of thymic lobes and ectopic location away from the midline (Fig.4.2D.) and ectopic small thymic lobes positioned beneath the carotid arteries (Fig4.2E., Fig.4.3B.). A similar range of great vessel defects was detected at 86% penetrance (12/14), often in conjunction with a thymic abnormality. In more mildly affected embryos the aortic arch was normal except for the positioning of the right subclavian which arose almost directly from the aortic arch, either as a result of abnormal positioning of the RSC or a reduction of the length of the RBC from which it arises (Fig4.2I.). Less severe phenotypes also included cervical aortic arch (CAo) where the aortic arch is pulled anteriorly by a shorter left common carotid artery (Fig4.2H.). More severe defects were also observed, particularly interrupted aortic arch type B (IAA-B) where the aortic arch is severed between the left common carotid and the left subclavian (Fig.4.2G., Fig.4.3E.). Retro-oesophageal right subclavian (ROSCA), in which the RSC arises from the descending aorta and passes behind the oesophagus, was also seen in these embryos (Fig.4.2G., Fig4.3C.). Both these defects arise as abnormalities of development of the right 4th PAA. In addition, it was noted that the pulmonary arteries appeared to have a reduced diameter in 10/13 (77%) of *Cyp26b1*$^{-/-}$ embryos which underwent OPT analysis. Some embryos (29%, 4/14) appeared to be dead at the time of dissection, and in one of these, distal aorticopulmonary septation appeared incomplete (Fig. 4.2J.).

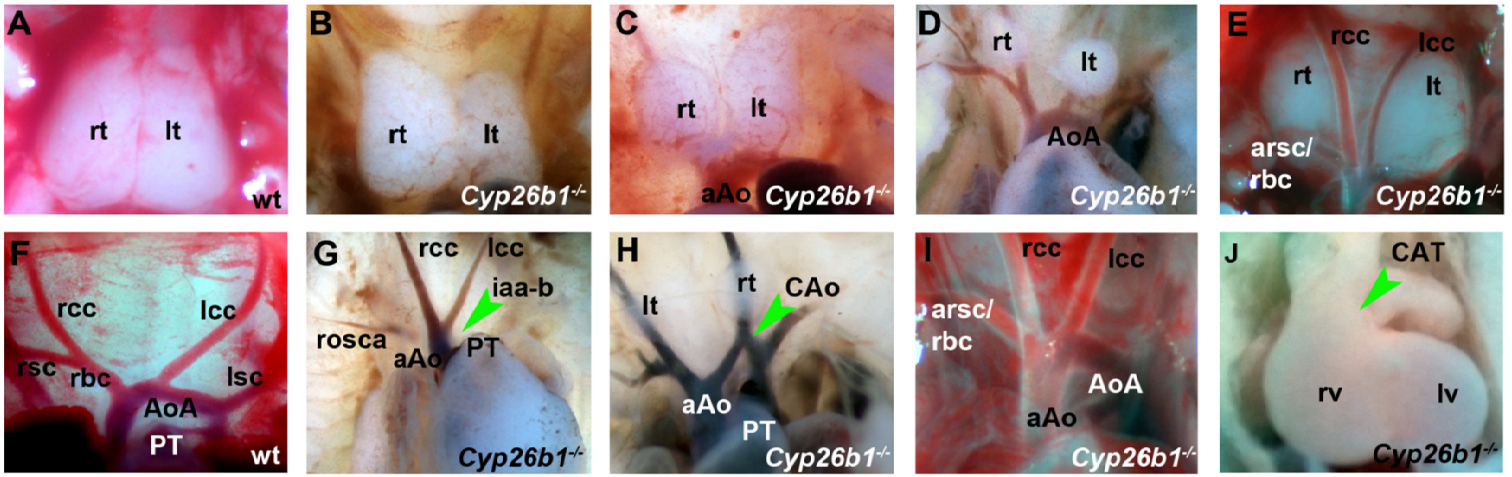

Figure 4.2 Thymic and great vessel defects in *Cyp26b1*$^{-/-}$ E15.5 embryos

A.-J.) Frontal views A.) Wild-type thymus lobes at the midline. B.-E.) Abnormal thymus development in *Cyp26b1* null embryos. B.) Reduced size left thymus lobe. C.) Small thymus lobes, which do not meet at the midline.D.) Small ectopic thymus lobes. D.) Common carotid arteries running over the top of reduced size ectopic thymus lobes. F.) Wild-type aortic arch. G.) *Cyp26b1*$^{-/-}$ embryo with an interrupted type-B aortic arch (iaa-b, green arrowhead) and retro-oesophageal right subclavian artery(rosca) . H.) *Cyp26b1*$^{-/-}$ embryo with a cervical aortic arch (CAo, green arrowhead) and small ectopic thymus. I.) Normal arch except for aberrant low position of the right subclavian (arsc/rbc). J.) Failure of distal aorticpulmonary septation (common arterial trunk, CAT, green arrowhead). Rt: right thymus lobe, lt: left thymus lobe, aAo: ascending aorta, AoA: aortic arch, rcc: right common carotid artery, lcc: left common carotid artery, rsc:, right subclavian artery, lsc: left subclavian artery, PT; pulmonary trunk, rv: right ventricle, lv: left ventricle.

The type of great vessel defects which were observed in the *Cyp26b1* null mutant embryos have characteristic associated intracardiac defects, typically peri-membranous ventricular septal defects (VSD) and anomalies in the rotation and alignment of the aorta and pulmonary trunk with the ventricles. This produces alignment defects such as double outlet right ventricle (DORV), where both the aorta and pulmonary trunk exit from the right ventricle or over-riding aorta (OAo), where the aorta is shifted slightly to the right and lies directly above the ventricular septal defect.

Optical projection tomography was used to investigate whether *Cyp26b1* null embryos also recapitulated this part of the 22q11DS/*Tbx1* null mutant phenotype.
Eighty-five percent of *Cyp26b1*$^{-/-}$ embryos (11/13) which underwent OPT displayed an alignment defect (DORV or OaO) and a peri-membranous VSD, with 91% (10/11) of these being found in association with a great vessel and thymic abnormality (Table 4.2).

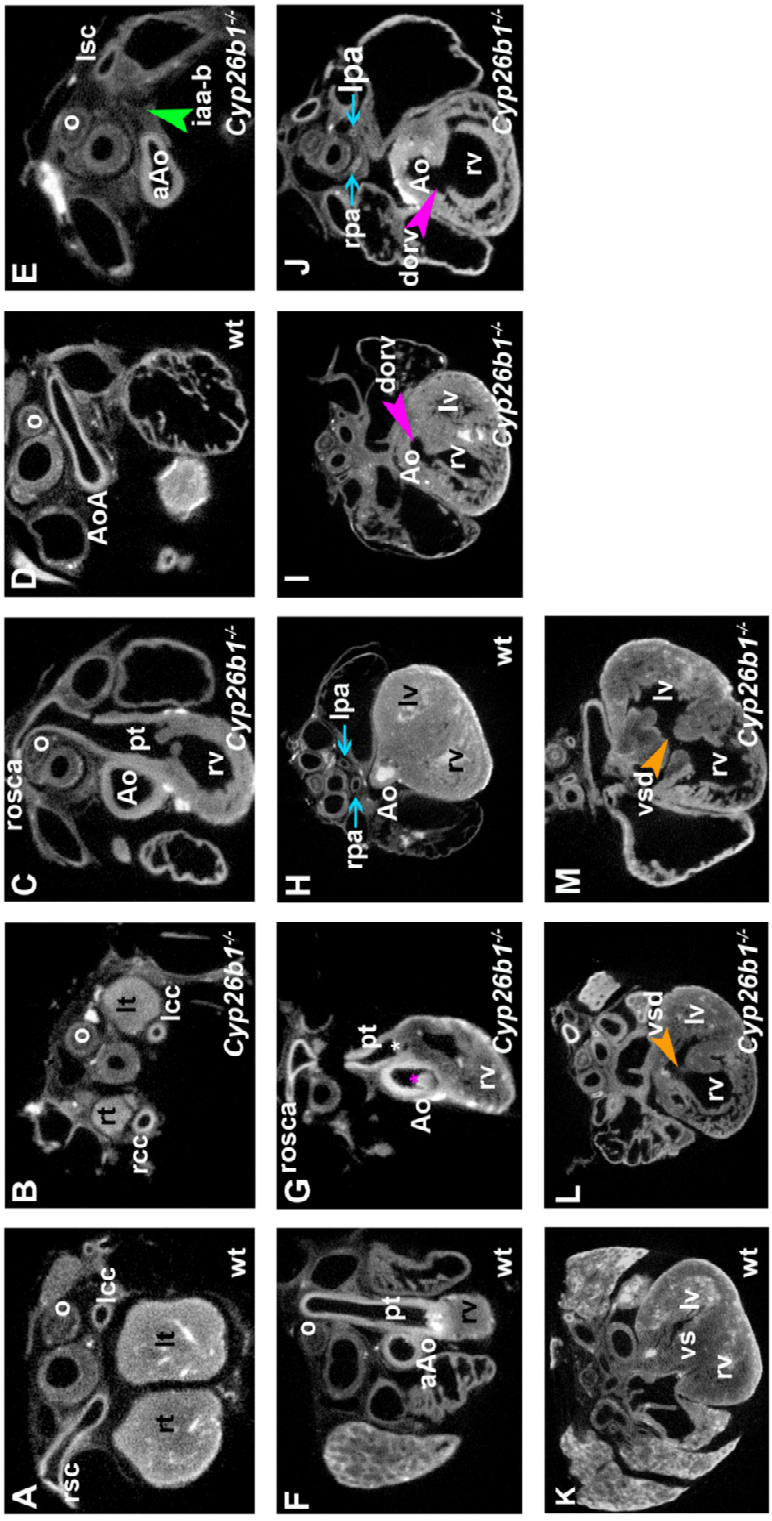

Figure 4.3 Optical projection tomography transverse sections of *Cyp26b1*$^{-/-}$ E15.5 embryos

A.) Wild-type control section through the thymus, common carotid and right subclavian arteries. B.) *Cyp26b*$^{-/-}$ section through a similar region to A.) showing small ectopic thymus positioned behind

the common carotid arteries. C.) *Cyp26b*$^{-/-}$ section showing a retro-oesophageal right subclavian artery originating from the descending aorta. D.) Wild type embryo showing a section through the normal left-sided aortic arch. E.) Section though *Cyp26b1*$^{-/-}$ embryo with interrupted aortic arch type B showing the missing segment of the aortic arch (green arrowhead).F.) Wild type section through the ascending aorta and pulmonary trunk. G.) Alignment defect in a *Cyp26b1*$^{-/-}$ embryo allows visualization of the aortic and pulmonary trunk valves ((pink and white asterisks respectively) in the same section. H.) Wild type section of the aorta exiting the left ventricle. Pulmonary arteries are indicated with blue arrows. I and J.) Double outlet right ventricle (pink arrowhead) where the aorta exits from the right ventricle. Blue arrows indicate reduced size pulmonary arteries in J. K.) Wild type section of the ventricular septum. L.) and M.) Ventricular septal defects in *Cyp26b1*$^{-/-}$ sections (orange arrowheads). rsc: right subclavian artery, lcc: left common carotid artery, rt: right thymus lobe, lt: left thymus lobe, o: oesophagus, rcc: right common carotid artery, Ao: aorta, pt: pulmonary trunk, rosca: retro-oesophageal right subclavian artery, rv: right ventricle, AoA:, aortic arch, aAo: ascending aorta, iaa-b: interrupted aortic arch type-b, lsc: left subclavian artery, lv: left ventricle, vs: ventricular septum.

Table 4.2 Table of frequency of thymic and cardiovascular defects at E15.5 in offspring from *Cyp26b1*$^{+/-}$ crosses

Phenotype	Wild-Type	*Cyp26b1*$^{+/-}$	*Cyp26b1*$^{-/-}$
Normal	18	23	0
Thymus defect only	0	6	1
Thymus and AoA defect	0	0	1
Thymus, alignment defect and VSD	0	0	1
Thymus, AoA and alignment defect and VSD	0	0	10 (4 IAA-B & ROSCA, 1RAA & ROSCA, 1CAo, 4ARSC)
Reabsorbed (did not undergo OPT)	0	0	1 (CAT)
Total defects	0	6	14
Total embryos	18	29	14

All embryos were examined for visible great vessel and thymus defects. All *Cyp26b1*$^{-/-}$ embryos also underwent OPT except for one reabsorbing embryo. Six embryos each of wild type and *Cyp26b1*$^{+/-}$ were also processed for OPT. P<0.0001 for all defects, great vessel defects only and alignment/VSD abnormalities only (Fishers Exact Probability Test [FEPT]). IAA-B: interrupted

aortic arch type-b, ROSCA: retro-oesophageal right subclavian artery, RAA: right aortic arch, CAo: cervical aortic arch, ARSC: aberrant right subclavian (not ROSCA), CAT: common arterial trunk. n=62.

4.2.3 Origin of the cardiovascular defects observed in E15.5 *Cyp26b1*$^{-/-}$ embryos

The great vessel defects present in *Cyp26b1* null embryos at E15.5 could have arisen through two mechanisms earlier in development; firstly, abnormal formation of the pharyngeal arch arteries or secondly, abnormal maintenance or remodelling of the pharyngeal arch arteries. The type of great vessel defects seen arise predominantly from defects of the 4th pharyngeal arch artery earlier in development, in models such as the *Tbx1* heterozygote mutant. The alignment anomalies which were also present in E15.5 *Cyp26b1*$^{-/-}$ embryos are frequently the result of developmental problems of the outflow tract at earlier developmental stages. Consequently, the offspring of *Cyp26b1* heterozygote crosses were investigated at E10.5 to determine the cause of the abnormalities found at E15.5. Unsurprisingly embryos of all genotypes were recovered in Mendelian ratios at this stage (Table 4.3).

Table 4.3 Table of genotypes recovered at E10.5 from *Cyp26b1*$^{+/-}$ crosses

	Wild-Type	*Cyp26b1*$^{+/-}$	*Cyp26b1*$^{-/-}$
Observed frequency	19	33	20
Expected frequency	18	36	18

P>0.05 from a chi-squared analysis, therefore genotype ratios are recovered as expected in a 1:2:1 Mendelian frequency for wild type: heterozygous: null *Cyp26b1* genotypes. n=72.

4.2.3.1 Pharyngeal arch artery anomalies

At E10.5 PAA 1 and 2 should be regressing, and PAA 4-6 should all be present, although the presence and size of PAA6 in particular varies with the precise age of the embryo. To score any defects in the formation of the pharyngeal arch arteries, embryos were injected with Indian ink into the outflow tract and PAA. The clearest abnormalities to recognize were those embryos where a non-patent to ink or thin 4th PAA was present

with a normally sized PAA3 and 6. *Cyp26b1* null embryos scored seven-fold higher numbers of these defects compared to wild-type and heterozygote controls (Table 4.4, Fig 4.4A.-E.) (P<0.0002, FEPT). Both unilateral and bilateral defects of the 4th and 6th PAA together (Fig.4.4F.) were observed in all genotypes. Unilateral 4th and 6th PAA defects were just statistically significantly higher in *Cyp26 b1*$^{-/-}$ embryos compared to controls (P=0.05). However, bilateral 4th and 6th defects and combined uni- and bilateral 4th and 6th PAA defects were not found to be statistically significant (P>0.05 FEPT) between genotype groups. The total number of embryos with aberrant PAA was 3.5-fold higher in *Cyp26b1*$^{-/-}$ embryos than wild type and *Cyp26b1*$^{+/-}$ embryos, which was statistically significant (P≤0.005, FEPT).

Table 4.4 Table of frequency of pharyngeal arch artery defects at E10.5 in offspring from *Cyp26b1*$^{+/-}$ crosses

Phenotype	Wild-Type	*Cyp26b1*$^{+/-}$	*Cyp26b1*$^{-/-}$
Normal	15	29	7
Unilateral small/non-patent PAA4 with patent PAA6	1	0	7*
Unilateral small/non-patent PAA 4 & 6	2	1	5*
Bilateral small/non-patent PAA4 & 6	1	3	1
Total defects	4	4	13*
Total embryos	19	33	20

Pharyngeal arch artery defects detected by Indian ink injection at E10.5. *P≤0.05, FEPT in *Cyp26b1*$^{-/-}$ embryos for the indicated classes of defects. n=72

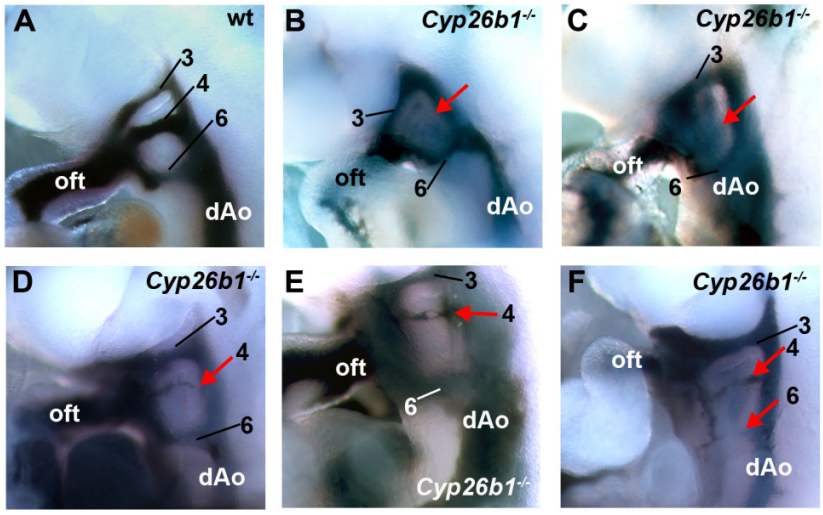

Figure 4.4 Pharyngeal arch artery defects at E10.5 in offspring of *Cyp26b1*$^{+/-}$ crosses

A.-F.) Side-views. Indian ink injection into the outflow tract of E10.5 embryos fills and visualizes the pharyngeal arch arteries. A.) Wild-type control with PAA3-6 fully present. B. and C.) *Cyp26b1*$^{-/-}$ embryos with non-patent/missing PAA4 D. and E.) *Cyp26b1*$^{-/-}$ embryos with thin 4th PAA. D.) PAA4 does not connect to the dorsal aorta. E.) PAA4 has a non-patent interruption in the centre of the vessel. F.) *Cyp26b1*$^{-/-}$ embryo where both PAA4 and 6 are reduced in size. Numbers 3-6 indicate the relevant pa, red arrows indicate non-patent/missing or small PAA, oft: outflow tract, dAo: dorsal aorta.

4.2.3.2 Outflow tract defects

The types of OFT alignment defects seen at E15.5 have been associated with abnormal rotation of the aorta and pulmonary trunk, possibly as the result of a shortened straighter OFT earlier in development. The OFT of offspring from *Cyp26b1*$^{+/-}$ crosses were accordingly examined at E10.5. The average length of the distal OFT was found to be 1.5-fold shorter in *Cyp26b1*$^{-/-}$ embryos, a significant reduction compared to wild-type embryos ($P<0.009$, unpaired two-tailed t test, Fig.4.5.). The proximal OFT had a similar length in wild-type and null embryos (1.06-fold shorter, $P>0.05$, unpaired two-tailed t test, Fig.4.5.). However, the proximal OFT appeared to be straighter, with a wider internal angle between the distal and proximal OFTs in *Cyp26b1*$^{-/-}$ embryos compared to wild type. The size and ballooning of the right ventricle also seemed to be diminished in some

null embryos and the right and left ventricles were positioned more parallel to each other than in controls (Fig.4.6A-D).

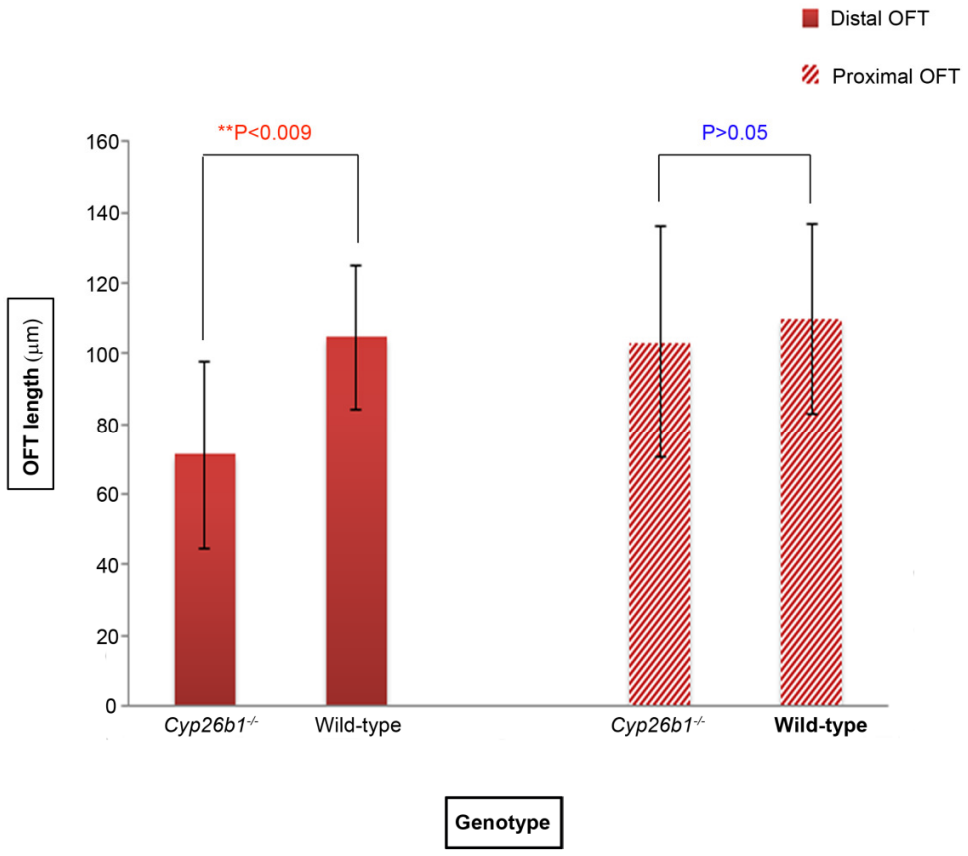

Figure 4.5. Graph of OFT lengths in wild-type and *Cyp26b1*$^{-/-}$ E10.5 embryos

Distal OFT length is significantly reduced in *Cyp26b1* null embryos (P<0.009, unpaired two-tailed t test).

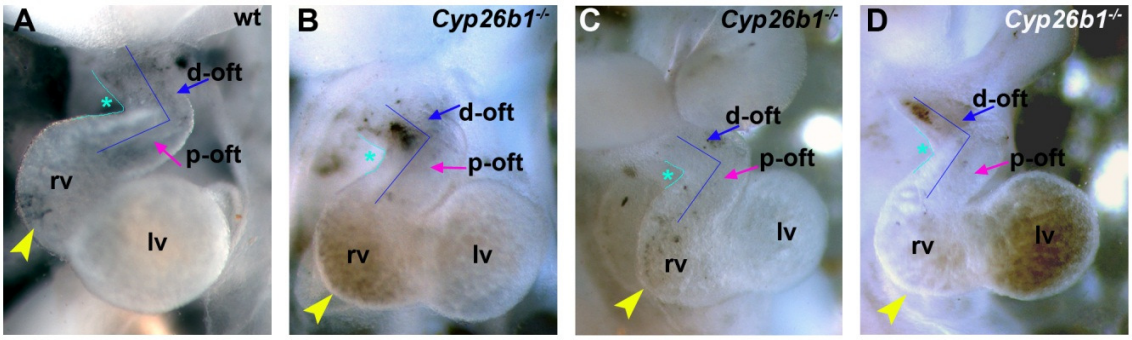

Figure 4.6 Outflow tract defects in wild-type and *Cyp26b1*$^{-/-}$ E10.5 embryos

A.-D.) Frontal views. A.) Wild-type embryos B.-D.) Cyp26b1-/- embryos. D-oft and blue arrow: distal outflow tract, p-oft and pink arrow: proximal outflow tract, rv: right ventricle, lv: left ventricle,

turquoise asterisk and outline indicate outer angle between distal and proximal OFT, yellow arrowhead: altered size/position of right ventricle relative to left ventricle.

4.2.4 Investigation of genetic interaction between *Tbx1* and *Cyp26b1*

Given the similar cardiovascular phenotypes observed in *Cyp26b1* and *Tbx1* null embryos and the isolation of *Cyp26b1* from a $Tbx1^{+/-}$ versus $Tbx1^{-/-}$ microarray and its altered expression in *Tbx1* null embryos, it was decided to investigate the possibility that these genes lie within the same genetic pathway. The approach taken, was to determine the severity/frequency of the cardiovascular defects in the offspring of $Cyp26b1^{+/-}$ and $Tbx1^{mcm/+}$ mice. At E15.5 all resulting genotypes were recovered in Mendelian ratios (Table 4.5) and all appeared normal externally. All embryos also appeared to be alive at the time of dissection.

Table 4.5 Table of genotypes recovered at E15.5 from $Cyp26b1^{+/-}$ and $Tbx1^{mcm/+}$crosses

	Wild-Type	$Cyp26b1^{+/-}$	$Tbx1^{mcm/+}$	$Cyp26b1^{+/-}$:$Tbx1^{mcm/+}$
Observed frequency	24	16	13	22
Expected frequency	18.75	18.75	18.75	18.75

P>0.05 from a chi-squared analysis, therefore genotype ratios are recovered as expected in a 1:1:1:1 Mendelian frequency for wild type: heterozygous: double heterozygote genotypes, n=75.

4.2.4.1 Great vessel and thymus defects from $Cyp26b1^{+/-}$ and $Tbx1^{mcm/+}$crosses

Thymus and great vessel defects were of a similar range and severity in $Cyp26b1^{+/-}$:$Tbx1^{mcm/+}$ double heterozygotes when compared to $Tbx1^{mcm/+}$ and $Cyp26b1^{-/-}$ embryos, including aortic arch abnormalities such as IAA-B, CAo and aberrant right subclavian (ARSC)(Table 4.6, Fig.4.7A.-D.). Wild type embryos displayed no defects of this type and 6% (1/16) $Cyp26b1^{+/-}$ embryos had a thymus defect. Twenty-three percent (3/13) of $Tbx1^{mcm/+}$ embryos had these characteristic thymic and cardiovascular defects, the frequency rising to 36% (8/22) in $Cyp26b1^{+/-}$:$Tbx1^{mcm/+}$ embryos. The association of the defects with all four genotypes is significant (P<0.02, FEPT). However, when only the

defects seen in *Tbx1*$^{mcm/+}$ versus *Cyp26b1*$^{+/-}$*:Tbx1*$^{mcm/+}$ were considered, this association was no longer significant, for either the total number of anomalies present or sub-categories (P>0.05, FEPT). To contrast synergistic with additive effects, it was assumed that in the case of summative effects, 6% of the *Cyp26b1*$^{+/-}$*:Tbx1*$^{mcm/+}$ embryos lacking a phenotype due to *Tbx1mcm/+* depletion would have a defect due to *Cyp26b1* reduction. Thus the expected number of defects assuming additive effects in double heterozygote embryos was 7/22 (32%). This was not significantly different from the 36% of abnormalities observed in *Cyp26b1*$^{+/-}$*:Tbx1*$^{mcm/+}$. Overall, the results with the current data set make it unlikely that there is a genetic interaction between *Cyp26b1* and *Tbx1* during great vessel and thymus development.

Table 4.6 Table of frequency of thymic and great vessel defects at E15.5 in offspring from *Cyp26b1*$^{+/-}$ and *Tbx1*$^{mcm/+}$ crosses

Phenotype	Wild-Type	*Cyp26b1*$^{+/-}$	*Tbx1*$^{mcm/+}$	*Cyp26b1*$^{+/-}$ *:Tbx1*$^{mcm/+}$
Normal	24	15	10	14
Thymus defect only	0	1	1	1
Thymus and ARSC	0	0	1	3
Thymus and AoA	0	0	0	1
Thymus, ARSC, AoA	0	0	1	3
Total defects	0	1	3	8
Total embryos	24	16	13	22

ARSC: aberrant right subclavian artery, including high RSC and ROSCA. AoA defects include IAA-B andCAo. n=75.

4.2.4.2 Intracardiac defects from Cyp26b1$^{+/-}$ *and Tbx1*$^{mcm/+}$*crosses*

To determine if *Cyp26b1* and *Tbx1* could be interacting to generate the type of intracardiac defects (VSD and alignment defects) seen in *Cyp26b1*$^{-/-}$ embryos a subset of all genotypes (including embryos with all observed great vessel phenotypes) were processed for OPT analysis. No defects were seen wild-type embryos but alignment

anomalies were present in small numbers in *Cyp26b1*$^{+/-}$, *Tbx1*$^{mcm/+}$ and double heterozygote embryos (Table 4.7, Fig.4.7E.-H.) in 20%, 30% and 16% of embryos respectively. The alignment defects observed were only of overriding aorta, whereas in *Cyp26b1*$^{-/-}$ embryos double outlet right ventricle, a more severe alignment anomaly, was observed. No significant association was found with genotype, indicating that for the current sample size these levels of intracardiac defects are not considered to be significantly different from wild type. It is unlikely that there is a *Tbx1/Cyp26b1* interaction involved in generating these anomalies.

Table 4.7 Table of frequency of VSD and alignment defects at E15.5 in offspring from *Cyp26b1*$^{+/-}$ and *Tbx1*$^{mcm/+}$ crosses

Phenotype	Wild-Type	*Cyp26b1*$^{+/-}$	*Tbx1*$^{mcm/+}$	*Cyp26b1*$^{+/-}$ *:Tbx1*$^{mcm/+}$
Normal	10	8	7	16
VSD	0	0	1	0
VSD and OAo	0	2	2	3
Total defects	0	2	3	3
Total embryos	10	10	10	19

VSD: ventricular septal defect. OAo: overriding aorta (alignment defect). n=49.

In the cohort that underwent OPT all *Cyp26b1*$^{+/-}$*:Tbx1*$^{mcm/+}$ intracardiac defects were found in association with great vessel or thymus defects. There were an additional three embryos with aberrant great vessel development but no obvious VSD. One *Cyp26b1*$^{+/-}$ embryo and one *Tbx1*$^{mcm/+}$ embryo were found to have a VSD without additional abnormalities.

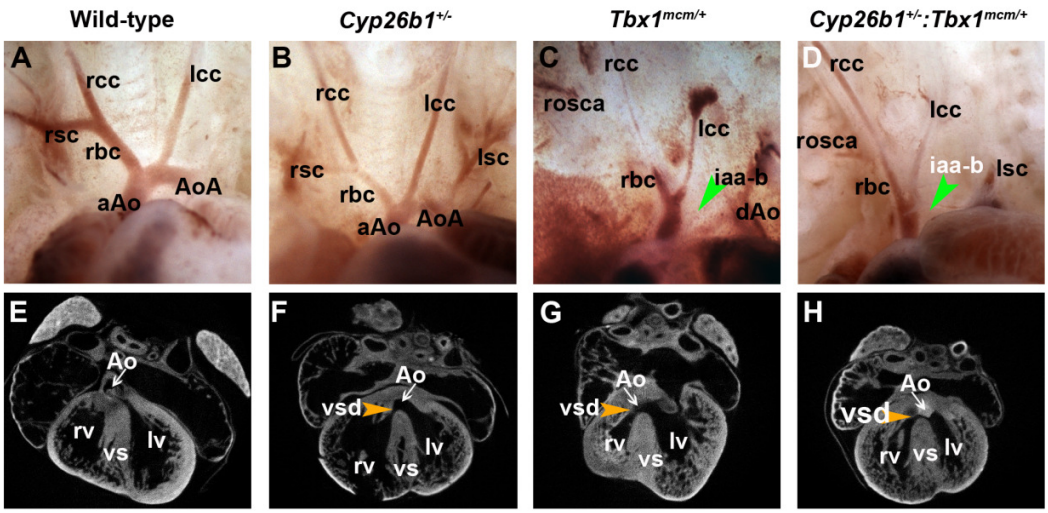

Figure 4.7. Cardiovascular defects in offspring of *Cyp26b1*$^{+/-}$ and *Tbx1*$^{mcm/+}$ crosses at E15.5.

A.-D.) Great vessel defects. A.) wild-type embryo with no abnormalities. B.) *Cyp26b1*$^{+/-}$ embryo with no abnormalities. C.) *Tbx1*$^{mcm/+}$ embryo with iaa-b and rosca. D.) *Cyp26b1*$^{+/-}$*:Tbx1*$^{mcm/+}$ embryo with iaa-b and rosca. E.-F.). OPT sections through E15.5 embryos. E.) Wild-type with normal aorta relative to the ventricular septum. F.-H.) *Cyp26b1*$^{+/-}$, *Tbx1*$^{mcm/+}$ and *Cyp26b1*$^{+/-}$*:Tbx1*$^{mcm/+}$ embryos respectively, all with overriding aorta and a VSD. rsc: right subclavian artery, rcc: right common carotid artery, rbc: right brachiocephalic artery, lcc: left common carotid artery, lsc: left subclavian artery, aAo: ascending aorta, AoA: aortic arch, dAo: descending aorta, rosca: retro-oesophageal right subclavian artery, iaa-b: interrupted aortic arch type-b (green arrowhead), Ao: position of aorta relative to ventricular septum (white arrow), vs: ventricular septum, rv: right ventricle, lv: left ventricle, vsd: ventricular septal defect (orange arrowhead).

4.2.4.3 Liveborn offspring from Cyp26b1$^{+/-}$ *and Tbx1*$^{mcm/+}$*crosses*

Genotype ratios in live-born mice from *Cyp26b1*$^{+/-}$ and *Tbx1*$^{mcm/+}$ crosses at P10+ were also calculated to determine whether any interaction might result in a post-natal lethality (Table 4.8). When all four genotype ratios were considered, the observed ratio was significantly different from that of the expected ratio ($P<0.004$, chi-squared test). The numbers of wild-type recovered were higher than expected, as were those of the *Tbx1*$^{mcm/+}$ mice, some of which should die at birth, reducing the number surviving at P10. Double heterozygote mice appeared to be under-represented, suggesting some peri-natal lethality maybe occurring in these animals. However, when *Cyp26b1*$^{+/-}$*:Tbx1*$^{mcm/+}$ numbers were

compared to single heterozygotes only, the difference between the ratios was no longer significant (P>0.05).

Table 4.8 Table of genotypes recovered at P10+ from *Cyp26b1*$^{+/-}$ and *Tbx1*$^{mcm/+}$ crosses

	Wild-Type	*Cyp26b1*$^{+/-}$	*Tbx1*$^{mcm/+}$	*Cyp26b1*$^{+/-}$ *:Tbx1*$^{mcm/+}$
Observed frequency	49	30	32	20
Expected frequency	32.75	32.75	32.75	32.75

P<0.004 from a chi-squared analysis, therefore genotype ratios are not recovered as expected in a 1:1:1:1 Mendelian frequency for wild type: heterozygous: double heterozygote genotypes, n=131.

4.2.5 Loss of one *Tbx1* allele may have a modifying effect upon the *Cyp26b1*$^{-/-}$ phenotype

The experiments described in section 4.2.5 suggested that there was no genetic interaction between *Cyp26b1* and *Tbx1* in determining the double heterozygote phenotype at the 95% confidence level. However, in light of the raised numbers of abnormalities in these animals, it was decided to investigate if any modifying effects were in operation in triple allele knock-outs. It is conceivable that phenotypic effects will only be evident when more than one *Cyp26* allele is lost due to possible redundancy between these genes. To this end it was decided to first focus upon the *Cyp26b1*$^{-/-}$*Tbx1*$^{mcm/+}$ phenotype, where RA should be increased more in the context of the *Tbx1* heterozygote background, adjacent to the *Cyp26b1*-expressing region. Additionally, the *Cyp26b1*$^{-/-}$ phenotype is milder than that of the *Tbx1*$^{mcm/mcm}$, which might make detecting any modifying influence easier. The offspring of double heterozygote embryos crossed with *Cyp26b1*$^{+/-}$ mice were genotyped and examined for thymic and great vessel defects at E15.5. Genotypes of mice from these crosses were found to be just within Mendelian ratios (P≤0.0514, chi-squared test). The external appearance of wild-type, *Cyp26b1*$^{+/-}$, *Tbx1*$^{mcm/+}$ and *Cyp26b1*$^{+/-}$*:Tbx1*$^{mcm/+}$ embryos was normal. Both *Cyp26b1*$^{-/-}$ and *Cyp26b1*$^{-/-}$*:Tbx1*$^{mcm/+}$ appeared very similar externally, both having severe meromelia and varying degrees of oedema and haemorrhage (Fig.4.8A.-D.).

Table 4.9 Table of genotypes recovered at 15.5 from *Cyp26b1*$^{+/-}$ and *Cyp26b1*$^{+/-}$*:Tbx1*$^{mcm/+}$ crosses

	Wild-type	*Cyp26b1*$^{+/-}$	*Tbx1*$^{mcm/+}$	*Cyp26b1*$^{+/-}$ *:Tbx1*$^{mcm/+}$	*Cyp26b1*$^{-/-}$	*Cyp26b1*$^{-/-}$ *:Tbx1*$^{mcm/+}$
Observed frequency	17	19	9	11	10	6
Expected frequency	9	18	9	18	9	9

P=0.0514 from a chi-squared analysis, therefore genotype ratios are recovered as expected in a 1:2:1:2:1:1 Mendelian frequency. n=72.

The cardiovascular phenotypes observed for wild types, *Tbx1* heterozygotes, *Tbx1*$^{mcm/+:}$ *Cyp26b1*$^{+/-}$ and *Cyp26*$^{-/-}$ were all very much as described previously (Table 4.10). All embryos with *Cyp26b1*$^{-/-}$ and *Cyp26b1*$^{-/-}$*:Tbx1*$^{mcm/+}$ genotypes presented with some form of aortic arch defect. Forty percent of *Cyp26b1* null embryos (4/10) and 50% of *Cyp26b1*$^{-/-}$*:Tbx1*$^{mcm/+}$embryos (3/6) were dead at dissection, although recently enough that cardiothoracic defects could still be distinguished (~E14.5-15). *Cyp26b1*$^{-/-}$ embryos exhibited the same range of anomalies seen previously, with the most severe set of defects seen in individual embryos comprising a small ectopic thymus, IAA-B and ARSC (Table 4.10). Twenty percent (n=2/10) of *Cyp26b1*$^{-/-}$ embryos exhibited this most severe phenotype, compared to a significantly increased 100% of *Cyp26b1*$^{-/-}$*:Tbx1*$^{mcm/+}$ embryos (n=6/6, P<0.002, FEPT). When the additive effects of a *Tbx1*$^{mcm/+}$ allele and the *Cyp26b1* null upon the frequency of the IAA-B plus ARSC and thymus defect phenotype were calculated (n=4/10) they were also found to be significantly different from those observed with the *Cyp26b1*$^{-/-}$*:Tbx1*$^{mcm/+}$ genotype (P<0.05, FEPT). There was also a significant difference between *Cyp26b1*$^{-/-}$*:Tbx1*$^{mcm/+}$ and *Cyp26b1*$^{-/-}$ embryos when the number of embryos with IAA-B with and without ARSC was compared (P<0.0001, FEPT). However, when only the presence or absence of IAA-B was compared between these two genotypes it was found not to be significant (P>0.05, FEPT). Thus, with the current numbers, a single *Tbx1*$^{mcm/+}$ allele in addition to a full *Cyp26b1* null knock-out may confer a higher frequency of the most severe cardiovascular phenotype in terms of the presence/absence of right 4th PAA defects in addition to that of the left 4th PAA.

Table 4.10 Table of frequency of thymic and cardiovascular defects at E15.5 in offspring from *Cyp26b1*$^{+/-}$ x *Cyp26b1*$^{+/-}$:*Tbx1*$^{mcm/+}$ crosses

Phenotype	Wild-type	*Cyp26b1*$^{+/-}$	*Tbx1*$^{mcm/+}$	*Cyp26b1*$^{+/-}$:*Tbx1*$^{mcm/+}$	*Cyp26b1*$^{-/-}$	*Cyp26b1*$^{-/-}$:*Tbx1*$^{mcm/+}$
Normal	17	16	5	6	0	0
Thymus defect	0	3	1	1	2	0
RSC defect	0	0	0	1	0	0
Thymus and RSC	0	0	1	2	3	0
Thymus, RSC, AoA	0	0	2 (IAA-B)	1 (IAA-B)	2 (IAA-B)	6 (IAA-B)
Thymus, AoA	0	0	0	0	3 (IAA-B)	0
Total defects	0	3	4	5	10	6
Total embryos	17	19	9	11	10	6

RSC: right subclavian artery, AoA : aortic arch defects,IAA-B or RAA.

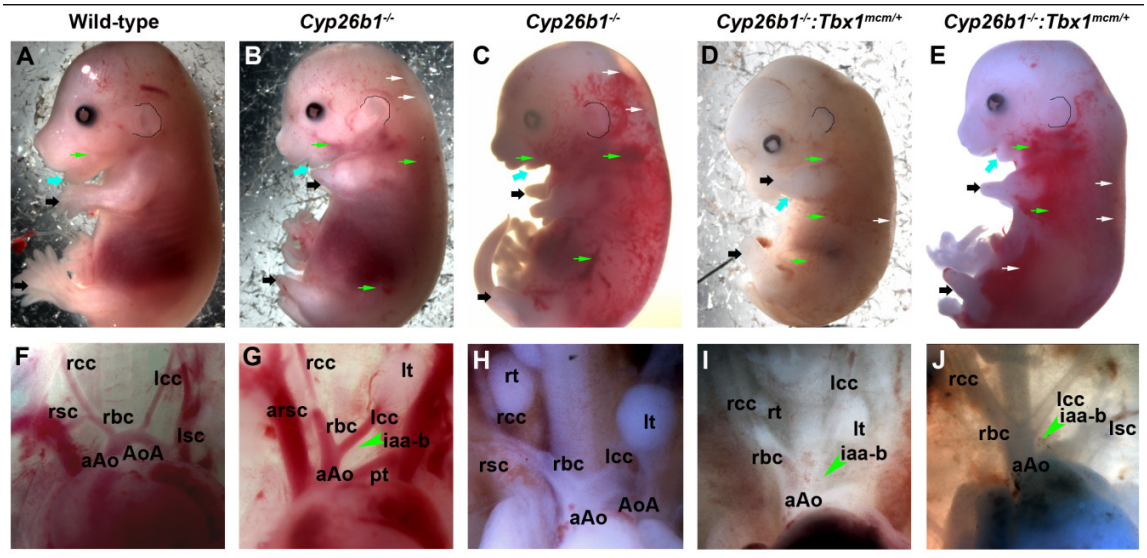

Figure 4.8 Great vessel defects in E15.5 *Cyp26b1*$^{-/-}$ and *Cyp26b1*$^{-/-}$*Tbx1*$^{mcm/+}$ embryos

A.-E.) External views. A. Wild-type. B. and C.) *Cyp26b1*$^{-/-}$ D. and E.) *Cyp26b1*$^{-/-}$:*Tbx1*$^{mcm/+}$

F.-J.) Great vessels. F.) Wild-type, normal aortic arch. G.) *Cyp26b1*$^{-/-}$ with iaa-b and arsc. H.) *Cyp26b1*$^{-/-}$ with small ectopic thymus, normal aortic arch. D. and E.) *Cyp26b1*$^{-/-}$*:Tbx1*$^{mcm/+}$ with iaa-b and arsc. External ear pinnae are outlined in white or black. Small green arrows: blood vessels in controls and sites of haemorrhage in mutant, small white arrows: oedema. large black arrows: meromelic limbs, large turquoise arrows: micrognathia, . rsc: right subclavian artery, rcc: right common carotid artery, rbc: right brachiocephalic artery, lcc: left common carotid artery, lsc: left subclavian artery, aAo: ascending aorta, AoA: aortic arch, pt: pulmonary trunk, arsca: aberrant right subclavian artery, iaa-b: interrupted aortic arch type-b (green arrowhead), lt: left thymus lobe, rt: right thymus lobe.

4.3 Discussion

4.3.1 *Cyp26b1*$^{-/-}$ phenotype

4.3.1.1 Cardiovascular defects

This study has focused on investigating the role that *Cyp26b1* may play in the development of pharyngeal and OFT derived structures classically affected in 22q11DS. It was discovered that *Cyp26b1* null embryos display characteristic great vessel remodeling and cardiac alignment and thymus defects, often associated with 22q11DS and its murine models. These types of cardiac anomalies were more akin to those seen in *Tbx1* heterozygous mouse phenotype, in that at E15.5 they consisted mainly of IAA-B, (occasionally right aortic arch), ROSCA or ARSC and DORV. Common arterial trunk, which is 100% penetrant in *Tbx1* null embryos and found in 3-10% of patients in clinical studies (Marino et al., 2002) but is normally not present in *Tbx1*$^{+/-}$ mice, was found only once in an *Cyp26b1*$^{-/-}$ embryo already dead at dissection.

The segments of the aortic arch which are affected in these specific great vessel anomalies are those derived from the 4th PAAs. These structures are known to be particularly sensitive to developmental disruption for reasons which are not yet fully understood. Animal models with these deficiencies of great vessel development frequently are found to have defects of 4th PAA formation or remodeling underlying the later aortic arch problem. This proved to be the case for *Cyp26b1*$^{-/-}$ embryos which failed to form the 4th PAA correctly at E10.5. A number of those embryos had a fully patent 6th

PAA whilst others did not, the 6th PAA also appearing small or non-patent. A number of these latter types of embryo were also seen in wild-type and *Cyp26b1* heterozygous embryos, making it difficult to assess their contribution to the E15.5 null phenotype. The frequency of great vessel defects at E15.5 was 86% (12/14). The non-patent 4th PAA with patent 6th PAA defects alone make up only 35% of *Cyp26b1* nulls at E10.5, which is significantly less than the frequency at E 15.5 ($P \leq 0.005$, Fishers Exact Probability Test). It was also found that at E10. 5, 5% (1/20) bilateral 4th PAA defects were found in *Cyp26*$^{-/-}$ embryos, whilst at E15.5, in a sample of similar size 36% of embryos (5/14) were shown to have defects affecting both left and right 4th PAA derivatives. Thus, while failure of 4th PAA formation contributes to the defects seen at E15.5, a later defect in remodelling of the PAA may also play a role. If, however, the non-patent 4th PAA with patent 6th PAA defects were combined with the small 4th and 6th PAA defects, then together these abnormalities make up 65% (13/20) of E10.5 *Cyp26b1* null embryos. This is sufficiently similar to the frequency at E15.5 ($P > 0.05$, FEPT) to account for the majority of the great vessel anomalies at E15.5. Examination of PAA defects E11.5-13.5 should be undertaken to distinguish whether remodeling defects also contribute to the aortic arch phenotype at E15.5. The types of great vessel defects observed in *Cyp26b1*$^{-/-}$ embryos are often associated with intra-cardiac defects which include alignment abnormalities of the great vessels with the cardiac chambers such as DORV and OAo and with PM-VSDs. These alignment defects were present in *Cyp26b1*$^{-/-}$ embryos at E15.5, as was an abnormally shortened OFT at E10.5 at similar frequencies (79% versus 72%, $P > 0.05$, FEPT). This is a relatively high frequency of DORV compared to other animal models with similar phenotypes, for example *Tbx1* mutants (Liao et al., 2004), suggesting *Cyp26b1* may be important for OFT rotation. Alignment defects have been suggested to arise as a result of abnormal looping and rotation of the outflow tract relative to the ventricular septum. This in turn has been linked to shortened outflow tracts, as proper elongation of the OFT is essential for correct alignment of the great vessels and the ventricular septum. Contributions to the OFT from the secondary heart fields and cardiac neural crest and regulation of cell proliferation, differentiation and apoptosis are all required for this complex remodelling process which involves many cell types and gene/signaling

pathways including *Tbx1* and retinoic acid signalling (Keyte and Hutson, 2012; Parisot et al., 2011; Vincent and Buckingham, 2010; Zaffran and Kelly, 2012).

Expression of the various *Cyp26* genes is important for the fine regulation of RA levels in different tissues necessary for normal development. *Cyp26b1* is expressed in the hindbrain and in both the pharyngeal endoderm and ectoderm. Loss of expression in the hindbrain could result in aberrant neural crest patterning; in zebrafish the *cyp26* genes including *cyp26b1* have been shown to be required for hindbrain patterning and *cyp26b1* is also necessary for the neural crest-derived component of the pharyngeal arches (Hernandez et al., 2007; Reijntjes et al., 2007). In mice it has been shown that proper patterning of the pharyngeal ectoderm and endoderm by various genes including *Tbx1*, *Gbx2*, *Chd7*, *Fgf8*, *Ripply 3*, endothelin receptor and ligand, *Hoxa3*, *Shh* and RA signalling amongst others, is necessary for normal development, including neural crest migration. Disruption of this patterning results in 4th pharyngeal arch artery and subsequent great vessel defects and thymus defects (Abu-Issa et al., 2002; Arnold et al., 2006b; Bayha et al., 2009; Calmont et al., 2009; Dupe et al., 1999; Ghyselinck et al., 1998; Kameda, ; Macatee et al., 2003; Matt et al., 2003; Okubo et al., 2008; Okubo et al., 2011; Randall et al., 2009; Tavares et al., 2012; Washington Smoak et al., 2005; Wendling et al., 2000; Zhang et al., 2005). This sets a precedent for the ablation of *Cyp26b1* in these expression domains to contribute to the phenotypes observed.

It has been reported that another *Cyp26b1* mutant mouse model has normal hindbrain patterning but mild neural crest migration defects. This particular knock-out line was also investigated for thymus and cardiovascular defects but was reported to be normal in this respect (MacLean et al., 2009). This is a very different result to the one obtained in this study and several different explanations are possible. Firstly the two different targeting constructs were used to make the two separate lines. Both of these constructs remove all exons down-stream of exon 2 and should therefore theoretically produce a similar phenotype. The mouse line used in the studies reported here (Yashiro et al., 2004) used a targeting vector containing a *PGK-puro* cassette cloned into intron 3 which was not removed following homologous recombination. Theoretically, this cassette can interfere with expression neighbouring genes. Consultation of Ensembl also did not reveal any near-by genes with any known role in development which, if interfered, with

could conceivably lead to the cardiovascular phenotypes observed. Therefore, the most likely explanation for this discrepancy in reported phenotype is that of genetic background. In this thesis all the engineered lines used were bred onto a C57Bl6 inbred background, which appears to potentiate for cardiovascular defects. No information was given in either publication for the other *Cyp26b1* mutant regarding the genetic background used for those experiments. However, if it was other than C57Bl6, then this could very well explain the variation in phenotype described as phenotypic variation with genetic background is a well-recognized phenomenon (Dixon and Dixon, 2004; Linder, 2001; Roberts et al., 2002; Strunk et al., 2004; Taddei et al., 2001).

4.3.1.2 External phenotype

At E15.5 *Cyp26b1*$^{-/-}$ were immediately recognizable due to previously described external developmental abnormalities. These included severe meromelia (Yashiro et al., 2004), shortened mandible, maxilla and nasal process (micrognathia) and small external pinnae (MacLean et al., 2009; Reijntjes et al., 2007). It was also determined that embryos displayed cleft palate as described before (MacLean et al., 2009; Okano et al., 2012).

A previously un-described phenotype was also apparent: the majority of *Cyp26b1* null embryos suffered from haemorrhage to varying degrees. *Cyp26b1* has been reported as being expressed in human endothelial and smooth muscle cells (Elmabsout et al., 2012; Ocaya et al., 2011) and in endothelial cells in the chick (Reijntjes et al., 2003). Normal functioning of either these cell types would be essential for the integrity of blood vessels in the embryo. Individual *Cyp26* gene expression varies widely between species and no vascular expression domain has been previously described in the mouse. However, this does not rule out either previously undetected low levels of expression of *Cyp26b1* in these tissues or their precursors early in development, or a secondary effect resulting from *Cyp26b1* knockdown in other expression domains and/or increased RA levels. Cytochrome P450 oxidoreductase (POR), acts as an electron donor for all cytochrome P450 enzymes, and is essential for the proper function of RA-metabolizing CYP26 enzymes. *Por* null embryos exhibit defects similar to both *Cyp26al* and *Cyp26b1* nulls, in the latter case having similar craniofacial and limb defects. They also have been shown to

have petechial haemorrhaging and greatly reduced vasculogenesis which can be rescued by reducing RA levels (Otto et al., 2003; Ribes et al., 2007b; Shen et al., 2002). It was also noticed that *Cyp26b1* null embryos frequently suffered from oedema, possibly related to the haemorrhagic phenotype. However, oedema is also associated with cardiac insufficiency, raising the possibility of the cardiac defects in *Cyp26b1* null mice contributing to this phenomenon.

Previously it has been stated that *Cyp26b1* null embryos die at birth (MacLean et al., 2009; Yashiro et al., 2004). While most null embryos do survive until birth, a number of embryos were already dead at E15.5. Cardiovascular insufficiency may contribute to this lethality and it can be speculated that the haemorrhagic phenotype observed may also affect the placental tissues and contribute to this early lethality.

4.3.2 Lack of interaction between *Tbx1* and *Cyp26b1*

Since *Cyp26b1* was identified from a microarray screen designed to isolate potential down-stream targets of *Tbx1* and has altered expression in *Tbx1* null mice it seemed reasonable to investigate whether a genetic interaction, placing these genes within the same pathway, existed. However, the results from crosses of heterozygous *Tbx1* and *Cyp26b1* mutant mice suggest this is not the case, as no significant synergistic rise in severity or frequency of the cardiovascular phenotype compared to single *Tbx1* heterozygotes was found. Therefore the similarities between the *Cyp26b1* and *Tbx1* mutant phenotypes are most likely the result of independent pathways operating upon the same tissues to produce a comparable phenotype. However, double heterozygotes did have a raised incidence of aortic arch defects in the current sample, which might become significant with a larger cohort. In addition, numbers of live-born animals from $Cyp26b1^{+/-}$ and $Tbx1^{mcm/+}$ crosses were not recovered in Mendelian ratios. Numbers of surviving $Cyp26b2^{+/-}/Tbx1^{mcm/+}$ animals were reduced, although not significantly so compared to $Tbx1^{mcm/+}$ embryos alone. Again this somewhat ambiguous result may become resolved further in a larger sample. While the incidence of intra-cardiac defects was examined in offspring from these crosses, only a subset of embryos underwent OPT, so analysis of the remaining samples may be required. Another possibility is that there

might be an observable synergistic effect upon a phenotype that has not been addressed so far. For example, both *Tbx1* and *Cyp26b1* null embryos suffer from defective palatogenesis (Funato et al., 2012; Goudy et al., 2010; Jerome and Papaioannou, 2001; MacLean et al., 2009; Okano et al., 2012) but this is not the case in heterozygous animals. It may therefore be worthwhile to investigate double heterozygote animals for genetic interactions affecting phenotypes other than the cardiovascular one described here, particularly given that defective palatogenesis leads to neonatal lethality due an inability to feed combined with milk inhalation leading to respiratory distress.

Alternatively, any interaction between heterozygous alleles of *Tbx1* and a single *Cyp26* gene may be too weak to detect, as in the *Tbx1* null mouse expression of all three *Cyp26* genes is altered. It is possible that the other *Cyp26* genes compensate for heterozygous deletion of *Cyp26b1* and that they too need to be reduced for a phenotypic interaction with *Tbx1* to become obvious. The first issue could be addressed initially by investigating double homozygous embryos or triple allele knockouts for any evidence of modifying effects.

4.3.3 Modifying effect of $Tbx1^{mcm/+}$ upon $Cyp26b1^{-/-}$ embryos

While there may be no grossly observable interaction between *Tbx1* and *Cyp26b1* in the pharyngeal and cardiovascular system in double heterozygote embryos, modifying effects of either allele upon the homozygous knock-out phenotype of the other might be present. In the current sample, 100% of $Cyp26b1^{-/-}$:$Tbx1^{mcm/+}$ embryos had the most severe combination of defects observed (IAA-B with ARSC and thymus defect), compared to 20% of $Cyp26b1^{-/-}$: $Tbx1^{+/+}$ embryos. This observation was statistically significantly different when compared to an additive effect. Thus, the presence of the $Tbx1^{mcm/+}$ allele may synergistically exacerbate the severity of defect seen in $Cyp26b1^{-/-}$ animals. This effect may well be mediated via the impact of *Tbx1* haploinsufficiency upon the other *Cyp26* genes in the context of *Cyp26b1* homozygosity. Whether the mechanism involved is simply that of needing to hit a certain threshold of increased pharyngeal RA levels to see phenotypic effects, or whether the specific alleles deleted are important to derive 22q11DS-like malformations, remains to be elucidated. For example, would $Cyp26b1^{-/-}$

:Cyp26a1$^{+/-}$ or *Cyp26a1*$^{+/-}$*: Cyp26b1*$^{+/-}$*: Tbx1*$^{+/-}$ embryos manifest a similar phenotype to *Cyp26b1*$^{-/-}$*:Tbx1*$^{mcm/+}$ embryos? As discussed in Chapter 3, at least some mice heterozygous for *Cyp26a1/b1/c1* are viable and fertile (Uehara et al., 2009), suggesting that triple heterozygosity of all three *Cyp26*s may not be enough to cause malformations in all animals. It would, however, be intriguing to investigate the effect of a *Tbx1* heterozygote allele upon this viability.

Prior studies upon *Tbx1* and genetic modifiers provide precedents for this type of genotype/phenotype variation and suggest that extending this work to consider compound homozygous mutants for *Tbx1*/*Cyp26b1* may be worthwhile, although understanding the severe phenotypes involved can be challenging. *Tbx1* has been shown to be necessary for the proper pharyngeal expression of *Tbx2* and *Tbx3* and they are redundantly required to restrict *Tbx1* expression to the lateral pharyngeal endoderm. However, double heterozygote mice for *Tbx1/Tbx2* or *Tbx1/Tbx3* were normal and *Tbx1*$^{-/-}$*:Tbx2*$^{+/-}$ mutants showed a mild endodermal expansion/segmentation defect. Conversely, in compound homozygous mutants *Tbx1*$^{-/-}$*:Tbx2*$^{-/-}$ or *Tbx1*$^{-/-}$*:Tbx3*$^{-/-}$, reduced expression of *Tbx2* and *Tbx3* in *Tbx1* null splanchnic mesoderm and endoderm could disrupt pharyngeal endoderm and OFT and right ventricle development more severely than in single null embryos (Mesbah et al., 2011). As in this example, there does appear to be a reciprocal effect of *Cyp26b1* and *Tbx1* upon each other in that *Tbx1* expression is down-regulated in *Cyp26b1* null mice, presumably as a consequence of raised levels of retinoic acid (Janesick et al., 2012; MacLean et al., 2009; Okano et al., 2012; Roberts et al., 2005). In *Tbx1* null embryos *Cyp26b1* pharyngeal endodermal expression is diminished and the pharyngeal ectodermal domain shifted. As discussed previously, it is difficult to dismiss this result as being caused by increased RA due to ectopic *Raldh2* expression as in previous studies excess RA induces *Cyp26b1* expression (Elmabsout et al., 2012; Lee et al., 2012; Ocaya et al., 2011; Reijntjes et al., 2005; White et al., 2000a; Yashiro et al., 2004). In another instance, *Chordin* (a Bmp signalling antagonist) was shown to be a modifier for the craniofacial phenotypes of *Tbx1* mutants. Chordin has been shown to up-regulate *Tbx1* expression whereas Bmp-signalling reduces it. *Chordin* mutations alone produce a low penetrance mandibular truncation. A point mutation in *Tbx1* produced a hypomorphic allele with a 22q11DS-like cardiovascular phenotype in which the

characteristic craniofacial malformations were infrequently present unless *Chordin* was also deleted. Therefore, *Chordin* acts as a modifier of the craniofacial abnormalities associated with loss of *Tbx1* (Choi and Klingensmith, 2009).

The data collected in this work so far suggest that *Tbx1* may act as modifier of the great vessel phenotype in *Cyp26b1* null embryos. However, the sample size of the *Cyp26b1*$^{-/-}$*:Tbx1*$^{mcm/+}$ cross is not particularly high, so increasing the size of the sample might alter this observation. In addition, the genotype ratio for the *Cyp26b1*$^{+/-}$*:Tbx1*$^{mcm/+}$ x *Cyp26b1*$^{+/-}$ cross was only just as statistically expected, so further numbers could also help to produce a more clear-cut result. Finally, OPT analysis of intra-cardiac defects has not yet been performed upon these embryos and *Tbx1*$^{mcm/+}$ might play an extra modifying role in this phenotype.

4.4 Future Directions

4.4.1 Further investigation of the *Cyp26b1*$^{-/-}$ phenotype

The work reported in this chapter shows that contrary to previous reports, *Cyp26b1* null mice can manifest a thymic and cardiovascular phenotype at E15.5 on a C57Bl6 background. These defects appear to result from pharyngeal and OFT defects earlier in development. However, further work remains to be performed to fully document the cause of these abnormalities. Firstly, proliferation and apoptosis studies with, for example, phosphohistone H3 and TUNEL staining respectively should be performed upon E10.5 or younger embryos to determine whether reduced proliferation and/or altered apoptosis in pharyngeal tissues and the splanchnic mesoderm of the SHF plays a role in the PAA and OFT observed in null embryos, particularly as retinoic acid has been shown to be involved in both these processes in OFT development (Ghyselinck et al., 1998; Li et al., 2010; Li et al., 2012).

OPT analysis of E10.5 embryos could further refine this phenotype giving insight into parameters known to be altered in other shortened OFT models (including the R115866 –treated chick) such as the angle of inner and outer ventricular curvature and the anterior levels of ventricular trabeculation and size of the right ventricle. *Hes1* and

Sema3C could be used as markers to examine OFT myocardium at the base of the pulmonary trunk which shows a counterclockwise rotation during formation of the great vessels (Bajolle et al., 2006; Bajolle et al., 2008; Rochais et al., 2009a; Yelbuz et al., 2002). Embryos between E10.5 and E15.5 could also be assessed for evidence of additional remodeling defects of the PAA in addition to those produced by the lack of formation of the 4th PAA at E10.5.

Molecular markers to delineate the development of the pharyngeal tissues including pharyngeal ectoderm (Ap2α, *Gbx2*, *Fgf8*), endoderm (*Pax1/9*, *Shh*, *Fgf8*), mesoderm (*Tbx1*, *Mesp1*), neural crest (*Sox10*, Crapbp1 and 2, p75) and the secondary heart field (*Fgf10*, *Isl1*, *Mef2c*, *Nkx2.5*) should be deployed. In addition embryos should be stained with endothelial markers (PECAM, endomucin) and vascular smooth muscle (sma22) to assess vasculogenesis in the 4th PAA defect, the yolk sac and across the embryo in general, for the haemorrhaging and early death phenotypes. Markers for lymphogenesis such as Lyve1 might also be employed to see if failure in development of the lymphatic system is contributing to the embryonic oedema observed. Levels of retinoic acid within the *Cyp26b1*$^{-/-}$ embryos should also be assessed. *RARE-Lacz* reporter alleles available in house do not function well on a C57Bl6 background, so expression of RA-responsive genes such as *Hoxb1* could be used as a read-out of RA levels instead. Expression levels of *Raldh2* and *Tbx1* could also be evaluated. Expression of the other *Cyp26* genes should be examined in *Cyp26b1*$^{-/-}$ embryos to elucidate if any redundancy is operating in these embryos. Previous work suggests that hindbrain patterning is normal in *Cyp26b1* null embryos (MacLean et al., 2009), but no cardiovascular defects were observed in those embryos, so this should be re-checked for this specific *Cyp26b1* deletion allele. Given that RA-signalling is important for epicardial function, development of the epicardium and coronary vessels could also be assessed *in Cyp26b1*$^{-/-}$ embryos (Guadix et al., 2011; Lavine et al., 2005; von Gise et al., 2011).

Conditional deletion experiments could be carried out using a floxed-*Cyp26b1* allele (Dranse et al., 2011) to delete *Cyp26b1* in specific expression domains. *Ap2α-Cre* (Macatee et al., 2003) and *Wnt1-Cre* (Danielian et al., 1998) drivers could be used in conjunction to assess the impact of ectodermal down-regulation of *Cyp26b1*. To perform the same task for the pharyngeal endoderm either the *Foxa2*^{mcm} (Park et al., 2008) or a

Sox17-2A-iCre (Engert et al., 2009) line could be used to delete *Cyp26b1* expression. Lineage experiments crossing *Wnt1Cre:yfp* (Jiang et al., 2000), *Pax3Cre:yfp* (Engleka et al., 2005) *Tbx1Cre:R26R* (Brown et al., 2004) reporter lines onto the *Cyp26b1* null background were attempted as part of this study but after a significant amount of breeding no *Cre/yfp/Cyp26b1* null embryos had been retrieved. The only three LacZ-positive embryos gave anomalous genotyping results so this line of enquiry was abandoned.

Finally, it has been shown that TBX1 recruits chromatin remodelling BAF60A and histone H3K4 monomethyltransferase SETD7 to the *Wnt5a* promoter to facilitate activation of transcription. Furthermore this paper suggested that TBX1 may require similar binding of BAF60A at target promoters such as *Fgf8*, *Fgf10* and *Cyp26a1* for transcriptional activity (Chen et al., 2012a). It would be useful to determine if this is the case for *Cyp26b1* using similar experimental protocols, including identification of T-box binding motifs in the *Cyp26b1* promoter, chromatin immunoprecipitation (ChIP) assays of TBX1 to determine if it binds these sites and co-immunoprecipitation of TBX1, BAF60A and SETD7, Furthermore, the histone methylation status in the presence of increased or decreased levels of TBX1 could be investigated via quantitative ChIP for H3K4me1. Whether the presence of BAF60A is necessary for target transactivation could also be assessed by evaluating the effect of BAF60A knock-down upon *Tbx1*-expression vector transactivation of targets.

4.4.2 Further investigation of any possible *Cyp26b1* and *Tbx1* interactions

As discussed in section 4.3.2 increasing the numbers for the $Cyp26b1^{+/-}$ x $Tbx1^{mcm/+}$ crosses would further confirm if the increase observed in the great vessel phenotype in double heterozygous embryos is indeed not significantly different to single heterozygous mice. Performing OPT analysis on all the embryos collected for this cross rather than a subset would also provide more definitive information regarding any interaction concerning the intracardiac phenotypes. Furthermore, potential interaction affecting other phenotypes such as palatogenesis could be investigated. Additionally, given that $Cyp26^{+/-}$:$Tbx1^{mcm/+}$ embryos did have an increased number of aortic arch abnormalities, investigation of the PAA defects at earlier stages might be warranted. *Tbx1*

heterozygotes have high penetrance of the 4th PAA defect at E10.5 but this is increasingly rescued with time. This rescue of the *Tbx1* phenotype may impinge upon any interaction with *Cyp26b1* and so analysis of PAA defects at earlier stages could be fruitful.

This work could also be extended by investigating if a genetic interaction is present when Tbx1 expression is reduced by more than half. One way to do this would be to take advantage of the different *Tbx1* knock-out and hypomorphic alleles which in different combinations allow relative *Tbx1* expression from in a gradual range from 100% in wild-type to 0.2% in $Tbx1^{-/-}$ mice and result in a sliding scale of developmental abnormalities reflecting the amount to *Tbx1* expressed. Perhaps the best initial approach would be to use the $Tbx1^{neo2}$ hypomorphic line. $Tbx1^{neo2/neo2}$ express roughly 34% of wild-type *Tbx1* levels and have a 100% penetrance of thymic and aortic arch defects, of which roughly 13% are IAA-B (Zhang and Baldini, 2008). $Tbx1^{neo2/+}$:$Cyp26b1^{+/-}$ mice would probably be viable and fertile as *Tbx1* levels at 70% would be above those found in $Cyp26b1^{+/-}$: $Tbx1^{mcm/+}$ mice. The double heterozygotes could then be bred back to each other to generate a range of genotypes including $Tbx1^{neo2/neo2}$:$Cyp26b1^{+/-}$ and $Tbx1^{neo2/neo2}$:$Cyp26b1^{-/-}$ which could then be investigated for evidence of genetic interaction.

Finally, as mentioned in more detail in section 4.3.3 above, studying different compound mutants, including more $Cyp26b1^{-/-}$: $Tbx1^{mcm/+}$ embryos and extending the study to include $Cyp2bb1^{+/-}$: $Tbx1^{mcm/mcm}$ and $Cyp26b1^{-/-}$: $Tbx1^{mcm/mcm}$ may provide further evidence of potential modifying effects between *Tbx1* and *Cyp26b1*.

CHAPTER 5

A genetic interaction between tbx1 and her6 plays a role in pharyngeal arch development in the zebrafish

5.1 Introduction

Hes-family bHLH genes are the mammalian homologues of the *hairy/Enhancer of split* family of Notch pathway effectors. *Hes1* functions as a transcriptional repressor in a Notch dependent or independent fashion. As discussed in more depth in Chapter 1, it is required for the regulation of many cellular processes including the maintenance of progenitor cells, regulation of boundary formation, and control of binary cell fate decisions in a variety of tissues, including the pituitary gland, thymus, pancreas, intestine and biliary system, sensory and nervous systems and somitogenesis (Ishibashi et al., 1995; Jensen et al., 2000; Jouve et al., 2000; Kita et al., 2007; Kodama et al., 2004; Raetzman et al., 2007; Sumazaki et al., 2004; Tomita et al., 1996; Tomita et al., 1999) and reviewed by (Kageyama et al., 2007)

A FACS-GAL microarray study was previously performed in our laboratory comparing *Tbx1*-expressing cells from heterozygous versus homozygous *Tbx1* mutant mouse embryos (Array 2). This work identified and validated a number of genes differentially expressed following loss of *Tbx1*, including *Hes1,* which was down-regulated greater than threefold in RTQ-PCR of *Tbx1*-null cells. Moreover, *Hes1* has been identified as a potential target in another microarray of SHF tissue between null and wild type embryos (Liao et al., 2008). Further, it was shown that *Hes1* was down-regulated in the *Tbx1* mutant mouse and that *Hes1* mutant mice recapitulate a number of the cardinal anomalies associated with 22q11DS including pharyngeal arch artery, thymic and OFT defects (Rochais et al., 2009a; van Bueren et al., 2010). However, due to confounding genetic backgrounds of the two mutant mouse lines, these studies were unable to provide any further evidence of a genetic interaction between *Tbx1* and *Hes1* contributing to the observed phenotypes.

To overcome the issue of genetic background and to discover whether these gene pathways are evolutionarily conserved it was decided to pursue the issue of whether a true genetic interaction is required between these genes for the development of the pharyngeal region in a zebrafish model system.

5.2 Results

5.2.1 *Her6* and *tbx1* are expressed in pharyngeal tissues during development

Her6 has previously been reported to be expressed in the pre-somitic mesoderm and in various regions of the presumptive CNS, including the thalamus (Pasini et al., 2001; Scholpp et al., 2009) of the developing zebrafish. This thesis reports additional expression within the pharyngeal region, which confirms that previously reported online at ZFIN (Thisse et al., 2001). At 26 somites, the primordiae of all pharyngeal arches (PA) 1-7 are present in zebrafish embryos. In situ hybridization of *her6* transcripts showed generalised *her6* expression throughout the pharyngeal arches at this stage (Fig.1Ai. and D.). In similarly staged embryos *tbx1* was strongly expressed in the tissues of the pharyngeal arches, except for the neural crest (Fig.5.1A. and C.). Expression of both genes was also evident in the otic vesicle. By 30hpf it is becoming easier to distinguish the separate pharyngeal arch elements from each other, with a clear division between presumptive PA1-2 and PA3-7. At 30hpf both *her6* and *tbx1* continued to be expressed in both presumptive PA1-2 and PA3-7 and in the otic vesicle (Fig.5.1Bi. and F. and Fig.5.1B. and E., respectively. Later in development the segmented structure of the pharyngeal arch cartilages and associated muscles and endodermal pouches becomes more evident. Expression of both *tbx1* and *her6* was maintained in the pharyngeal region at these stages. *Tbx1* is expressed in the pharyngeal musculature and pouch endoderm (Fig.5.1G.) at 52hpf. A similar distribution of pharyngeal *her6* transcripts was observed at 52hpf (Fig.5.1H.), although *her6* expression was not seen in the intermandibularis muscles, unlike *tbx1,* whereas *her6* expression was visible in the medial rectus muscle and *tbx1* transcripts were not (Fig.5.1G. and H.).

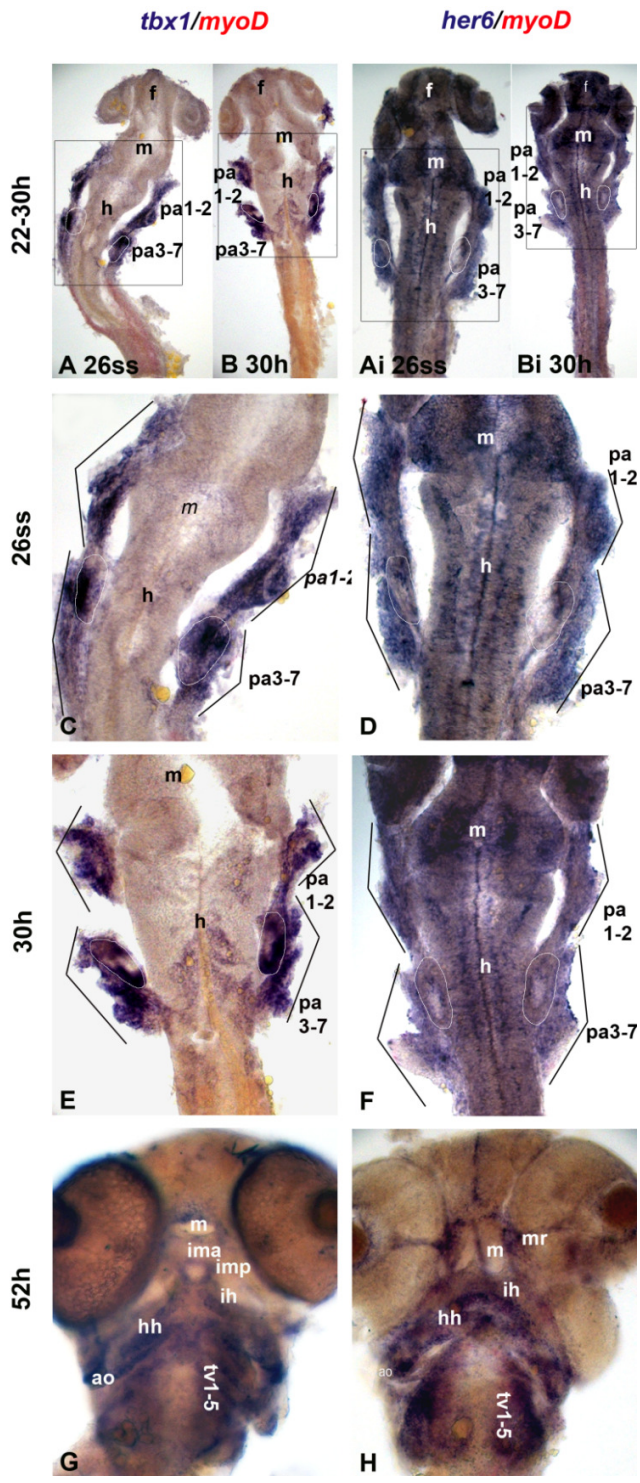

Figure 5.1 Whole mount in situ hybridization comparing expression of *her6* and *tbx1* in flat-mounted embryos

A and B.). *tbx1* expression in the presumptive pharyngeal arches at 22hpf (26 somites) and 30hpf respectively. Ai and Bi.). *her6* expression at equivalent developmental stages to (A.) and (B.) in

the presumptive pharyngeal arches and fore, mid and hindbrain. C and D.). Boxed regions of (A.) and (Ai.) at higher magnification. E and F.). Boxed regions of (B.) and (Bi.) at higher magnification. G and H.). Expression of *tbx1* (G.) and *her6* (H.) in the pharyngeal region of 52hpf embryos. myoD staining is in Fast Red. f: forebrain, m: midbrain, h: hindbrain, pa1-2: presumptive pharyngeal arches 1-2, pa3-7 presumptive pharyngeal arches 3-7. White circular outlines indicate the otic vesicles, m: mouth, mr: medial rectus muscle, ih: interhyoideus muscle, hh: hyohyoideus muscle, ao: adductor opercula muscle, tv1-5: tranversus ventralis muscles.

5.2.2 Overlapping expression of *her6* and *tbx1* during pharyngeal development

To establish whether *tbx1* and *her6* expression truly overlap we performed double fluorescent in situ hybridization visualized with the TSA system. At 5 somites *her6* expression is widespreadwith particularly high expression in rhombomere 6 (Fig.5.2B.). Strong *tbx1* expression is observed in the presumptive pharyngeal tissues just caudal to rhombomere 6 (Fig.5.2C.). Overlapping expression of the two genes was seen in the presumptive pharyngeal arches, particularly in those regions close to the neural tube (Fig.5.2D., white arrows). This overlapping expression was maintained at the 12 somite stage. The presumptive pharyngeal region as marked by *tbx1* has expanded antero-posteriorly (Fig.5.2G.) and continues to express *her6* (Fig.5.2F.). Co-expression of *her6* with *tbx1* transcripts is maintained, with the overlap being most noticeable in the medial region of the presumptive pharyngeal arches (Fig.5.2H.). At 30hpf high levels of *her6* transcripts were still detected in the CNS, with particularly high levels in the midbrain and the midbrain/hindbrain boundary. Widespread expression in the presumptive pharyngeal arches and otic vesicle was maintained (Fig.5.2J.). Expression of *tbx1* was retained in the mesoderm and endoderm of all the presumptive pharyngeal arches at this stage (Fig.5.2K). Overlap with *her6* transcripts could be seen in in these tissues in presumptive pharyngeal arches 1-2 and 3-7 and the otic vesicle (Fig.5.2L., Fig.5.2 M-P.), with especially extensive co-expression in the pharyngeal peri-otic mesenchyme, in both confocal stack single slices (Fig.5.2L., Fig.5.2M., N.) and 3D-projections of the confocal stack through the entire embryo (Fig.5.2O., P.). Transient overlapping expression of both genes was also detected in the pharyngeal ectoderm (Fig.5.2R.-U.) As previously shown with standard in situ experiments, transcripts for both genes were detected at 48hpf, when the individual

pharyngeal arches are more clearly delineated. The endoderm and mesoderm of the pharyngeal arches continue to express *tbx1* in a clearly segmented fashion (Fig.5.2X.) whereas *her6* transcripts, as before, were more generally distributed within the pharyngeal region (Fig.5.2W.). In the merged view, *her6* expression was present in non-*tbx1* expressing neural crest-derived pharyngeal arch regions and was also co-expressed in *tbx1*-positive pharyngeal tissues (Fig.5.2Y.).

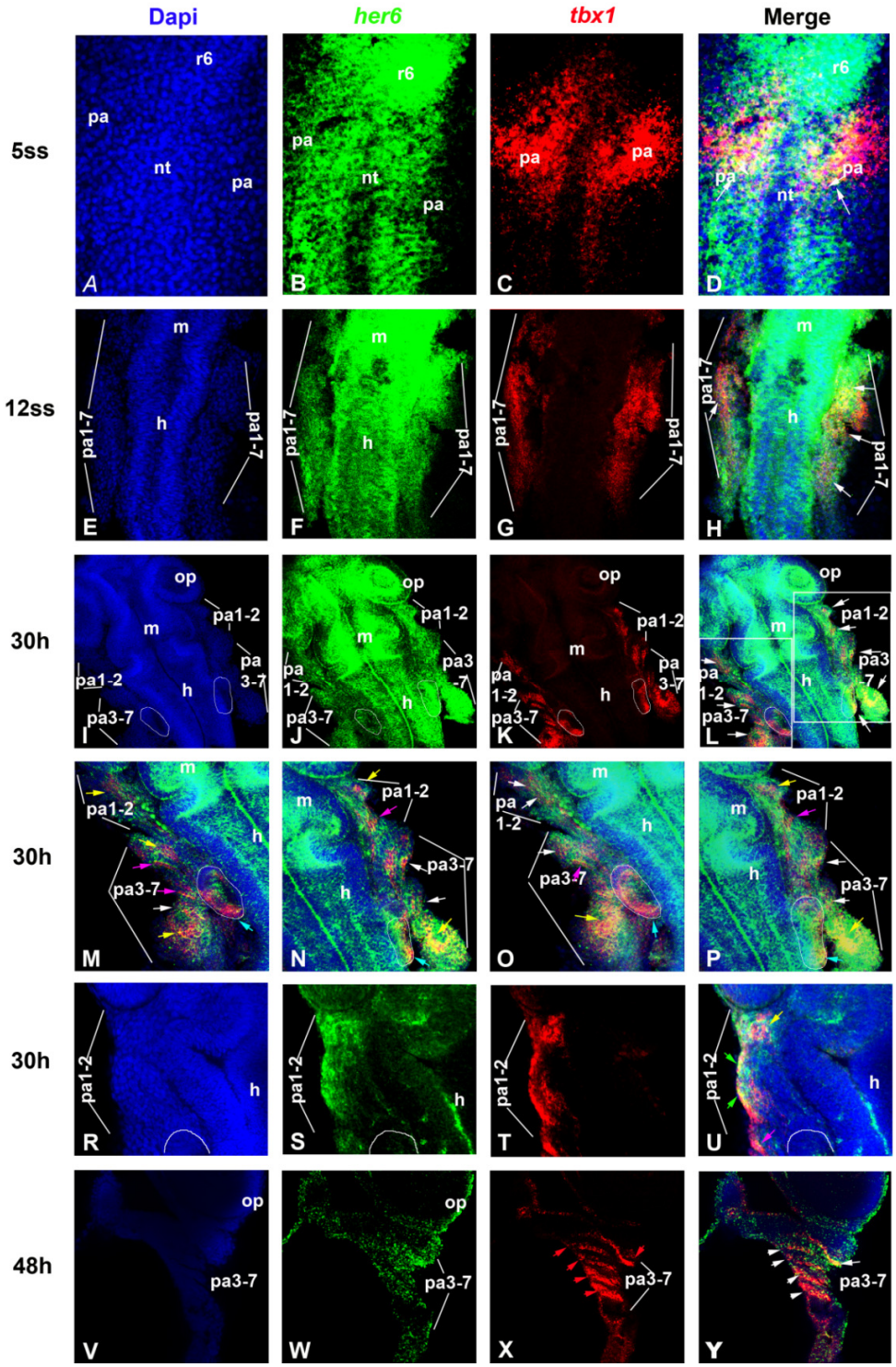

Figure 5.2 Whole mount double fluorescent in situ hybridization for *her6* and *tbx1*in flat-mounted embryos

In all panels DAPI staining is shown in blue, *her6* in green and *tbx1* in red. A-D.). Confocal stack single slice at 5 somites A.). DAPI. B.). *her6* expression C.). *tbx1* expression D.). Overlap of *her6*

and *tbx1* expression in the presumptive pharyngeal arches (white arrows). E-H.). Confocal stack single slice, 12 somites. E.). DAPI. F.). *her6* expression in the neuroepithelium and presumptive pharyngeal arches. G.). *tbx1* in the presumptive pharyngeal arches. H.). Overlap of expression of the two genes in the presumptive pharyngeal tissue, particularly in the central-anterior pharyngeal region (white arrows). I-L.). Confocal stack single slice, 30h. I.). DAPI. J.). Neuroepithelial and pharyngeal expression of *her6*. K.). Strong expression of *tbx*1 in the pharyngeal arches L.). Overlap of expression of *her6* and *tbx1* along the length of the pharyngeal primordiae (white arrows) and the otic vesicle (white outline). M and N.). Confocal stack single slice. Higher magnification of the merged boxed pharyngeal regions in (L.). O and P.). Images of the confocal stack 3D projection for (M.) and (N.). Arrows indicate overlap of *her6* and *tbx1* expression. Yellow arrows: mesoderm, pink arrows: endoderm, blue arrows: otic vesicle. R-U.). Confocal stack single slice, 30h. R.). DAPI. S.). *her6* expression. T.). *tbx1* expression. U.). Overlap of *tbx1* and *her6* expression in pharyngeal ectoderm (green arrows). V-Y.). Confocal stack 3D projection images, 48h.V.). DAPI. W.). *her6* expression X. *tbx1* expression in the pharyngeal arches. Y.). Overlap of expression of both genes. r6: rhombomere 6. m: midbrain, h: hindbrain, pa1-2: presumptive pharyngeal arches 1-2, pa3-7 presumptive pharyngeal arches 3-7, op: optic vesicle. White circular outlines indicate the otic vesicles, red arrows mesendoderm of individual pharyngeal arches and white arrows indicate regions of overlapping expression in the pharyngeal arches.

5.2.3 Overlapping expression of *her6* with muscle and neural crest markers

Double fluorescent in situ with *myoD* at 36hpf (Fig.3C. and G.) confirmed that *her6* (Fig.5.3B. and F.) is co-expressed in mesodermally-derived pharyngeal muscles (Fig.3D.and H.). Fluorescent in situ hybridization for *her6* (Fig.5.3I., N. and R.) in 22 and 30 hpf *Tg(sox10:gfp)* embryos (Fig.5.3K., O. and S.) revealed *her6* transcription in some of the *sox10*-positive neural crest cells migrating into the pharyngeal arches to contribute to the formation of the pharyngeal arch cartilage at all antero-posterior levels (Fig.5.3L., P.and T.).

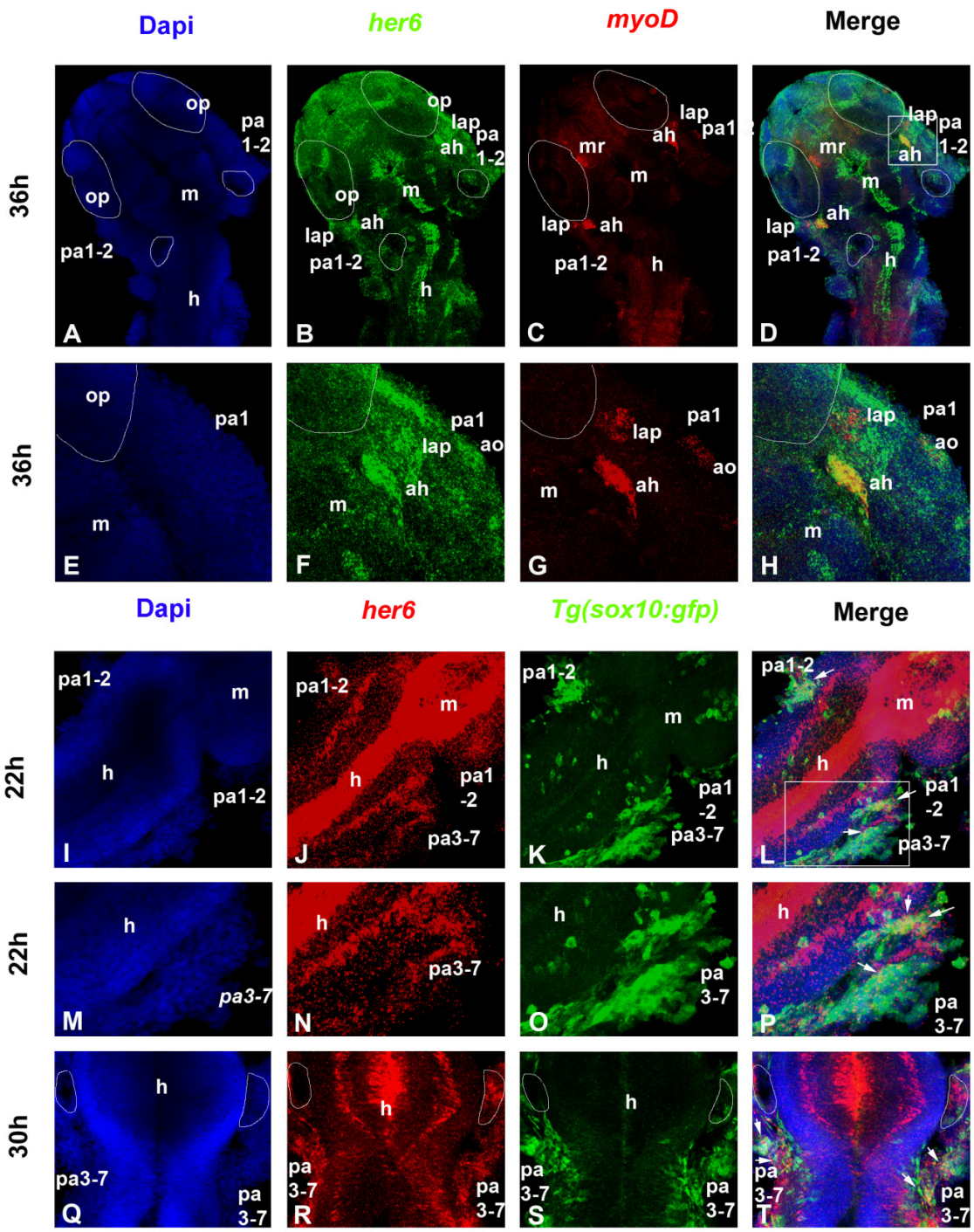

Figure 5.3 Double fluorescent in situ hybridization for *her6* and *myoD* or *sox10*

A-D. Images of confocal stack 3D projections at 36hpf. A.). DAPI. B.). *her6* green fluorescent expression C.). *myoD* red fluorescent (Cy3) expression. D.). Co-expression of *her6* and *myoD* in forming muscles of the head and pharyngeal region. adductor hyoideus: ah, adductor opercula: ao, levator arcus palatine: lap . E-H.). Higher magnification of the boxed region in (D). I-T.).

Images of confocal stack 3D projections. *her6* red fluorescent (Cy3) in situ hybridization in *Tg(sox10:gfp)* embryos. I-L.). 22hpf. I.). DAPI. J.). *her 6* expression in pharyngeal arches K.). *sox10-gfp* green fluorescent (Alexa 488) expression in neural crest cells invading the pharyngeal arches L.). Overlap in some regions of the pharyngeal neural crest (L). M-P.). Higher magnification of boxed pharyngeal arch region in (L). Q-T.). 30hpf. Q.). DAPI. R.). *her6* expression S.). *sox10-gfp* expression T.). Co-expression in neural crest cells. m: midbrain, h: hindbrain, pa1-2: presumptive pharyngeal arches 1-2, pa3-7 presumptive pharyngeal arches 3-7, op: optic vesicle. White circular outlines indicate the otic vesicles and white arrows indicate regions of overlapping expression in the pharyngeal arches.

5.2.4 *Her6* expression responds to altered expression of *tbx1* : down-regulation in *vgo*$^{tm208/tm208}$ *tbx1* null embryos

If *her6* is directly or indirectly regulated by *tbx1*, then alteration of *tbx1* expression levels should be reflected in *her6* expression. The expression of *her6* in *vgo*$^{tm208/tm208}$ *tbx1* null embryos was therefore examined over a developmental time course. In the pharyngeal primordium at 30hpf much less *her6* expression was evident in *vgo*$^{tm208/tm208}$ embryos compared to wild-type controls, particularly caudally to presumptive pharyngeal arch 1. (Fig.5.4.A.-C.). Fluorescent in situ hybridization for *her6* (Fig.5.4G. and K.) at 36hpf in *Tg(fli-1:gfp)* embryos (Fig.5.4F. and J.) allowed separate and overlaid visualization of the neural-crest derived elements of the forming arches with *her6* expression (Fig.5.4D. and H.) and showed that while GFP-positive pharyngeal cells are present in *vgo*$^{tm208/tm208}$ they are disorganized compared to wild type controls with reduced *her6* expression (Fig.5.4G.and K.). Average integrated density was used as a measure of the intensity of *her6* staining and was reduced 2.7-fold (Fig.5.5.) ($P<0.0001$ unpaired, two-tailed t test) in *vgo*$^{tm208/tm208}$ embryos compared to wild-type embryos ($n>3$)(Fig.5.4G. and K., boxed region). This reduction of *her6* expression persisted at later stages, with greatly down-regulated levels of *her6* transcripts detected within the pharyngeal region of 60hpf embryos compared to wild-type embryos (Fig.5.4L-N.). Real-time PCR on dissected pharyngeal arches at 72hpf gave a 2.32-fold reduction of relative *her6* expression in *vgo*$^{tm208/tm208}$ embryos compared to normal controls ($P<0.05$, unpaired two-tailed t test)(see Fig.5.6 for graph).

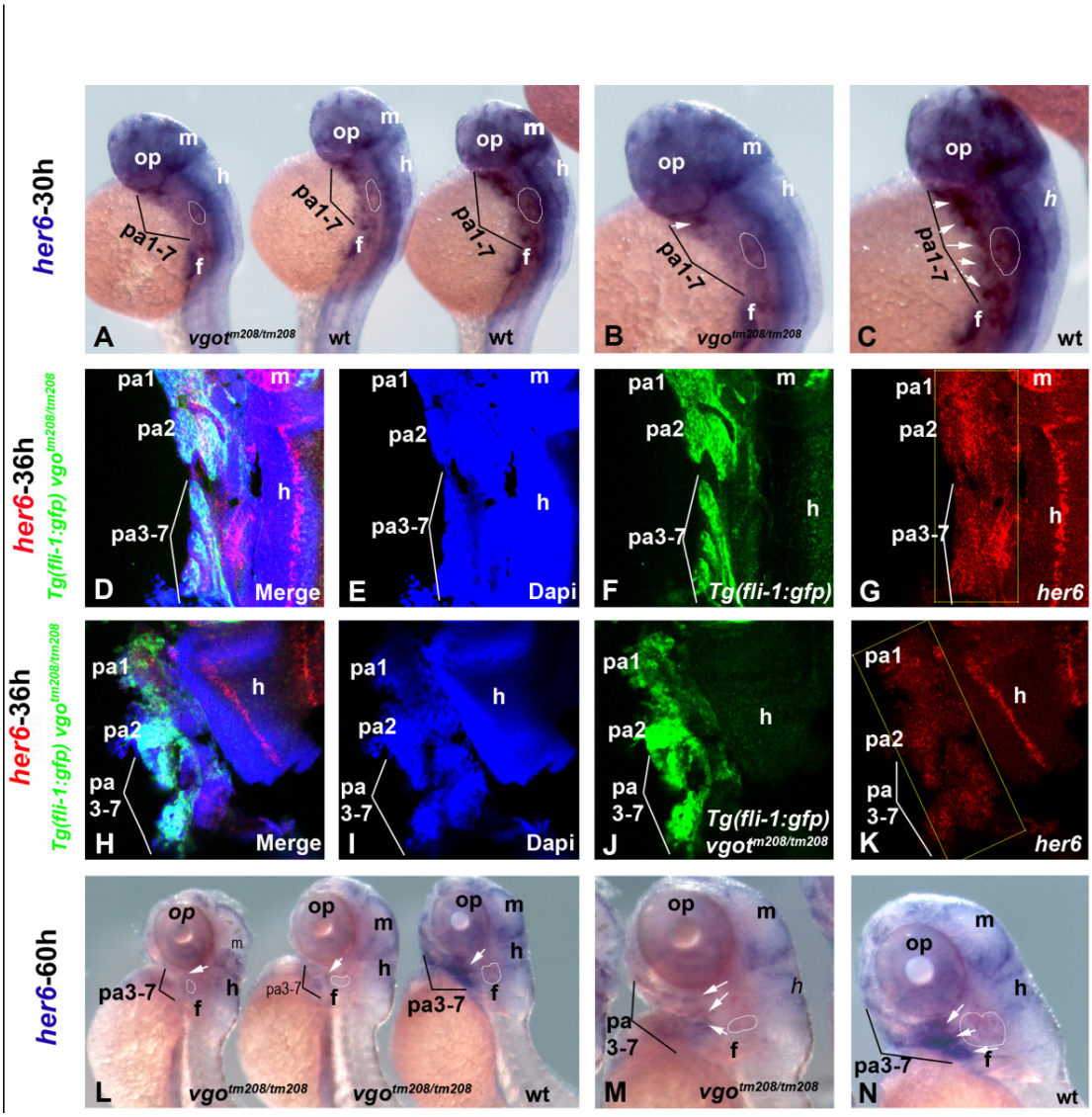

Figure 5.4 Altered *her6* expression with altered levels of *tbx1* expression: down-regulation in *vgo*$^{tm208/tm208}$ *tbx1* null embryos

A-C.). In situ hybridization of *her6* at 30hpf. A.). Reduced levels of pharyngeal staining in *vgo*$^{tm208/tm208}$ embryos compared to wild type (wt) controls. B and C.). Higher magnification of embryos shown in (A.). D-K.). Confocal stack single slice 30hpf. Red fluorescent (Cy3) in situ hybridization for *her6* in a *Tg(fli-1:gfp)* background allowing visualization of pharyngeal arch neural crest. D-G.). Wild-type control. D.). Combined staining for DAPI, *her6* and *fli-1:gfp*.E.). DAPI. F.). *fli-1:gfp* expression in pharyngeal arches. G.). *her6* expression, with pharyngeal region outlined by box. H-K.). *vgo*$^{tm208/tm208}$ H.). Combined staining for DAPI, *her6* and *fli-1:gfp*. I..) DAPI. J.) *fli-1:gfp* expression in disorganized pharyngeal arches. K.). Reduced *her6* expression, with pharyngeal region outlined by box. L-N.). In situ hybridization of *her6* at 60hpf. L.). Reduced levels of

pharyngeal staining in *vgo*$^{tm208/tm208}$ embryos compared to wild type (wt) controls. M.). and N.). Higher magnification of embryos shown in (L.).

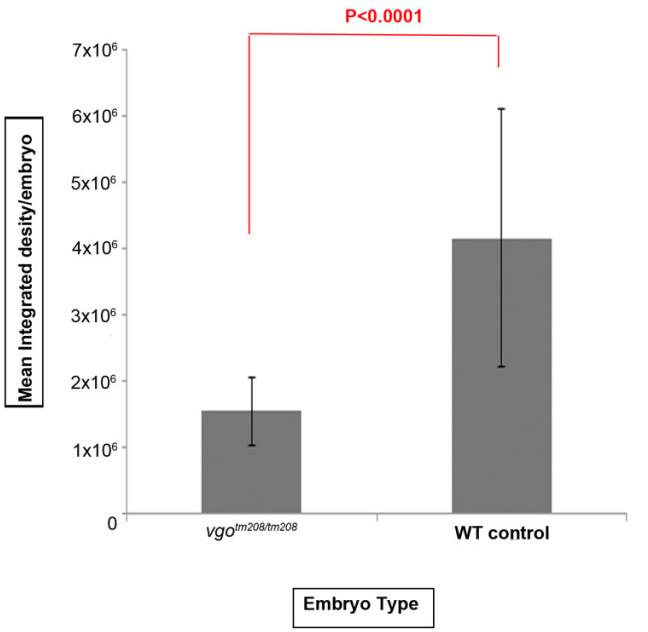

Figure 5.5 Graph of mean integrated density of *her6* staining/embryo comparing wild type control and *vgo*$^{tm208/tm208}$ embryos

Unpaired two-tailed t tests showed expression in *vgo*$^{tm208/tm208}$ embryos to be significantly reduced (P<0.0001). Integrated density measurements were used as a measure of the level of *her6* expression and were compiled from confocal stacks of n=3 embryos per group using the image processing package Fiji (http://fiji.sc/wiki/index.php/Fiji). Error bars represent standard deviation.

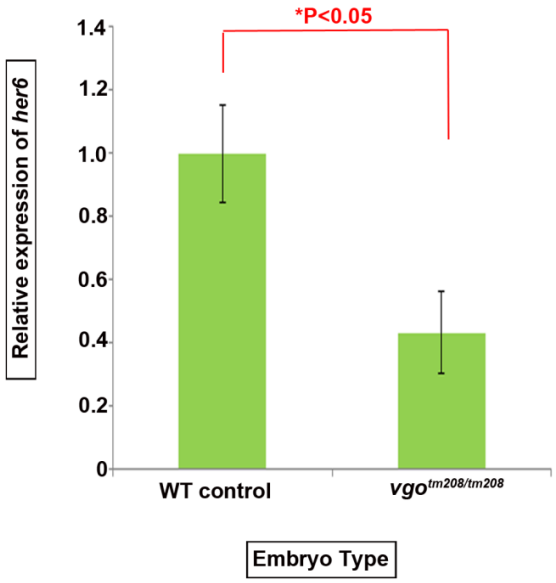

Figure 5.6 Quantitative real-time PCR. Relative expression of *her6* in control versus *vgo*$^{tm208/tm208}$ pharyngeal regions at 72hpf

Error bars represent normalized co-efficient of variance. P<0.05, unpaired, two-tailed *t* test.

5.2.5 *Her6* expression responds to altered expression of *tbx1* : up-regulation in *XTbx1*-injected embryos

We then examined *her6* levels in the presence of increased *tbx1*. Capped *XTbx1* mRNA (100-200pg/nl) was injected into 1 cell embryos, which were then incubated as normal for 8 and 24 hours. In situ hybridization detected no change in expression levels after 8h of incubation (Fig.5.7A.-C.) with all experimental classes displaying equivalent levels of *her6* expression in in situ hybridizations. However, after 24h of culture *XTbx1* mRNA injected embryos had increased levels of *her6* pharyngeal expression after in situ hybridization, both when compared to un-injected wild type controls (Fig.5.8A.and B.) and when compared to embryos injected equivalent levels of control *nrfp* mRNA as *XTbx1* mRNA (Fig.5.8C. and D.). This increased expression after *XTbx1* injection was evident in most tissues where *her6* is expressed, not just those where *tbx1* is endogenously co-expressed, presumably because injection of capped *XTbx1* mRNA at the 1 cell stage will lead to its presence in most cells of the embryo. This result suggests that while *tbx1*

can act to increase *her6* expression, it can only do so in those tissues already competent to express *her6*, as no spatial or temporal ectopic *her6* expression was detected.

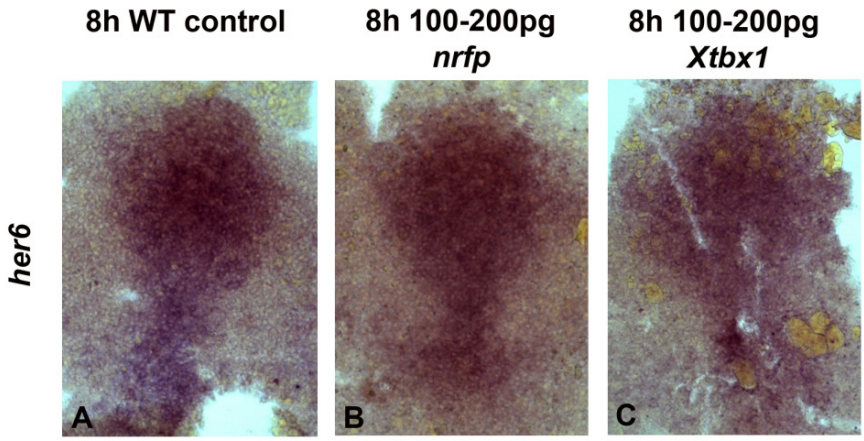

Figure 5.7 In situ hybridization of *her6* in WT control, 100-200 pg *nrfp* mRNA-injected and 100-200pg *XTbx1* mRNA-injected embryos

After 8h of culture post-injection expression of *her6* was seen at similar levels in all embryo classes. A).. WT control. B.). 100-200 pg *nrfp* mRNA. C.). 100-200pg *Xtbx1* mRNA.

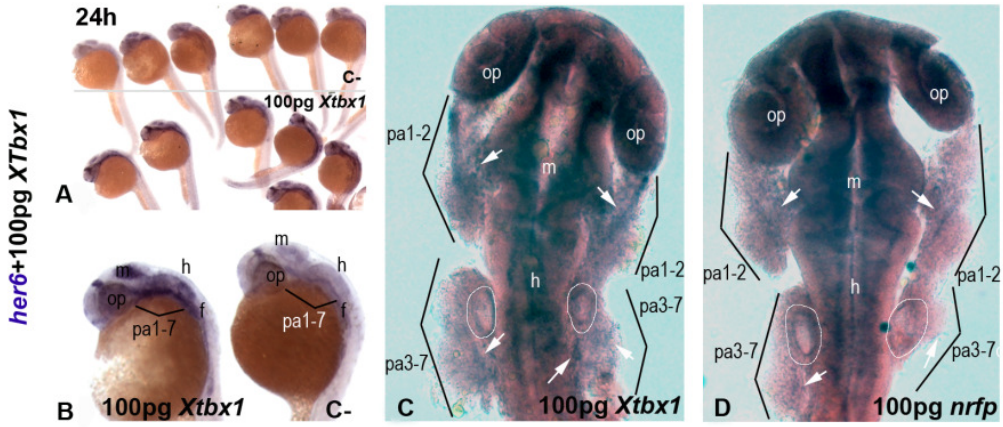

Figure 5.8 Altered *her6* expression with altered levels of *tbx1* expression: up- regulation in *XTbx1*-injected embryos

A-D.). *her6* in situ hybridization at 24hpf. A.). and B.). Side views of *her6* expression in 24hpf *XTbx1*-injected embryos compared to wild-type controls (C-).C.). and D.). *Xtbx1* and *nrfp*-injected flat-mounted embryos respectively. m: midbrain, h: hindbrain, pa1-2: presumptive pharyngeal arches 1-2, pa3-7 presumptive pharyngeal arches 3-7, op: optic vesicle. White circular outlines indicate the otic vesicles and white arrows indicate pharyngeal *her6* expression or regions where it is absent in morphant/mutant embryos.

5.2.6 *Her6* morphants phenocopy *tbx1* morphants and mutants

Knockdown of *tbx1* using a previously validated antisense, translation-blocking morpholino (750µM)(Stalmans et al., 2003) phenocopied previously published $vgo^{tm208/tm208}$ pharyngeal defects(Piotrowski et al., 2003; Piotrowski and Nusslein-Volhard, 2000) in 47.5% (37/78) of morphants. An independent non-overlapping, translation-blocking MO gave the same phenotype as reported previously (Stalmans et al., 2003). Here we show that a *her6* MO (200µM) previously demonstrated to abrogate translation and knockdown *her6* activity (Pasini et al., 2004), also produced pharyngeal defects in 61% (47/77) of embryos. These abnormalities, observed in both morphants, phenocopy those of $vgo^{tm208/tm208}$ embryos (Fig.5.9).

In situ hybridization with a *tie1/2* probe revealed that in *her6* morphants, as in $vgo^{tm208/tm208}$ mutants, only one or two pharyngeal arch arteries (PAA) could be detected, compared to the four PAA present in equivalent staged controls. This suggests a compromised pharyngeal vasculature and haemodynamic flow in these embryos, particularly as most embryos exhibit cardiac oedema by 3dpf (Fig.5.9C-Cv., Fig.5.10B.). *Fli-1* in situ hybridization demonstrated abnormal development of the pharyngeal arch cartilages where posterior pharyngeal arches appeared to be small, misshapen or missing in both morphants and *tbx1* null embryos (Fig.5.9A.-Av.) This was confirmed by Alcian blue staining which showed the mandibular and hyoid arches were often missing or malformed as were the more posterior ceratobrachial arches. It was also often difficult to distinguish individual arches from each other. The neurocranial cartilage elements, including the posterior mesodermally derived parochordalia were frequently absent, or abnormal in size and shape (Fig.5.9B.-Bv.). To investigate these observations further confocal 3D analysis was performed after morpholino injection into *Tg(fli-1:gfp)* embryos. In these embryos the neural crest cell derived pharyngeal arch cartilage is gfp-positive, allowing the pharyngeal cartilage defects to be viewed in more detail (Fig.5.9D.-Dv.). In wild-type embryos all posterior pharyngeal arches were clearly segmented (Fig.5.9D.-Di.). Loss of segmentation was visible in $vgo^{tm208/tm208}$ embryos, both *tbx1* and *her6* morphants (Fig.5.9Dii. and Dii.i) and double morphants (Fig.5.9Diii.) where an amorphous mass of gfp-positive cells could be seen. Other aspects of pharyngeal arch

development were abnormal, as arches were often short, hypoplastic or missing. In addition the shape of the arch was frequently dysmorphic, seeming more rounded and irregular compared to the beautifully regimented appearance of control pharyngeal arches (Fig.5.9Dii.-Dv.).

These pharyngeal abnormalities lie within the range of pharyngeal phenotypes found in *Hes1* null and *Tbx1* null mouse models (Lindsay et al., 2001; van Bueren et al., 2010; Vitelli et al., 2002a). In addition, somitic and notochordal defects similar to those described previously (Pasini et al., 2004) were seen with higher concentrations (250-500µM) of the *her6* MO. Somites were found to be irregularly shaped compared the normal chevron pattern and also had irregular boundaries(Fig.5.10C.-E.). Bent tails, possibly the result of an abnormal notochord development, were also seen (Fig.5.10E.). These embryos also exhibited loss of jaw and caudal pharyngeal structures as discussed above, and had cardiac oedema (Fig.5.10A.and B.).

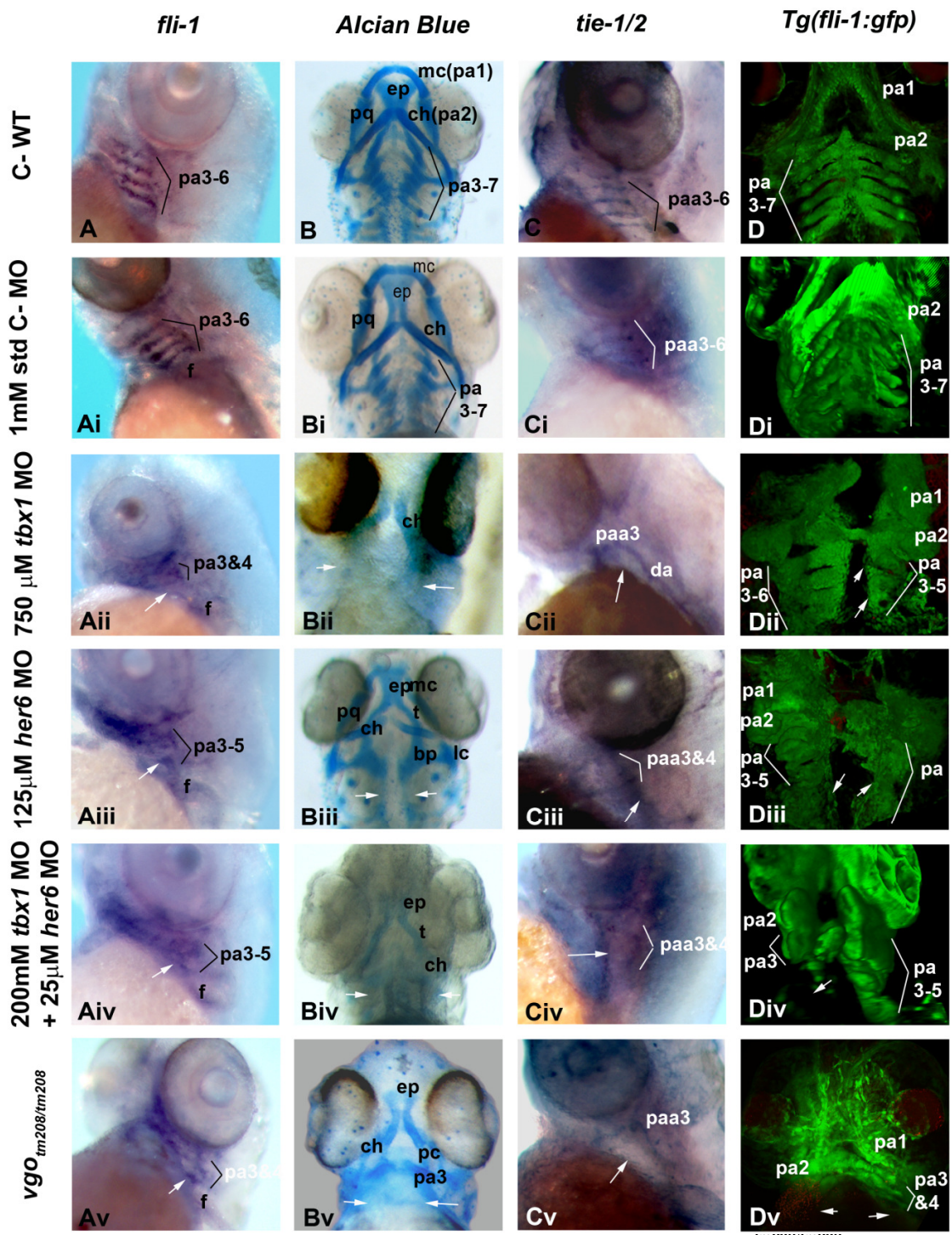

Figure 5.9 Pharyngeal phenotypes in her6 and tbx1 morphant and *vgo*$^{tm208/tm208}$ embryos at 72hpf

A-D.). Wild type controls.Ai-Di.). Standard control MO. Aii-Dii.). *tbx1* MO, Aiii-Diii.). *her6* MO, Aiv-Div.). double morphants, Av-Dv.). *vgo*$^{tm208/tm208}$ embryos. A-Av.). Whole -mount *fli-1* in situ hybridization for ncc-derived pharyngeal cartilage. B-Bv.). Alcian blue staining for cartilage. C-

Cv.).Whole-mount in situ hybridization for *tie1/2* labels the vascular endothelium of pharyngeal arch arteries. D-Dv.). Images of confocal stack 3D-projections on a *Tg(Fli1:gfp)* background show pharyngeal arch segmentation and shape. pa3-7 pharyngeal arches 3-7(ceratobrachial cartilages), mc : Meckels' cartilage, bh, basihyal cartilage, ch: ceratohyal cartilage, ethmoid plate, pq: paloquadrate, bp: basal plate, lc: lateral commissure, t: trabeculae. White arrows indicate abnormal PA development

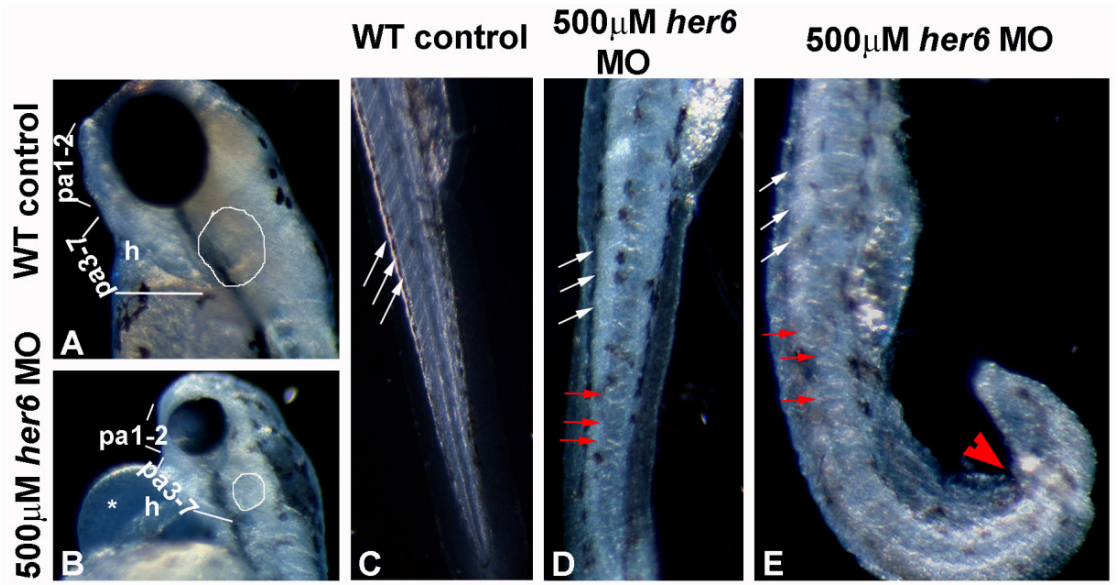

Figure 5.10 *her6* morphant phenotypes

500μM *her6* morphants at 72hpf. A.). Wild type control with fully formed pharyngeal region, arches 1-7 (p1-7) and a normal heart (h) and normal sized otic vesicle (ov). B.). *her6* morphant with reduced pharyngeal arch domain, cardiac oedema (*) and smaller otic vesicle compared to wild type (ov). C.). Wild type control with normal trunk and somites (white arrows). D.). and E.). Trunk and tail of similarly staged *her6* morphant embryos with abnormal tail and somite development. Anteriorly, somites have a less pronounced chevron shape and posteriorly, somites appear rounded and irregular in shape and spacing (red arrows). The embryonic tail in (E.). is severely curved suggesting a possibly notochord defect (red arrowhead).pa1-2, pa3-7: pharyngeal arches 1-2, 3-7.

5.2.7 Morphant control experiments

It should be noted that all morpholinos described have been previously published (Pasini et al., 2004; Stalmans et al., 2003). Either mRNA translation or splicing were altered as expected by each MO (Pasini et al., 2004) or at least two MOs per gene

produced an equivalent phenotype, that also recapitulated the ENU mutant (Stalmans et al., 2003). Additional control experiments were also performed for each morpholino. Mismatch morpholinos for the *tbx1* and *her6* morphant-producing MOs, or MOs against human beta-globin (standard control), were injected at equivalent concentrations and were found to produce no defects (n=50 for each mismatch MO) (Fig.5.11A.and B.).

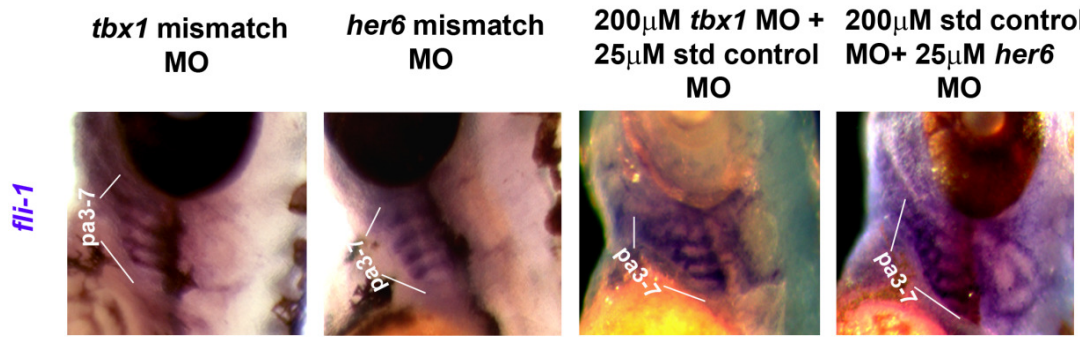

Figure 5.11 Normal pharyngeal arch phenotypes in mismatch and sub-phenotype morphant control embryos

A.). 72hpf *tbx1* mismatch morphant embryo. B.). 72hpf *her6* mismatch morphant embryo. C.). 72hpf sub-phenotypic control injection embryo; 200μM *tbx1* MO + 25μM standard control MO. D.). 72hpf sub-phenotypic control injection embryo; 200μM standard control MO+ 25μM *her6* MO. All embryos display normal pharyngeal development (white numberss 3-6; pharyngeal arches 3-6).

Rescue experiments with the corresponding mRNA were carried out for both morpholinos to check their specificity. In these sets of injections, the percentage of embryos with normal pharyngeal development rose from 18.6 % (n=13/70) for the *her6* MO alone to 72.2% (n=70/97) when the *her6* mRNA was also injected (P<0.0001). In the same experiment for the *tbx1* MO the percentage of embryos with normal pharyngeal development rose from 37.3% (n=25/67) for the *tbx1*MO alone to 87.4% (n=90/103) when the *tbx1*mRNA was also injected (P<0.0001).

To check that the MO phenotypes observed were not the result of off-target *p53* activation, *her6* and *tbx1* MOs were injected with a *p53* MO (Robu et al., 2007a) and the numbers of embryos with pharyngeal abnormalities assessed. The percentage of embryos with abnormal pharyngeal arches seen with *tbx1* MO injection in this set of experiments was 53% (n=171/333) and 52.7% (n=125/237) when *p53* MO was injected concurrently

(not significant). The same was true of experiments for the *her6* MO, where the MO gave a defective pharyngeal arch frequency of 59.8% (n=55/92) alone and a frequency of 56.6% when injected with the *p53* MO (208/367) (not significant). It was therefore unlikely that the observed phenotypes were the result of non-specific activation of the *p53*-apoptosis pathway.

5.2.8 Synergistic rise in pharyngeal defects with co-injection of *tbx1* and *her6* MOs

Simultaneous pair-wise knockdown of *tbx1* and *her6* was used to reveal any genetic interaction existing between these genes. a sub-phenotypic concentration was first identified for each morpholino. This was defined as the highest MO dose that generated a pharyngeal phenotype in 10% or fewer injected zebrafish embryos, either when the MO was injected alone, or with the corresponding pair-concentration of standard control MO. When these sub-phenotypic doses for both the *tbx1* (200µM) and *her6* (25µM) MOs were co-injected, the frequency of embryos with defective pharyngeal development rose from 10% in the case of the *tbx1* MO alone (22/214) and 5% with the *her6* MO only (7/138), to 50.6% (42/83) (P<0.0001)(Table 1). To contrast synergistic with additive effects, it was assumed that in the case of summative effects, 5% of the *tbx1* MO treated embryos lacking a phenotype due to *tbx1* knockdown would have a defect due to *her6* knockdown. Thus the expected number of defects assuming additive effects in co-injected embryos was 12/83 (14.5%). The actual number of defective embryos observed following co-injection was 42/83 (P<.0001). This synergistic increase in the occurrence of pharyngeal abnormalities is strongly suggestive of a genetic interaction between *tbx1* and *her6* (Table 1). The synergistic interaction between *her6* and *tbx1* is such that despite the concentration of each morpholino being sub-phenotypic when injected alone, when injected together, the pharyngeal defect phenotype was at levels similar to that observed in, the single, higher concentration, morphants, and $vgo^{tm208/tm208}$ mutants (Fig.5.9Aiv-Div.). *Fli-1* in situ hybridization (Fig.5.9Aiv.), Alcian blue staining (Fig.5.9Biv.) and *Tg(fli-1:gfp)* confocal analysis (Fig.5.9Div.), revealed that the nature of the defects was also similar between dual MO knockdowns and $vgo^{tm208/tm208}$ fish. Observed malformations included loss of segmentation, particularly in caudal regions of the pharyngeal apparatus, along with short,

hypoplastic, abnormally shaped or missing pharyngeal arches. Arches had reduced vascularisation by pharyngeal arch arteries, as marked by *tie1/2* in situ hybridization (Fig.5.9Civ.). Control embryos were injected with 200µM *tbx1* MO + 25 µM standard control MO or 200µM standard control MO + 25µM *her6* MO developed normally (Fig.5.11C.and D.).

Table 5.1 Co-injection of *her6* and *tbx1* MOs produces a synergistic rise in pharyngeal defects.

Concentration control MO(µM)	Concentration *Tb x1* MO(µM)	Concentration *her6* MO(µM)	% (n) embryos with pharyngeal defects	*P* value
200	-	25	10.0% (22/214)$^{\#}$*	
50	200	-	5.0% (7/138)*§	*0.1
-	200	25	50.6% (42/83) $^{\#\S}$	$^{\S\#}$<0.0001

Results of 1nl co-injections for *tbx1*, *her6* and control MO's. * denotes P value using a chi-squared contingency table, comparing the control injections to each other $^{\#}$ and § denotes P value comparing experimental to control injection.

5.2.9 Loss of pharyngeal muscle, endoderm and neural crest markers in morphant zebrafish

Head muscle precursors including the extraocular and pharyngeal muscles express *myoD* in zebrafish embryos (Schilling and Kimmel, 1997). Transcripts were observed in the normal pattern in wild-type embryos and standard control MO embryos at 72hpf (Fig.5.12A. and B.). This expression was greatly reduced in all morphants (Fig5.12C-E.) in a similar fashion; small pockets of pharyngeal and extraocular expression remained, but these were diminished in both size and intensity of staining and often expression was almost completely abrogated in the muscle precursors of pharyngeal region, as in the *vgo*$^{tm208/tm208}$ mutants (Fig.5.12F.). A similar reduction of expression was evident when *pax9a* was used as marker for pharyngeal endoderm. Wild type and standard control MO-injected embryos exhibited strong expression in the endodermal pharyngeal pouches at 72hpf (Fig.5.12G. and H.). Expression was down-regulated in all morphant classes, with only small patches of expression remaining more anteriorly, and complete loss of expression in often observed in caudal pharyngeal pouches (Fig.5.12I.-K.). The

vgo$^{tm208/tm208}$ mutant displayed a very similar phenotype, with only a few patches of *pax9a* expression still being present in the pharyngeal region (Fig.5.12L.).

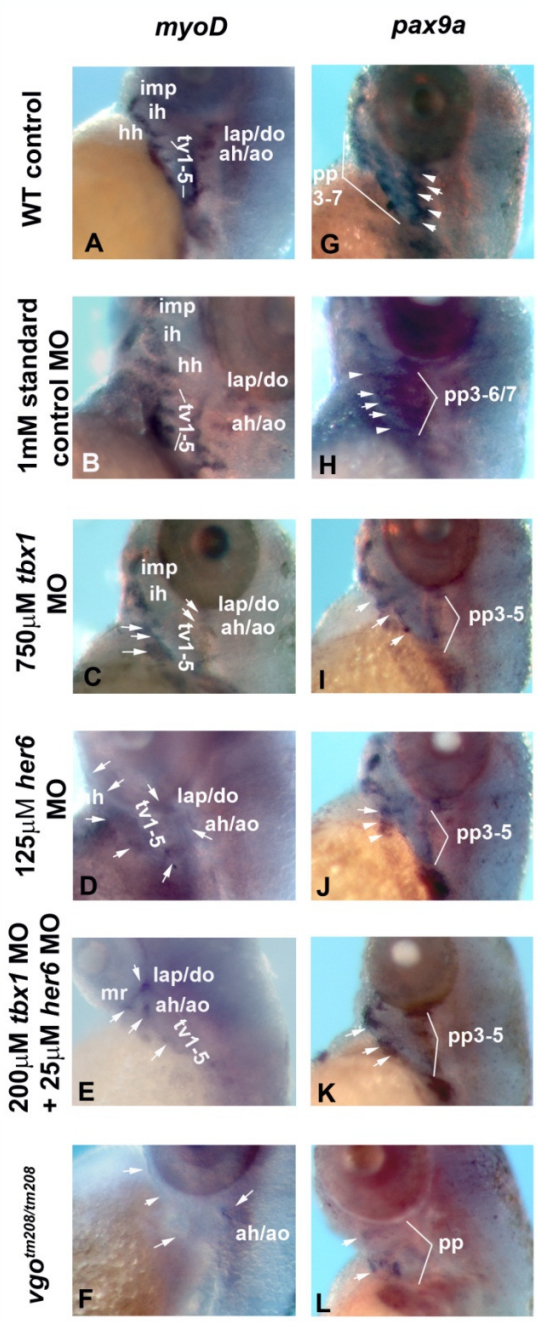

Figure 5.12 Altered pharyngeal expression of *myoD* and *pax9a* in morphant and *vgo*$^{tm208/tm208}$ embryos.

A-F.). *myod* expression at 72hpf. A.). and B.). Normal expression of *myoD* in the pharyngeal muscles of wild type (A.) and 1mM standard control morphants (B.). C-E.). Down-regulated

expression of pharyngeal *myoD* C.) *tbx1* ,D.) *her6* and E.) double morphants.F.) *vgo*$^{tm208/tm208}$ embryos . G-L.). *pax9a* expression at 72hpf. Normal expression of *pax9a* in the pharyngeal endoderm of wild type (G.) and 1mM standard control morphants (H.). I-K.). Down-regulated expression of *pax9a*. I.) tbx1 , J.) *her6* and K.) double morphants. L.). *vgo*$^{tm208/tm208}$ embryos. mr: medial rectus muscle, ima: intermandibularis anterior, ih: interhyoideus muscle, hh: hyohyoideus muscle, ah: adductor hyoideus, ao: adductor opercula muscle, tv1-5: tranversus ventralis muscles, pp: pharyngeal pouch. White arrows indicate presence/absence of *myod/pax9a* staining.

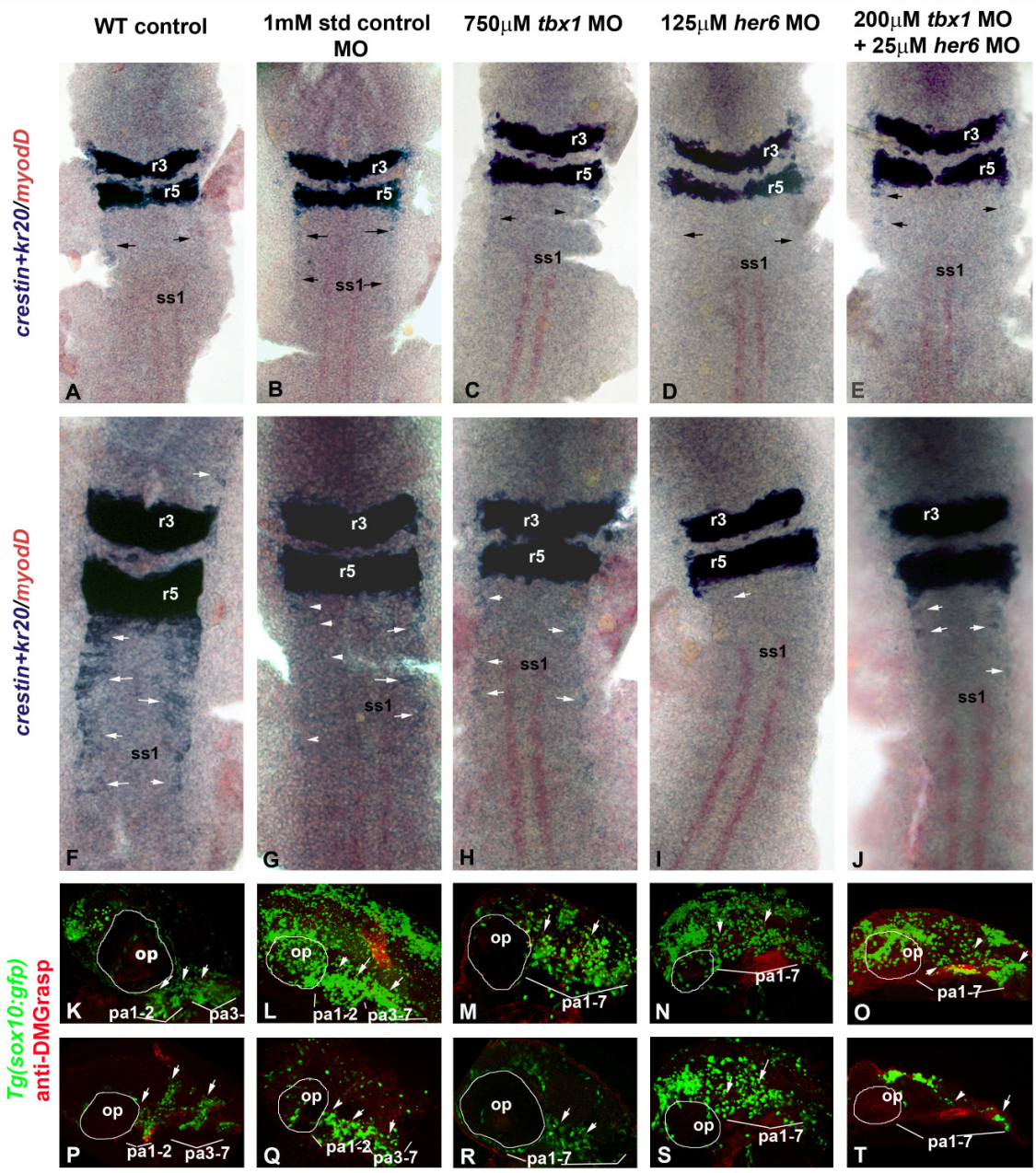

Figure 5.13 Neural crest development in *her6* and *tbx1* morphant embryos

A-J.). *crestin* (neural crest) and *kr20* (rhombomeres 3 and 5) expression. A-E.). 3-4 somite embryos. A.). Wild type. B.). Standard control morphant. C.). *tbx1*, D.). *her6* and E.). double morphants. F-J.). 6-7 somite embryos. F.). Wild-type control. G.). Standard control morphant. H.). *tbx1*, I.). *her6* and J.). double morphants. K-O.). Confocal stack 3D-projection images of *Tg(sox10:gfp)*(neural crest) 30hpf embryos and Dm-Grasp-Alexa-568 staining (endoderm and heart). P-T.). Confocal stack single slices from the same embryos as shown in (K-O.). K and P.). Wild-type control. L and Q.). 1mM standard control morphant. M and R.). 750μM *tbx1* morphant. N and S.). 125μM *her6* morphant. O and T.). 25μM *her6* + 200μM *tbx1* double morphant. Ncc

streams in controls (K, P and L, Q.) are forming pharyngeal arches whereas in morphants (M-O. and R-T.) ncc seem more disorganized and forming pharyngeal arch primordia are harder to distinguish. pa1-2, 3-7, 1-7: pharyngeal arches 1-2, 3-7, 1-7, op/white outline: optic vesicle, white arrows indicate ncc forming pa.

Pan-neural crest marker *crestin* (Luo et al., 2001) expression was diminished caudally in a number of morphants of all classes at 3-4 somite (Fig.5.13C.-E.) and 6-7 somite stages (Fig.5.13H.-J.) compared to controls (Fig.5.13A.and B. and Fig.5.13F.and G.). Examination of *Tg(sox10-gfp)* embryos at 30hpf revealed neural crest migration anomalies similar to those described for the $vgo^{tm208/tm208}$ mutant where crest from individual arches fuse together (Fig.5.13. K.-T.). Finally, counts of *sox10-gfp*-positive cells within the pharyngeal arches at 30hpf were decreased in all morphant groups compared to controls ($P<0.05$) (Table 2, Fig.5.14.). Interestingly, quantification of neural crest cells also resulted in a significantly reduced number in the caudal pharynx of *Hes1* null mouse embryos at E9.5, (Rochais et al., 2009a).

Table 5.2 Decreased numbers of *sox10:gfp*-positive neural crest cells in morphants

Embryo Type	Mean. no. of pharyngeal *sox10:gfp*-positive cells/embryo	P value
WT control	181.8±68.9*	NS*
1mM standard control MO	159.3±91.5*#	NS*
125µM her6 MO	97.2±33.2#	<0.05
750µM tbx1 MO	88.6±51.61664#	<0.05
25µM her6 MO+ 200µM tbx1 MO	92.9±51.9#	<0.05

Numbers of *sox10:gfp*-positive neural crest cells are significantly decreased in all morphant classes(#) compared to controls(*).(n>5, P<0.05 using an unpaired two-tailed t test.). NS: not statistically significant P>0.05

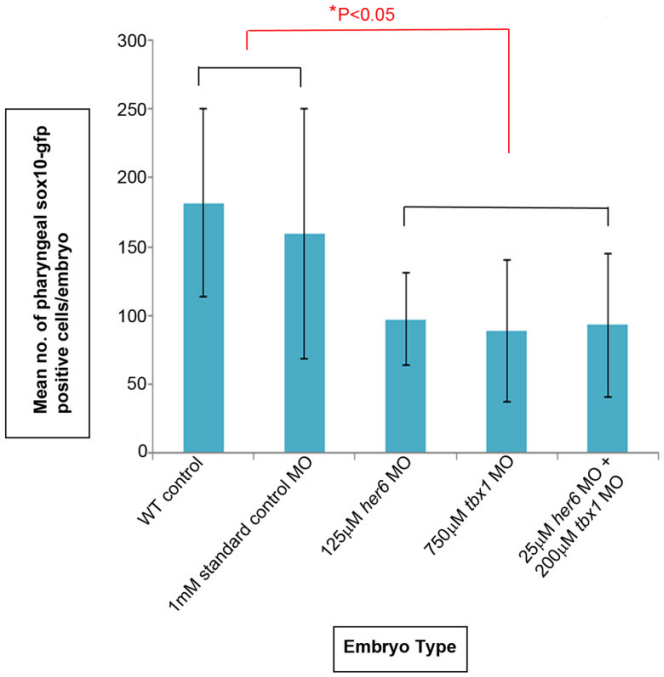

Figure 5.14 Graph of mean number of gfp-positive cells in the pharyngeal region of 30hpf *Tg(sox10:gfp)* embryos

Numbers of *sox10:gfp*-positive neural crest cells are significantly decreased in all morphant classes compared to controls (n>5, P<0.05 using an unpaired two-tailed t test.). Error bars denote standard deviation.

5.2.10 Decreased pharyngeal proliferation may contribute to the morphant phenotype

Since defective pharyngeal proliferation has been demonstrated in both *Tbx1* and *Hes1* mutants (Ai et al., 2006; Chen et al., 2009; Liao et al., 2008; Rochais et al., 2009a; van Bueren et al., 2010; Xu et al., 2004; Xu et al., 2005; Zhang et al., 2006b) we used whole mount immunohistochemistry against phosphohistone H3 as a marker for proliferating cells. Using confocal microscopy the number of positive cells within the pharyngeal tissues of n>5 embryos at 24hpf was counted for all embryo types and the mean number of proliferating pharyngeal cells/embryo compared across all groups (see Fig.5.15. for graph). No significant difference was observed between wild type and standard control morphants. However, all morphant groups and $vgo^{tm208/tm208}$ had a

significantly reduced number of proliferating cells (2.4-1.6-fold) in the pharyngeal region (P<0.0001)(Table 3). This therefore suggests that the pharyngeal phenotypes observed in zebrafish with reduced *tbx1* and *her6* levels maybe partially the result of reduced proliferation during development.

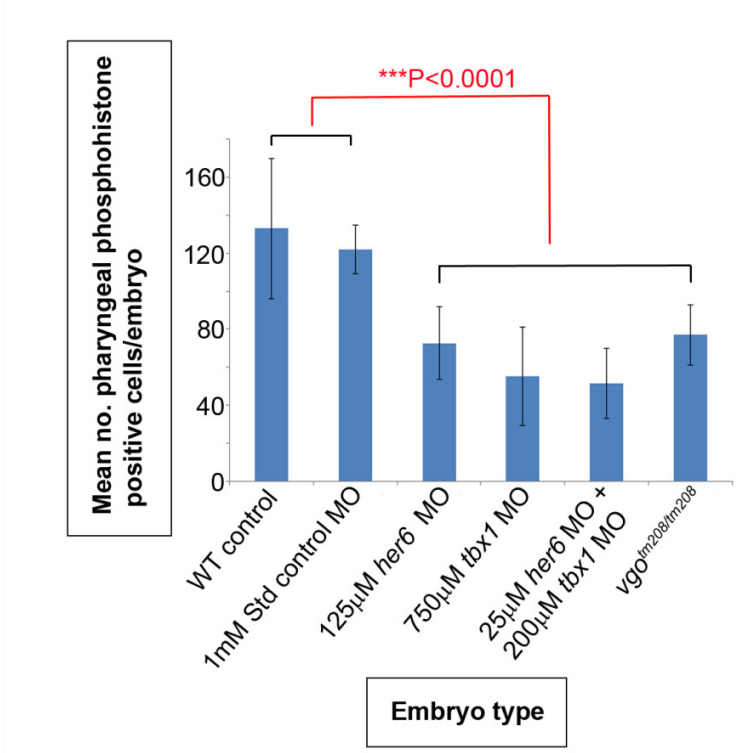

Figure 5.15 Graph of mean number of phosphohistone H3-positive proliferating cells in morphant, *vgo*$^{tm208/tm208}$ and control zebrafish pharyngeal arches at 24hpf

Proliferation in the pharyngeal tissues, as measured by phosphohistone positive cells, was decreased in morphant and mutant embryos compared to control embryos. Using an unpaired t test no statistically significant difference was observed in the numbers of positive cells between wild type (WT) controls and embryos injected with 1mM standard control MO, P>0.05. Compared to control embryos all morphant classes and *vgo*$^{tm208/tm208}$ embryos displayed statistically significantly reduced numbers of phosphohistone positive cells with the unpaired t test, P<0.0001. Error bars display standard deviation.

5.2.11 Apoptosis remains unaltered at 24hpf in morphant and *vgo*$^{tm208/tm208}$ fish

Previously, experiments injecting *p53* MO with the MOs of interest ruled out any off-target non-specific activation of *p53*-mediated apoptosis. However, a specific role for

apoptosis in the generation of the observed phenotypes remained to be investigated. Whole-mount Tunel staining was used to label apoptotic cells within the pharyngeal region of n>5 embryos at 24hpf for all embryo types and the mean number of Tunel-positive pharyngeal cells/embryo compared across all groups (see Fig.5.16 for graph). No significant difference was observed between wild type and standard control morphants. Morphant groups and *vgo*$^{tm208/tm208}$ appeared to have slightly raised number of apoptotic cells but this difference was found to be non-significant (Table 3) suggesting increased apoptosis at 24hpf does not play a role in the pharyngeal defects described here.

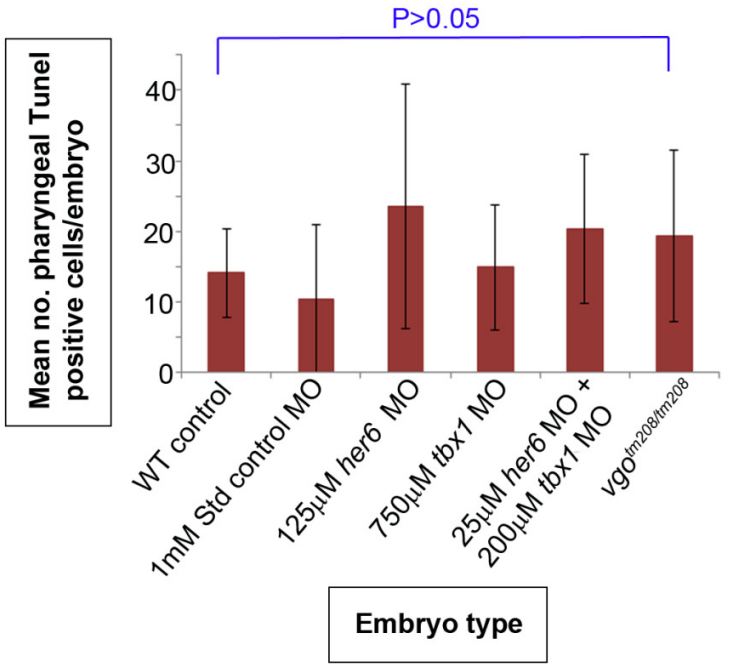

Figure 5.16. Graph of mean number of Tunel positive cells in in morphant, *vgo*$^{tm208/tm208}$ and control zebrafish pharyngeal arches at 24hpf

Apoptosis in the pharyngeal tissue, as measured by Tunel positive cells, was increased in morphant and mutant embryos compared to control embryos. Using an unpaired t test no statistically significant difference was observed in the numbers of positive cells between wild type (WT) controls and embryos injected with 1mM standard control MO, P>0.05. The numbers of Tunel positive cells in the morphant groups and *vgo*$^{tm208/tm208}$ embryos were not found to be statistically significant compared to controls with the unpaired t test, P>0.05. Error bars display standard deviation.

Table 5. 3. Proliferation and apoptosis in pharyngeal region of 24hpf zebrafish embryos

Embryo Type	Mean. no. of pharyngeal phosphohistone-positive cells/embryo	P value	Mean. no. of pharyngeal Tunel-positive cells/embryo	P value
WT control	133± 36.7*	NS*	14.1± 6.2*	NS*
1mM standard control MO	122.1± 12.7*	NS*	10.4± 10.5*	NS*
125µM her6 MO	72.7± 19.1$^{\#}$ (1.7-fold decrease)	P<0.0001$^{\#}$	23.6± 17.3§	NS§
750µM tbx1 MO	55.3± 25.9$^{\#}$ (2.2-fold decrease)	P<0.0001$^{\#}$	14.9± 8.8§	NS§
25µM her6 MO+ 200µM tbx1 MO	51.5± 18.5$^{\#}$ (2.4-fold decrease)	P<0.0001$^{\#}$	20.4± 10.5§	NS§
vgo$^{tm208/tm208}$	77± 16.0$^{\#}$ (1.6-fold decrease)	P<0.0001$^{\#}$	19.3± 12.1§	NS§

Number of proliferating (phosphohistone-positive)cells and cells undergoing apoptosis (Tunel positive) in pharyngeal region at 24hpf. The number of proliferating cells were significantly decreased (P<0.0001) in all morphant embryos($^{\#}$) compared to controls(*) whereas the number of apoptotic cells(§) were not significantly altered compared to controls(*).Statistical significance was calculated using an unpaired two-tailed t test and n>5 in all cases. NS: not statistically significant P>0.05

5.2.12 Injection of *her6* mRNA rescues the *tbx1* morphant phenotype

If *her6* is downstream of *tbx1* in zebrafish, and diminished expression of *her6* contributed to the *tbx1* loss of function phenotype, then increasing levels of *her6* may ameliorate the malformations secondary to *tbx1* knockdown. Thus, an attempt was made to rescue the *tbx1* knockdown phenotype using *her6* mRNA in *Tg(fli-1:gfp)* embryos. It was found that embryos co-injected with *tbx1* MO and *her6* mRNA and examined at 72hpf exhibited little sign of anomalous pharyngeal development, appearing very similar

to un-injected controls (Fig.5.17A. and D.). Only 10% (14/142) of embryos had relevant defects compared to the 58% (116/201) incidence observed with *tbx1* MO alone ($P<$ 0.0001, Table 5.4) (Fig.5.17B.). In addition, very similar results were obtained with *tbx1* MO plus *her6* mRNA injections into wild-type fish, analysed by *fli-1* in situ hybridization (data not shown), where only 10% (20/200) of fish had pharyngeal development defects.

In order to check that the rescue effect of the *her6* mRNA was not caused by non-specific effects such as interactions between MO and mRNA sequences, *tbx1* MO was co-injected with a truncated *her6ΔWRPW* construct. This is a deletion construct encoding *her6* without the C-terminal four amino acids comprising the WRPW functional domain, which interacts with co-repressors of the Groucho-related/Transducin-like E(Spl) (TLE) family to repress target genes via histone deacetylase mediated chromatin inactivation. Previous work has shown that while *her6ΔWRPW* retains some function, activity is abrogated by at least half with this deletion (Pasini et al., 2004). In these *tbx1* MO+*her6ΔWRPW* control injections 42% (102/243) of embryos had defective pharyngeal development (similar to that seen when the *tbx1* MO is injected alone) (Fig.5.17B. and C.) as opposed to the 10% of defects seen with *tbx1* MO plus full-length *her6*. Thus, little rescue takes place with *her6ΔWRPW*, the truncated her6 mRNA construct, suggesting that the rescue effect is specific to full-length *her6* and requires the C-terminal WRPW domain.

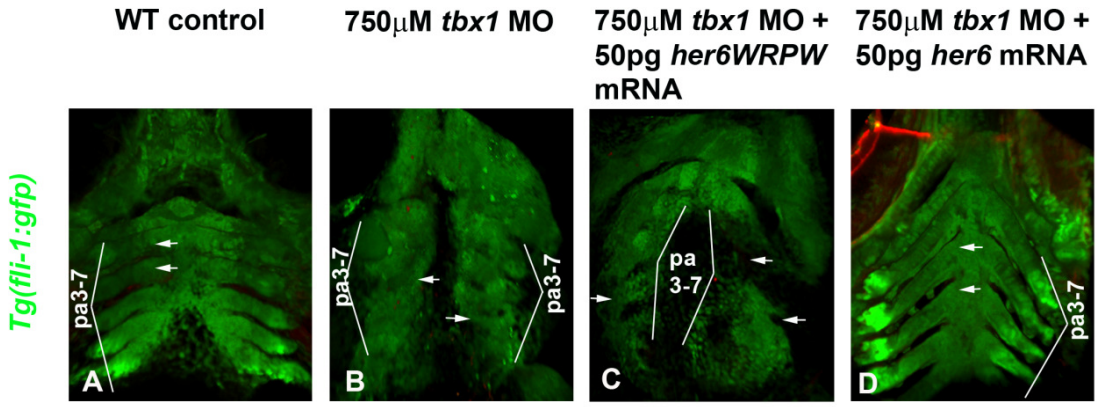

Figure 5.17 *her6* mRNA rescues the *tbx1* morphant pharyngeal phenotype

Images of confocal stack 3D projections at 72hpf. A.). Wild-type *Tg(fli-1:gfp)* control with normally segmented pharyngeal arches. B.). *tbx1* morphant with abnormal pharyngeal arch formation. C.).

Injection of a truncated *her6* mRNA, *her6WRPW* cannot rescue the *tbx1* morphant phenotype. D.). Injection of *her6* mRNA restores the normal pharyngeal phenotype in *tbx1* morphants. pa3-7: pharyngeal arches 3-7, white arrows indicate normal/abnormal pharyngeal arches.

Table 5.4 *her6* mRNA injection can rescue *tbx1* MO pharyngeal defects

Embryo Type	% embryos with abnormal pharyngeal development at 3dpf	*P* value
1nl 750µM *tbx1* MO	58% (116/201)[#]	
1nl 750µM *tbx1* MO+ 50pg/nl *her6WRPW* mRNA	42% (102/243)*	
1nl 750µM *tbx1* MO 50pg/nl *her6* mRNA	10% (20/200) [#]*	[#]*<0.0001

Results of target gene (*her6*) rescue of *tbx1* MO phenotype in *Tg(fli-1:GFP)* embryos. Rescue with *her6* mRNA is statistically significant at P<0.0001 when compared to both *tbx1* MO alone ([#]) and *tbx1* MO+*her6ΔWRPW*(*), using a chi-squared contingency table.

5.2.13 Pharyngeal proliferation is rescued in *tbx1* morphants injected with *her6* mRNA

Furthermore, proliferative studies were performed as described above (section 5.2.10) upon *tbx1* morphants injected with *her6ΔWRPW* mRNA or full-length *her6* mRNA and wild-type control embryos at 24hpf. Full-length *her6* mRNA was found to be able to rescue the *tbx1* MO-induced proliferation defect back to wild-type control levels, whereas the truncated *her6ΔWRPW* mRNA could not (P>0.05)(Table 5.5, see Fig.5.18 for graph).

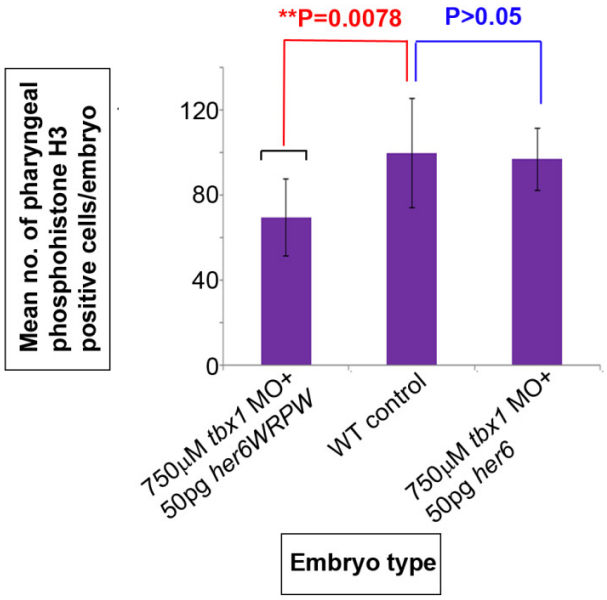

Figure 5.18 Graph of mean number of phosphohistone H3 positive cells in control and rescued *tbx1* morphant zebrafish pharyngeal arches at 24hpf

Proliferation in the pharyngeal tissues of *tbx1* morphants injected with *her6* mRNA was not statistically significantly different from proliferation levels in wild type control embryos (unpaired t test, P=0.7648. In control experiments using the deleted *her6WRPW* mRNA *tbx1* morphants proliferation was statistically significantly reduced compared to wild type controls (unpaired two-tailed t test, P=0.0078.) Error bars represent standard deviation.

Table 5.5 *her6* mRNA rescues the *tbx1* MO proliferation defect

Embryo Type	Mean. no. of pharyngeal phosphohistone-positive cells/embryo	P value
WT control	100± 25.72936*#	
1nl 750µM *tbx1* MO+ 50pg/nl *her6WRPW* mRNA	69.4± 18.22209#	P<0.05#
1nl 750µM *tbx1* MO 50pg/nl *her6* mRNA	97± 14.5688*	NS*

The significantly decreased number of proliferating (phosphohistone-positive) cells in the pharyngeal region of *tbx1* morphants at 24hpf can be rescued back to wild-type levels with *her6* full-length mRNA(#) but not with a *her6* C'-terminal deletion mRNA(*).Statistical significance was calculated using an unpaired two-tailed t test and n>5 in all cases. NS: not statistically significant P>0.05

5.2.14 Notch signaling partially rescues the *tbx1* morphant phenotype

The next question to be investigated, was whether activation of the notch pathway, which up-regulates *her6*, could similarly abrogate the *tbx1* morphant phenotype. We injected *tbx1* MO into embryos from a cross between *Tg*(*hsp70:gal4)* and *Tg(UAS:nicd)* fish. Those embryos carrying both effector and responder transgenes will constitutively express the notch-1a intra-cellular (NICD) domain thus activating notch signalling upon undergoing heat-shock treatment. This treatment was carried out at around 50% epiboly, the stage at which *tbx1* expression is first reported in zebrafish (Kochilas et al., 2003; Piotrowski et al., 2003). Pharyngeal development was then assessed at 3dpf using *fli-1* in situ hybridization as previously and embryos subsequently genotyped.

Injection of *tbx1* MO alone produced pharyngeal defects in 41% (18/44) of surviving injected embryos at 72hpf. However, after heat-shock activation of the nicd, the percentage of live embryos at 72hpf exhibiting pharyngeal arch defects had dropped to 23.5% (27/115) (P=0.047, Table 5.6) suggesting that activation of the Notch pathway was able to ameliorate some of the effects of *tbx1* knock-down.

Together, these data suggest that in the zebrafish, *tbx1* and *her6* are individually required for normal pharyngeal development, interact in this process, and that the C-terminal WRPW motif is required for rescue of *tbx1* knock down phenotypes.

Table 5.6 Partial rescue of the *tbx1* MO pharyngeal phenotype by activation of the Notch intracellular domain

Embryo Type	% embryos with abnormal pharyngeal development at 3dpf
Un-injected (negative control)	3% (3/112)
Un-injected+heat-shock (nicd activation alone)	10% (9/87)
tbx1 MO alone	41% (18/44)*
tbx1 MO + heat-shock (nicd activation)	23.5% (27/115)*

Heat-shock activation of a constitutively active Notch intracellular domain can partially rescue the *tbx1* morphant phenotype. Rescue of the pharyngeal arch phenotype by heat-shock nicd activation(*) is significant at $P<0.047$ using a chi-squared contingency table.

5.3 Discussion

5.3.1 Experimental summary

The studies presented here show that the Notch pathway bHLH repressor *her6* is expressed in several tissues of the zebrafish embryonic pharyngeal apparatus, including the ectoderm, mesoderm, endoderm and neural crest throughout development. Furthermore, both *her6* and *tbx1* are expressed together within the mesoderm, ectoderm and endoderm of the pharyngeal arches as in the mouse (van Bueren et al., 2010). Similarly, we find *her6* expression is reduced in the *tbx1* null zebrafish mutant, $vgo^{tm208/tm208}$. In situ hybridization experiments suggested that *Xtbx1* can up-regulate the expression of *her6*, further evidence suggesting that these genes lie within the same genetic pathway.

These results are consistent with the hypothesis that *tbx1* and *her6* interact within the same genetic pathway controlling development of the pharyngeal apparatus. Two further experiments support this idea. Firstly, co-injection of *tbx1* and *her6* morpholinos at

sub-phenotypic concentrations increases the number of pharyngeal defects 3.5-fold, compared to the low number of defects observed when each morpholino is injected at the same concentration but with an inactive control MO as a partner. Secondly, the *tbx1* morphant phenotype can be rescued by injection of full-length *her6* mRNA, but not by a truncated *her6* mRNA lacking the WRPW C-terminal repression domain. This rescue can also be partially recapitulated by induction of the notch pathway.

5.3.2 Expression of *her6/tbx1* matches known tissue-specific roles in the mouse

Normal development of the pharyngeal-cardiovascular system in vertebrates requires the co-ordination of many complex signalling events between all the tissues comprising this complicated apparatus; namely the pharyngeal epithelia (both ectoderm and endoderm), pharyngeal, splanchnic and secondary heart field mesoderm and the neural crest [reviewed in (Graham A. et al., 2005; Graham, 2008; Rochais et al., 2009b; Scambler, 2010; Tzahor E. and Evans S.M., 2011; Vincent and Buckingham, 2010)]. Expression of *Tbx1* in all these tissues except for the neural crest has been shown to be necessary for normal pharyngeal development, as conditional loss of *Tbx1* expression in any of these tissues in the mouse leads to a phenotype similar to that of the *Tbx1* null allele, including aberrant NCC development, loss of PA segmentation and PAA defects (Arnold et al., 2006b; Calmont et al., 2009; Randall et al., 2009; Xu et al., 2005; Zhang et al., 2005; Zhang et al., 2006b). In addition, the pharyngeal defects of the $vgo^{tm208/tm208}$ mutant can be partially rescued by the transplantation of wild-type cells into the pharyngeal mesendoderm of $vgo^{tm208/tm208}$ embryos (Piotrowski et al., 2003). Furthermore, a number of neural crest derived tissues including vascular smooth muscle and craniofacial structures including the mandible, maxilla and palate do not develop properly in *Hes1* null mice (Akimoto et al., 2010; van Bueren et al., 2010). Conditional knock-out experiments for *Hes1* in the mouse reveal a requirement for *Hes1* in neural crest for normal thymic development and an additional partial PAA phenotype when expression was deleted in the AP2α expression domain of the pharyngeal ectoderm and neural crest (van Bueren et al., 2010). This suggests the loss of expression on the pharyngeal mesoderm/secondary heart field and endoderm contribute to the remaining PAA and

partially penetrant OFT phenotypes observed in the full *Hes1* knockout. Using a *Mef2cCre*-driver to produce specific loss of function in the secondary heart field did not produce PAA phenotypes, and more surprisingly did not result in OFT abnormalities either (Papangeli, 2010). However, the numbers for the latter experiment were relatively small. Loss-of-function experiments using a pan-mesodermal allele might be more revealing of any mesoderm-specific requirement for *Hes1*. Two inducible *Cre-loxp* approaches [*Foxa2mcm* (Park et al., 2008) and *Sox17-2A-iCre* (Engert et al., 2009)] were made to determine the role of the endoderm in the *Hes1* cardiovascular development but neither was successful as *ROSA26* reporter alleles showed that on *Hes1* backgrounds Cre recombination was variable and always less than expected (Papangeli, 2010).

The observation that both *tbx1* and *her6* are co-expressed in pharyngeal mesoderm, endoderm and ectoderm during the development suggests that a similar multi-tissue requirement may exist in the fish as in the mouse. Interestingly, in *Xenopus laevis, XTbx6*, a paraxial mesoderm gene, is required for *XTbx1* expression and normal cranial chondrogenesis and myogenesis. Knock-down of either gene caused delayed NCC migration, severe defects in pharyngeal cartilage and hypoplasia of head muscle.(Tazumi et al., 2010), phenotypes strikingly similar to those observed in our zebrafish *tbx1* knock-down models.

5.3.3 Comparison of zebrafish morphant and mouse mutant phenotypes

3D confocal analysis with *Tg(fli-1:gfp)* zebrafish indicates that segmentation, formation and patterning of the arches in *tbx1* morphants is disrupted in a similar fashion to that previously described for $vgo^{tm208/tm208}$ mutants (Piotrowski et al., 2003; Piotrowski and Nusslein-Volhard, 2000). These malformations were also phenocopied with knock-down of *her6*. The formation and patterning of the pharyngeal arch arteries within each pharyngeal arch are severely disrupted in both *her6* morphants and *tbx1* morphants and mutants. These phenotypes are very reminiscent of those observed in *Tbx1* null and hypomorphic mutant mice (Lindsay et al., 2001), in which pharyngeal arch hypoplasia, loss of pharyngeal segmentation and loss of the pharyngeal arch arteries are all observed. However, the phenotype in *Tbx1* null mice consistently affects bilateral segmentation

below PA2, whereas in the zebrafish this phenomenon is frequently unilateral. In the case of *tbx1* knock-down these differences could be attributed to the more efficient loss of function achieved by a null allele versus MO injection, particularly as bilateral pharyngeal defects are more common in the *vgo*$^{tm208/tm208}$ mutant model, although unilateral defects are still observed. The phenotype in *Hes1* null mice is somewhat milder than seen in the zebrafish; while pharyngeal arch artery, palatal and glandular morphogenesis is affected in mouse, the pharyngeal apparatus expands and segments normally. Here, species differences may play a role. Incomplete penetrance of pharyngeal defects in *Hes1* mouse mutants compared to *her6* knock-down phenotypes maybe the result of functional redundancy with other *Hes*-related genes, in particular the *Hey* genes or the modifying effects of genetic background.. Alternatively, the degree of requirement for *her6* in pharyngeal tissues may be greater in the fish than in the mouse and thus be more susceptible to the effects of genetic knockdown.

5.3.4 Morphant/mutant phenotypes and genetic interaction between *her6* and *tbx1*

Both the *tbx1* and *her6* morphants phenocopy the *tbx1* mutant *vgo*$^{tm208/tm208}$ as described previously (Piotrowski et al., 2003; Piotrowski and Nusslein-Volhard, 2000), Alcian Blue staining for cartilage of the pharyngeal skeleton and the neurocranium and analysis of pharyngeal cartilage elements in *Tg(fli-1:gfp)* fish in *tbx1* and *her6* morphants show that neural crest-derived cartilage development is severely affected. Moreover, this study documents an early neural crest phenotype with reduced staining of markers early in development and a decrease in the number of NCC in the pharyngeal region at 30hpf. Quantification of the number of *Ap2ά*-positive neural crest cells also showed a significantly reduced number in the caudal pharynx of *Hes1* null embryos at E9.5, (Papangeli, 2010; Rochais et al., 2009a).

Signals from the pharyngeal endoderm, particularly FGF signaling, have been shown to direct neural-crest chondrogenesis and the development of the pharyngeal cartilages (Couly et al., 2002; Crump et al., 2004; David et al., 2002; Kumar et al., 2012; Walshe and Mason, 2003), showing the importance of normal pharyngeal endoderm development for correct cartilage development. As suggested previously for *vgo*$^{tm208/tm208}$

mutants (Piotrowski et al., 2003; Piotrowski and Nusslein-Volhard, 2000), the abnormalities in *tbx1* and *her6* morphants may be at least in part due to loss of segmentation of the pharyngeal arches by the pharyngeal endodermal pouches as evident from the morphant segmentation defects in *Tg(fli-1:gfp)* experiments and the loss of pharyngeal endoderm marker expression.

Abnormal mesodermal development was also apparent in in *tbx1* and *her6* morphants. As in *vgo*$^{tm208/tm208}$ mutants expression of *myoD* in the pharyngeal muscles was greatly reduced and it has been shown that that *Tbx1* in the mouse regulates pharyngeal muscle progenitor fate (Sambasivan et al., 2009). Loss of endothelial pharyngeal arch artery marker *tie1/2* could also originate as a mesodermal defect as endothelial cells are mesodermally derived and again expression of *Tbx1* in the mesoderm has been shown to be required for pharyngeal arch artery development (Zhang et al., 2006b). During craniofacial development there is a tight linkage between NCC-derived skeletal and connective tissue elements and mesodermally-derived skeletal muscle, with interplay between neural crest and mesoderm required for the proper formation of the structures derived from both tissues (Grenier et al., 2009; Rinon et al., 2007; Schilling and Kimmel, 1997).

Neural crest defects could also contribute to the PAA phenotype as a neural crest contribution is required for proper segmentation and development of the pharyngeal arch cartilage (Hall, 1980; LeDouarin, 1982; Noden, 1983; Schilling and Kimmel, 1994) and the smooth muscle layer of the pharyngeal arch arteries, which is in turn required to maintain the integrity of the endothelial PAA (Bockman et al., 1987; Bockman et al., 1989; Ito and Sieber-Blum, 1991; Nakamura, 1982).

The fact that the *tbx1* and *her6* morphants phenocopy both the *vgo*$^{tm208/tm208}$ and each other closely, as described above, implies that they may lie in the same genetic pathway. Importantly, in support of this theory a synergistic rise in the same phenotype in pharyngeal arches, endoderm and mesoderm as discussed above was seen in subphenotypic double morphants when both active morpholinos (against *tbx1* and *her6*) were injected, but controls with either active morpholino plus control morpholino developed normally. A second corroboration of the hypothesis of a genetic interaction

between *tbx1* and *her6* as being important for normal pharyngeal development was provided by the rescue experiments in which *her6* mRNA was able to ameliorate the phenotype induced by the *tbx1* morpholino. In addition, cell proliferation is implicated in both knock-down and rescue embryos.

5.3.5 Why is a *tbx1/her6* interaction seen in the zebrafish and not the mouse?

The experiments presented here, were originally begun in an attempt to determine whether *Tbx1* and *Hes1* (*her6*) were indeed part of the same genetic pathway during pharyngeal development. Previous work had shown that *Hes1* expression is greatly reduced in $Tbx1^{-/-}$ compared to $Tbx1^{+/-}$ mouse embryo cells(van Bueren et al., 2010). *Hes1* expression is also diminished in the pharyngeal arches of the *Tbx1* null mouse, particularly in the mesoderm and endoderm (van Bueren et al., 2010). In addition, both *Tbx1* and *Hes1* heterozygote embryos exhibit similar 4th pharyngeal arch artery defects and concomitant great vessel defects at later stages, as well as outflow tract alignment defects and ventricular septal defects (Jerome and Papaioannou, 2001; Lindsay et al., 2001; Rochais et al., 2009a; van Bueren et al., 2010). However, investigation of double heterozygote mice did not reveal any differences in severity of frequency of pharyngeal arch artery defects as compared to single heterozygotes. This result suggested that there was no genetic interaction between *Tbx1* and *Hes1* during development in the mouse. Taken together, the results presented here infer that this interaction is present in the zebrafish, leading to the question of why this difference is apparent between the two species.

In the mouse it is possible that confounding factors could have influenced the result of genetic interaction experiments. As mentioned briefly in the Introduction both mutant lines exhibited a variable phenotype depending upon the genetic background employed. On a pure MF1 background *Hes1* null embryos died at E12.5 from vascular defects and presented with severe neural tube defects. On a mixed MF1:C57Bl6 genetic background Mendelian ratios were normal at E15.5 and no neural tube defects were observed (Lammerts van Bueren, 2008). The penetrance and severity of *Tbx1* null alleles has previously been shown to vary greatly with background (Taddei et al., 2001) and on

the mixed MF1: C57Bl6 background only 14% of *Tbx1* heterozygotes embryos had 4th pharyngeal arch artery defects at E12.5 compared to 50% on the C57Bl6 background. Thus the effect of the MF1 background upon the *Tbx1* pharyngeal arch artery phenotype combined with the recovery of the *Hes1*$^{-/-}$ vascular defects on the C57Bl6 background may have prevented the identification of an epistatic interaction between *Hes1* and *Tbx1* in the development of the mouse pharyngeal arch artery system. The phenotype of zebrafish mutants can also be affected by differing genetic background. For example the *tbx1* null fish, *vgo*$^{tm208/tm208}$ has a much more severe phenotype on the AB* background compared to the Tubingen background, in that the first pharyngeal arch is also highly reduced, whereas on the Tubingen background it is rarely affected (Piotrowski et al., 2003). However, this issue can be circumvented in the fish using knock-down morpholino experiments and mRNA rescues where the reagents are injected within the same embryo. The dosage for the required effect can be titrated for each experimental element, thus eliminating the problem of modifying genetic background for most experiments.

A further confounding effect which could have affected the results of the epistasis experiments is the effect of functional redundancy upon phenotype. The hairy/enhancer of split (Hes) family contains not only *Hes1* in the mouse, but also *Hes2*, *3*, *5*, 6 and *7* and the Hes-related (Hey/Hesr) *Hey1*, *2* and *L* genes, which are functionally related effectors of Notch signaling (Iso et al., 2003), having a YPPW C-terminal domain rather than WRPW. All three *Hey* genes are co-expressed in the mou myocardium, endocardium and vasculature (Wiese et al., 2010). Combined loss of *Hey1* and *HeyL* produces atrioventricular valve defects and VSDs whereas each mutant alone is unaffected (Fischer et al., 2004; Fischer et al., 2007; Kokubo et al., 2005). Similarly although *Hey2* null mutants exhibit a wide range of cardiovascular defects including cardiac hypertrophy (Gessler et al., 2002), Tetralogy of Fallot, VSDs, ASDs and tricuspid atresia (Donovan et al., 2002; Kokubo et al., 2004; Sakata et al., 2002), and coronary vascular defects (Watanabe et al., 2010) Addition of a second null allele for *Hey1* exacerbates these abnormalities, causing embryonic lethality at an earlier stage from severe vascular defects (Fischer et al., 2004; Kokubo et al., 2005). In the pharyngeal region *Hes1* expression overlaps with all three *Hey* genes in the pharyngeal mesenchyme and with *Hey1* and *Hey L* in the pharyngeal endoderm (High et al., 2007; Papangeli, 2010), raising the possibility

that functional redundancy between these genes may ameliorate any epistatic interaction between *Hes1* and *Tbx1*. Similarly, *Hes1*, *3* or *5* and *Hey1* have been shown to compensate for one another, in that compound mutant animals display defects of greater severity in neurogenesis, sensory organ, glandular and intestinal development compared to mutants for single genes, although no redundancy in pharyngeal or cardiovascular tissues has been reported (Cau et al., 2000; Hatakeyama et al., 2006; Hatakeyama et al., 2004; Hirata et al., 2001; Hojo et al., 2000; Ishibashi et al., 1995; Kita et al., 2007; Ohtsuka et al., 1999; Ohtsuka et al., 2001; Tateya et al., 2011; Ueo et al., 2012; Zine et al., 2001).

In the zebrafish, published reports of functional redundancy between *Hes/Hey* gene homologues are much harder to find, and it has been suggested that individual *hey* gene expression is more restricted than in the mouse (Winkler et al., 2003). Using the gene expression programme on ZFIN, the reported expression patterns of all the zebrafish *her(hes)/hey* genes were compared to that of *her6*. Very few possible candidates with overlapping expression were detected for the other *her* genes, despite a larger number of zebrafish *her(hes)* genes as a result of gene duplication events in teleosts. However, both *hey1* and *hey2* expression were found in the pharyngeal region at similar stages to *her6* (Thisse et al., 2001; Thisse and Thisse, 2004; Thisse and Thisse, 2005). The *gridlock (hey2*) null mutant has similar developmental anomalies to the mouse including defects in cardiac valve, myocardial proliferation, atrioventricular patterning and vascular development (Jia et al., 2007; Rutenberg et al., 2006; Weinstein et al., 1995; Zhong et al., 2000; Zhong et al., 2001) and *hey1* expression is required for the proper regulation of skeletal dorsoventral specification in the zebrafish face (Zuniga et al., 2010).Thus both these genes could be possible candidates for functional compensation for loss of *her6* expression.

However, it seems more likely that any mechanism masking the lack of epistasis between *Hes1* and *Tbx1* in the mouse would involve the modifying effects of genetic background, rather than functional redundancy, unless there are species differences which allow compensation to be more common in mouse than the fish, despite overlapping expression patterns of potential compensatory genes in both species.

The final reason for this difference of interaction between the species could be that *Tbx1* and *Hes1* simply do not interact during pharyngeal development in the mouse, but

do in the fish. However, given that *Hes1* was originally isolated as a potential *Tbx1* target from the mouse embryo this seems a more unlikely explanation than the potential confounding factors which may be acting in the mouse.

5.3.6 Roles in proliferation for *Tbx1/tbx1* and *Hes1/her6*

Tbx1 has been shown to be required for cellular proliferation in a number of different tissues in the mouse including the otic epithelium (Xu et al., 2007b), periotic mesoderm (Xu et al., 2007a), hair follicles (Chen et al., 2012b), dental epithelium (Cao et al., 2010; Catón et al., 2009), palatal mesenchyme (Funato et al., 2012) pharyngeal/cardiac mesoderm including splanchnic and secondary heart field mesoderm (Ai et al., 2006; Chen et al., 2009; Liao et al., 2008; Xu et al., 2004; Zhang et al., 2006b) , and pharyngeal endoderm (Xu et al., 2005).

Hes1 is also known to play an important role in the maintenance of progenitor cells in the nervous system (Hatakeyama et al., 2004; Ohtsuka et al., 1999; Ohtsuka et al., 2001), the eye (Lee et al., 2005; Tomita et al., 1996), the pituitary gland (Kita et al., 2007; Raetzman et al., 2007), pancreas (Jensen et al., 2000), thymus (Tomita et al., 1999) and hair follicle melanoblasts (Aubin-Houzelstein et al., 2008). *Hes1* also controls proliferation via repression of the cyclin-dependent kinase inhibitor $p27^{kip1}$ in the brain, liver, thymus (Murata et al., 2005) and cochlear epithelium(Murata et al., 2009). Similarly *Hes1* regulation of proliferation via inhibition of $p27^{kip1}$ and/or $p57^{kip1}$ has been observed in the pituitary (Georgia et al., 2006; Monahan et al., 2009; Raetzman et al., 2007). Decreased proliferation has also been reported in the corneal epithelium (Nakamura et al., 2008) and retina (Wall et al., 2009) in the absence of *Hes1* expression. Importantly, reduced proliferation has been demonstrated in the pharyngeal ectoderm of *Hes1* null mice (van Bueren et al., 2010). Decreased proliferation along with up-regulated $p27^{kip1}$ levels have also been observed in the secondary heart field mesoderm of $Hes1^{-/-}$ embryos (Rochais et al., 2009a).

Overall, levels of pharyngeal proliferation were reduced in *tbx1* and *her6* morphants as in $vgo^{tm208/tm208}$ mutants suggesting similar requirements for these two genes

in cellular proliferation in the zebrafish as in the mouse, although proliferation within individual tissues was not dissected in the fish as in the mouse. Similar decreases in pharyngeal proliferation were observed in the subphenotypic double morphants in which *her6* and *tbx1* genetically interact to produce the morphant pharyngeal phenotype. Finally, full length *her6* mRNA can rescue the proliferation defect produced by the injection of *tbx1* MO, further indicating that the genetic interaction between *her6* and *tbx1* in pharyngeal development may involve a mechanism influencing pharyngeal proliferation.

5.3.7 Potential mechanisms for *tbx1/her6* genetic interaction

The alteration of *her6* expression concomitant with *tbx1* expression levels, epistatic loss-of function and rescue experiments combined, suggest that *tbx1* and *her6* lie in a common pathway. However, despite being isolated from a FACS-Gal microarray designed to identify cell autonomous targets the length of time required for injection of *XTbx1* to up-regulate expression of *her6* suggests that this activation is likely not to be direct. Indeed, experiments in this laboratory have so far failed to achieve activation of (murine) *Hes1* promoter constructs with *Tbx1* in cell transfections (unpublished data), although there are potential T-box binding sites (TBEs) within *Hes1* genomic DNA. This raises the question as to how events downstream of *tbx1* and *her6* might converge in a common pathway. In the mouse *Tbx6* directly regulates *Dll1* transcription in the tailbud and presomitic mesoderm (PSM), in concert with canonical Wnt signaling, and thereby activates the Notch pathway (Hofmann et al., 2004). Thus, in light of our experiments in which activation of the notch pathway was able to partially rescue *tbx1* morphants, it is tempting to speculate that within the pharyngeal apparatus *tbx1* may have analogous effects on notch pathway ligands, and thus activate notch signaling which in turn activates *her6* transcription (Fig.5.19A.). Of interest, *Notch3* was found to have significantly reduced expression in $Tbx1^{-/-}$ vs $Tbx1^{+/-}$ cells (van Bueren et al., 2010) and has been reported to be important in smooth muscle cell differentiation in vitro (Liu et al., 2009) and in vivo (Domenga et al., 2004). Knock-down of all four Notch receptors using a dominant-negative MAML construct (DNMAML) expressed in neural crest cells also produces aortic arch defects resembling 22q11DS in addition to pulmonary artery stenosis

and ventricular septal defects (High et al., 2007). The phenotype of secondary heart field specific DNMAML mice is also akin to 22q11DS with its animal models displaying outflow tract and aortic arch anomalies (High, 2009). In the future knock-down of Notch-receptors/signalling using a *Tbx1Cre* line could shed light upon the functional importance of Notch signaling in the *Tbx1* Expression domain, ChIP and yeast one-hybrid studies could identify direct transcriptional binding sites within the *her6/Hes1* promoter. $Tbx^{neo2/neo2}$ mice, which are thought to represent the 22q11DS phenotype most accurately. Rescue experiments utilizing conditional NICD activation in these animals could be carried out to further elucidate the role of Notch-signalling in the tissues affected in 22q11DS.

An alternative mechanism for *tbx1/her6* interaction could involve shared target genes. Within the PSM *Tbx6* activates expression of *Mesp2* and can drive reporter gene expression from a *Mesp2* promoter-luciferase construct. Notably while the Notch intracellular domain (NICD) alone has no effect on the *Mesp2* reporter, it significantly co-activates TBX6-driven activity via both RBPJκ-dependent and independent mechanisms. Mutation of the TBX6 binding sites results in impaired skeletogenesis in mouse, which could be rescued by the medaka *mespb* core enhancer and chromatin immunoprecipitation confirmed T-box binding to the *Mesp2* consensus sequences (Yasuhiko et al., 2006; Yasuhiko et al., 2008). Thus, by analogy, normal activity of TBX1 at a target promoter may also require that of HER6 (Fig.5.19B). A second, intriguing, potential mechanism for the action of HER6 and TBX1 at a common target promoter, is provided by the recently elucidated role of RIPPLY3 in repressing the transactivation function of TBX1. RIPPLY3 binds to TBX1 at the promoter of common targets such as *Pax9* in the pharyngeal endoderm. Like HER6, RIPPLY3 contains a WPRW domain, via which it recruits Groucho/TLE/HDAC complexes, which then act to repress TBX1-driven transcriptional activation. There is also evidence suggesting *Tbx1* expression is necessary for that of *Ripply3* (Janesick et al., 2012; Okubo et al., 2011). It is possible to imagine a similar mechanism operating, whereby HER6 instead acts as the Groucho/TLE/HDAC recruiter, thus repressing TBX1 activity at target genes (Fig.5.19C). These hypotheses could be further investigated by using ChIP to identify potential TBX1/HES1 common targets. The promoter sequences of these could then be analysed for T-box and N-box binding motifs

and constructs made for in vitro experiments to determine if binding of TBX1 and HES1/HER6 together affected target gene transcription.

A recent publication reports that *tbx1* also regulates *her9* within the zebrafish inner ear to repress neurogenic fate (Radosevic et al., 2011). *Her9* is another zebrafish *Hes1* orthologue, albeit more distantly related to *hes1* than *her6*, and is expressed within the neuroectoderm, ear and axial mesoderm (Leve et al., 2001). This interaction in the ear is suggested to be direct and Notch independent, raising the possibility of multiple complex interactions between *Tbx1* and *Hes* family genes within different tissues during development, particularly since *Hes1* and other *hes/her* genes are known to auto-regulate in conjunction with other factors to control their oscillatory expression (Brend and Holley, 2009a; Hirata et al., 2002; Hirata et al., 2004; Kageyama R et al., 2007; Kageyama et al., 2009; Takebayashi et al., 1994) . Interestingly, retinoic acid is proposed to act up-stream of both *tbx1* and *her9* (Radosevic et al., 2011). RA is implicated both up and down-stream of *Tbx1* in mouse, chick and zebrafish pharyngeal development (Guris et al., 2006; Roberts et al., 2005; Roberts et al., 2006; Zhang et al., 2006a) and *Hes1* has been shown to be down-regulated by RA in vitro (Murata et al., 2005), so further studies to pursue the role of RA with regard to the *Tbx1*/*tbx1 Hes1*/*her6* interaction within pharyngeal tissues maybe relevant.

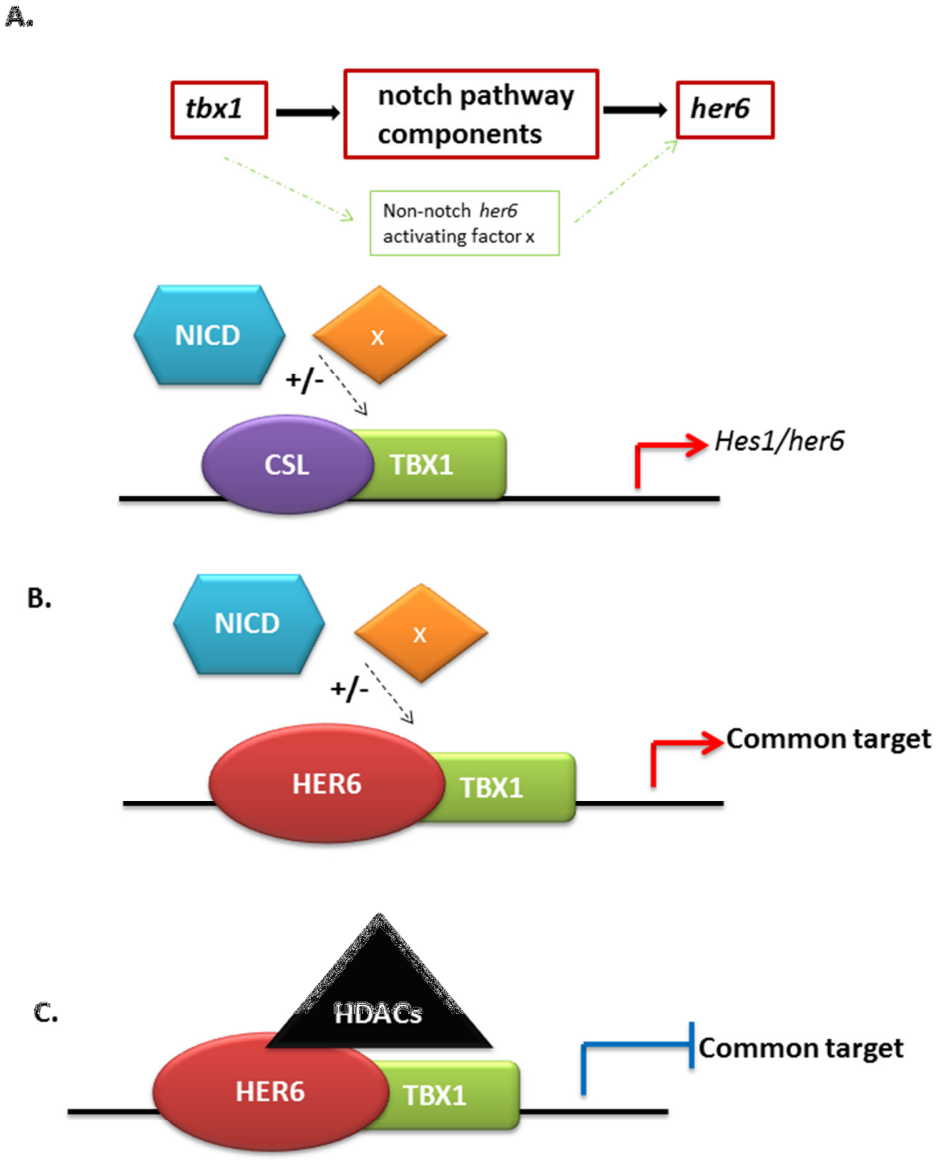

Figure 5.19 Potential mechanisms for *tbx1/her6* interaction based on mechanisms postulated in the literature

A.) *tbx1* activates the notch pathway which in turn activates *her6*. X represents a possible non-canonical Notch activating factor [based on (Hofmann et al., 2004)]. B.) Binding of TBX1 and HER6 at a common target promoter is required for TBX1 target activation. C.) HES1/HER6 acts to repress TBX1 transactivation of a common target gene [based on (Janesick et al., 2012; Okubo et al., 2011).

5.3.8 A role for Notch independent pathways?

As described above NICD activation can partially rescue the *tbx1* morphant phenotype. This rescue is not as successful as with *her6* mRNA, which may simply be due to experimental variation, but does raise the possibility that *tbx1/her6* interaction may also be mediated by a Notch-independent activation of *her6* expression. Pathways such as *Shh/Gli2* (Ingram et al., 2007; Wall et al., 2005), *Pax3* (Nakazaki et al., 2008) and *Frs2α*/ERK (Sato et al., 2010) have been shown to activate *Hes1* independently of Notch signaling. It is also suggested that HES1 can serve as a convergent signaling node within early retinal progenitor cells to integrate various cell-extrinsic cues, including VEGF and SHH (Hashimoto et al., 2006). All of these pathways have been linked to 22q11DS in various ways. *Shh* is thought to regulate *Tbx1* expression via the *Foxc1/c2* transcription factors and similar knock-out phenotypes to *Tbx1* null mice are observed for these genes (Garg et al., 2001; Yamagishi et al., 2003). VEGF signaling is a modifier of the 22q11 phenotype (Stalmans et al., 2003) and may act downstream of *Tbx1* in lymphogenesis (Chen et al., 2010). In *Pax3 Splotch* mutant mice a comparable phenotype to that of 22q11DS/*Tbx1* mutant mice is observed. Common arterial trunk and defects of the pharyngeal arches and arch arteries and thymus, parathyroids and thyroid glands are manifest as a result of a decreased contribution of neural crest cells to the pharyngeal and outflow regions (Bradshaw et al., 2009; Chan et al., 2004; Conway et al., 1997). *Hes1* expression is decreased in the NCC of *Splotch* mutants and is up-regulated by the direct binding of *Pax3* to the *Hes1* promoter in wild type embryos but not in *Sp/Sp* mutants (Nakazaki et al., 2008). Finally, FGF signaling downstream of *Tbx1* particularly via *Fgf8*, is important for normal development.

In light of the interaction we have uncovered in zebrafish, it will be of interest to investigate whether increased expression of *Hes1*, the Notch pathway, or pathways which can independently activate *Hes1* can rescue aspects of the *Tbx1* loss of function phenotype in the mouse. These experiments should be initiated using a hypomorphic allele such as that described by Zhang and Baldini 2008 (Zhang and Baldini, 2008) as these models are believed to more accurately reflect the patient situation.

5.4 Future Directions

5.4.1 Tissue-specific experiments in the zebrafish

Tol2 contains a gene encoding an active transposase that can catalyze DNA transposition in vertebrate cells. In zebrafish, *Tol2* generates genomic integrations in the germ cells very efficiently. Using the *Tol2* transposition system, has resulted in the development of important genetic methods including single insertion transgenesis, gene trapping, enhancer trapping, and the Gal4-UAS system in zebrafish. *Tol2* transposition has been combined with *Cre-loxp/Flp* systems in the zebrafish to drive a gene-trap cassette, FT1, that can be stably inverted by both Cre and Flp recombinases. Host gene expression is not greatly affected when gene-trap intronic insertions are inverted, in the neutral orientation. However, when the gene trap is in the same orientation as the host gene, severe disruption of endogenous expression is expected. Cre- and Flp-mediated recombination switches the orientation of the gene-trap cassette, permitting conditional rescue in one orientation and conditional knockout in the other. Constructs of this type combined with tissue-specific inducible Cre-transgenic lines could provide an approach to allow investigation of *tbx1* and *her6* tissue-specific pharyngeal arch requirements in the zebrafish (Curado et al., 2007; Halpern et al., 2008; Li et al., 2009; Mosimann and Zon, 2011; Ni et al., 2012; Suster et al., 2011). Recently, zinc finger nucleases (ZFNs) and artificial transcription activator-like effector nucleases (TALENs) have been used to introduce specific double-stranded breaks in the zebrafish genome, allowing the targeted generation of mutant alleles. In 2012, the TALEN technology has been used with synthetic single-stranded oligonucleotides designed to span a specific TALEN cut site to serve as a template for homology directed repair. This allowed the introduction of specific RE sites, and, most importantly, the introduction of a *loxp* sites at a targeted location. Both these engineered chromosomes were germline transmitted, offering the potential to generate targeted conditional alleles in the zebrafish [(Bedell et al., 2012) and references therein]. Thus in the future, it may be possible to produce conditional alleles for both *tbx1* and *her6*. Caged morpholinos could also be used to achieve temporally conditional knockdown of *her6/tbx1*. This approach temporarily inhibits the activity of the MO with a

photocaged moiety until it is released by exposure to laser light at an appropriate time point (Wang et al., 2012) and references therein.

Further investigation the cell proliferation defects observed in the morphant pharyngeal regions toidentify which tissues carry this deficiency might also be informative. These experiments could be performed by combining immunohistochemistry for proliferative markers such as phosphohistone H3 with either tissue specific gfp-transgenic fish such as *Tg(sox10:gfp)* for the different pharyngeal lineages or with fluorescent in situ hybridization for marker genes expressed within specific cell types.

Attempts to finish the conditional work in the mouse for *Hes1* by characterizing its role in the pharyngeal mesoderm and endoderm could also be considered. Using the pan-mesodermal Cre-driver *Mesp1Cre* would answer the first, but the second may prove more problematic since both endodermal Cre lines (*Foxa2mcmCre* and *Sox17Cre*) tried in this laboratory suggested Cre recombination on the *Hes1* background was variable and always less than expected. This could be overcome by crossing to a different background, but would depend upon finding a background that did not ameliorate the *Hes1* phenotype. An alternative driver is *Foxg1Cre* but this has been shown to have non-endodermal expression in the mesoderm (A. Baldini pers. comm.). *Sox17Cre* is also expressed in the vascular endothelium (K.Yashiro, pers. comm.) Experiments with *Tbx1Cre* (Huynh et al., 2007) could help to determine whether knockdown of *Hes1* in *Tbx1*-positive pharyngeal tissues is sufficient to produce the 22q11-like phenocopy and increase the evidence for likelihood of an interaction between the two genes in the mouse. This experiment would also exclude any direct role of *Hes1* within the NCC, as *Tbx1* is not expressed in this lineage.

5.4.2 Interaction between *her6* and *tbx1* in cardiac development?

The work presented here is focused upon identifying an interaction between *her6* and *tbx1* in pharyngeal arch/artery development. However, during these studies we observed that single and double morphant embryos frequently presented with abnormal looking hearts and cardiac oedema was often present by 3dpf. Both *Tbx1* and *Hes1* mutant mice share common cardiac phenotypes including secondary heart field proliferation

deficiencies, OFT extension failure and later defects including VSDs and overriding aorta. It may therefore be of interest to extend this study further to consider whether *her6* and *tbx1* co-operate not only in pharyngeal arch/artery development but in cardiac development as well. Recent studies have confirmed that as for higher vertebrates the zebrafish contains two heart fields, both of which are important for cardiac development. As in other models, in the fish the second heart field makes a late contribution to the myocardium, smooth muscle and endothelium of the OFT and the distal ventricle and conserved molecular pathways including *tbx1*, *isl1*, *shh*, *mef2cb nkx2.5*, and TGF-B, BMP and FGF signaling are required for the development of the zebrafish arterial pole (Hami et al., 2011; Hinits et al., ; Lazic and Scott, 2011; Zhou et al., 2011), also reviewed in (Liu and Stainier, 2012). Development of the SHF is perturbed in $vgo^{tm208/tm208}$ embryos with reduced pSmad1/5/8 expression indicating reduced numbers of differentiating cells at the animal pole and fewer cells being added to the OFT from the SHF population (Hami et al., 2011). Further studies could investigate the function of the SHF in *her6* and *her/tbx1* double morphants in similar experiments, and moreover, cellular proliferation in the SHF could be examined to see if a decrease in proliferation plays a role in any abnormal phenotype as it does in the *Tbx1* and *Hes1* mouse mutant OFT.

5.4.3 Mechanism of *her6/tbx1* interaction

The evidence provided in this chapter overall demonstrates that *tbx1* and *her6* most likely act in a common pathway. However, the mechanism of action of the *tbx1/her6* interaction remains obscure. Indeed, whether this is a direct interaction or mediated by other factor is currently unknown. Bioinformatic analyses could be carried out to identify potential *tbx1* binding sites within the *her6* regulatory regions. Subsequent testing with transient transfection experiments can be carried out to see if *tbx1* can bind to these elements and induce *her6* expression. If so, mutation of the binding sites can be carried out to confirm the specific binding of *tbx1* to these sites. In addition, given the potential role of notch signalling, co-transfection with an NICD construct could be performed to see if a synergistic activation of *her6* can be observed with both *tbx1* and NICD present. Relatively few direct targets for *Tbx1* have been described in mouse; *Pitx2*, *Fgf10*, *Wnt5a*,

Vegfr3 and *Smad7*. Only the latter three of these targets, have been have been confirmed by ChIP. Genome-wide ChIP-sequence experiments in murine embryos and cell lines, currently underway in several labs, may also indicate potential elements via which *Tbx1* might regulate *Hes1*. Similar experiments in zebrafish, or quantitative-ChIP analysis of any conserved binding elements, would determine whether such direct regulation is present in this species. If, however, the common target hypothesis is correct, then comparison of HER6 (HES1) and TBX1 ChIP sequence data could be used to determine potential common target genes. If any of these approaches were successful then further assays to confirm combinatorial binding at target promoters could be carried out using the zebrafish as an *in vivo* model.

CHAPTER 6
Final Discussion

6.1 Tbx1 networks

Tbx1 plays a crucial role pharyngeal and cardiovascular development. Loss of *Tbx1* produces a specific pharyngeal and cardiovascular phenotype in animal models that phenocopies human 22q11DS, in which *Tbx1* is haploinsufficient in most cases. The development of the pharyngeal region and SHF during embryogenesis requires an extremely complex system of cross-talk between several different tissues, mediated by an equally complex molecular interactive network. *Tbx1* has been shown to be important for the normal development of all the tissues of the pharyngeal region, including the NCC. *Tbx1* promotes the proliferation of progenitor cells at the expense of differentiation. It also plays a role in developmental patterning of the pharyngeal region and OFT and is required for normal NCC migratory behaviour. *Tbx1* functions at the genetic level, controlling the transcription of down-stream target genes and also takes part in protein-protein interactions that further impact upon pharyngeal and OFT development. The number of identified molecular interactors, which act both up-stream and down-stream of *Tbx1*(Fig.6.1), is growing rapidly, and includes a wide range of different pathways including transcription factors, chromatin remodelling factors, growth factors and the retinoic acid pathway. The work presented in thesis has been undertaken to ascertain the functional roles of potential *Tbx1* targets, Notch-pathway effector bHLH gene *Hes1* and the Cyp26 enzyme family, in the production of the *Tbx1* mutant phenotype, in particular the cardiovascular defects observed.

6.1.1 *Tbx1*, *her6* and *Cyp26* genes

Potential *Tbx1* targets *Hes1*/(*her6*) and members of the *Cyp26* gene family were previously identified and validated by microarray and RTQ-PCR. As discussed above the aim of this thesis was to further investigate any roles they may play in the *Tbx1* mutant

phenotype, particularly the cardiovascular aspects. As a result of this study, and additional circumstantial evidence in the mouse, it seems likely that there is an interaction between *tbx1* and *her6* in the zebrafish. *Tbx1* and *her6* are required for normal patterning and proliferation of the pharyngeal arches and arteries in this model. Given the cardiovascular phenotype of the *Hes1*$^{-/-}$ mouse, this is also quite possibly the case this species, although further epistasis experiments will be required to prove this. *Hes1* null embryos also have *Tbx1*/22q11DS-related heart defects. Although this phenotype was not pursued in this study, cardiac oedema and malformation were observed in *her6* morphant zebrafish, similar to abnormalities in *vgo*$^{tm080/tm2088}$ embryos, making it tempting to speculate that the *Hes1/her6/Tbx1* interaction also operates during the development of the outflow tract/ventricle.

The case for interaction of *Tbx1* with the *Cyp26*s is more complicated. *Tbx1* is required for normal Cyp26 expression and abrogated function of all three Cyp26 enzymes provides a phenocopy of 22q11DS as does the *Cyp26b1* full knockout mouse. However, although more cardiovascular defects were seen in double heterozygous *Cyp26b1:Tbx1* mice, this was not statistically significant with the sample size analysed. An increased penetrance of the most severe aortic arch phenotype was observed in the deleted triple allele *Cyp26b1*$^{-/-}$*Tbx1*$^{mcm/+}$ embryos. This phenomenon cannot be described in terms of epistasis, as in the *Cyp26b1* nulls there is no *Cyp26b1* gene present. However, it could be thought of in terms of a modifying effect of the *Tbx1*^{mcm} allele on the *Cyp26b1* pathway, via interaction with *Cyp26b1* targets, i.e. genes whose expression is altered by activity levels of *Cyp26b1*. Interestingly, Chen et al (Chen et al., 2012a) report that *Tbx1* may activate transcription of several down-stream targets, including *Wnt5a*, *Fgf8*, *Fgf10* and *Cyp26a1*, via recruitment of the chromatin remodelling complex Baf60a. By analogy it is possible a similar mechanism may operate for the activation of *Cyp26b1* (and *c1*). The interaction between *Tbx1*$^{mcm/+}$*:Cyp26b1*$^{+/-}$ is not strong enough to be obviously phenotypically synergistic with the sample size observed. However, a possible mechanism involving additional contributions from these other *Tbx1* interactors may be necessary and/or sufficient to lead to phenotypically noticeable synergistic change. It is clear that any phenotype with triple heterozyote null mutations in all three *Cyp26* genes is not fully penetrant as triple heterozygotes are reported as being bred together to produce triple

homozygote null animals (Uehara et al., 2009). Thus down-regulation of some/all of the *Cyp26* genes/other interactors in combination with *Tbx1* may be required, and for this reason it would be interesting to investigate the phenotype of *Cyp26a1/b1/c1* heterozygotes in the context of a $Tbx1^{+/-}$ background. Viewed in this combinatorial fashion i.e. that each interaction contributes an incremental change of varying degree, it is possible to see that this type of network (Fig.6.1.) could potentially produce a very sensitive down-stream response. This would fit well with the known dosage sensitivity of *Tbx1*. Allelic series which produce a gradient of *Tbx1* expression give rise to a similar phenotypic gradient, with different tissues exhibiting varied responses to the level of *Tbx1* expression (Zhang and Baldini, 2008). It can be imagined that this outcome is only possible if a very fine combinatorial control of down-stream targets is achievable.

Whilst further experiments are required to determine the exact nature of the *Tbx1/Cyp26* interaction, that *Tbx1* can act to modify this pathway, and therefore available RA, seems probable. It is also already proven that *Tbx1* performs this function at the level of the *Raldh2* synthesizing enzymes by regulating their anterior expression (Guris et al., 2006; Ivins et al., 2005). Thus *Tbx1* does act up-stream of RA-synthesizing/metabolizing enzymes to regulate pharyngeal RA levels during development.

6.1.2 Regulatory feedback between Tbx1 and RA

A potential feedback loop exists between *Tbx1* and RA-signalling (Fig 6.1). *Tbx1* regulates the availability of RA for development signalling via the synthesizing and metabolizing genes. Various groups have shown that RA signalling, in turn, can down-regulate the expression of *Tbx1* itself (Roberts et al., 2005; Zhang et al., 2006a), although the exact nature of these effects seems to be somewhat variable between experimental systems (Table 6.1). In VAD quail embryos ectopic early expression was followed by complete loss of expression later in development and RA bead implants at stage 10 repress pharyngeal *Tbx1* expression (Roberts et al., 2005). In vitro experiment in P19 cells and in zebrafish embryos has shown this response to exogenous RA to be dose-dependent (Roberts et al., 2005; Zhang et al., 2006a). Additionally, in Xenopus treated with an RAR antagonist, *Tbx1* expression was at first increased relative to controls, then decreased and

later unaffected. RAR agonist treatment lead to early expression of *Tbx1* being up-regulated before becoming down-regulated later in development. The early up-regulation of *Tbx1* in response to RA was also confirmed by morpholino experiments (Janesick et al., 2012). There are also reports suggesting exogenous RA in early presumptive otic placodal tissue can induce *Tbx1* expression as (Bok et al., 2011; Radosevic et al., 2011) (Table 6.1). The function of other T-box genes has been shown to be negatively regulated by members of the *Ripply* family during somitogenesis (Kawamura et al., 2008; Moreno et al., 2008). Recent reports upon the function of RIPPLY3 suggest this protein could be at least partially mediating the response of *Tbx1* to RA. *Ripply3* is co-expressed with *Tbx1* in the murine pharyngeal endoderm and ectoderm and *Ripply3* mutants exhibit aberrant cardiovascular and thymus defects and abnormal pharyngeal mesodermal development as a result of increased non-cell autonomous apoptosis (Janesick et al., 2012; Okubo et al., 2011). TBX1 and RIPPLY3 proteins physically interact at target promter sequences, via the T-box WRPW domains respectively, and RIPPLY3 represses TBX1 target transactivation. This repression probably functions via RIPPLY3 mediated recruitment of GROUCHO/TLE co-repressors to the TBX1 protein, at the target gene promoter (Okubo et al., 2011). In *Xenopu*s, TBX1 was necessary for *Ripply3* induction, whereas *Ripply3* overexpression reduced *Tbx1* expression, suggesting an possible autoregulatory loop. *Ripply3* is strongly induced by increased RAR-signalling and decreased in its absence (Janesick et al., 2012). This leads to the possibility that part of the tight control of *Tbx1* and its target genes could be RA-RIPPLY3-mediated, i.e. increased RA expression induces *Ripply3* thus further repressing TBX1 transactivation. This might explain why RA-mediated reduction of *Tbx1* requires 8-12h and is partially dependent upon protein synthesis. However, two RARE motifs are present in the *Tbx1* upstream locus suggesting direct regulation of *Tbx1* by RA may also be possible (Roberts et al., 2005).

Table 6.1 Effects of RA upon *Tbx1* expression

Experimental system	*Tbx1* expression relative to control	
	Decreased RA	Increased RA
Xenopus whole embryo (Janesick et al., 2012)	(RTQ-PCR after addition of RAR antagonist) St14 Increased St16 Decreased St 18-32 Unaffected (Anti-RARα2 MO) Decreased expression at neurala stages (in situ hybridization)	(RTQ-PCR after addition of RAR agonist) St14 Increased St16 Increased St18 Unaffected St23-32 Decreased N/A
Avian embryo (Roberts et al., 2005) (Bok et al., 2011)	(VAD quail in situ hybridization) St10-12 Ectopic caudal expansion & lateral reduction in PPE St14+ Greatly decreased (Chick, in situ hybridization) (Chick, in situ hybridization 0.4g/ml citral soaked bead implants in 8ss otic mesenchyme) St12 loss in posterior OV	(Chick. St12-14 2 x10^{-3}M RA soaked bead pharyngeal st12-14 implants, in situ hybridization)) St 20 decreased all pharyngeal tissues (Global RA treatment St10-14) +24h decreased (Chick, in situ hybridization ss8 0.5mg/ml RA soaked bead implants in otic mesenchyme) St12 Anterior ectopic OV expansion. Decreased in PM
P19 cells (Roberts et al., 2005)	Unknown	(3 x 10^{-6}M-1.5x10^{-8}M RA treatment, RTQ-PCR)) Dose dependent decrease from +8h culture
Zebrafish otic vesicle (Radosevic et al., 2011) Zebrafish whole embryo (Zhang et al., 2006a)	(DEAB treatment 10.5-24hpf) 24h Decreased Unknown	(2x10^{-8}M RA 10.5-12hpf) 24hpf anterior ectopic expression (5 x10^{-8}M/10^{-7} RA 12.5-14hpf) 36hpf+ Greatly decreased all pharyngeal tissues (RTQ-PCR and in situ hybridization)
Mouse	*Raldh2* $^{-/-}$ (Ryckebusch et al., 2008; Ryckebusch et al., 2010) 3-4ss, Ectopic caudal OFT expansion 8ss decreased PE and PSE Anterior expansion pharyngeal mesenchyme.	(Maternal diet supplementation, 100μgRA/g chow E7.5-9.5 *Tbx1*$^{lacz/+}$ x wild-type C.Roberts unpublished data). Decrease β-galactosidase expression E9.5 (50mg/kg maternal gavage E7.75 In situ hybridization) Anterior ectopic OV expansion Decreased in PM(Bok et al., 2011)

Combined results for different experimental systems for the effect of increased/decreased RA upon *Tbx1* expression. St: Stage of development, hpf: hours post-fertilization, PE: pharyngeal endoderm, PSE: pharyngeal surface ectoderm, PM: pharyngeal mesoderm, OV: otic vesicle, ss: somites, RTQ-PCR: real time quantitative PCR, VAD: Vitamin A deficient, DEAB: Diethylaminobenzaldehyde RA inhibitor

6.1.3 Environmental factors influence the outcome of genetic lesions

Very recently, it has been shown that *Tbx1* is regulated by the action of histone acteyltransferease MOZ at the *Tbx1* locus (Fig.6.1). Occupancy of the *Tbx1* promoter by MOZ was required for H39K acetylation and transcription of *Tbx1* early in development, and also at the *Tbx5* and *Tbx2* loci at later stages. *Tbx1* expression was reduced in *Moz* homozygous null embryos and these embryos phenocopied 22q11. A synergistic rise in frequency and severity of these malformations was demonstrated in $Tbx1^{+/-}Moz^{+/-}$ embryos. The null *Moz* phenotypes could also be rescued by a *Tbx1* BAC transgene. $Moz^{+/-}$ embryos are developmentally normal under usual circumstances. However, increased dietary RA between E8.25 and E9.5 produced increased 22q11-like abnormalities in $Moz^{+/-}$ embryos compared to wild-type controls (Voss et al., 2012). Thus environmental RA variations can affect the phenotypic outcome of pre-existing congenital lesions. The presence of the *Moz* haploinsufficiency probably confers an increased sensitivity to local levels of RA, since RA also reduces *Tbx1* expression levels. Relative levels of buffering against excess RA, determined by *Cyp26* expression, may also contribute to the ability of embryos to overcome environmental fluctuations such as varying RA levels in normal versus mutant embryogenesis. A new paper also suggests that alterations of SHH and RA signalling, that are benign in the wild type state, can increase the severity and/or frequency of craniofacial/cardiovascular defects in $Ldgel^{/+}$ embryos, in a *Tbx1*-independent fashion. *Ldgel* is a mouse 16 chromosomal deletion model for 22q11Ds, as described in Chapter 1. These experiments imply that environmental factors may act upon the other deleted genes (and their targets) in 22q11DS to generate some of the phenotypic variation and diversity observed between different patients (Maynard et al., 2012).

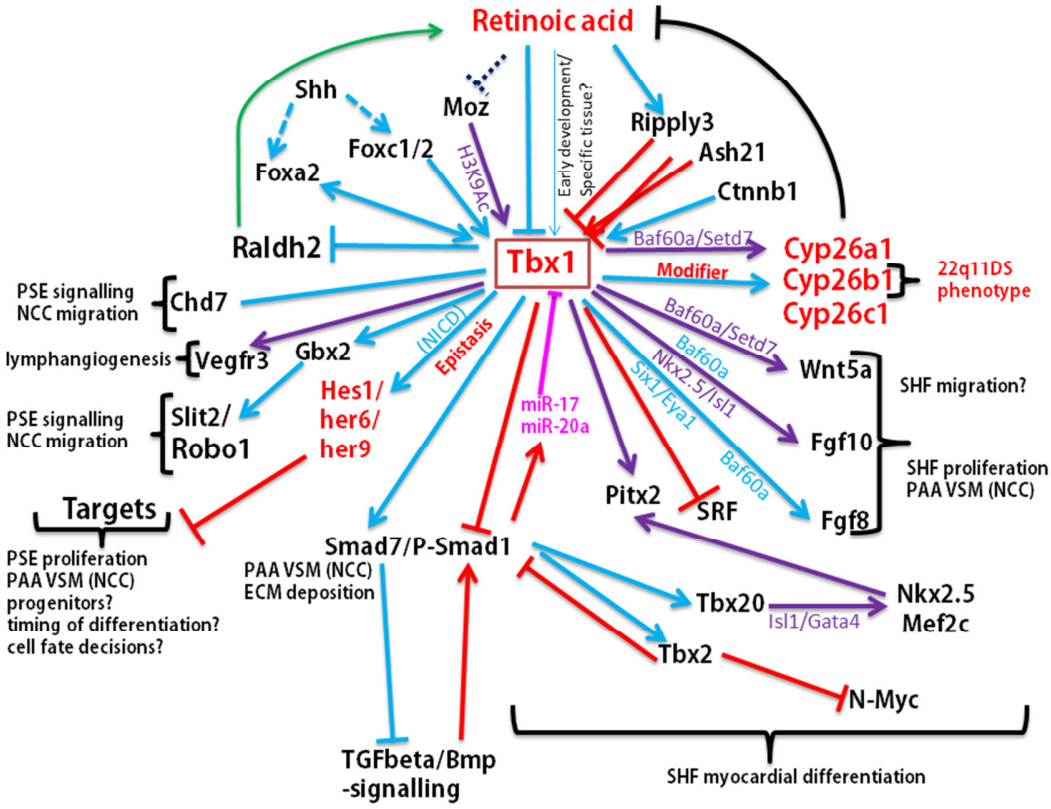

Figure 6.1 Schematic of and overview of possible Tbx1 interactions during development. Results from published data and this thesis. Included interactions are from varying tissues/species/developmental stages [reviewed in (Greulich et al., 2011; Papangeli and Scambler, 2012b; Scambler, 2010)]. Protein-protein interactions: red lines, genetic experiments/expression data: blue lines, direct transcriptional regulation at promoter, includes in vivo and in vitro experiments: purple lines, synthesizing enzymes: green lines, degrading enzymes: black lines, miRNAs: pink lines. Large dotted line: indirect, small dotted lines: hypothesis.

In a similar vein, environment in the form of diet can induce a pre-disposing genetic defect to lead to a disease phenotype in calcified aortic valve disease (CAVD). CAVD and bicuspid aortic valve disease are the commonest form of adult valve disease affecting 1-2% of the Western population. Eventually over time with the influence of environmental factors including diet, aging and smoking CAVD and bicuspid aortic valve (BAoV) disease leads to improper function of the valve, obstructed blood-flow and regurgitation, which in turn increases the workload on the left ventricle and over time the outcome is heart failure (Freeman and Otto, 2005; Goldbarg et al., 2007). *RBPJκ*-heterozygous

animals have normal tricuspid valve leaflets but after 16 weeks on a hypercholesterolemic diet valve calcification is induced in conjunction with down-regulation of *Hey1* and activation of osteogenic markers (Nus et al., 2011). BAoV causes improper valve function in its own right and can predispose towards valve calcification, thus increasing the likelihood of developing aortic valve disease (Garg et al., 2005). Various studies of BAov in mouse and human have elucidated that *Nos3* is a common target of both *Notch* and *Gata5* and *Gata5* may regulate *Nos3* expression both directly, and indirectly, via Notch signalling. This signalling pathway is required for normal EMT and to prevent to abnormal up-regulation of osteogenic gene expression in developing and maturing valves (Chang et al., 2011; Garg et al., 2005; Laforest et al., 2011; Lee et al., 2000; Padang et al., 2012) (Fig.6.3). Interestingly, both *Tbx1* and *Fgf8* heterozygous mouse models are also found to have a bicuspid aortic valve [my unpublished observations and (Macatee et al., 2003)] suggesting that these genes may impact upon this pathway or act via a parallel mechanism upon a common target gene/tissue. In addition, mouse models suggest possible roles for transcription factors NFAT/calcineurin (Chang et al., 2004; Lin et al., 2012; Schulz and Yutzey, 2004) and *Nkx2.5* (Beffagna et al., 2012; Biben et al., 2000) and BMP-signalling (Girdauskas et al., 2011; Thomas et al., 2012) during this process. Further investigation of a $Tbx1^{+/-}$ BAoV phenotype could include analysis as to whether it is always associated with a LVOT defect, expression patterns of the known genetic players in BAoV and the effects of aging and a high cholesterol diet upon surviving adult $Tbx1^{+/-}$ valve calcification.

6.2 Interactive signalling between *Tbx1*, RA and Notch signalling pathways in 22q11DS developmental systems?

Tbx1 has been implicated in both the Notch pathway via *Hes1/her6* and the RA pathway via the genes controlling availability of RA in the development of the pharyngeal and cardiovascular systems. More than likely these pathways function in parallel to each other during the development of these tissues. However, there have been some publications that suggest combinatorial functions of these signalling pathways which could, theoretically be integrated with *Tbx1*.

6.2.1 Combinatorial RA and Notch signalling in the acquisition of mesodermal fate

Intriguingly, there are hints in the literature that RA, in combination with NOTCH and BMP signalling, can together regulate the acquisition of mesodermal fate in ES cells. PA6 cells which can be used as a feeder layer for ES cells mediate their differentiation activity through activation of NOTCH signalling. In the presence of BMP4, ES cells favoured either a mesodermal fate as indicated by increased expression of *Desmin*, or the maintenance of self-renewal, as many colonies were also positive for *Oct4*. If RA was added into the culture medium with BMP4, then nearly 100% of colonies were positive for *Desmin* alone and acquired a mesodermal cell morphology indicating a switch towards mesodermal fate. Notch-signalling from PA6 cells was important for this process as in the presence of γ-secretase inhibitors to down-regulate NOTCH signalling reduced the number of *Desmin*-positive cells. RTQ-PCR in serially-passaged differentiated cells showed down-regulation of pluripotency, endodermal and ectodermal marker genes and up-regulation of smooth muscle markers. Furthermore, RA and Notch signalling during this process directly impacted on BMP-mediated activation canonical SMAD-luciferase reporter. BMP4 supplementation of the culture media increased luciferase activation, but this effect was attenuated in co-cultures with PA6 cells, and abrogated further with the addition of RA (Torres et al., 2012). Clearly, careful regulation of BMP-signalling by NOTCH and RA is required to for activation of a mesodermal direction of differentiation in this system. This thesis describes work from this laboratory and others, which show that *Tbx1* acts to regulate both RA and down-stream Notch effectors in PAA development. It has also been shown to interact with the BMP pathway at both the genetic and protein level. TBX1 binds SMAD1 and inhibits SMAD1/4 signalling (Fulcoli et al., 2009) and induces expression of TGF-B inhibitory *Smad7* (Papangeli and Scambler, 2012a). It has also previously been shown that *Tbx1* is expressed cardiac progenitor cells, which can give rise to three types of cardiovascular lineages including smooth muscle. *Tbx1* expression is necessary to maintain the proliferation of the multipotent undifferentiated progenitor cells and is down-regulated with differentiation (Chen et al., 2009). Additional multifaceted interactions in a number of systems have also been shown to exist between

between RA-signalling and Notch signalling via the NICD and the SMADs (Andersson et al., 2011; Greene and Pisano, 2005). It could therefore be hypothesized that *Tbx1* may sit up-stream of a similar BMP,-Notch -RA -signalling cascade during smooth muscle development, controlling the balance between the maintenance of multipotency versus mesodermal fate (Fig 6.2).

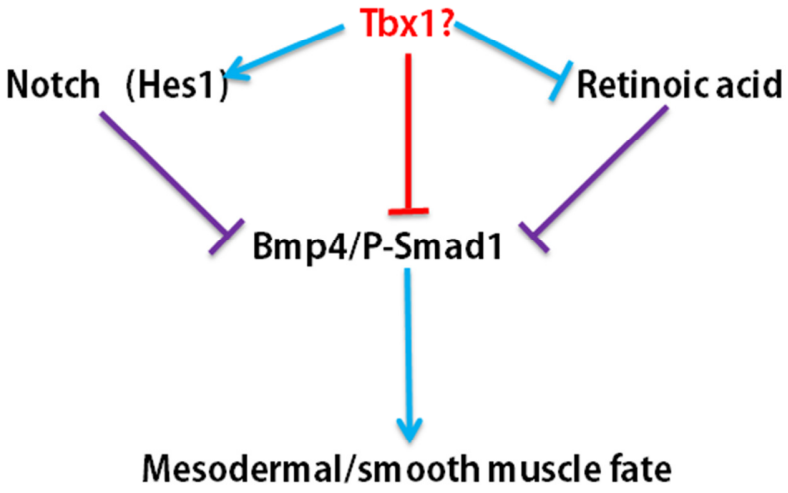

Figure 6.2 Schematic of hypothetical Tbx1 signalling during acquisition of mesodermal cell fate in ES cells.

Protein-protein interactions: red lines, genetic experiments/expression data: blue lines, direct transcriptional regulation at promoter.

6.2.2 RA, *Tbx1* and *her9* during zebrafish otic development

As discussed in Chapter 5, there also appears to be a potential interaction between *Tbx1*, RA and *her9*, another zebrafish paralogue of *Hes1*, [albeit less conserved than *her6* (Leve et al., 2001)] although this has not yet been proven by epistasis experiments. *Her9* is co-expressed with *tbx1* in the non-neurogenic domain of the ear in zebrafish embryos. Knock-down of *her9* in this domain resulted in ectopic expression of pro-neural genes and decreased cell proliferation. Examination of *her9* expression in *tbx1* null *vgo*$^{tm208/tm208}$ mutants and embryos over-expressing *tbx1*, showed *tbx1* to be necessary and sufficient for

her9 otic expression, as it is for *her6* pharyngeal expression. This interaction appeared to be completely NOTCH independent, unlike that of *tbx1* and *her6*. Blocking RA signalling abolished expression of *tbx1* and *her9* and non-teratogenic doses of RA shifted the expression domain of both genes. Inhibition of HH signalling ectopically induced otic *tbx1* and there was a strong potentiation of this effect in the presence of RA. FGF-signalling was found to be necessary for otic induction at gastrulation stages and altered expression of *raldh2* and *cyp26c1* was observed, but RA activity later in otic development appeared to be FGF- independent. So it seems that in the otic vesicle a potential signalling network between RA, *her9* and *tbx1* may regulate otic patterning to preserve a non-neurogenic proliferative domain (Radosevic et al., 2011). The effect of RA upon *tbx1* and thus *her9* appears somewhat different to that reported previously in other species (Table 6.1). Ectopic expression of *her9* in experiments with exogenous RA was different to the loss of expression observed in $vgo^{tm208/tm208}$ embryos. This was unexpected as $vgo^{tm208/tm208}$ embryos might be expected to have increased levels of RA as in the *Tbx1* null mouse. Some studies report down-regulation of *Tbx1* in pharyngeal tissues, including the otic vesicle after incubation with exogenous RA (Roberts et al., 2005; Zhang et al., 2006a), whereas others, where RA was applied earlier, report ectopic anterior *Tbx1* expression in the otic vesicle (Bok et al., 2011; Radosevic et al., 2011). These differences may be due to species variation, tissue specific effects, timing of the RA application or varying RA dosage and suggest that the exact functions of RA/*Tbx1/Hes1* family interactions during development are extremely dynamic and context dependent. It might be interesting to attempt to elucidate if there is a role for RA in the *tbx1/her6* interaction. However, it is also possible to argue that the exact nature of the fluctuation from the norm induced by disrupted RA signalling may be unimportant, since the effects upon development of altered RA homeostasis in either direction tend to affect the same systems in a similar fashion.

6.2.3 RA, Notch and *Tbx1* during dental development

Additionally, there seems to be complex interplay between *Tbx1*, Notch and RA signalling during dental development, in interactions between the neural crest-derived

dental mesenchyme and the adjacent dental epithelium. RA up-regulates Notch receptor expression in dental mesenchyme, but Notch expression is absent from presumptive ameloblast epithelium. Notch ligands however, are expressed in a complementary fashion in the dental epithelium (Mitsiadis et al., 1995). Signals from the mesenchyme including FGF and BMP4 are necessary for the expression of both *Jag2* and *Tbx1*. These are in turn required for the enamel-producing ameloblast progenitors of the dental epithelium for normal tooth development. Loss of either *Jag2* or *Tbx1* induced tooth defects reminiscent of those observed in 22q11DS (Catón et al., 2009; Mitsiadis et al., 2008; Mitsiadis et al., 2010).

6.2.4 A role for Notch/hypoxia signalling in the 22q11DS phenotype of congenital scoliosis?

RA, Notch, Wnt and FGF-signalling and expression of *Ripply* and *Tbx6* genes all are part of the complex genetic network necessary for the "wave and clockfront" mechanism of somitogenesis, whereby the axial skeleton is derived from the presomitic mesoderm (PSM) (Pourquie, 2011; Saga, 2012). Recently, deleterious dominant haploinsufficient but weakly penetrant mutations in NOTCH pathway genes *HES7* and *MESP2* have been identified for congenital scoliosis, which is defined as a lateral curve of the spine exceeding ten degrees and caused by structural vertebral abnormalities. Haploinsufficiency of *Hes7* was found to cause a similar phenotype. *Mesp2*$^{+/-}$ mice did not manifest vertebral anomalies unless they were subjected to a further environmental insult; namely hypoxic conditions in utero, which induced an increased severity and penetrance of vertebral defects compared to wild-type siblings. Hypoxic treatment also increased the severity and penetrance of vertebral malformation in both *Hes7*$^{+/-}$ mice and *Dll1* and *Notch1* heterozygotes. The molecular mechanism behind this interaction of the Notch and hypoxia pathways appeared to be temporary down-regulation of FGF-WNT-signalling in the PSM and disruption of cyclical Notch signalling leading to aberrant somitogenesis (Sparrow et al., 2012)(Fig6.3).

In addition to this mechanism, there are more than fifty mouse mutants with disrupted somitogenesis and vertebral malformations, including many of the members of the Notch

pathway family, *Raldh2*, *Cyp26a1* and *Cyp26b1*, *Foxc1* and *Foxc2*, *Ripply* and *Tbx*-family genes (Sparrow et al., 2011). Interestingly, at least 10-20% of 22q11DS patients also manifest a congenital scoliosis phenotype (Brunet et al., 2006; Hay, 2007; Morava et al., 2002; Ryan et al., 1997; Swillen et al., 2000), raising the question of whether *TBX1* haploinsufficiency plus additional environmental factors such as in utero hypoxia or altered maternal RA levels might play a role in this phenotype (Fig.6.3). *Tbx1* mice have not been reported with vertebral malformations, but *Tbx1* is expressed during somitogenesis and in the vertebral column. It might be interesting to investigate the effect of hypoxia upon vertebral development in *Tbx1*$^{+/-}$ embryos, particularly given that *Fgf8* is known to be a key down-stream target of Tbx1 in other systems. In addition, compound mutant mice deleted for *Tbx1* and RA-pathway alleles could be investigated for vertebral phenotypes, given the role of RA in somitogenesis and a reported vertebral phenotype for potential *Tbx1* down-stream targets within the RA-pathway.

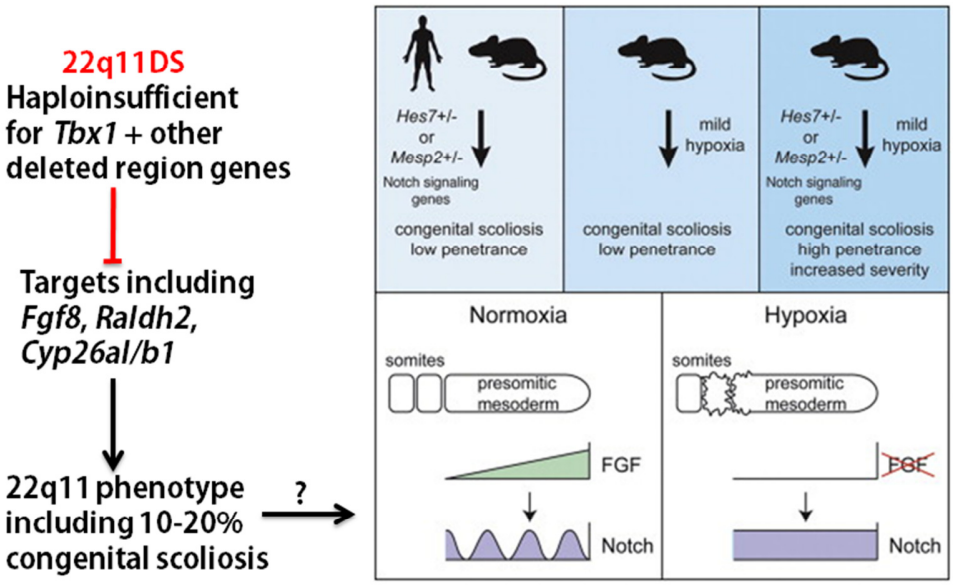

Figure 6.3 Mechanism for congenital scoliosis

Congenital scoliosis, a lateral curvature of the spine caused by vertebral defects, occurs in approximately 1 in 1,000 live births. Haploinsufficiency of Notch signalling pathway genes and the 22q11DS region in humans can cause this congenital abnormality. In a mouse model, the combination of the Notch genetic risk factor with an environmental condition (short-term gestational hypoxia) significantly increases the penetrance and severity of vertebral defects. Hypoxia disrupts FGF signaling, leading to a temporary failure of embryonic somitogenesis. These

results potentially provide a mechanism for the genesis of a host of common sporadic congenital abnormalities through gene-environment interaction Adapted from (Sparrow et al., 2012).

6.3 Regeneration

Tbx1, Notch and RA signalling have all been implicated in regenerative processes. The *Notch1* receptor is expressed on cardiac stem cells located in cardiac niches and Notch activity is also required post-natally for cardiomyogenesis. In the zebrafish Notch-signalling is activated in cardiomyocytes, during the repair of ventricular apex amputation. Different studies have shown positive and negative effects of Notch overexpression upon cardiac cell fate choices. Overexpression of NICD inhibits ESC cardiac differentiation, but expression in the right time and place in mesodermal cells can promote a cardiac fate via BMP/WNT activation/inhibition respectively. Adult *c-kit*-positive cardiac progenitor cells express NOTCH-receptors and are surrounded by supporting niche cells which express JAG1-ligand. NOTCH signalling then drives proliferation and expression of *Nkx2.5*, thus allowing a brief amplifying pool of early myocytes whilst also promoting commitment to a myocyte fate. In addition, a NOTCH-activated epicardial cell population with inherent fibrosis-repair potential which are increased after injury has recently been identified in the mouse heart [reviewed in (Gude and Sussman, 2012)]. The adult zebrafish is able to regenerate *gata4*-positive cardiac ventricular muscle from remaining cardiomyocytes following a range of different injuries including surgical resection, cryoinjury and conditional diphtheria-toxin mediated cell death. This process involves increased retinoic acid synthesis by up-regulation of *raldh2* in first the epicardium, and then the endocardium. Similar regenerative ability has been observed in neonatal mice, but not in adult mice and understanding these different mechanisms between species could lead to novel therapies for human cardiac disease [reviewed in(Choi and Poss, 2012)].

Cyp26a1 has also been associated with a stem cell population albeit not in cardiovascular development. Rather, posterior embryonic development of the zebrafish depends upon a *brachyury/wnt* autoregulatory loop in mesodermal progenitor cells. This feedback mechanism is normally protected from excess RA, thus preventing caudal truncation, by *brachyury* activation of *cyp26a1* (Martin and Kimelman, 2010). It is tempting to speculate

that similar mechanisms might exist for cardiac progenitors with regulation of RA levels via *raldh/cyp26* genes necessary for balance between proliferation and differentiation. Finally, as discussed above *Tbx1* is required to maintain proliferation of a number of cell types including cardiac progenitor cells during development. SMAD-mediated BMP-signalling, which can in turn be negatively regulated by TBX1 at the protein level, may act as a negative modulator of SHF proliferation (Chen et al., 2009; Fulcoli et al., 2009; Prall et al., 2007; Xu et al., 2004). Very recently, a role for *Tbx1* has been identified in stem cell biology, using hair follicle stem cells (HFSCs) as a model system. *Tbx1* is required for stem-cell self-renewal. Progressive depletion of HFSCs and stem cell niche cells by successive rounds of depilation in skin epithelium of *Tbx1* conditionally-ablated mice led to a loss of more 70% of HFSC cells and thinning of the hair coat compared to wild type. The mechanism involved in regulating the switch between HFSC quiescence and proliferation appears to involve fine-tuning the response to BMP signalling, where *Tbx1* acts to inhibit the BMP-signalling pathway. TBX1 functions in the replenishment of HF-SCs during tissue regeneration diminished stem cell self-renewal, coupled with enhanced sensitization to intrinsic BMP

That *Tbx1* and so many of its major down-stream target pathways have a potential role in tissue renewal is intriguing. However, it remains to be determined if this capacity is mostly restricted to the maintenance of embryonic progenitors or whether this function of *Tbx1* could extend to adult cardiac tissues, since to date no role for *Tbx1* has been reported in adult cardiac function.

6.4 Future Directions

The work in this thesis has shown that both *her6* and *Cyp26b1* are likely to interact with *Tbx1* during cardiovascular development. *Her6* has been shown part of the *tbx1* pathway regulating the formation of the PAA during zebrafish development. The *Cyp26*s', in particular *Cyp26b1*, have been determined to be necessary for the development of the tissues affecting in 22q11DS. Moreover, epistasis experiments suggest that *Cyp26b1* and *Tbx1* may interact during cardiovascular development.

However, further experiments could be conducted to refine our understanding of these pathways. It would be useful to be able to confirm the *her6/tbx1* interaction in the mammalian system, Given this issues with phenotype penetrance and expressivity depending on genetic background, this might not be straightforward. However, a *Tbx1* knock-in null allele expressing *Hes1* in the *Tbx1* domain could be made, as previously described for *Fgf8* (Vitelli et al., 2006). This would simultaneously inactivate *Tbx1* and drive *Hes1*-cDNA expression by *Tbx1* regulatory elements. If no rescue of the *Tbx1* null phenotype was observed in these animals, then again, analogous to experiments for *Tbx1* and *Fgf8*, *Hes1* could be expressed in the $Tbx1^{neo2/-}$ background. This line has the advantage of expression a small amount of *Tbx1*, whilst fully recapitulating the 22q11DS human phenotype. This would also address the issue of whether *Hes1* and *Tbx1* interact during OFT development as well as PAA formation. Equivalent experimental approaches to those reported here for the PAA, could also be used to investigate the requirement for *her6* and *tbx1* in cardiac embryogenesis in the zebrafish.

As discussed in Chapter 4, ChIP-sequence experiments could be used to identify if *tbx1* is directly regulating *her6*, and to identify common target genes. This technique uses an antibody against the protein of interest to isolate cross-linked DNA-protein complexes from specific tissues. The resulting DNA fragments are then sequenced, using a next generation sequencing platform. This produces a large amount of data regarding potential targets which can be further analysed in a number of ways including statistical significance of enriched regions compared to controls, binding motif algorithms and location of enriched regions in relation to genomic features such as transcriptional start sites [reviewed in (Park, 2009)]. Once potential target sequence have been identified, further analyses could be performed, as have been used previously [e.g. (Chen et al., 2012a)]. These would include analysis of potential targets sequences for binding elements such as N and T-box binding sites and other possible biding motifs of interest. Luciferase assays could determine if *Tbx1/Hes1* bound to these sites *in vitro*. Furthermore, standard and quantitative ChIP (q-ChIP) could then be used to assay endogenous *Tbx1/Hes1* binding to these regions. Co-immunopreciptation and qChIP could also help to identify any transcriptional modifying complexes recruited to these regions, such as chromatin modifying factors BAF60A/BAF60C.

ChIP-based approaches could assist in assessing whether *Tbx1* directly regulates the activity of all or any of the *Cyp26* genes as suggested by reduced RTQ-PCR read-out for *Cyp26a1* in *Tbx1*-expression assays with knocked-down *Baf60a* expression (Chen et al., 2012a). Similarly, it could provide data on possible common genetic pathways affected down-stream of *Tbx1* and the *Cyp26* genes, although this is unlikely to be via dual-regulation of target transcription as CYP26 proteins are RA degrading enzymes, not transcription factors.

Given the recent identification of "off-DNA" regulatory activity for *Tbx1* at the protein-protein level, a proteomics screens could be an effective way to further characterize *Tbx1* functions during development. Affinity purification mass spectrophotometry has been used for this purpose and is based upon biochemical purification of proteins from cell/tissue extracts. Chemical cross-linking approaches allow the identification of even weak and transient interactions. Quantitative interaction proteomics allows the identification of differentially abundant proteins from two different samples i,e wild-type versus *Tbx1* null samples. Again, data sets have to be statistically analysed to determine the most likely target interactions. These must then be validated in various ways, including confirmation of binding with mammalian two-hybrid assays, co-immunopreciptation and in vivo binding or fluorescence resonance energy transfer (FRET)] [reviewed in (Sardiu and Washburn, 2011)].

Finally, the role of *Tbx1* in the post-natal heart might be further investigated. Preliminary expression experiments in this laboratory suggest *Tbx1* may continue to be expressed in some cardiac tissues in late development/early post-natal stages. Given the developmental role of *Tbx1* to promote cardiac progenitor proliferation it is tempting to suggest this expression might reflect adult cells with regenerative capacities. A first step to investigating this possibility might be to fully confirm and categorize these sites of expression along with expression of cardiac stem cell markers such as C-KIT, SCA-1, SSEA-1, CD34, CD29, ISL1, NKX2.5 and GATA4. Depending upon the results from such an expression analysis, roles for *Tbx1* post-natally could be initially assessed by conditional spatiotemporal deletion of *Tbx1* using inducible Cre-drivers in conjunction with the *Tbx1*-floxed allele in normal and infarcted hearts.

6.5 Conclusion

In summary, I have used a variety of functional *in vivo* approaches including genetic knock-down and rescue and drug-based protein-inhibition studies to further increase our understanding of the *Tbx1* down-stream cascade. In particular, this work has refined our knowledge of the interactions between *Tbx1* and the Notch and RA-signalling pathways, such that it is now possible to place *her6/Hes1* and *Cyp26b1* as functionally down-stream of *Tbx1*.

References

.

Aanhaanen,W.T.J., Boukens,B.J.D., Sizarov,A., Wakker,V., de Gier-de Vries,C., van Ginneken,A.C., Moorman,A.F.M., Coronel,R., and Christoffels,V.M. (2011). Defective Tbx2-dependent patterning of the atrioventricular canal myocardium causes accessory pathway formation in mice. *J Clin Invest* **121,** 534-544.

Aanhaanen,W.T.J., Brons,J.F., Dominguez,J.N., Rana,M.S., Norden,J., Airik,R., Wakker,V., de Gier-de Vries,C., Brown,N.A., Kispert,A. et al. (2009). The Tbx2+ Primary Myocardium of the Atrioventricular Canal Forms the Atrioventricular Node and the Base of the Left Ventricle. *Circ Res* **104,** 1267-1274.

Abu-Abed,S., Dolle,P., Metzger,D., Beckett,B., Chambon,P., and Petkovich,M. (2001). The retinoic acid-metabolizing enzyme, CYP26A1, is essential for normal hindbrain patterning, vertebral identity, and development of posterior structures. *Genes Dev.* **15,** 226-240.

Abu-Abed,S.S., Beckett,B.R., Chiba,H., Chithalen,J.V., Jones,G., Metzger,D., Chambon,P., and Petkovich,M. (1998). Mouse P450RAI (CYP26) Expression and Retinoic Acid-inducible Retinoic Acid Metabolism in F9 Cells Are Regulated by Retinoic Acid Receptor gamma and Retinoid X Receptor alpha. *J. Biol. Chem.* **273,** 2409-2415.

Abu-Issa,R., Smyth,G., Smoak,I., Yamamura,K., and Meyers,E.N. (2002). Fgf8 is required for pharyngeal arch and cardiovascular development in the mouse. *Development* **129,** 4613-4625.

Aggarwal,V.S., Liao,J., Bondarev,A., Schimmang,T., Lewandoski,M., Locker,J., Shanske,A., Campione,M., and Morrow,B.E. (2006). Dissection of Tbx1 and Fgf interactions in mouse models of 22q11DS suggests functional redundancy. *Hum. Mol. Genet.* **15,** 3219-3228.

Ai,D., Liu,W., Ma,L., Dong,F., Lu,M.F., Wang,D., Verzi,M.P., Cai,C., Gage,P.J., and Evans,S. (2006). Pitx2 regulates cardiac left-right asymmetry by patterning second cardiac lineage-derived myocardium. *Developmental Biology* **296,** 437-449.

Akimoto,M., Kameda,Y., Arai,Y., Miura,M., Nishimaki,T., Takeda,A., and Uchinuma.E. (2010). Hes1 is required for the development of craniofacial structures derived from ectomesenchymal neural crest cells. *Journal of Craniofacial Surgery* **5,** 1443-1449.

Andersen,P., Uosaki,H., Shenje,L.T., and Kwon,C. (2012). Non-canonical Notch signaling: emerging role and mechanism. *Trends in Cell Biology* **22,** 257-265.

Andersson,E.R., Sandberg,R., and Lendahl,U. (2011). Notch signaling: simplicity in design, versatility in function. *Development* **138,** 3593-3612.

Androutsellis-Theotokis,A., Leker,R.R., Soldner,F., Hoeppner,D.J., Ravin,R., Poser,S.W., Rueger,M.A., Bae,S.K., Kittappa,R., and McKay,R.D.G. (2006). Notch signalling regulates stem cell numbers in vitro and in vivo. *Nature* **442,** 823-826.

Ang,H.L. and Duester,G. (1999). Stimulation of premature retinoic acid synthesis in Xenopus embryos following premature expression of aldehyde dehydrogenase ALDH1. *Eur J Biochem* **260,** 227-234.

Arinami,T. (2006). Analyses of the associations between the genes of 22q11 deletion syndrome and schizophrenia. *Journal of Human Genetics* **51,** 1037-1045.

Arnold,J.S., Braunstein,E.M., Ohyama,T., Groves,A.K., Adams,J.C., Brown,M.C., and Morrow,B.E. (2006a). Tissue specific roles of Tbx1 in the development of the outer, middle and inner ear, defective in 22q11DS patients. *Hum. Mol. Genet.* ddl084.

Arnold,J.S., Werling,U., Braunstein,E.M., Liao,J., Nowotschin,S., Edelmann,W., Hebert,J.M., and Morrow,B.E. (2006b). Inactivation of Tbx1 in the pharyngeal endoderm results in 22q11DS malformations. *Development* **133,** 977-987.

Arsenian,S., Weinhold,B., Oelgeschlager,M., Ruther,U., and Nordheim,A. (1998). Serum response factor is essential for mesoderm formation during mouse embryogenesis. *EMBO J* **17,** 6289-6299.

Ataliotis,P., Ivins,S., Mohun,T.J., and Scambler,P.J. (2005). XTbx1 is a transcriptional activator involved in head and pharyngeal arch development in Xenopus laevis. *Dev. Dyn.* **232,** 979-991.

Aubin-Houzelstein,G., Djian-Zaouche,J., Bernex,F., Gadin,S., Delmas,V., Larue,L., and Panthier,J.J. (2008). Melanoblasts' Proper Location and Timed Differentiation Depend on Notch/RBP-J Signaling in Postnatal Hair Follicles. *J Invest Dermatol* **128,** 2686-2695.

Bachiller,D., Klingensmith,J., Shneyder,N., Tran,U., Anderson,R., Rossant,J., and De Robertis,E.M. (2003). The role of chordin/Bmp signals in mammalian pharyngeal development and DiGeorge syndrome. *Development* **130,** 3567-3578.

Baek,J.H., Hatakeyama,J., Sakamoto,S., Ohtsuka,T., and Kageyama,R. (2006). Persistent and high levels of Hes1 expression regulate boundary formation in the developing central nervous system. *Development* **133,** 2467-2476.

Bajolle,F., Zaffran,S., Kelly,R.G., Hadchouel,J., Bonnet,D., Brown,N.A., and Buckingham,M. (2006). Rotation of the Myocardial Wall of the Outflow Tract Is Implicated in the Normal Positioning of the Great Arteries. *Circ Res* 01.

Bajolle,F., Zaffran,S., Meilhac,S.M., Dandonneau,M., Chang,T., Kelly,R.G., and Buckingham,M.E. (2008). Myocardium at the base of the aorta and pulmonary trunk is prefigured in the outflow tract of the heart and in subdomains of the second heart field. *Developmental Biology* **313,** 25-34.

Bakker,M.L., Boukens,B.J., Mommersteeg,M.T.M., Brons,J.F., Wakker,V., Moorman,A.F.M., and Christoffels,V.M. (2008). Transcription Factor Tbx3 Is Required for the Specification of the Atrioventricular Conduction System. *Circ Res* **102,** 1340-1349.

Bamshad,M., Lin,R.C., Law,D.J., Watkins,W.S., Krakowiak,P.A., Moore,M.E., Franceschini,P., Lala,R., Holmes,L.B., Gebuhr,T.C. et al. (1997). Mutations in human TBX3 alter limb, apocrine and genital development in ulnar-mammary syndrome. *Nat Genet* **16,** 311-315.

Baron,J.M., Heise,R., Blaner,W.S., Neis,M., Joussen,S., Dreuw,A., Marquardt,Y., Saurat,J.H., Merk,H.F., Bickers,D.R. et al. (2005). Retinoic Acid and its 4-Oxo Metabolites are Functionally Active in Human Skin Cells In Vitro. *J Investig Dermatol* **125,** 143-153.

Basson,C.T., Bachinsky,D.R., Lin,R.C., Levi,T., Elkins,J.A., Soults,J., Grayzel,D., Kroumpouzou,E., Traill,T.A., Leblanc-Straceski,J. et al. (1997). Mutations in human cause limb and cardiac malformation in Holt-Oram syndrome. *Nat Genet* **15,** 30-35.

Batourina,E., Gim,S., Bello,N., Shy,M., Clagett-Dame,M., Srinivas,S., Costantini,F., and Mendelsohn,C. (2001). Vitamin A controls epithelial/mesenchymal interactions through *Ret* expression. *Nat. Genet.* **27,** 74-78.

Bayha,E., Jorgensen,M.C., Serup,P., and Grapin-Botton,A. (2009). Retinoic Acid Signaling Organizes Endodermal Organ Specification along the Entire Antero-Posterior Axis. *PLoS ONE* **4,** e5845.

Bedell,V.M., Wang,Y., Campbell,J.M., Poshusta,T.L., Starker,C.G., Krug II,R.G., Tan,W., Penheiter,S.G., Ma,A.C., Leung,A.Y.H. et al. (2012). In vivo genome editing using a high-efficiency TALEN system. *Nature* **advance online publication**.

Beffagna,G., Cecchetto,A., Dal Bianco,L., Lorenzon,A., Angelini,A., Padalino,M., Vida,V., Bhattacharya,S., Stellin,G., Rampazzo,A. et al. (2012). R25C mutation in the NKX2.5 gene in Italian patients affected with non-syndromic and syndromic congenital heart disease. *Journal of Cardiovascular Medicine* **Publish Ahead of Print**.

Begemann,G., Schilling,T.F., Rauch,G.J., Geisler,R., and Ingham,P.W. (2001). The zebrafish neckless mutation reveals a requirement for raldh2 in mesodermal signals that pattern the hindbrain. *Development* **128,** 3081-3094.

Bel-Vialar,S., Core,N., Terranova,R., Goudot,V., Boned,A., and Djabali,M. (2000). Altered Retinoic Acid Sensitivity and Temporal Expression of Hox Genes in Polycomb-M33-Deficient Mice. *Developmental Biology* **224,** 238-249.

Bertrand,J.Y., Cisson,J.L., Stachura,D.L., and Traver,D. (2010). Notch signaling distinguishes 2 waves of definitive hematopoiesis in the zebrafish embryo. *Blood* **115,** 2777-2783.

Bessho,Y., Sakata,R., Komatsu,S., Shiota,K., Yamada,S., and Kageyama,R. (2001). Dynamic expression and essential functions of Hes7 in somite segmentation. *Genes Dev.* **15,** 2642-2647.

Biben,C., Weber,R., Kesteven,S., Stanley,E., McDonald,L., Elliott,D.A., Barnett,L., Köentgen,F., Robb,L., Feneley,M. et al. (2000). Cardiac Septal and Valvular Dysmorphogenesis in Mice Heterozygous for Mutations in the Homeobox Gene Nkx2-5. *Circ Res* **87,** 888-895.

Bjerknes,M., Khandanpour,C., Moroy,T., Fujiyama,T., Hoshino,M., Klisch,T.J., Ding,Q., Gan,L., Wang,J., Martin G. et al. (2012). Origin of the brush cell lineage in the mouse intestinal epithelium. *Developmental Biology* **362,** 194-218.

Blanco,R. and Gerhardt,H. (2012). VEGF and Notch in Tip and Stalk Cell Selection. *Cold Spring Harbor Perspectives in Medicine*.

Blentic,A., Gale,E., and Maden,M. (2003). Retinoic acid signalling centres in the avian embryo identified by sites of expression of synthesising and catabolising enzymes. *Dev. Dyn.* **227,** 114-127.

Bockman,D., Redmond,M., and Kirby,M. (1989). Alteration of early vascular development after ablation of cranial neural crest. *Anatomical Record* **225,** 209-217.

Bockman,D., Redmond,M., Waldo,K., Davis,H., and Kirby,M. (1987). Effect of neural crest ablation on development of the heart and arch arteries in the chick. *American Journal of Anatomy* **180,** 332-341.

Bohnsack,B.L., Lai,L., Dolle,P., and Hirschi,K.K. (2004). Signaling hierarchy downstream of retinoic acid that independently regulates vascular remodeling and endothelial cell proliferation. *Genes Dev.* **18,** 1345-1358.

Bok,J., Raft,S., Kong,K.A., Koo,S.K., Drager,U.C., and Wu,D.K. (2011). Transient retinoic acid signaling confers anterior-posterior polarity to the inner ear. *PNAS* **108,** 161-166.

Boogerd,C.J.J., Moorman,A.F.M., and Barnett,P. (2009). Protein interactions at the heart of cardiac chamber formation. *Annals of Anatomy - Anatomischer Anzeiger* **191,** 505-517.

Borggrefe,T. and Liefke,R. (2012). Fine-tuning of the intracellular canonical Notch signaling pathway. *Cell Cycle* **11,** 264-276.

Bothe,I., Tenin,G., Oseni,A., and Dietrich,S. (2011). Dynamic control of head mesoderm patterning. *Development* **138,** 2807-2821.

Bradshaw,L., Chaudhry,B., Hildreth,V., Webb,S., and Henderson,D.J. (2009). Dual role for neural crest cells during outflow tract septation in the neural crest-deficient mutant Splotch2H. *Journal of Anatomy* **214,** 245-257.

Brand,M., Beuchle,D., Endres,F., Haffter,P., Hammerschmidt,M., Mullins,M., Schulte-Merker,S., Nusslein-Volhard,C., Luck,R., Swchartz,K.J. et al. (1995). Keeping and raising zebrafish (Danio rerio) in Tubingen. *Zebrafish Science Monitor* **3,** 2-7.

Braunstein,E., Monks,D., Aggarwal,V., Arnold,J., and Morrow,B. (2009). Tbx1 and Brn4 regulate retinoic acid metabolic genes during cochlear morphogenesis. *BMC Developmental Biology* **9,** 31.

Braunstein,E., Crenshaw III,E.B., Morrow,B., and Adams,J. (2008). Cooperative Function of Tbx1 and Brn4 in the Periotic Mesenchyme is Necessary for Cochlea Formation. *JARO* **9,** 33-43.

Braybrook,C., Doudney,K., Marcano,A.C., Arnason,A., Bjornsson,A., Patton,M.A., Goodfellow,P.J., Moore,G.E., and Stanier,P. (2001). The T-box transcription factor gene TBX22 is mutated in X-linked cleft palate and ankyloglossia. *Nat Genet* **29,** 179-183.

Brend,T. and Holley,S.A. (2009a). Expression of the oscillating gene her1 is directly regulated by hairy/enhancer of split, T-box, and suppressor of hairless proteins in the zebrafish segmentation clock. *Developmental Dynamics* **238,** 2745-2759.

Brend,T. and Holley,S.A. (2009b). Zebrafish Whole Mount High-Resolution Double Fluorescent In Situ Hybridization. *J Vis Exp* e1229.

Broom,E.R., Gilthorpe,J.D., Butts,T., Campo-Paysaa,F., and Wingate,R.J.T. (2012). The roof plate boundary is a bi-directional organiser of dorsal neural tube and choroid plexus development. *Development* **139,** 4261-4270.

Brown,C.B., Wenning,J.M., Lu,M.M., Epstein,D.J., Meyers,E.N., and Epstein,J.A. (2004). Cre-mediated excision of Fgf8 in the Tbx1 expression domain reveals a critical role for Fgf8 in cardiovascular development in the mouse. *Dev. Biol.* **267,** 190-202.

Brown,L.A., Rodaway,A.R.F., Schilling,T.F., Jowett,T., Ingham,P.W., Patient,R.K., and Sharrocks,A.D. (2000). Insights into early vasculogenesis revealed by expression of the ETS-domain transcription factor Fli-1 in wild-type and mutant zebrafish embryos. *Mechanisms of Development* **90,** 237-252.

Bruneau,B.G., Nemer,G., Schmitt,J.P., Charron,F., Robitaille,L., Caron,S., Conner,D.A., Gessler,M., Nemer,M., Seidman,C.E. et al. (2001). A Murine Model of Holt-Oram Syndrome Defines Roles of the T-Box Transcription Factor Tbx5 in Cardiogenesis and Disease. *Cell* **106,** 709-721.

Brunet,A., Gabau,E., Perich,R.M., Valdesoiro,L., Brun,C., Caballin,M.R., and Guitart,M. (2006). Microdeletion and microduplication 22q11.2 screening in 295 patients with clinical features of DiGeorge/Velocardiofacial syndrome. *American Journal of Medical Genetics Part A* **140A,** 2426-2432.

Buckingham,M., Meilhac,S., and Zaffran,S. (2005). Building the Mammalian Heart from Two Sources of Myocardial Cells. *Nat Rev Genet* **6,** 826-837.

Budhu,A.S. and Noy,N. (2002). Direct Channeling of Retinoic Acid between Cellular Retinoic Acid-Binding Protein II and Retinoic Acid Receptor Sensitizes Mammary Carcinoma Cells to Retinoic Acid-Induced Growth Arrest. *Mol. Cell. Biol.* **22,** 2632-2641.

Byrd,N.A. and Meyers,E.N. (2005). Loss of Gbx2 results in neural crest cell patterning and pharyngeal arch artery defects in the mouse embryo. *Developmental Biology* **284,** 233-245.

Cai,C.L., Liang,X., Shi,Y., Chu,P.H., Pfaff,S.L., Chen,J., and Evans,S. (2003). Isl1 Identifies a Cardiac Progenitor Population that Proliferates Prior to Differentiation and Contributes a Majority of Cells to the Heart. *Developmental Cell* **5,** 877-889.

Cai,C.L., Zhou,W., Yang,L., Bu,L., Qyang,Y., Zhang,X., Li,X., Rosenfeld,M.G., Chen,J., and Evans,S. (2005). T-box genes coordinate regional rates of proliferation and regional specification during cardiogenesis. *Development* dev.

Calmont,A.l., Ivins,S., van Bueren,K.L., Papangeli,I., Kyriakopoulou,V., Andrews,W.D., Martin,J.F., Moon,A.M., Illingworth,E.A., Basson,M.A. et al. (2009). Tbx1 controls cardiac neural crest cell migration during arch artery development by regulating Gbx2 expression in the pharyngeal ectoderm. *Development* **136,** 3173-3183.

Cao,H., Florez,S., Amen,M., Huynh,T., Skobe,Z., Baldini,A., and Amendt,B.A. (2010). Tbx1 regulates progenitor cell proliferation in the dental epithelium by modulating Pitx2 activation of p21. *Developmental Biology* **347,** 289-300.

Carreira,S., Dexter,T.J., Yavuzer,U., Easty,D.J., and Goding,C.R. (1998). Brachyury-Related Transcription Factor Tbx2 and Repression of the Melanocyte-Specific TRP-1 Promoter. *Mol. Cell. Biol.* **18,** 5099-5108.

Catón,J., Luder,H.U., Zoupa,M., Bradman,M., Bluteau,G., Tucker,A.S., Klein,O., and Mitsiadis,T.A. (2009). Enamel-free teeth: Tbx1 deletion affects amelogenesis in rodent incisors. *Developmental Biology* **328,** 493-505.

Cau,E., Gradwohl,G., Casarosa,S., Kageyama,R., and Guillemot,F. (2000). Hes genes regulate sequential stages of neurogenesis in the olfactory epithelium. *Development* **127,** 2323-2332.

Chambers,D., Wilson,L., Maden,M., and Lumsden,A. (2007). RALDH-independent generation of retinoic acid during vertebrate embryogenesis by CYP1B1. *Development* dev.

Chan,W.Y., Cheung,C.S., Yung,K.M., and Copp,A.J. (2004). Cardiac neural crest of the mouse embryo: axial level of origin, migratory pathway and cell autonomy of the splotch (Sp2H) mutant effect. *Development* **131,** 3367-3379.

Chang,A.C., Fu,Y., Garside,V.C., Niessen,K., Chang,L., Fuller,M., Setiadi,A., Smrz,J., Kyle,A., Minchinton,A. et al. (2011). Notch Initiates the Endothelial-to-Mesenchymal Transition in the Atrioventricular Canal through Autocrine Activation of Soluble Guanylyl Cyclase. *Developmental Cell* **21,** 288-300.

Chang,C.P., Neilson,J.R., Bayle,J.H., Gestwicki,J.E., Kuo,A., Stankunas,K., Graef,I.A., and Crabtree,G.R. (2004). A Field of Myocardial-Endocardial NFAT Signaling Underlies Heart Valve Morphogenesis. *Cell* **118,** 649-663.

Chapman,D.L., Garvey,N., Hancock,S., Alexiou,M., Agulnik,S.I., Gibson-Brown,J.J., Cebra-Thomas,J., Bollag,R.J., Silver,L.M., and Papaioannou,V.E. (1996). Expression of the T-box family genes, Tbx1-Tbx5, during early mouse development. *Dev. Dyn.* **206,** 379-390.

Chatzi,C., Brade,T., and Duester,G. (2011). Retinoic Acid Functions as a Key GABAergic Differentiation Signal in the Basal Ganglia. *PLoS Biol* **9,** e1000609.

Chen,L., Fulcoli,F.G., Ferrentino,R., Martucciello,S., Illingworth,E.A., and Baldini,A. (2012a). Transcriptional Control in Cardiac Progenitors: Tbx1 Interacts with the BAF Chromatin Remodeling Complex and Regulates *Wnt5a*. *PLoS Genet* **8,** e1002571.

Chen,L., Fulcoli,F.G., Tang,S., and Baldini,A. (2009). Tbx1 Regulates Proliferation and Differentiation of Multipotent Heart Progenitors. *Circulation Research* **105,** 842-851.

Chen,L., Mupo,A., Huynh,T., Cioffi,S., Woods,M., Jin,C., McKeehan,W., Thompson-Snipes,L., Baldini,A., and Illingworth,E. (2010). Tbx1 regulates Vegfr3 and is required for lymphatic vessel development. *The Journal of Cell Biology* **189,** 417-424.

Chen,T., Heller,E., Beronja,S., Oshimori,N., Stokes,N., and Fuchs,E. (2012b). An RNA interference screen uncovers a new molecule in stem cell self-renewal and long-term regeneration. *Nature* **485,** 104-108.

Cheng,Y.C., Cheung,M., Abu-Elmagd,M.M., Orme,A., and Scotting,P.J. (2000). Chick Sox10, a transcription factor expressed in both early neural crest cells and central nervous system. *Developmental Brain Research* **121,** 233-241.

Chithalen,J.V., Luu,L., Petkovich,M., and Jones,G. (2002). HPLC-MS/MS analysis of the products generated from all-trans-retinoic acid using recombinant human CYP26A. *Journal of Lipid Research* **43,** 1133-1142.

Choi,M. and Klingensmith,J. (2009). *Chordin* Is a Modifier of *Tbx1* for the Craniofacial Malformations of 22q11 Deletion Syndrome Phenotypes in Mouse. *PLoS Genet* **5,** e1000395.

Choi,W.Y. and Poss,K.D. (2012). Chapter eleven - Cardiac Regeneration. In *Current Topics in Developmental Biology*
Heart Development. (ed. Benoit,G.B.), pp. 319-344. Academic Press.

Christoffels,V.M., Hoogaars,W.M.H., Tessari,A., Clout,D.E.W., Moorman,A.F.M., and Campione,M. (2004). T-box transcription factor Tbx2 represses differentiation and formation of the cardiac chambers. *Dev. Dyn.* **229,** 763-770.

Christoffels,V.M., Mommersteeg,M.T.M., Trowe,M.O., Prall,O.W.J., de Gier-de Vries,C., Soufan,A.T., Bussen,M., Schuster-Gossler,K., Harvey,R.P., Moorman,A.F.M. et al. (2006). Formation of the Venous Pole of the Heart From an Nkx2-5-Negative Precursor Population Requires Tbx18. *Circ Res* **98,** 1555-1563.

Chrysostomou,E., Gale,J.E., and Daudet,N. (2012). Delta-like 1 and lateral inhibition during hair cell formation in the chicken inner ear: evidence against cis-inhibition. *Development* **139,** 3764-3774.

Conley,M., Beckwith,J., Mancer JFK, and Tenckhoff,L. (1979). The spectrum of the DiGeorge syndrome. *The Journal of Pediatrics* **94,** 883-890.

Conlon,F.L., Sedgwick,S.G., Weston,K.M., and Smith,J.C. (1996). Inhibition of Xbra transcription activation causes defects in mesodermal patterning and reveals autoregulation of Xbra in dorsal mesoderm. *Development* **122,** 2427-2435.

Conlon,F.L., Fairclough,L., Price,B.M.J., Casey,E.S., and Smith,J.C. (2001). Determinants of T box protein specificity. *Development* **128,** 3749-3758.

Conti,E., Grifone,N., Sarkozy,A., Tandoi,C., Marino,B., Digilio,M.C., Mingarelli,R., Pizzuti,A., and Dallapiccola,B. (2003). DiGeorge subtypes of nonsyndromic conotruncal defects: evidence against a major role of TBX1 Gene. *Eur. J. Hum. Genet.* **11,** 349-351.

Conway,S.J., Henderson,D.J., and Copp,A.J. (1997). Pax3 is required for cardiac neural crest migration in the mouse: evidence from the splotch (Sp2H) mutant. *Development* **124,** 505-514.

Cordell,H.J. (2002). Epistasis: what it means, what it doesn't mean, and statistical methods to detect it in humans. *Hum. Mol. Genet.* **11,** 2463-2468.

Couly,G., Creuzet,S., Bennaceur,S., Vincent,C., and Le Douarin,N.M. (2002). Interactions between Hox-negative cephalic neural crest cells and the foregut endoderm in patterning the facial skeleton in the vertebrate head. *Development* **129,** 1061-1073.

Crosnier,C., Stamataki,D., and Lewis,J. (2006). Organizing cell renewal in the intestine: stem cells, signals and combinatorial control. *Nat Rev Genet* **7,** 349-359.

Crump,J.G., Maves,L., Lawson,N.D., Weinstein,B.M., and Kimmel,C.B. (2004). An essential role for Fgfs in endodermal pouch formation influences later craniofacial skeletal patterning. *Development* **131,** 5703-5716.

Curado,S., Anderson,R.M., Jungblut,B., Mumm,J., Schroeter,E., and Stainier,D.Y.R. (2007). Conditional targeted cell ablation in zebrafish: A new tool for regeneration studies. *Dev. Dyn.* **236,** 1025-1035.

Danielian,P.S., Muccino,D., Rowitch,D.H., Michael,S.K., and McMahon,A.P. (1998). Modification of gene activity in mouse embryos in utero by a tamoxifen-inducible form of Cre recombinase. *Curr Biol* **8,** 1323-13S2.

Davenport,T.G., Jerome-Majewska,L.A., and Papaioannou,V.E. (2003). Mammary gland, limb and yolk sac defects in mice lacking Tbx3, the gene mutated in human ulnar mammary syndrome. *Development* **130,** 2263-2273.

David,N.B., Saint-Etienne,L., Tsang,M., Schilling,T.F., and Rosa,F.M. (2002). Requirement for endoderm and FGF3 in ventral head skeleton formation. *Development* **129,** 4457-4468.

de la Pompa,J.L. and Epstein,J.A. (2012). Coordinating Tissue Interactions: Notch Signaling in Cardiac Development and Disease. *Developmental Cell* **22,** 244-254.

de Pater,E., Clijsters,L., Marques,S.R., Lin,Y.F., Garavito-Aguilar,Z.V., Yelon,D., and Bakkers,J. (2009). Distinct phases of cardiomyocyte differentiation regulate growth of the zebrafish heart. *Development* **136,** 1633-1641.

de Roos,K., Sonneveld,E., Compaan,B., ten Berge,D., Durston,A.J., and van der Saag,P.T. (1999). Expression of retinoic acid 4-hydroxylase (CYP26) during mouse and Xenopus laevis embryogenesis. *Mechanisms of Development* **82,** 205-211.

Deltour,L., Foglio,M.H., and Duester,G. (1999). Metabolic Deficiencies in Alcohol Dehydrogenase Adh1,Adh3, and Adh4 Null Mutant Mice: Overlapping Roles of Adh1 and Adh4 in Ethanol Clearance and Metabolism of Retinol to Retinoic Acid. *J. Biol. Chem.* **274,** 16796-16801.

Desmaze,C., Prieur,M., Amblard,F., Aïkem,M., LeDeist,F., Demczuk,S., Zucman,J., Plougastel,B., Delattre,O., Croquette,M.-F. et al. (1993). Physical mapping by FISH of the DiGeorge critical region (DGCR): Involvement of the region in familial cases. *Am J Hum Genet.* **53,** 1239-1249.

Dixon,J. and Dixon,M.J. (2004). Genetic background has a major effect on the penetrance and severity of craniofacial defects in mice heterozygous for the gene encoding the nucleolar protein treacle. *Dev. Dyn.* **229,** 907-914.

Dobbs-McAuliffe,B., Zhao,Q., and Linney,E. (2004). Feedback mechanisms regulate retinoic acid production and degradation in the zebrafish embryo. *Mechanisms of Development* **121,** 339-350.

Dolle,P. (2009). Developmental expression of retinoic acid receptors (RARs). *Nuclear Receptor Signaling* **7**.

Domenga,V., Fardoux,P., Lacombe,P., Monet,M., Maciazek,J., Krebs,L.T., Klonjkowski,B., Berrou,E., Mericskay,M., Li,Z. et al. (2004). Notch3 is required for arterial identity and maturation of vascular smooth muscle cells. *Genes Dev.* **18,** 2730-2735.

Dong,F., Sun,X., Liu,W., Ai,D., Klysik,E., Lu,M.F., Hadley,J., Antoni,L., Chen,L., Baldini,A. et al. (2006). Pitx2 promotes development of splanchnic mesoderm-derived branchiomeric muscle. *Development* dev.

Donovan,J., Kordylewska,A., Jan,Y.N., and Utset,M.F. (2002). Tetralogy of Fallot and Other Congenital Heart Defects in Hey2 Mutant Mice. *Current Biology* **12,** 1605-1610.

Dragin,N., Shi,Z., Madan,R., Karp,C.L., Sartor,M.A., Chen,C., Gonzalez,F.J., and Nebert,D.W. (2008). Phenotype of the Cyp1a1/1a2/1b1-/- Triple-Knockout Mouse. *Molecular Pharmacology* **73,** 1844-1856.

Dranse,H.J., Sampaio,A.V., Petkovich,M., and Underhill,T.M. (2011). Genetic deletion of Cyp26b1 negatively impacts limb skeletogenesis by inhibiting chondrogenesis. *Journal of Cell Science* **124,** 2723-2734.

Duester,G. (1996). Involvement of alcohol dehydrogenase, short-chain dehydrogenase/reductase, aldehyde dehydrogenase, and cytochrome P450 in the control of retinoid signaling by activation of retinoic acid synthesis. *Biochemistry.* **35,** 12221-12227.

Duester,G., Mic,F.A., and Molotkov,A. (2003). Cytosolic retinoid dehydrogenases govern ubiquitous metabolism of retinol to retinaldehyde followed by tissue-specific metabolism to retinoic acid. *Chemico-Biological Interactions* **143-144,** 201-210.

Dupe,V., Ghyselinck,N.B., Wendling,O., Chambon,P., and Mark,M. (1999). Key roles of retinoic acid receptors alpha and beta in the patterning of the caudal hindbrain, pharyngeal arches and otocyst in the mouse. *Development* **126,** 5051-5059.

Dupe,V., Matt,N., Garnier,J.M., Chambon,P., Mark,M., and Ghyselinck,N.B. (2003). A newborn lethal defect due to inactivation of retinaldehyde dehydrogenase type 3 is prevented by maternal retinoic acid treatment. *PNAS* **100,** 14036-14041.

Durston,A.J., Timmermans,J.P.M., Hage,W.J., Hendriks,H.F.J., de Vries,N.J., Heideveld,M., and Nieuwkoop,P.D. (1989). Retinoic acid causes an anteroposterior transformation in the developing central nervous system. *Nature* **340,** 140-144.

Dutton,J., Antonellis,A., Carney,T., Rodrigues,F., Pavan,W., Ward,A., and Kelsh,R. (2008). An evolutionarily conserved intronic region controls the spatiotemporal expression of the transcription factor Sox10. *BMC Developmental Biology* **8,** 105.

Edelmann,L., Pandita,R.K., Spiteri,E., Funke,B., Goldberg,R., Palanisamy,N., Chaganti,R.S.K., Magenis,E., Shprintzen,R.J., and Morrow,B.E. (1999). A common molecular basis for rearrangement disorders on chromosome 22q11. *Hum. Mol. Genet.* **8,** 1157-1167.

Edmondson,D.G., Lyons,G.E., Martin,J.F., and Olson,E.N. (1994). Mef2 gene expression marks the cardiac and skeletal muscle lineages during mouse embryogenesis. *Development* **120,** 1251-1263.

Elmabsout,A.A., Kumawat,A., Saenz-Mendez,P., Krivospitskaya,O., Savenstrand,H., Olofsson,P.S., Eriksson,L.A., Strid,A., Valen,G., Torma,H. et al. (2012). Cloning and Functional Studies of a Splice Variant of CYP26B1 Expressed in Vascular Cells. *PLoS ONE* **7,** e36839.

Emanuel,B.S., Budarf,M.L., and Scambler P.J. (1999). The Genetic Basis of Contotruncal Cardiac defects: The Chromosome 22q11 Deletion. In *Heart Development*. (ed. Harvey,R.P. and Rosenthal.N.), pp. 463-478. Academic Press.

Emoto,Y., Wada,H., Okamoto,H., Kudo,A., and Imai,Y. (2005). Retinoic acid-metabolizing enzyme Cyp26a1 is essential for determining territories of hindbrain and spinal cord in zebrafish. *Developmental Biology* **278,** 415-427.

Engert,S., Liao,W.P., Burtscher,I., and Lickert,H. (2009). Sox17-2A-iCre: A knock-in mouse line expressing Cre recombinase in endoderm and vascular endothelial cells. *genesis* **47,** 603-610.

Engleka,K.A., Gitler,A.D., Zhang,M., Zhou,D.D., High,F.A., and Epstein,J.A. (2005). Insertion of Cre into the Pax3 locus creates a new allele of Splotch and identifies unexpected Pax3 derivatives. *Developmental Biology* **280,** 396-406.

Fan,X., Molotkov,A., Manabe,S.I., Donmoyer,C.M., Deltour,L., Foglio,M.H., Cuenca,A.E., Blaner,W.S., Lipton,S.A., and Duester,G. (2003). Targeted Disruption of Aldh1a1 (Raldh1) Provides Evidence for a Complex Mechanism of Retinoic Acid Synthesis in the Developing Retina. *Mol. Cell. Biol.* **23,** 4637-4648.

Fantel,A.G., Shepard,T.H., Newell-Morris,L.L., and Moffett,B.C. (1977). Teratogenic effects of retinoic acid in pigtail monkeys (Macaca nemestrina). I. General features. *Teratology* **15,** 65-71.

Farin,H.F., Bussen,M., Schmidt,M.K., Singh,M.K., Schuster-Gossler,K., and Kispert,A. (2007). Transcriptional Repression by the T-box Proteins Tbx18 and Tbx15 Depends on Groucho Corepressors. *J. Biol. Chem.* **282,** 25748-25759.

Feng,X., Krebs,L.T., and Gridley,T. (2010). Patent ductus arteriosus in mice with smooth muscle-specific Jag1 deletion. *Development* **137,** 4191-4199.

Fischer,A. and Gessler,M. (2007). Delta Notch and then? Protein interactions and proposed modes of repression by Hes and Hey bHLH factors. *Nucl. Acids Res.* **35,** 4583-4596.

Fischer,A., Schumacher,N., Maier,M., Sendtner,M., and Gessler,M. (2004). The Notch target genes Hey1 and Hey2 are required for embryonic vascular development. *Genes & Development* **18,** 901-911.

Fischer,A., Steidl,C., Wagner,T.U., Lang,E., Jakob,P.M., Friedl,P., Knobeloch,K.P., and Gessler,M. (2007). Combined Loss of Hey1 and HeyL Causes Congenital Heart Defects Because of Impaired Epithelial to Mesenchymal Transition. *Circ Res* **100,** 856-863.

Fortini,M.E. (2009). Notch Signaling: The Core Pathway and Its Posttranslational Regulation. *Developmental Cell* **16,** 633-647.

Fouillade,C., Monet-Lepêtre,M., Baron-Menguy,C., and Joutel,A. (2012). Notch signalling in smooth muscle cells during development and disease. *Cardiovascular Research* **95,** 138-146.

Frank,D.U., Fotheringham,L.K., Brewer,J.A., Muglia,L.J., Tristani-Firouzi,M., Capecchi,M.R., and Moon,A.M. (2002). An Fgf8 mouse mutant phenocopies human 22q11 deletion syndrome. *Development* **129,** 4591-4603.

Freeman,R.V. and Otto,C.M. (2005). Spectrum of Calcific Aortic Valve Disease. *Circulation* **111,** 3316-3326.

Fujii,H., Sato,T., Kaneko,S., Gotoh,O., Fujii-Kuriyama,Y., Osawa,K., Kato,S., and Hamada,H. (1997). Metabolic inactivation of retinoic acid by a novel P450 differentially expressed in developing mouse embryos. *EMBO J.* **16,** 4163-4173.

Fukuda,A., Kawaguchi,Y., Furuyama,K., Kodama,S., Horiguchi,M., Kuhara,T., Koizumi,M., Boyer,D.F., Fujimoto,K., Doi,R. et al. (2006). Ectopic pancreas formation in Hes1 -knockout mice reveals plasticity of endodermal progenitors of the gut, bile duct, and pancreas. *J Clin Invest* **116,** 1484-1493.

Fulcoli,F.G., Huynh,T., Scambler,P.J., and Baldini,A. (2009). Tbx1 Regulates the BMP-Smad1 Pathway in a Transcription Independent Manner. *PLoS ONE* **4,** e6049.

Funato,N., Nakamura,M., Richardson,J.A., Srivastava,D., and Yanagisawa,H. (2012). Tbx1 regulates oral epithelial adhesion and palatal development. *Hum. Mol. Genet.*

Funke,B., Epstein,J.A., Kochilas,L.K., Lu,M.M., Pandita,R.K., Liao,J., Bauerndistel,R., Schuler,T., Schorle,H., Brown,M.C. et al. (2001). Mice overexpressing genes from the 22q11 region deleted in velo-cardio-facial syndrome/DiGeorge syndrome have middle and inner ear defects. *Hum. Mol. Genet.* **10,** 2549-2556.

Gaemers,I.C., van Pelt,A.M., van der Saag,P.T., and de Rooij,D.G. (1996). All-trans-4-oxo-retinoic acid: a potent inducer of in vivo proliferation of growth-arrested A spermatogonia in the vitamin A-deficient mouse testis. *Endocrinology* **137,** 479-485.

Gale,E., Prince,V., Lumsden,A., Clarke,J., Holder,N., and Maden,M. (1996). Late effects of retinoic acid on neural crest and aspects of rhombomere. *Development* **122,** 783-793.

Gale,E., Zile,M., and Maden,M. (1999). Hindbrain respecification in the retinoid-deficient quail. *Mechanisms of Development* **89,** 43-54.

Gale,N.W., Dominguez,M.G., Noguera,I., Pan,L., Hughes,V., Valenzuela,D.M., Murphy,A.J., Adams,N.C., Lin,H.C., Holash,J. et al. (2004). Haploinsufficiency of delta-like 4 ligand results in embryonic lethality due to major defects in arterial and vascular development. *Proceedings of the National Academy of Sciences of the United States of America* **101,** 15949-15954.

Garg,V., Yamagishi,C., Hu,T., Kathiriya,I.S., Yamagishi,H., and Srivastava,D. (2001). Tbx1, a DiGeorge syndrome candidate gene, is regulated by sonic hedgehog during pharyngeal arch development. *Dev. Biol.* **235,** 62-73.

Garg,V., Kathiriya,I.S., Barnes,R., Schluterman,M.K., King,I.N., Butler,C.A., Rothrock,C.R., Eapen,R.S., Hirayama-Yamada,K., Joo,K. et al. (2003). GATA4 mutations cause human congenital heart defects and reveal an interaction with TBX5. *Nature* **424,** 443-447.

Garg,V., Muth,A.N., Ransom,J.F., Schluterman,M.K., Barnes,R., King,I.N., Grossfeld,P.D., and Srivastava,D. (2005). Mutations in NOTCH1 cause aortic valve disease. *Nature* **437,** 270-274.

Georgia,S., Soliz,R., Li,M., Zhang,P., and Bhushan,A. (2006). p57 and Hes1 coordinate cell cycle exit with self-renewal of pancreatic progenitors. *Developmental Biology* **298,** 22-31.

Gerhardt,H., Golding,M., Fruttiger,M., Ruhrberg,C., Lundkvist,A., Abramsson,A., Jeltsch,M., Mitchell,C., Alitalo,K., Shima,D. et al. (2003). VEGF guides angiogenic sprouting utilizing endothelial tip cell filopodia. *J. Cell Biol.* **161,** 1163-1177.

Gessler,M., Knobeloch,K.P., Helisch,A., Amann,K., Schumacher,N., Rohde,E., Fischer,A., and Leimeister,C. (2002). Mouse gridlock: No Aortic Coarctation or Deficiency, but Fatal Cardiac Defects in Hey2 -/- Mice. *Current Biology* **12,** 1601-1604.

Ghosh,T.K., Packham,E.A., Bonser,A.J., Robinson,T.E., Cross,S.J., and Brook,J.D. (2001). Characterization of the TBX5 binding site and analysis of mutations that cause Holt-Oram syndrome. *Hum. Mol. Genet.* **10,** 1983-1994.

Ghyselinck,N.B., Wendling,O., Messaddeq,N., Dierich,A., Lampron,C., Decimo,D., Viville,S., Chambon,P., and Mark,M. (1998). Contribution of retinoic acid receptor beta isoforms to the formation of the conotruncal septum of the embryonic heart. *Dev. Biol.* **198,** 303-318.

Girdauskas,E., Schulz,S., Borger,M.A., Mierzwa,M., and Kuntze,T. (2011). Transforming Growth Factor-Beta Receptor Type II Mutation in a Patient With Bicuspid Aortic Valve Disease and Intraoperative Aortic Dissection. *The Annals of Thoracic Surgery* **91,** e70-e71.

Gittenberger-de-Groot,A.C., Bartelings Margot M., Deruiter,M.C., and Poelmann,R.E. (2005). Basics of Cardiac Development for the Understanding of Congenital Heart Malformations. *Pediatr Res* **57,** 169-176.

Goldbarg,S.H., Elmariah,S., Miller,M.A., and Fuster,V. (2007). Insights Into Degenerative Aortic Valve Disease. *Journal of the American College of Cardiology* **50,** 1205-1213.

Gong,W., Gottlieb,S., Collins,J., Blescia,A., Dietz,H., Goldmuntz,E., McDonald-McGinn,D.M., Zackai,E.H., Emanuel,B.S., Driscoll,D.A. et al. (2001). Mutation analysis of TBX1 in non-deleted patients with features of DGS/VCFS or isolated cardiovascular defects. *J. Med. Genet.* **38,** E45.

Goodman,D.S. and Blaner,W.S. (1984). Biosynthesis, absorption, and hepatic metabolism of retinol. In *The Retinoids*. (ed. Sporn,M.B., Roberts,A.B., and Goodman,D.S.), pp. 1-39. Academic Press: New York, NY, USA.

Goudy,S., Law,A., Sanchez,G., Baldwin,H.S., and Brown,C. (2010). Tbx1 is necessary for palatal elongation and elevation. *Mechanisms of Development* **127,** 292-300.

Graham A., Okabe M., and Quinlan R. (2005). The role of the endoderm in the development and evolution of the pharyngeal arches. *Journal of Anatomy* **207,** 479-487.

Graham,A. (2008). Deconstructing the pharyngeal metamere. *J. Exp. Zool.* **310B,** 336-344.

Greene,R.M. and Pisano,M.M. (2005). Recent advances in understanding transforming growth factor beta regulation of orofacial development. *Human & Experimental Toxicology* **24,** 1-12.

Grego-Bessa,J., Luna-Zurita,L., del Monte,G., Bolós,V., Melgar,P., Arandilla,A., Garratt,A.N., Zang,H., Mukouyama,Y.s., Chen,H. et al. (2007). Notch Signaling Is Essential for Ventricular Chamber Development. *Developmental Cell* **12,** 415-429.

Grenier,J., Teillet,M.A.e., Grifone,R.l., Kelly,R.G., and Duprez,D. (2009). Relationship between Neural Crest Cells and Cranial Mesoderm during Head Muscle Development. *PLoS ONE* **4,** e4381.

Greulich,F., Rudat,C., and Kispert,A. (2011). Mechanisms of T-box gene function in the developing heart. *Cardiovascular Research* **91,** 212-222.

Grifone,R. and Kelly,R.G. (2007). Heartening news for head muscle development. *Trends in Genetics* **23,** 365-369.

Guadix,J.A., Ruiz-Villalba,A., Lettice,L., Velecela,V., Munoz-Chapuli,R., Hastie,N.D., Perez-Pomares,J.M., and Martinez-Estrada,O.M. (2011). Wt1 controls retinoic acid signalling in embryonic epicardium through transcriptional activation of Raldh2. *Development* **138,** 1093-1097.

Gude,N. and Sussman,M. (2012). Notch signaling and cardiac repair. *Journal of Molecular and Cellular Cardiology* **52,** 1226-1232.

Guidato,S., Barrett,C., and Guthrie,S. (2003). Patterning of motor neurons by retinoic acid in the chick embryo hindbrain in vitro. *Molecular and Cellular Neuroscience* **23,** 81-95.

Guo,C., Sun,Y., Zhou,B., Adam,R.M., Li,X., Pu,W.T., Morrow,B.E., Moon,A., and Li,X. (2011). A Tbx1-Six1/Eya1-Fgf8 genetic pathway controls mammalian cardiovascular and craniofacial morphogenesis. *J Clin Invest* **121,** 1585-1595.

Guris,D.L., Duester,G., Papaioannou,V.E., and Imamoto,A. (2006). Dose-Dependent Interaction of Tbx1 and Crkl and Locally Aberrant RA Signaling in a Model of del22q11 Syndrome. *Developmental Cell* **10,** 81-92.

Guris,D., Fantes,J., Tara,D., Drucker,B.J., and Imamoto,A. (2001). Mice lacking the homologue of the human 22q11.2 gene *CRKL* phenocopy neurocristopathies of DiGeorge syndrome. *Nature Genetics* **27,** 293-298.

Habets,P.E.M.H., Moorman,A.F.M., Clout,D.E.W., van Roon,M.A., Lingbeek,M., van Lohuizen,M., Campione,M., and Christoffels,V.M. (2002). Cooperative action of Tbx2 and Nkx2.5 inhibits ANF expression in the atrioventricular canal: implications for cardiac chamber formation. *Genes & Development* **16,** 1234-1246.

Hall,B.K. (1980). Tissue interactions and the initiation of osteogenesis and chondrogenesis in the neural-crest derived mandibular skeleton of the emebryonic mouse as seen in isolated murine tissues and in recombinations of murine and avian tissues. *J. Embryol. Exp. Morph.* **58,** 251-264.

Halpern,M.E., Rhee,J., Goll,M.G., Akitake,C., Parsons,M., and Leach,S.D. (2008). Gal4/UAS Transgenic Tools and Their Application to Zebrafish. *Zebrafish* **5,** 97-110.

Hamburger,V. and Hamilton,H.L. (1951). A series of normal stages in the development of the chick embryo. *Journal of Morphology* **88,** 49-92.

Hami,D., Grimes,A.C., Tsai,H.J., and Kirby,M.L. (2011). Zebrafish cardiac development requires a conserved secondary heart field. *Development* **138,** 2389-2398.

Happle,R., Traupe,H., Bounameaux,Y., and Fisch,T. (1984). [Teratogenic effects of etretinate in humans]. *Dtsch. Med. Wochenschr.* **109,** 1476-1480.

Harel,I., Maezawa,Y., Avraham,R., Rinon,A., Ma,H.Y., Cross,J.W., Leviatan,N., Hegesh,J., Roy,A., Jacob-Hirsch,J. et al. (2012). Pharyngeal mesoderm regulatory network controls cardiac and head muscle morphogenesis. *Proceedings of the National Academy of Sciences* **109,** 18839-18844.

Harrelson,Z., Kelly,R.G., Goldin,S.N., Gibson-Brown,J.J., Bollag,R.J., Silver,L.M., and Papaioannou,V.E. (2004). Tbx2 is essential for patterning the atrioventricular canal

and for morphogenesis of the outflow tract during heart development. *Development* **131,** 5041-5052.

Hashimoto,T., Zhang,X.M., Chen,B.Y., and Yang,X.J. (2006). VEGF activates divergent intracellular signaling components to regulate retinal progenitor cell proliferation and neuronal differentiation. *Development* **133,** 2201-2210.

Hatakeyama,J., Sakamoto,S., and Kageyama,R. (2006). *Hes1* and *Hes5* Regulate the Development of the Cranial and Spinal Nerve Systems. *Developmental Neuroscience* **28,** 92-101.

Hatakeyama,J., Bessho,Y., Katoh,K., Ookawara,S., Fujioka,M., Guillemot,F., and Kageyama,R. (2004). Hes genes regulate size, shape and histogenesis of the nervous system by control of the timing of neural stem cell differentiation. *Development* **131,** 5539-5550.

Hay,B.N. (2007). Deletion 22q11: Spectrum of Associated Disorders. *Seminars in Pediatric Neurology* **14,** 136-139.

He,M.l., Wen,L., Campbell,C.E., Wu,J.Y., and Rao,Y. (1999). Transcription repression by Xenopus ET and its human ortholog TBX3, a gene involved in ulnar-mammary syndrome. *Proceedings of the National Academy of Sciences* **96,** 10212-10217.

Heathcote,K., Braybrook,C., Abushaban,L., Guy,M., Khetyar,M.E., Patton,M.A., Carter,N.D., Scambler,P.J., and Syrris,P. (2005). Common arterial trunk associated with a homeodomain mutation of NKX2.6. *Hum. Mol. Genet.* **14,** 585-593.

Hellstrom,M., Phng,L.K., and Gerhardt,H. (2007a). VEGF and Notch Signaling: The Yin and Yang of Angiogenic Sprouting. *Cell Adhesion & Migration* **1,** 133-136.

Hellstrom,M., Phng,L.K., Hofmann,J.J., Wallgard,E., Coultas,L., Lindblom,P., Alva,J., Nilsson,A.K., Karlsson,L., Gaiano,N. et al. (2007b). Dll4 signalling through Notch1 regulates formation of tip cells during angiogenesis. *Nature* **445,** 776-780.

Hernandez,R.E., Putzke,A.P., Myers,J.P., Margaretha,L., and Moens,C.B. (2007). Cyp26 enzymes generate the retinoic acid response pattern necessary for hindbrain development. *Development* **134,** 177-187.

Herrmann,K. (1995). Teratogenic effects of retinoic acid and related substances on the early development of the zebrafish (Brachydanio rerio) as assessed by a novel scoring system. *Toxicology in Vitro* **9,** 267-283.

High,F.A. (2009). Murine Jagged1/Notch signaling in the second heart field orchestrates Fgf8 expression and tissue-tissue interactions during outflow tract development. *J Clin Invest* **0,** 0.

High,F.A., Lu,M.M., Pear,W.S., Loomes,K.M., Kaestner,K.H., and Epstein,J.A. (2008). Endothelial expression of the Notch ligand Jagged1 is required for vascular smooth muscle development. *PNAS* **105,** 1955-1959.

High,F.A., Zhang,M., Proweller,A., Tu,L., Parmacek,M.S., Pear,W.S., and Epstein,J.A. (2007). An essential role for Notch in neural crest during cardiovascular development and smooth muscle differentiation. *J. Clin. Invest.* **117,** 353-363.

Hinits,Y., Pan,L., Walker,C., Dowd,J., Moens,C.B., and Hughes,S.M. Zebrafish Mef2ca and Mef2cb are essential for both first and second heart field cardiomyocyte differentiation. *Developmental Biology*.

Hirata,H., Bessho,Y., Kokubu,H., Masamizu,Y., Yamada,S., Lewis,J., and Kageyama,R. (2004). Instability of Hes7 protein is crucial for the somite segmentation clock. *Nat Genet* **36,** 750-754.

Hirata,H., Tomita,K., Bessho,Y., and Kageyama,R. (2001). Hes1 and Hes3 regulate maintenance of the isthmic organizer and development of the mid/hindbrain. *EMBO J* **20,** 4454-4466.

Hirata,H., Yoshiura,S., Ohtsuka,T., Bessho,Y., Harada,T., Yoshikawa,K., and Kageyama,R. (2002). Oscillatory Expression of the bHLH Factor Hes1 Regulated by a Negative Feedback Loop. *Science* **298,** 840-843.

Hiroi,Y., Kudoh,S., Monzen,K., Ikeda,Y., Yazaki,Y., Nagai,R., and Komuro,I. (2001). Tbx5 associates with Nkx2-5 and synergistically promotes cardiomyocyte differentiation. *Nat Genet* **28,** 276-280.

Hochgreb,T., Linhares,V.L., Menezes,D.C., Sampaio,A.C., Yan,C.Y.I., Cardoso,W.V., Rosenthal,N., and Xavier-Neto,J. (2003). A caudorostral wave of RALDH2 conveys anteroposterior information to the cardiac field. *Development* **130,** 5363-5374.

Hofmann,J.J., Briot,A., Enciso,J., Zovein,A.C., Ren,S., Zhang,Z.W., Radtke,F., Simons,M., Wang,Y., and Iruela-Arispe,M.L. (2012). Endothelial deletion of murine Jag1 leads to valve calcification and congenital heart defects associated with Alagille syndrome. *Development* **139,** 4449-4460.

Hofmann,M., Schuster-Gossler,K., Watabe-Rudolph,M., Aulehla,A., Herrmann,B.G., and Gossler,A. (2004). WNT signaling, in synergy with T/TBX6, controls Notch signaling by regulating Dll1 expression in the presomitic mesoderm of mouse embryos. *Genes Dev.* **18,** 2712-2717.

Hojo,M., Ohtsuka,T., Hashimoto,N., Gradwohl,G., Guillemot,F., and Kageyama,R. (2000). Glial cell fate specification modulated by the bHLH gene Hes5 in mouse retina. *Development* **127,** 2515-2522.

Hollander,D.A., Sarfarazi,M., Stoilov,I., Wood,I.S., Fredrick,D.R., and Alvarado,J.A. (2006). Genotype and Phenotype Correlations in Congenital Glaucoma: CYP1B1 Mutations, Goniodysgenesis, and Clinical Characteristics. *Am J Ophthalmol* **142,** 993-1004.

Hollemann,T., Chen,Y., Grunz,H., and Pieler,T. (1998). Regionalized metabolic activity establishes boundaries of retinoic acid signalling. *EMBO J.* **17,** 7361-7372.

Hoogaars,W.M.H., Engel,A., Brons,J.F., Verkerk,A.O., de Lange,F.J., Wong,L.Y.E., Bakker,M.L., Clout,D.E., Wakker,V., Barnett,P. et al. (2007). Tbx3 controls the sinoatrial node gene program and imposes pacemaker function on the atria. *Genes Dev.* **21,** 1098-1112.

Hoover,L.L., Burton,E.G., Brooks,B.A., and Kubalak,S.W. (2008). The Expanding Role for Retinoid Signaling in Heart Development. *Scientific World Journal* **8,** 194-211.

Horb,M.E. and Thomsen,G.H. (1999). Tbx5 is essential for heart development. *Development* **126,** 1739-1751.

Hu,P., Tian,M., Bao,J., Xing,G., Gu,X., Gao,X., Linney,E., and Zhao,Q. (2008). Retinoid regulation of the zebrafish cyp26a1 promoter. *Dev. Dyn.* **237,** 3798-3808.

Hu,T., Yamagishi,H., Maeda,J., McAnally,J., Yamagishi,C., and Srivastava,D. (2004). Tbx1 regulates fibroblast growth factors in the anterior heart field through a reinforcing autoregulatory loop involving forkhead transcription factors. *Development* **131,** 5491-5502.

Huh,S.H. and Ornitz,D.M. (2010). β-catenin deficiency causes DiGeorge syndrome-like phenotypes through regulation of Tbx1. *Development* **137,** 1137-1147.

Humphreys,R., Zheng,W., Prince,L.S., Qu,X., Brown,C., Loomes,K., Huppert,S.S., Baldwin,S., and Goudy,S. (2012). Cranial neural crest ablation of Jagged1 recapitulates the craniofacial phenotype of Alagille syndrome patients. *Hum. Mol. Genet.* **21,** 1374-1383.

Hutson,M.R. and Kirby,M.L. (2007). Model systems for the study of heart development and disease: Cardiac neural crest and conotruncal malformations. *Seminars in Cell & Developmental Biology* **18,** 101-110.

Huynh,T., Chen,L., Terrell,P., and Baldini A (2007). A fate map of Tbx1 expressing cells reveals heterogeneity in the second cardiac field. *Genesis* **45,** 470-475.

Ingram,W.J., McCue,K.I., Tran,T.H., Hallahan,A.R., and Wainwright,B.J. (2007). Sonic Hedgehog regulates Hes1 through a novel mechanism that is independent of canonical Notch pathway signalling. *Oncogene* **27,** 1489-1500.

Ishibashi,M., Ang,S.L., Shiota,K., Nakanishi,S., Kageyama,R., and Guillemot,F. (1995). Targeted disruption of mammalian hairy and Enhancer of split homolog-1 (HES-

1) leads to up-regulation of neural helix-loop-helix factors, premature neurogenesis, and severe neural tube defects. *Genes Dev.* **9,** 3136-3148.

Iso,T., Kedes,L., and Hamamori,Y. (2003). HES and HERP families: multiple effectors of the Notch signaling pathway. *J Cell Physiol* **194,** 237-255.

Ito,K. and Sieber-Blum,M. (1991). In vitro clonal analysis of quail cardiac neural crest development. *Developmental Biology* **148,** 95-106.

Iulianella,A., Beckett,B., Petkovich,M., and Lohnes,D. (1999). A Molecular Basis for Retinoic Acid-Induced Axial Truncation. *Developmental Biology* **205,** 33-48.

Ivins,S., Lammerts van Beuren,K., Roberts,C., James,C., Lindsay,E., Baldini,A., Ataliotis,P., and Scambler,P.J. (2005). Microarray analysis detects differentially expressed genes in the pharyngeal region of mice lacking Tbx1. *Developmental Biology* **285,** 554-569.

Jain,R., Engleka,K.A., Rentschler,S.L., Manderfield,L.J., Li,L., Yuan,L., and Epstein,J.A. (2011). Cardiac neural crest orchestrates remodeling and functional maturation of mouse semilunar valves. *J Clin Invest* **121,** 422-430.

Janesick,A., Shiotsugu,J., Taketani,M., and Blumberg,B. (2012). RIPPLY3 is a retinoic acid-inducible repressor required for setting the borders of the pre-placodal ectoderm. *Development* **139,** 1213-1224.

Jarriault,S., Brou,C., Logeat,F., Schroeter,E.H., Kopan,R., and Israel,A. (1995). Signalling downstream of activated mammalian Notch. *Nature* **377,** 355-358.

Jensen,J., Pedersen,E.E., Galante,P., Hald,J., Heller,R.S., Ishibashi,M., Kageyama,R., Guillemot,F., Serup,P., and Madsen,O.D. (2000). Control of endodermal endocrine development by Hes-1. *Nat Genet* **24,** 36-44.

Jerome,L.A. and Papaioannou,V.E. (2001). DiGeorge syndrome phenotype in mice mutant for the T-box gene, Tbx1. *Nat. Genet.* **27,** 286-291.

Jia,H., King,I.N., Chopra,S.S., Wan,H., Ni,T.T., Jiang,C., Guan,X., Wells,S., Srivastava,D., and Zhong,T.P. (2007). Vertebrate heart growth is regulated by functional antagonism between Gridlock and Gata5. *PNAS* **104,** 14008-14013.

Jiang,X., Rowitch,D.H., Soriano,P., McMahon,A.P., and Sucov,H.M. (2000). Fate of the mammalian cardiac neural crest. *Development* **127,** 1607-1616.

Jouve,C., Palmeirim,I., Henrique,D., Beckers,J., Gossler,A., Ish-Horowicz,D., and Pourquie,O. (2000). Notch signalling is required for cyclic expression of the hairy-like gene HES1 in the presomitic mesoderm. *Development* **127,** 1421-1429.

Kageyama R, Yoshiura S, Masamizu Y, and Niwa Y. (2007). Ultradian oscillators in somite segmentation and other biological events. *Cold Spring Harb Symp Quant Biol.* **72,** 451-457.

Kageyama,R., Ohtsuka,T., and Kobayashi,T. (2008a). Roles of Hes genes in neural development. *Development Growth and Differentiation* **50, Suppl.1,** 97-103.

Kageyama,R., Niwa,Y., and Shimojo,H. (2009). Rhythmic gene expression in somite formation and neural development. *Molecules and Cells* **27,** 497-502.

Kageyama,R., Niwa,Y., Shimojo,H., Kobayashi,T., and Ohtsuka,T. (2010). Chapter Ten - Ultradian Oscillations in Notch Signaling Regulate Dynamic Biological Events. In *Current Topics in Developmental Biology*
Notch Signaling. (ed. Raphael,K.), pp. 311-331. Academic Press.

Kageyama,R., Ohtsuka,T., and Kobayashi,T. (2007). The Hes gene family: repressors and oscillators that orchestrate embryogenesis. *Development* dev.

Kageyama,R., Ohtsuka,T., Shimojo,H., and Imayoshi,I. (2008b). Dynamic Notch signaling in neural progenitor cells and a revised view of lateral inhibition. *Nat Neurosci* **11,** 1247-1251.

Kalter,H. (1960). The teratogenic effects of hypervitaminosis A upon the face and mouth of inbred mice. *Ann. N. Y. Acad. Sci.* **85,** 42-55.

Kalter,H. and Warkany,J. (1961). Experimental production of congenital malformations in strains of inbred mice by maternal treatment with hypervitaminosis A. *Am. J. Pathol.* **38,** 1-21.

Kameda,Y. Hoxa3 and signaling molecules involved in aortic arch patterning and remodeling. *Cell and Tissue Research*.

Kameda,Y., Saitoh,T., Nemoto,N., Katoh,T., and Iseki,S. (2012). Hes1 is required for the development of the superior cervical ganglion of sympathetic trunk and the carotid body. *Developmental Dynamics* **241,** 1289-1300.

Kastner,P., Mark,M., Ghyselinck,N., Krezel,W., Dupe,V., Grondona,J.M., and Chambon,P. (1997). Genetic evidence that the retinoid signal is transduced by heterodimeric RXR/RAR functional units during mouse development. *Development* **124,** 313-326.

Kawamura,A., Koshida,S., and Takada,S. (2008). Activator-to-Repressor Conversion of T-Box Transcription Factors by the Ripply Family of Groucho/TLE-Associated Mediators. *Mol. Cell. Biol.* **28,** 3236-3244.

Kelly,R.G. and Buckingham,M.E. (2002). The anterior heart-forming field: voyage to the arterial pole of the heart. *Trends Genet.* **18,** 210-216.

Kelly,R.G., Brown,N.A., and Buckingham,M.E. (2001). The Arterial Pole of the Mouse Heart Forms from Fgf10-Expressing Cells in Pharyngeal Mesoderm. *Developmental Cell* **1,** 435-440.

Kelly,R.G., Jerome-Majewska,L.A., and Papaioannou,V.E. (2004). The del22q11.2 candidate gene Tbx1 regulates branchiomeric myogenesis. *Hum. Mol. Genet.* **13,** 2829-2840.

Kelly,R.G. and Papaioannou,V.E. (2007). Visualization of outflow tract development in the absence of Tbx1 using an FgF10 enhancer trap transgene. *Dev. Dyn.* **236,** 821-828.

Keyte,A. and Hutson,M.R. (2012). The neural crest in cardiac congenital anomalies. *Differentiation* **84,** 25-40.

Kinkel,M.D., Sefton,E.M., Kikuchi,Y., Mizoguchi,T., Ward,A.B., and Prince,V.E. (2009). Cyp26 enzymes function in endoderm to regulate pancreatic field size. *PNAS* **106,** 7864-7869.

Kipp,J.L., Golebiowski,A., Rodriguez,G., Demczuk,M., Kilen,S.M., and Mayo,K.E. (2011). Gene Expression Profiling Reveals Cyp26b1 to Be an Activin Regulated Gene Involved in Ovarian Granulosa Cell Proliferation. *Endocrinology* **152,** 303-312.

Kirby,M. (2002). Molecular embryogenesis of the heart. *Pediatr Dev Pathol* **5,** 516-543.

Kirby,M., Turnage,K.3., and Hays,B. (1985). Characterization of conotruncal malformations following ablation of "cardiac" neural crest. *Anatomical Record* **213,** 87-93.

Kirk,E.P., Sunde,M., Costa,M.W., Rankin,S.A., Wolstein,O., Castro,M.L., Butler,T.L., Hyun,C., Guo,G., Otway,R. et al. (2007). Mutations in Cardiac T-Box Factor Gene TBX20 Are Associated with Diverse Cardiac Pathologies, Including Defects of Septation and Valvulogenesis and Cardiomyopathy. *Am J Hum Genet* **81,** 280-291.

Kispert,A. and and Herrman,B.G. (1993). The Brachyury gene encodes a novel DNA binding protein. *EMBO J* **12,** 3211-3220.

Kispert,A., Koschorz,B., and Hermann,B.G. (1995). The T protein encoded by Brchyury is a tissue-specific transcription factor. *EMBO J* **14,** 4763-4772.

Kistler,A. (1981). Teratogenesis of retinoic acid in rats: susceptible stages and suppression of retinoic acid-induced limb malformations by cycloheximide. *Teratology* **23,** 25-31.

Kita,A., Imayoshi,I., Hojo,M., Kitagawa,M., Kokubu,H., Ohsawa,R., Ohtsuka,T., Kageyama,R., and Hashimoto,N. (2007). Hes1 and Hes5 Control the Progenitor Pool, Intermediate Lobe Specification, and Posterior Lobe Formation in the Pituitary Development. *Mol Endocrinol* **21,** 1458-1466.

Kitamura,K., Miura,H., Miyagawa-Tomita,S., Yanazawa,M., Katoh-Fukui,Y., Suzuki,R., Ohuchi,H., Suehiro,A., Motegi,Y., Nakahara,Y. et al. (1999). Mouse Pitx2 deficiency leads to anomalies of the ventral body wall, heart, extra- and periocular mesoderm and right pulmonary isomerism. *Development* **126,** 5749-5758.

Klingberg,G., Oskarsdottir,S., Johannesson,E.L., and Noren,J.G. (2002). Oral manifestations in 22q11 deletion syndrome. *International Journal of Paediatric Dentistry* **12,** 14-23.

Kobayashi,T., Mizuno,H., Imayoshi,I., Furusawa,C., Shirahige,K., and Kageyama,R. (2009). The cyclic gene Hes1 contributes to diverse differentiation responses of embryonic stem cells. *Genes & Development* **23,** 1870-1875.

Kochhar,D.M. and Johnson,E.M. (1965). Morphological and autoradiographic studies of cleft palate induced in rat embryos by maternal hypervitaminosis A. *J. Embryol. Exp. Morphol.* **14,** 223-238.

Kochilas,L., Merscher-Gomez,S., Lu,M.M., Potluri,V., Liao,J., Kucherlapati,R., Morrow,B., and Epstein,J.A. (2002). The role of neural crest during cardiac development in a mouse model of DiGeorge syndrome. *Dev. Biol.* **251,** 157-166.

Kochilas,L.K., Potluri,V., Gitler,A., Balasubramanian,K., and Chin,A.J. (2003). Cloning and characterization of zebrafish tbx1. *Gene Expr. Patterns.* **3,** 645-651.

Kodama,Y., Hijikata,M., Kageyama,R., Shimotohno,K., and Chiba,T. (2004). The role of notch signaling in the development of intrahepatic bile ducts. *Gastroenterology* **127,** 1775-1786.

Kokubo,H., Miyagawa-Tomita,S., Nakazawa,M., Saga,Y., and Johnson,R.L. (2005). Mouse hesr1 and hesr2 genes are redundantly required to mediate Notch signaling in the developing cardiovascular system. *Developmental Biology* **278,** 301-309.

Kokubo,H., Miyagawa-Tomita,S., Tomimatsu,H., Nakashima,Y., Nakazawa,M., Saga,Y., and Johnson,R.L. (2004). Targeted Disruption of hesr2 Results in Atrioventricular Valve Anomalies That Lead to Heart Dysfunction. *Circ Res* **95,** 540-547.

Kokubo,H., Tomita-Miyagawa,S., Hamada,Y., and Saga,Y. (2007). Hesr1 and Hesr2 regulate atrioventricular boundary formation in the developing heart through the repression of Tbx2. *Development* **134,** 747-755.

Kopinke,D., Sasine,J., Swift,J., Stephens,W.Z., and Piotrowski,T. (2006). Retinoic acid is required for endodermal pouch morphogenesis and not for pharyngeal endoderm specification. *Dev. Dyn.* **235,** 2695-2709.

Krebs,L.T., Shutter,J.R., Tanigaki,K., Honjo,T., Stark,K.L., and Gridley,T. (2004). Haploinsufficient lethality and formation of arteriovenous malformations in Notch pathway mutants. *Genes Dev.* **18,** 2469-2473.

Krebs,L.T., Xue,Y., Norton,C.R., Shutter,J.R., Maguire,M., Sundberg,J.P., Gallahan,D., Closson,V., Kitajewski,J., Callahan,R. et al. (2000). Notch signaling is essential for vascular morphogenesis in mice. *Genes & Development* **14,** 1343-1352.

Kumar,M., Ray,P., and Chapman,S.C. (2012). Fibroblast growth factor and bone morphogenetic protein signaling are required for specifying prechondrogenic identity in neural crest-derived mesenchyme and initiating the chondrogenic program. *Dev. Dyn.* **241,** 1091-1103.

Laforest,B., Andelfinger,G., and Nemer,M. (2011). Loss of Gata5 in mice leads to bicuspid aortic valve. *J Clin Invest* **121,** 2876-2887.

Lai,E.C. and Rubin,G.M. (2001). neuralized is essential for a subset of Notch pathway-dependent cell fate decisions during Drosophila eye development. *PNAS* **98,** 5637-5642.

Lai,L., Bohnsack,B.L., Niederreither,K., and Hirschi,K.K. (2003). Retinoic acid regulates endothelial cell proliferation during vasculogenesis. *Development* **130,** 6465-6474.

Lammer,E.J., Chen,D.T., Hoar,R.M., Agnish,N.D., Benke,P.J., Braun,J.T., Curry,C.J., Fernhoff,P.M., Grix,A.W., Jr., Lott,I.T. et al. (1985). Retinoic acid embryopathy. *N. Engl. J. Med.* **313,** 837-841.

Lammerts van Bueren,K. (2008). Genomic and Transcriptomic Approaches to Pathways affected in DiGeorge Syndrome. *UCL-Institute of Child Health*.

Lanford,P.J., Lan,Y., Jiang,R., Lindsell,C., Weinmaster,G., Gridley,T., and Kelley,M.W. (1999). Notch signalling pathway mediates hair cell development in mammalian cochlea. *Nat Genet* **21,** 289-292.

Laue,K., Janicke,M., Plaster,N., Sonntag,C., and Hammerschmidt,M. (2008). Restriction of retinoic acid activity by Cyp26b1 is required for proper timing and patterning of osteogenesis during zebrafish development. *Development* **135,** 3775-3787.

Lavine,K.J., Yu,K., White,A.C., Zhang,X., Smith,C., Partanen,J., and Ornitz,D.M. (2005). Endocardial and Epicardial Derived FGF Signals Regulate Myocardial Proliferation and Differentiation In Vivo. *Developmental Cell* **8,** 85-95.

Lawson,N.D., Scheer,N., Pham,V.N., Kim,C.H., Chitnis,A.B., Campos-Ortega,J.A., and Weinstein,B.M. (2001). Notch signaling is required for arterial-venous differentiation during embryonic vascular development. *Development* **128,** 3675-3683.

Lazic,S. and Scott,I.C. (2011). Mef2cb regulates late myocardial cell addition from a second heart field-like population of progenitors in zebrafish. *Developmental Biology* **354,** 123-133.

LeDouarin,N.M. (1982). *The Neural Crest*. Cambridge: Cambridge University Press.

Lee,H.Y., Wroblewski,E., Philips,G.T., Stair,C.N., Conley,K., Reedy,M., Mastick,G.S., and Brown,N.L. (2005). Multiple requirements for Hes1 during early eye formation. *Developmental Biology* **284,** 464-478.

Lee,L.M.Y., Leung,C.Y., Tang,W.W.C., Choi,H.L., Leung,Y.C., McCaffery,P.J., Wang,C.C., Woolf,A.S., and Shum,A.S.W. (2012). A paradoxical teratogenic mechanism for retinoic acid. *PNAS* **109,** 13668-13673.

Lee,T.C., Zhao,Y.D., Courtman,D.W., and Stewart,D.J. (2000). Abnormal Aortic Valve Development in Mice Lacking Endothelial Nitric Oxide Synthase. *Circulation* **101,** 2345-2348.

Leslie,J.D., Ariza-McNaughton,L., Bermange,A.L., McAdow,R., Johnson,S.L., and Lewis,J. (2007). Endothelial signalling by the Notch ligand Delta-like 4 restricts angiogenesis. *Development* **134,** 839-844.

Leve,C., Gajewski,M., Rohr,K., and Tautz,D. (2001). Homologues of c-hairy1 and lunatic fringe in zebrafish are expressed in the developing central nervous system, but not in the presomitic mesoderm. *Development Genes and Evolution* **211,** 493-500.

Li,H., Wagner,E., McCaffery,P., Smith,D., Andreadis,A., and Dräger,U.C. (2000). A retinoic acid synthesizing enzyme in ventral retina and telencephalon of the embryonic mouse. *Mechanisms of Development* **95,** 283-289.

Li,L., Krantz,I.D., Deng,Y., Genin,A., Banta,A.B., Collins,C.C., Qi,M., Trask,B.J., Kuo,W.L., Cochran,J. et al. (1997a). Alagille syndrome is caused by mutations in human Jagged1, which encodes a ligand for Notch1. *Nat Genet* **16,** 243-251.

Li,P., Pashmforoush,M., and Sucov,H.M. (2010). Retinoic Acid Regulates Differentiation of the Secondary Heart Field and TGFβ Mediated Outflow Tract Septation. *Developmental Cell* **18,** 480-485.

Li,P., Pashmforoush,M., and Sucov,H.M. (2012). Mesodermal retinoic acid signaling regulates endothelial cell coalescence in caudal pharyngeal arch artery vasculogenesis. *Developmental Biology* **361,** 116-124.

Li,Q.Y., Newbury-Ecob,R.A., Terrett,J.A., Wilson,D.I., Curtis,A.R.J., Ho Yi,C., Gebuhr,T., Bullen,P.J., Robson,S.C., Strachan,T. et al. (1997b). Holt-Oram syndrome is caused by mutations in TBX5, a member of the Brachyury (T) gene family. *Nat Genet* **15,** 21-29.

Li,Z., Korzh,V., and Gong,Z. (2009). DTA-mediated targeted ablation revealed differential interdependence of endocrine cell lineages in early development of zebrafish pancreas. *Differentiation* **78,** 241-252.

Liao,J., Aggarwal,V.S., Nowotschin,S., Bondarev,A., Lipner,S., and Morrow,B.E. (2008). Identification of downstream genetic pathways of Tbx1 in the second heart field. *Developmental Biology* **316,** 524-537.

Liao,J., Kochilas,L., Nowotschin,S., Arnold,J.S., Aggarwal,V.S., Epstein,J.A., Brown,M.C., Adams,J., and Morrow,B.E. (2004). Full spectrum of malformations in velo-cardio-facial syndrome/DiGeorge syndrome mouse models by altering Tbx1 dosage. *Hum. Mol. Genet.* **13,** 1577-1585.

Lin,C.Y., Lin,C.J., Chen,C.H., Chen,R.M., Zhou,B., and Chang,C.P. (2012). The secondary heart field is a new site of calcineurin/Nfatc1 signaling for semilunar valve development. *Journal of Molecular and Cellular Cardiology* **52,** 1096-1102.

Linder,C.C. (2001). The influence of genetic background on spontaneous and genetically engineered mouse models of complex diseases. *Lab Anim (NY).* **30,** 34-39.

Lindsay,E.A., Botta,A., Jurecic,V., Carattini-Rivera,S., Cheah,Y.C., Rosenblatt,H.M., Bradley,A., and Baldini,A. (1999). Congenital heart disease in mice deficient for the DiGeorge syndrome region. *Nature* **401,** 379-383.

Lindsay,E.A., Vitelli,F., Su,H., Morishima,M., Huynh,T., Pramparo,T., Jurecic,V., Ogunrinu,G., Sutherland,H.F., Scambler,P.J. et al. (2001). Tbx1 haploinsufficieny in the DiGeorge syndrome region causes aortic arch defects in mice. *Nature* **410,** 97-101.

Lindsay,E.A. (2001). Chromosomal microdeletions: dissecting del22q11 syndrome. *Nat Rev Genet* **2,** 858-868.

Lindsay,E.A. and Baldini,A. (2001). Recovery from arterial growth delay reduces penetrance of cardiovascular defects in mice deleted for the DiGeorge syndrome region. *Hum. Mol. Genet.* **10,** 997-1002.

Liu,C., Liu,W., Lu,M.F., Brown,N.A., and Martin,J.F. (2001). Regulation of left-right asymmetry by thresholds of Pitx2c activity. *Development* **128,** 2039-2048.

Liu,C., Liu,W., Palie,J., Lu,M.F., Brown,N.A., and Martin,J.F. (2002). Pitx2c patterns anterior myocardium and aortic arch vessels and is required for local cell movement into atrioventricular cushions. *Development* **129,** 5081-5091.

Liu,H., Kennard,S., and Lilly,B. (2009). NOTCH3 Expression Is Induced in Mural Cells Through an Autoregulatory Loop That Requires Endothelial-Expressed JAGGED1. *Circ Res* **104,** 466-475.

Liu,J. and Stainier,D.Y.R. (2012). Zebrafish in the Study of Early Cardiac Development. *Circ Res* **110,** 870-874.

Lohnes,D., Mark,M., Mendelsohn,C., Dolle,P., Dierich,A., Gorry,P., Gansmuller,A., and Chambon,P. (1994). Function of the retinoic acid receptors (RARs) during development (I). Craniofacial and skeletal abnormalities in RAR double mutants. *Development* **120,** 2723-2748.

Lohnes,D., Kastner,P., Dierich,A., Mark,M., LeMeur,M., and Chambon,P. (1993). Function of retinoic acid receptor gamma in the mouse. *Cell* **73,** 643-658.

Loudig,O., Maclean,G.A., Dore,N.L., Luu,L., and Petkovich,M. (2005). Transcriptional co-operativity between distant retinoic acid response elements in regulation of Cyp26A1 inducibility. *Biochem. J.* **392,** 241-248.

Louvi,A. and Artavanis-Tsakonas,S. (2012). Notch and disease: A growing field. *Seminars in Cell & Developmental Biology* **23,** 473-480.

Luna-Zurita,L., Prados,B.n., Grego-Bessa,J., Luxan,G., del Monte,G., Benguria,A., Adams,R.H., Perez-Pomares,J.M., and de la Pompa,J.L. (2010). Integration of a Notch-dependent mesenchymal gene program and Bmp2-driven cell invasiveness regulates murine cardiac valve formation. *J Clin Invest* **120,** 3493-3507.

Luo,R., An,M., Arduini,B.L., and Henion,P.D. (2001). Specific pan-neural crest expression of zebrafish Crestin throughout embryonic development. *Dev. Dyn.* **220,** 169-174.

Lyons,M.S., Bell,B., Stainier,D., and Peters,K.G. (1998). Isolation of the zebrafish homologues for the tie-1 and tie-2 endothelium-specific receptor tyrosine kinases. *Dev. Dyn.* **212,** 133-140.

Ma,L., Lu,M.F., Schwartz,R.J., and Martin,J.F. (2005). Bmp2 is essential for cardiac cushion epithelial-mesenchymal transition and myocardial patterning. *Development* **132,** 5601-5611.

Macatee,T.L., Hammond,B.P., Arenkiel,B.R., Francis,L., Frank,D.U., and Moon,A.M. (2003). Ablation of specific expression domains reveals discrete functions of ectoderm- and endoderm-derived FGF8 during cardiovascular and pharyngeal development. *Development* **130,** 6361-6374.

MacGrogan,D., Luna-Zurita,L., and de la Pompa,J.L. (2011). Notch signaling in cardiac valve development and disease. *Birth Defects Research Part A: Clinical and Molecular Teratology* **91,** 449-459.

MacLean,G., Abu-Abed,S., Dolle,P., Tahayato,A., Chambon,P., and Petkovich,M. (2001). Cloning of a novel retinoic-acid metabolizing cytochrome P450, Cyp26B1, and comparative expression analysis with Cyp26A1 during early murine development. *Mechanisms of Development* **107,** 195-201.

MacLean,G., Dolle,P., and Petkovich,M. (2009). Genetic disruption of CYP26B1 severely affects development of neural crest derived head structures, but does not compromise hindbrain patterning. *Dev. Dyn.* **238,** 732-745.

MacLean,G., Li,H., Metzger,D., Chambon,P., and Petkovich,M. (2007). Apoptotic Extinction of Germ Cells in Testes of Cyp26b1 Knockout Mice. *Endocrinology* **148,** 4560-4567.

Maden,M., Gale,E., Kostetskii,I., and Zile,M. (1996). Vitamin A-deficient quail embryos have half a hindbrain and other neural defects. *Current Biology* **6,** 417-426.

Malpel,S., Mendelsohn,C., and Cardoso,W.V. (2000). Regulation of retinoic acid signaling during lung morphogenesis. *Development* **127,** 3057-3067.

Malpeli G., Folli C., and Berni R. (1996). Retinoid bindin to retinol-binding protein and the interference with the interaction with transthyretin. *Biochim. Biophys. Acta* **1294,** 48-54.

Mandel,E.M., Kaltenbrun,E., Callis,T.E., Zeng,X.X., Marques,S.R., Yelon,D., Wang,D.Z., and Conlon,F.L. (2010). The BMP pathway acts to directly regulate Tbx20 in the developing heart. *Development* **137,** 1919-1929.

Marino,B., Digilio,M.C., and Toscano,A. (2002). Common arterial trunk, DiGeorge syndrome and microdeletion 22q11. *Progress in Pediatric Cardiology* **15,** 9-17.

Mark,M., Ghyselinck,N.B., and Chambon,P. (2004). Retinoic acid signalling in the development of branchial arches. *Current Opinion in Genetics & Development* **14,** 591-598.

Mark,M., Gyselinck,N.B., and Chambon,P. (2009). Function of retinoic acid receptors during embryonic development. *Nuclear Receptor Signaling* **7,** 1-15.

Martin,B.L. and Kimelman,D. (2010). Brachyury establishes the embryonic mesodermal progenitor niche. *Genes & Development* **24,** 2778-2783.

Matt,N., Ghyselinck,N.B., Wendling,O., Chambon,P., and Mark,M. (2003). Retinoic acid-induced developmental defects are mediated by RARbeta/RXR heterodimers in the pharyngeal endoderm. *Development* **130,** 2083-2093.

Matt,N., Dupe,V., Garnier,J.M., Dennefeld,C., Chambon,P., Mark,M., and Ghyselinck,N.B. (2005). Retinoic acid-dependent eye morphogenesis is orchestrated by neural crest cells. *Development* **132,** 4789-4800.

Maynard,T.M., Gopalakrishna,D., Meechan,D., Paronett,E., Newbern,J., and LaMantia,A.S. (2012). 22q11 gene dosage establishes an adaptive range for sonic hedgehog and retinoic acid signaling during early development. *Human Molecular Genetics*.

McCarthy,K., Ho,S., and Anderson,R. (2000). Ventricular Septal Defects: Morphology of the Doubly Committed Juxtaarterial and Muscular Variants. *Images in Paediatric Cardiology* **4,** 5-23.

McCright,B., Lozier,J., and Gridley,T. (2002). A mouse model of Alagille syndrome: Notch2 as a genetic modifier of Jag1 haploinsufficiency. *Development* **129,** 1075-1082.

McDaniell,R., Warthen,D.M., Sanchez-Lara,P.A., Pai,A., Krantz,I.D., Piccoli,D.A., and Spinner,N.B. (2006). NOTCH2 Mutations Cause Alagille Syndrome, a Heterogeneous Disorder of the Notch Signaling Pathway. *The American Journal of Human Genetics* **79,** 169-173.

Meechan,D.W., Tucker,E.S., Maynard,T.M., and LaMantia,A.S. (2009). Diminished dosage of 22q11 genes disrupts neurogenesis and cortical development in a mouse model of 22q11 deletion/DiGeorge syndrome. *PNAS* **106,** 16434-16445.

Mendelsohn,C., Batourina,E., Fung,S., Gilbert,T., and Dodd,J. (1999). Stromal cells mediate retinoid-dependent functions essential for renal development. *Development* **126,** 1139-1148.

Mendelsohn,C., Lohnes,D., Decimo,D., Lufkin,T., LeMeur,M., Chambon,P., and Mark,M. (1994). Function of the retinoic acid receptors (RARs) during development (II). Multiple abnormalities at various stages of organogenesis in RAR double mutants. *Development* **120,** 2749-2771.

Merscher,S., Funke,B., Epstein,J.A., Heyer,J., Puech,A., Lu,M.M., Xavier,R.J., Demay,M.B., Russell,R.G., Factor,S. et al. (2001). TBX1 is responsible for cardiovascular defects in velo-cardio-facial/DiGeorge syndrome. *Cell* **104,** 619-629.

Mesbah,K., Harrelson,Z., Theveniau-Ruissy,M., Papaioannou,V.E., and Kelly,R.G. (2008). Tbx3 Is Required for Outflow Tract Development. *Circ Res* **103,** 743-750.

Mesbah,K., Rana,M.S., Francou,A., van Duijvenboden,K., Papaioannou,V.E., Moorman,A.F., Kelly,R.G., and Christoffels,V.M. (2011). Identification of a Tbx1/Tbx2/Tbx3 genetic pathway governing pharyngeal and arterial pole morphogenesis. *Hum. Mol. Genet.*

Meyers,E.N., Lewandoski1,M., and Martin,G.R. (1998). An Fgf8 mutant allelic series generated by Cre- and Flp-mediated recombination. *Nat Genet* **18,** 136-141.

Mic,F.A., Haselbeck,R.J., Cuenca,A.E., and Duester,G. (2002). Novel retinoic acid generating activities in the neural tube and heart identified by conditional rescue of Raldh2 null mutant mice. *Development* **129,** 2271-2282.

Mic,F.A., Molotkov,A., Benbrook,D.M., and Duester,G. (2003). Retinoid activation of retinoic acid receptor but not retinoid X receptor is sufficient to rescue lethal defect in retinoic acid synthesis. *PNAS* **100,** 7135-7140.

Mic,F.A., Molotkov,A., Fan,X., Cuenca,A.E., and Duester,G. (2000). RALDH3, a retinaldehyde dehydrogenase that generates retinoic acid, is expressed in the ventral retina, otic vesicle and olfactory pit during mouse development. *Mechanisms of Development* **97,** 227-230.

Mitsiadis,T.A., Lardelli,M., Lendahl,U., and Thesleff,I. (1995). Expression of Notch 1, 2 and 3 is regulated by epithelial-mesenchymal interactions and retinoic acid in the developing mouse tooth and associated with determination of ameloblast cell fate. *The Journal of Cell Biology* **130,** 407-418.

Mitsiadis,T.A., Graf,D., Luder,H., Gridley,T., and Bluteau,G. (2010). BMPs and FGFs target Notch signalling via jagged 2 to regulate tooth morphogenesis and cytodifferentiation. *Development* **137,** 3025-3035.

Mitsiadis,T.A., Tucker,A.S., De Bari,C., Cobourne,M.T., and Rice,D.P.C. (2008). A regulatory relationship between Tbx1 and FGF signaling during tooth morphogenesis and ameloblast lineage determination. *Developmental Biology* **320,** 39-48.

Molotkov,A., Deltour,L., Foglio,M.H., Cuenca,A.E., and Duester,G. (2002a). Distinct Retinoid Metabolic Functions for Alcohol Dehydrogenase Genes Adh1 and Adh4 in Protection against Vitamin A Toxicity or Deficiency Revealed in Double Null Mutant Mice. *J. Biol. Chem.* **277,** 13804-13811.

Molotkov,A., Fan,X., Deltour,L., Foglio,M.H., Martras,S., Farrés,J., Parés,X., and Duester,G. (2002b). Stimulation of retinoic acid production and growth by ubiquitously expressed alcohol dehydrogenase Adh3. *PNAS* **99,** 5337-5342.

Molotkov,A., Fan,X., and Duester,G. (2002c). Excessive vitamin-A toxicity in mice genetically deficient in either alcohol dehydrogenase Adh1 or Adh3. *European Journal of Biochemistry* **269,** 2607-2612.

Monahan,P., Rybak,S., and Raetzman,L.T. (2009). The Notch Target Gene Hes1 Regulates Cell Cycle Inhibitor Expression in the Developing Pituitary. *Endocrinology* **150,** 4386-4394.

Monks,D.C. and Morrow,B.E. (2012). Identification of putative retinoic acid target genes downstream of mesenchymal Tbx1 during inner ear development. *Dev. Dyn.* **241,** 563-573.

Moon,A.M., Guris,D.L., Seo,J.h., Li,L., Hammond,J., Talbot,A., and Imamoto,A. (2006). Crkl Deficiency Disrupts Fgf8 Signaling in a Mouse Model of 22q11 Deletion Syndromes. *Developmental Cell* **10,** 71-80.

Morava,E., Lacassie,Y., King,A., Illes,T., and Marble,M. (2002). Scoliosis in Velo-Cardio-Facial Syndrome. *Journal of Pediatric Orthopaedics* **22**.

Moreno,T.A., Jappelli,R., Belmonte,J.C.I.a., and Kintner,C. (2008). Retinoic acid regulation of the Mesp-Ripply feedback loop during vertebrate segmental patterning. *Developmental Biology* **315,** 317-330.

Morimoto,M., Liu,Z., Cheng,H.T., Winters,N., Bader,D., and Kopan,R. (2010). Canonical Notch signaling in the developing lung is required for determination of arterial smooth muscle cells and selection of Clara versus ciliated cell fate. *Journal of Cell Science* **123,** 213-224.

Mosimann,C. and Zon,L.I. (2011). Chapter 10 - Advanced Zebrafish Transgenesis with Tol2 and Application for Cre/lox Recombination Experiments. In *Methods in Cell Biology*

The Zebrafish: Genetics, Genomics and Informatics. (ed. Detrich,H.W.), pp. 173-194. Academic Press.

Mulder,G.B., Manley,N., Grant,J., Schmidt,K., Zeng,W., Eckhoff,C., and Maggio-Price,L. (2000). Effects of excess vitamin A on development of cranial neural crest-derived structures: a neonatal and embryologic study. *Teratology* **62,** 214-226.

Mulder,G.B., Manley,N., and Maggio-Price,L. (1998). Retinoic acid-induced thymic abnormalities in the mouse are associated with altered pharyngeal morphology, thymocyte maturation defects, and altered expression of Hoxa3 and Pax1. *Teratology* **58,** 263-275.

Murata,J., Ohtsuka,T., Tokunaga,A., Nishiike,S., Inohara,H., Okano,H., and Kageyama,R. (2009). Notch-Hes1 pathway contributes to the cochlear prosensory formation potentially through the transcriptional down-regulation of p27Kip1. *J. Neurosci. Res.* **87,** 3521-3534.

Murata,K., Hattori,M., Hirai,N., Shinozuka,Y., Hirata,H., Kageyama,R., Sakai,T., and Minato,N. (2005). Hes1 Directly Controls Cell Proliferation through the Transcriptional Repression of p27Kip1. *Mol. Cell. Biol.* **25,** 4262-4271.

Murphy,K.C., Jones,L.A., and Owen,M.J. (1999). High Rates of Schizophrenia in Adults With Velo-Cardio-Facial Syndrome. *Arch Gen Psychiatry* **56,** 940-945.

Naiche,L.A., Harrelson Z., Kelly R.G., and Papaioannou V.E. (2005). T-Box Genes in Vertebrate Development. *Annual Reviews of Genetics* **39,** 219-239.

Nakamura,H. (1982). Mesenchymal derivatives from the neural crest. *Arch. Histol. Jpn.* **45,** 127-138.

Nakamura,T., Ohtsuka,T., Sekiyama,E., Cooper,L.J., Kokubu,H., Fullwood,N.J., Barrandon,Y., Kageyama,R., and Kinoshita,S. (2008). Hes1 Regulates Corneal Development and the Function of Corneal Epithelial Stem/Progenitor Cells. *STEM CELLS* **26,** 1265-1274.

Nakayama,K., Satoh,T., Igari,A., Kageyama,R., and Nishida,E. (2008). FGF induces oscillations of Hes1 expression and Ras/ERK activation. *Current Biology* **18,** R332-R334.

Nakazaki,H., Reddy,A.C., Mania-Farnell,B.L., Shen,Y.W., Ichi,S., McCabe,C., George,D., McLone,D.G., Tomita,T., and Mayanil,C.S.K. (2008). Key basic helix-loop-helix transcription factor genes Hes1 and Ngn2 are regulated by Pax3 during mouse embryonic development. *Developmental Biology* **316,** 510-523.

Ni,T.T., Lu,J., Zhu,M., Maddison,L.A., Boyd,K.L., Huskey,L., Ju,B., Hesselson,D., Zhong,T.P., Page-McCaw,P.S. et al. (2012). Conditional control of gene function by an invertible gene trap in zebrafish. *Proceedings of the National Academy of Sciences*.

Niederreither,K., Abu-Abed,S., Schuhbaur,B., Petkovich,M., Chambon,P., and Dolle,P. (2002a). Genetic evidence that oxidative derivatives of retinoic acid are not involved in retinoid signaling during mouse development. *Nat. Genet.* **31,** 84-88.

Niederreither,K., Subbarayan,V., Dolle,P., and Chambon,P. (1999). Embryonic retinoic acid synthesis is essential for early mouse post-implantation development. *Nat. Genet.* **21,** 444-448.

Niederreither,K., Vermot,J., Messaddeq,N., Schuhbaur,B., Chambon,P., and Dolle,P. (2001). Embryonic retinoic acid synthesis is essential for heart morphogenesis in the mouse. *Development* **128,** 1019-1031.

Niederreither,K., Vermot,J., Schuhbaur,B., Chambon,P., and Dolle,P. (2000). Retinoic acid synthesis and hindbrain patterning in the mouse embryo. *Development* **127,** 75-85.

Niederreither,K. and Dolle,P. (2008). Retinoic acid in development: towards an integrated view. *Nat Rev Genet* **9,** 541-553.

Niederreither,K., McCaffery,P., Drager,U.C., Chambon,P., and Dolle,P. (1997). Restricted expression and retinoic acid-induced downregulation of the retinaldehyde dehydrogenase type 2 (RALDH-2) gene during mouse development. *Mechanisms of Development* **62,** 67-78.

Niederreither,K., Vermot,J., Roux,I.L., Schuhbaur,B., Chambon,P., and Dolle,P. (2003). The regional pattern of retinoic acid synthesis by RALDH2 is essential for the development of posterior pharyngeal arches and the enteric nervous system. *Development* **130,** 2525-2534.

Niederreither,K., Vermot,J., Schuhbaur,B., Chambon,P., and Dolle,P. (2002b). Embryonic retinoic acid synthesis is required for forelimb growth and anteroposterior patterning in the mouse. *Development* **129,** 3563-3574.

Nigam,V. and Srivastava,D. (2009). Notch1 represses osteogenic pathways in aortic valve cells. *Journal of Molecular and Cellular Cardiology* **47,** 828-834.

Nishibatake,M., Kirby,M., and Van Mierop,L. (1987). Pathogenesis of persistent truncus arteriosus and dextroposed aorta in the chick embryo after neural crest ablation. *Circulation* **75,** 255-264.

Noden,D.M. (1983). The role of neural crest in patterning of avian cranial skeletal, connective and muscle tissues. *Developmental Biology* **96,** 144-165.

Nordgarden,H., Lima,K., Skogedal,N., Folling,I., Storhaug,K., and Abrahamsen,T.G. (2011). Dental developmental disturbances in 50 individuals with the 22q11.2 deletion syndrome; relation to medical conditions? *Acta Odontol Scand* **70,** 194-201.

Nornes,S., Mikkola,I., Krauss,S., Delghandi,M., Perander,M., and Johansen,T. (1996). Zebrafish Pax9 Encodes Two Proteins with Distinct C-terminal Transactivating Domains of Different Potency Negatively Regulated by Adjacent N-terminal Sequences. *Journal of Biological Chemistry* **271,** 26914-26923.

Nowotschin,S., Liao,J., Gage,P.J., Epstein,J.A., Campione,M., and Morrow,B.E. (2006). Tbx1 affects asymmetric cardiac morphogenesis by regulating Pitx2 in the secondary heart field. *Development* **133,** 1565-1573.

Nus,M., MacGrogan,D., Martinez-Poveda,B., Benito,Y., Casanova,J.C., Fernandez-Aviles,F., Bermejo,J., and de la Pompa,J.L. (2011). Diet-Induced Aortic Valve Disease in Mice Haploinsufficient for the Notch Pathway Effector RBPJK/CSL. *Arteriosclerosis, Thrombosis, and Vascular Biology* **31,** 1580-1588.

Ocaya,P.A., Elmabsout,A.A., Olofsson,P.S., Törm,H., and Sirj,A. (2011). CYP26B1 plays a major role in the regulation of all-trans-retinoic acid metabolism and signaling in human aortic smooth muscle cells. *Journal of Vascular Research* **48,** 23-30.

Ocaya,P., Gidlof,A.C., Olofsson,P.S., Torma,H., and Sirsjo,A. (2007). CYP26 Inhibitor R115866 Increases Retinoid Signaling in Intimal Smooth Muscle Cells. *Arteriosclerosis, Thrombosis, and Vascular Biology* **27,** 1542-1548.

Oda,T., Elkahloun,A.G., Pike,B.L., Okajima,K., Krantz,I.D., Genin,A., Piccoli,D.A., Meltzer,P.S., Spinner,N.B., Collins,F.S. et al. (1997). Mutations in the human Jagged1 gene are responsible for Alagille syndrome. *Nat Genet* **16,** 235-242.

Ohtsuka,T., Ishibashi,M., Gradwohl,G., Nakanishi,S., Guillemot,F., and Kageyama,R. (1999). Hes1 and Hes5 as Notch effectors in mammalian neuronal differentiation. *EMBO J* **18,** 2196-2207.

Ohtsuka,T., Sakamoto,M., Guillemot,F., and Kageyama,R. (2001). Roles of the Basic Helix-Loop-Helix Genes Hes1 and Hes5 in Expansion of Neural Stem Cells of the Developing Brain. *J. Biol. Chem.* **276,** 30467-30474.

Okano,J., Kimura,W., Papaionnou,V.E., Miura,N., Yamada,G., Shiota,K., and Sakai,Y. (2012). The regulation of endogenous retinoic acid level through CYP26B1 is required for elevation of palatal shelves. *Dev. Dyn.* **241,** 1744-1756.

Okubo,T., Kawamura,A., Takahashi,J., Ohbayashi,A., and Takada,S. (2008). Tbx-associated transcriptional corepressor, Ripply3, plays essential roles in pharyngeal development. *Developmental Biology* **319,** 601.

Okubo,T., Kawamura,A., Takahashi,J., Yagi,H., Morishima,M., Matsuoka,R., and Takada,S. (2011). Ripply3, a Tbx1 repressor, is required for development of the pharyngeal apparatus and its derivatives in mice. *Development* **138,** 339-348.

Otto,D.M.E., Henderson,C.J., Carrie,D., Davey,M., Gundersen,T.E., Blomhoff,R., Adams,R.H., Tickle,C., and Wolf,C.R. (2003). Identification of Novel Roles of the

Cytochrome P450 System in Early Embryogenesis: Effects on Vasculogenesis and Retinoic Acid Homeostasis. *Mol. Cell. Biol.* **23,** 6103-6116.

Padang,R., Bagnall,R.D., Richmond,D.R., Bannon,P.G., and Semsarian,C. (2012). Rare non-synonymous variations in the transcriptional activation domains of GATA5 in bicuspid aortic valve disease. *Journal of Molecular and Cellular Cardiology* **53,** 277-281.

Pane,L.S., Zhang,Z., Ferrentino,R., Huynh,T., Cutillo,L., and Baldini,A. (2012). Tbx1 is a negative modulator of Mef2c. *Hum. Mol. Genet.*

Papangeli,I. (2010). Tbx1: potential targets and interactors relevant to development of structures affected in Digeorge Syndrome. *UCL-Institute of Child Health*.

Papangeli,I. and Scambler,P. (2012a). Tbx1 Genetically Interacts With the TGF+¦/BMP Inhibitor Smad7 During Great Vessel Remodeling. *Circulation Research*.

Papangeli,I. and Scambler,P. (2012b). The 22q11 deletion: DiGeorge and velocardiofacial syndromes and the role of TBX1. *WIREs Dev Biol*.

Parisot,P., Mesbah,K., Theveniau-Ruissy,M., and Kelly,R.G. (2011). Tbx1, subpulmonary myocardium and conotruncal congenital heart defects. *Birth Defects Research Part A: Clinical and Molecular Teratology* **91,** 477-484.

Park,E.J., Ogden,L.A., Talbot,A., Evans,S., Cai,C.L., Black,B.L., Frank,D.U., and Moon,A.M. (2006). Required, tissue-specific roles for Fgf8 in outflow tract formation and remodeling. *Development* **133,** 2419-2433.

Park,E.J., Watanabe,Y., Smyth,G., Miyagawa-Tomita,S., Meyers,E., Klingensmith,J., Camenisch,T., Buckingham,M., and Moon,A.M. (2008). An FGF autocrine loop initiated in second heart field mesoderm regulates morphogenesis at the arterial pole of the heart. *Development* **135,** 3599-3610.

Park,P.J. (2009). ChIP-seq: advantages and challenges of a maturing technology. *Nat Rev Genet* **10,** 669-680.

Pasini,A., Henrique,D., and Wilkinson,D.G. (2001). The zebrafish Hairy/Enhancer-of-split-related gene her6 is segmentally expressed during the early development of hindbrain and somites. *Mechanisms of Development* **100,** 317-321.

Pasini,A., Jiang,Y.J., and Wilkinson,D.G. (2004). Two zebrafish Notch-dependent hairy/Enhancer-of-split-related genes, her6 and her4, are required to maintain the coordination of cyclic gene expression in the presomitic mesoderm. *Development* **131,** 1529-1541.

Pasutto,F., Sticht,H., Hammersen,G., Gillessen-Kaesbach,G., FitzPatrick,D.R., Nurnberg,G., Brasch,F., Schirmer-Zimmermann,H., Tolmie,J.L., Chitayat,D. et al. (2007). Mutations in STRA6 Cause a Broad Spectrum of Malformations Including

Anophthalmia, Congenital Heart Defects, Diaphragmatic Hernia, Alveolar Capillary Dysplasia, Lung Hypoplasia, and Mental Retardation. *Am J Hum Genet* **80,** 550-560.

Paylor,R., Glaser,B., Mupo,A., Ataliotis,P., Spencer,C., Sobotka,A., Sparks,C., Choi,C.H., Oghalai,J., Curran,S. et al. (2006). Tbx1 haploinsufficiency is linked to behavioral disorders in mice and humans: Implications for 22q11 deletion syndrome. *PNAS* **103,** 7729-7734.

Paylor,R. and Lindsay,E. (2006). Mouse Models of 22q11 Deletion Syndrome. *Biol Psychiatry* **59,** 1172-1179.

Pei,D.S., Sun,Y.H., Chen,C.H., Chen,S.P., Wang,Y.P., Hu,W., and Zhu,Z.Y. (2008). Identification and characterization of a novel gene differentially expressed in zebrafish cross-subfamily cloned embryos. *BMC Developmental Biology* **8,** 29.

Pennimpede,T., Cameron,D.A., Maclean,G.A., Li,H., Abu-Abed,S., and Petkovich,M. (2010a). The role of CYP26 enzymes in defining appropriate retinoic acid exposure during embryogenesis. *Birth Defects Research Part A: Clinical and Molecular Teratology* **88,** 883-894.

Pennimpede,T., Cameron,D.A., Maclean,G.A., and Petkovich,M. (2010b). Analysis of Cyp26b1/Rarg compound-null mice reveals two genetically separable effects of retinoic acid on limb outgrowth. *Developmental Biology* **339,** 179-186.

Penton,A.L., Leonard,L.D., and Spinner,N.B. (2012). Notch signaling in human development and disease. *Seminars in Cell & Developmental Biology* **23,** 450-457.

Pijnappel,W.W.M., Hendriks,H.F.J., Folkers,G.E., van den Brink,C.E., Dekker,E.J., Edelenbosch,C., van der Saag,P.T., and Durston,A.J. (1993). The retinoid ligand 4-oxo-retinoic acid is a highly active modulator of positional specification. *Nature* **366,** 340-344.

Piotrowski,T., Ahn,D.G., Schilling,T.F., Nair,S., Ruvinsky,I., Geisler,R., Rauch,G.J., Haffter,P., Zon,L.I., Zhou,Y. et al. (2003). The zebrafish van gogh mutation disrupts tbx1, which is involved in the DiGeorge deletion syndrome in humans. *Development* **130,** 5043-5052.

Piotrowski,T. and Nusslein-Volhard,C. (2000). The Endoderm Plays an Important Role in Patterning the Segmented Pharyngeal Region in Zebrafish (Danio rerio). *Developmental Biology* **225,** 339-356.

Piotrowski,T., Schilling,T.F., Brand,M., Jiang,Y.J., Heisenberg,C.P., Beuchle,D., Grandel,H., van Eeden,F.J., Furutani-Seiki,M., Granato,M. et al. (1996). Jaw and branchial arch mutants in zebrafish II: anterior arches and cartilage differentiation. *Development* **123,** 345-356.

Plageman,T.F. and Yutzey,K.E. (2005). T-Box genes and Heart development: Putting the "T" in HearT. *Dev. Dyn.* **232,** 11-20.

Pourquie,O. (2011). Vertebrate Segmentation: From Cyclic Gene Networks to Scoliosis. *Cell* **145,** 650-663.

Prall,O.W.J., Menon,M.K., Solloway,M.J., Watanabe,Y., Zaffran,S., Bajolle,F., Biben,C., McBride,J.J., Robertson,B.R., Chaulet,H. et al. (2007). An Nkx2-5/Bmp2/Smad1 Negative Feedback Loop Controls Heart Progenitor Specification and Proliferation. *Cell* **128,** 947-959.

Priston,M., Glase,r.T., Oliver,E., Walter,M., Ritch,R., Levin,A., and Heon,E. (2006). Further support of the role of CYP1B1 in patients with Peters anomaly. *Molecular Vision* **12,** 506-510.

Probst,S., Kraemer,C., Demougin,P., Sheth,R., Martin,G.R., Shiratori,H., Hamada,H., Iber,D., Zeller,R., and Zuniga,A. (2011). SHH propagates distal limb bud development by enhancing CYP26B1-mediated retinoic acid clearance via AER-FGF signalling. *Development* **138,** 1913-1923.

Quintana,L. and Sharpe,J. (2011). Optical Projection Tomography of Vertebrate Embryo Development. *Cold Spring Harb Protoc* **2011,** db.

Radosevic,M., Robert-Moreno,A., Coolen,M., Bally-Cuif,L., and Alsina,B. (2011). Her9 represses neurogenic fate downstream of Tbx1 and retinoic acid signaling in the inner ear. *Development* **138,** 397-408.

Raetzman,L.T., Cai,J.X., and Camper,S.A. (2007). Hes1 is required for pituitary growth and melanotrope specification. *Developmental Biology* **304,** 455-466.

Raft,S., Nowotschin,S., Liao,J., and Morrow,B.E. (2004). Suppression of neural fate and control of inner ear morphogenesis by Tbx1. *Development* **131,** 1801-1812.

Randall,V., McCue,K., Roberts,C., Kyriakopoulou,V., Beddow,S., Barrett,A.N., Vitelli,F., Prescott,K., Shaw-Smith,C., Devriendt,K. et al. (2009). Great vessel development requires biallelic expression of Chd7 and Tbx1 in pharyngeal ectoderm in mice. *Journal of Clinical Investigation* **119,** 3301-3310.

Rauch,A., Zink,S., Zweier,C., Thiel,C.T., Koch,A., Rauch,R., Lascorz,J., Huffmeier,U., Weyand,M., Singer,H. et al. (2005). Systematic assessment of atypical deletions reveals genotype-phenotype correlation in 22q11.2. *J Med Genet* **42,** 871-876.

Reijntjes,S., Gale,E., and Maden,M. (2004). Generating gradients of retinoic acid in the chick embryo: Cyp26C1 expression and a comparative analysis of the Cyp26 enzymes. *Dev. Dyn.* **230,** 509-517.

Reijntjes,S., Rodaway,A., and Maden,M. (2007). The retinoic acid metabolising gene, CYP26B1, patterns the cartilaginous cranial neural crest in zebrafish. *International Journal of Developmental Biology* **51,** 351-360.

Reijntjes,S., Blentic,A., Gale,E., and Maden,M. (2005). The control of morphogen signalling: Regulation of the synthesis and catabolism of retinoic acid in the developing embryo. *Developmental Biology* **285,** 224-237.

Reijntjes,S., Gale,E., and Maden,M. (2003). Expression of the retinoic acid catabolising enzyme CYP26B1 in the chick embryo and its regulation by retinoic acid. *Gene Expression Patterns* **3,** 621-627.

Rentschler,S., Harris,B.S., Kuznekoff,L., Jain,R., Manderfield,L., Lu,M.M., Morley,G.E., Patel,V.V., and Epstein,J.A. (2011). Notch signaling regulates murine atrioventricular conduction and the formation of accessory pathways. *J Clin Invest* **121,** 525-533.

Rhinn,M. and Dolle,P. (2012). Retinoic acid signalling during development. *Development* **139,** 843-858.

Rhinn,M., Schuhbaur,B., Niederreither,K., and Dolle,P. (2011). Involvement of retinol dehydrogenase 10 in embryonic patterning and rescue of its loss of function by maternal retinaldehyde treatment. *PNAS* **108,** 16687-16692.

Ribes,V., Fraulob,V., Petkovich,M., and Dolle,P. (2007a). The oxidizing enzyme CYP26a1 tightly regulates the availability of retinoic acid in the gastrulating mouse embryo to ensure proper head development and vasculogenesis. *Dev. Dyn.* **236,** 644-653.

Ribes,V., Otto,D.M.E., Dickmann,L., Schmidt,K., Schuhbaur,B., Henderson,C., Blomhoff,R., Wolf,C.R., Tickle,C., and Dolle,P. (2007b). Rescue of cytochrome P450 oxidoreductase (Por) mouse mutants reveals functions in vasculogenesis, brain and limb patterning linked to retinoic acid homeostasis. *Developmental Biology* **303,** 66-81.

Riley,M.F., McBride,K.L., and Cole,S.E. (2011). NOTCH1 missense alleles associated with left ventricular outflow tract defects exhibit impaired receptor processing and defective EMT. *Biochimica et Biophysica Acta (BBA) - Molecular Basis of Disease* **1812,** 121-129.

Rinon,A., Lazar,S., Marshall,H., Büchmann-Møller,S., Neufeld,A., Elhanany-Tamir,H., Taketo,M.M., Sommer,L., Krumlauf,R., and Tzahor,E. (2007). Cranial neural crest cells regulate head muscle patterning and differentiation during vertebrate embryogenesis. *Development* **134,** 3065-3075.

Rizzoti,K. and Lovell-Badge,R. (2007). SOX3 activity during pharyngeal segmentation is required for craniofacial morphogenesis. *Development* **134,** 3437-3448.

Roberts,C., Ivins,S., Cook,A.C., Baldini,A., and Scambler,P.J. (2006). Cyp26 genes a1, b1 and c1 are down-regulated in Tbx1 null mice and inhibition of Cyp26 enzyme function produces a phenocopy of DiGeorge Syndrome in the chick. *Hum. Mol. Genet.* **15,** 3394-3410.

Roberts,C., Ivins,S.M., James,C.T., and Scambler,P.J. (2005). Retinoic acid down-regulates Tbx1 expression in vivo and in vitro. *Dev. Dyn.* **232,** 928-938.

Roberts,C., Sutherland,H.F., Farmer,H., Kimber,W., Halford,S., Carey,A., Brickman,J.M., Wynshaw-Boris,A., and Scambler,P.J. (2002). Targeted Mutagenesis of the Hira Gene Results in Gastrulation Defects and Patterning Abnormalities of Mesoendodermal Derivatives Prior to Early Embryonic Lethality. *Mol. Cell. Biol.* **22,** 2318-2328.

Robu,M.E., Larson,J.D., Nasevicius,A., Beiraghi,S., Brenner,C., Farber,S.A., and Ekker,E.C. (2007a). p53 Activation by Knockdown Technologies. *PLoS Genetics* **3,** 787-801.

Robu,M.E., Larson,J.D., Nasevicius,A., Beiraghi,S., Brenner,C., Farber,S.A., and Ekker,S.C. (2007b). p53 Activation by Knockdown Technologies. *PLoS Genet* **3,** e78.

Rochais,F., Dandonneau,M., Mesbah,K., Jarry,T., Mattei,M.G., and Kelly,R.G. (2009a). *Hes1* Is Expressed in the Second Heart Field and Is Required for Outflow Tract Development. *PLoS ONE* **4,** e6267.

Rochais,F., Mesbah,K., and Kelly,R.G. (2009b). Signaling Pathways Controlling Second Heart Field Development. *Circ Res* **104,** 933-942.

Roman,B.L., Pham,V.N., Lawson,N.D., Kulik,M., Childs,S., Lekven,A.C., Garrity,D.M., Moon,R.T., Fishman,M.C., Lechleider,R.J. et al. (2002). Disruption of acvrl1 increases endothelial cell number in zebrafish cranial vessels. *Development* **129,** 3009-3019.

Rosa,F.W., Wilk,A.L., and Kelsey,F.O. (1986). Teratogen update: vitamin A congeners. *Teratology* **33,** 355-364.

Ross,C.A. and Zolfaghari,R. (2011). Cytochrome P450s in the Regulation of Cellular Retinoic Acid Metabolism. *Annu. Rev. Nutr.* **31,** 65-87.

Rothenberg,F. and Fisher,S.W.M. (2003). Sculpting the Cardiac Outflow Tract. *Birth Defects Research (Part C)* **69,** 38-45.

Rutenberg,J.B., Fischer,A., Jia,H., Gessler,M., Zhong,T.P., and Mercola,M. (2006). Developmental patterning of the cardiac atrioventricular canal by Notch and Hairy-related transcription factors. *Development* **133,** 4381-4390.

Ryan,A., Goodship,J., Wilson,D., Philip,N., Levy,A., Seidel,H., Schuffenhauer,S., Oechsler,H., Belohradsky,B., Prieur,M. et al. (1997). Spectrum of clinical features associated with interstitial chromosome 22q11 deletions: a European collaborative study. *J Med Genet* **34,** 798-804.

Ryckebusch,L., Bertrand,N., Mesbah,K., Bajolle,F., Niederreither,K., Kelly,R.G., and Zaffran,S. (2010). Decreased Levels of Embryonic Retinoic Acid Synthesis

Accelerate Recovery From Arterial Growth Delay in a Mouse Model of DiGeorge Syndrome. *Circ Res* **106,** 686-694.

Ryckebusch,L., Wang,Z., Bertrand,N., Lin,S.C., Chi,X., Schwartz,R., Zaffran,S., and Niederreither,K. (2008). Retinoic acid deficiency alters second heart field formation. *PNAS* **105,** 2913-2918.

Saga,Y. (2012). The mechanism of somite formation in mice. *Current Opinion in Genetics & Development* **22,** 331-338.

Sakai,Y., Meno,C., Fujii,H., Nishino,J., Shiratori,H., Saijoh,Y., Rossant,J., and Hamada,H. (2001). The retinoic acid-inactivating enzyme CYP26 is essential for establishing an uneven distribution of retinoic acid along the anterio-posterior axis within the mouse embryo. *Genes Dev.* **15,** 213-225.

Sakata,Y., Kamei,C.N., Nakagami,H., Bronson,R., Liao,J.K., and Chin,M.T. (2002). Ventricular septal defect and cardiomyopathy in mice lacking the transcription factor CHF1/Hey2. *Proceedings of the National Academy of Sciences of the United States of America* **99,** 16197-16202.

Sambasivan,R., Gayraud-Morel,B., Dumas,G., Cimper,C., Paisant,S., Kelly,R.G., and Tajbakhsh,S. (2009). Distinct Regulatory Cascades Govern Extraocular and Pharyngeal Arch Muscle Progenitor Cell Fates. *Developmental Cell* **16,** 810-821.

Sandell,L.L., Sanderson,B.W., Moiseyev,G., Johnson,T., Mushegian,A., Young,K., Rey,J.P., Ma,J.x., Staehling-Hampton,K., and Trainor,P.A. (2007). RDH10 is essential for synthesis of embryonic retinoic acid and is required for limb, craniofacial, and organ development. *Genes Dev.* **21,** 1113-1124.

Sardiu,M.E. and Washburn,M.P. (2011). Building Protein-Protein Interaction Networks with Proteomics and Informatics Tools. *Journal of Biological Chemistry* **286,** 23645-23651.

Sasai,Y., Kageyama,R., Tagawa,Y., Shigemoto,R., and Nakanishi,S. (1992). Two mammalian helix-loop-helix factors structurally related to Drosophila hairy and Enhancer of split. *Genes Dev.* **6,** 2620-2634.

Sato,A., Scholl,A.M., Kuhn,E.B., Stadt,H.A., Decker,J.R., Pegram,K., Hutson,M.R., and Kirby,M.L. (2011). FGF8 signaling is chemotactic for cardiac neural crest cells. *Developmental Biology* **354,** 18-30.

Sato,T., Shimazaki,T., Naka,H., Fukami,S.I., Satoh,Y., Okano,H., Lax,I., Schlessinger,J., and Gotoh,N. (2010). FRS2α Regulates Erk Levels to Control a Self-Renewal Target Hes1 and Proliferation of FGF-Responsive Neural Stem/Progenitor Cells. *STEM CELLS* **28,** 1661-1673.

Sato,Y., Yasuda,K., and Takahashi,Y. (2002). Morphological boundary forms by a novel inductive event mediated by Lunatic fringe and Notch during somitic segmentation. *Development* **129,** 3633-3644.

Scambler,P. (2010). 22q11 Deletion Syndrome: A Role for TBX1 in Pharyngeal and Cardiovascular Development. *Pediatric Cardiology* **31,** 378-390.

Scambler,P.J. (2000). The 22q11 deletion syndromes. *Hum. Mol. Genet.* **9,** 2421-2426.

Scheer,N., Groth,A., Hans,S., and Campos-Ortega,J.A. (2001). An instructive function for Notch in promoting gliogenesis in the zebrafish retina. *Development* **128,** 1099-1107.

Scheer,N. and Campos-Ortega,J.A. (1999). Use of the Gal4-UAS technique for targeted gene expression in the zebrafish. *Mechanisms of Development* **80,** 153-158.

Scheer,N., Riedl,I., Warren,J.T., Kuwada,J.Y., and Campos-Ortega,J.A. (2002). A quantitative analysis of the kinetics of Gal4 activator and effector gene expression in the zebrafish. *Mechanisms of Development* **112,** 9-14.

Schilling,T.F. and Kimmel,C.B. (1994). Segment and cell-type restricted lineages during pharyngeal arch development in the zebrafish embryo. *Development* **120,** 483-494.

Schilling,T.F. and Kimmel,C.B. (1997). Musculoskeletal patterning in the pharyngeal segments of the zebrafish embryo. *Development* **124,** 2945-2960.

Schindelin,J., Arganda-Carreras,I., Frise,E., Kaynig,V., Longair,M., Pietzsch,T., Preibisch,S., Rueden,C., Saalfeld,S., Schmid,B. et al. (2012). Fiji: an open-source platform for biological-image analysis. *Nat Meth* **9,** 676-682.

Schneider,R.A., Hu,D., Rubenstein,J.L.R., Maden,M., and Helms,J.A. (2001). Local retinoid signaling coordinates forebrain and facial morphogenesis by maintaining FGF8 and SHH. *Development* **128,** 2755-2767.

Scholpp,S., Delogu,A., Gilthorpe,J., Peukert,D., Schindler,S., and Lumsden,A. (2009). Her6 regulates the neurogenetic gradient and neuronal identity in the thalamus. *PNAS* **106,** 19895-19900.

Schulz,R.A. and Yutzey,K.E. (2004). Calcineurin signaling and NFAT activation in cardiovascular and skeletal muscle development. *Developmental Biology* **266,** 1-16.

Seo,J.h., Suenaga,A., Hatakeyama,M., Taiji,M., and Imamoto,A. (2009). Structural and Functional Basis of a Role for CRKL in a Fibroblast Growth Factor 8-Induced Feed-Forward Loop. *Mol. Cell. Biol.* **29,** 3076-3087.

Seo,S. and Kume,T. (2006). Forkhead transcription factors, Foxc1 and Foxc2, are required for the morphogenesis of the cardiac outflow tract. *Developmental Biology* **296,** 421-436.

Sharpe,J., Ahlgren,U., Perry,P., Hill,B., Ross,A., Hecksher-Sorensen,J., Baldock,R., and Davidson,D. (2002). Optical projection tomography as a tool for 3D microscopy and gene expression studies. *Science* **296,** 541-545.

Shen,A.L., O'Leary,K.A., and Kasper,C.B. (2002). Association of Multiple Developmental Defects and Embryonic Lethality with Loss of Microsomal NADPH-Cytochrome P450 Oxidoreductase. *J. Biol. Chem.* **277,** 6536-6541.

Shenefelt,R.E. (1972). Gross congenital malformations. Animal model: treatment of various species with a large dose of vitamin A at known stages in pregnancy. *Am. J. Pathol.* **66,** 589-592.

Shimojo,H., Ohtsuka,T., and Kageyama,R. (2008). Oscillations in Notch Signaling Regulate Maintenance of Neural Progenitors. *Neuron* **58,** 52-64.

Shirai,M., Imanaka-Yoshida,K., Schneider,M.D., Schwartz,R.J., and Morisaki,T. (2009). T-box 2, a mediator of Bmp-Smad signaling, induced hyaluronan synthase 2 and Tgfβ2 expression and endocardial cushion formation. *PNAS* **106,** 18604-18609.

Siekmann,A.F. and Lawson,N.D. (2007). Notch signalling limits angiogenic cell behaviour in developing zebrafish arteries. *Nature* **445,** 781-784.

Simoes-costa,M.S., Azambuja,A.P., and Xavier-Neto,J. (2008). The search for non-chordate retinoic acid signaling: lessons from chordates. *J. Exp. Zool.* **310B,** 54-72.

Singh,M.K., Christoffels,V.M., Dias,J.M., Trowe,M.O., Petry,M., Schuster-Gossler,K., Burger,A., Ericson,J., and Kispert,A. (2005). Tbx20 is essential for cardiac chamber differentiation and repression of Tbx2. *Development* **132,** 2697-2707.

Singh,R., Horsthuis,T., Farin,H.F., Grieskamp,T., Norden,J., Petry,M., Wakker,V., Moorman,A.F.M., Christoffels,V.M., and Kispert,A. (2009). Tbx20 Interacts With Smads to Confine Tbx2 Expression to the Atrioventricular Canal. *Circ Res* **105,** 442-452.

Sinha,S., Abraham,S., Gronostajski,R.M., and Campbell,C.E. (2000). Differential DNA binding and transcription modulation by three T-box proteins, T, TBX1 and TBX2. *Gene* **258,** 15-29.

Sirbu,I.O., Gresh,L., Barra,J., and Duester,G. (2005). Shifting boundaries of retinoic acid activity control hindbrain segmental gene expression. *Development* **132,** 2611-2622.

Sockanathan,S. and Jessell,T.M. (1998). Motor Neuron-Derived Retinoid Signaling Specifies the Subtype Identity of Spinal Motor Neurons. *Cell* **94,** 503-514.

Sparrow,D.B., Chapman,G., Smith,A.J., Mattar,M.Z., Major,J.A., O'Reilly,V.C., Saga,Y., Zackai,E.H., Dormans,J.P., Alman,B.A. et al. (2012). A Mechanism for Gene-Environment Interaction in the Etiology of Congenital Scoliosis. *Cell* **149,** 295-306.

Sparrow,D., Chapman,G., and Dunwoodie,S. (2011). The mouse notches up another success: understanding the causes of human vertebral malformation. *Mamm Genome* **22,** 362-376.

Spoorendonk,K.M., Peterson-Maduro,J., Renn,J., Trowe,T., Kranenbarg,S., Winkler,C., and Schulte-Merker,S. (2008). Retinoic acid and Cyp26b1 are critical regulators of osteogenesis in the axial skeleton. *Development* **135,** 3765-3774.

Stalmans,I., Lambrechts,D., De Smet,F., Jansen,S., Wang,J., Maity,S., Kneer,P., von der,O.M., Swillen,A., Maes,C. et al. (2003). VEGF: a modifier of the del22q11 (DiGeorge) syndrome? *Nat. Med.* **9,** 173-182.

Stamataki,D., Holder,M., Hodgetts,C., Jeffery,R., Nye,E., Spencer-Dene,B., Winton,D.J., and Lewis,J. (2011). Delta1 Expression, Cell Cycle Exit, and Commitment to a Specific Secretory Fate Coincide within a Few Hours in the Mouse Intestinal Stem Cell System. *PLoS ONE* **6,** e24484.

Stennard,F.A., Costa,M.W., Elliott,D.A., Rankin,S., Haast,S.J.P., Lai,D., McDonald,L.P.A., Niederreither,K., Dolle,P., and Bruneau,B.G. (2003). Cardiac T-box factor Tbx20 directly interacts with Nkx2-5, GATA4, and GATA5 in regulation of gene expression in the developing heart. *Developmental Biology* **262,** 206-224.

Stennard,F.A., Costa,M.W., Lai,D., Biben,C., Furtado,M.B., Solloway,M.J., McCulley,D.J., Leimena,C., Preis,J.I., Dunwoodie,S.L. et al. (2005). Murine T-box transcription factor Tbx20 acts as a repressor during heart development, and is essential for adult heart integrity, function and adaptation. *Development* **132,** 2451-2462.

Stoller,J.Z. and Epstein,J.A. (2005). Cardiac neural crest. *Seminars in Cell & Developmental Biology* **16,** 704-715.

Stoller,J.Z., Huang,L., and Epstein,J.A. (2008). Ash2l: A Novel interacting cofactor of DiGeorge syndrome transcription factor Tbx1. *Developmental Biology* **319,** 596-597.

Stoppie,P., Borgers,M., Borghgraef,P., Dillen,L., Goossens,J., Sanz,G., Szel,H., Van Hove,C., Van Nyen,G., Nobels,G. et al. (2000). R115866 Inhibits All-trans-Retinoic Acid Metabolism and Exerts Retinoidal Effects in Rodents. *J Pharmacol Exp Ther* **293,** 304-312.

Stratford,T., Logan,C., Zile,M., and Maden,M. (1999). Abnormal anteroposterior and dorsoventral patterning of the limb bud in the absence of retinoids. *Mechanisms of Development* **81,** 115-125.

Stratford,T., Horton,C., and Maden,M. (1996). Retinoic acid is required for the initiation of outgrowth in the chick limb bud. *Current Biology* **6,** 1124-1133.

Streit,A., Lee,K.J., Woo,I., Roberts,C., Jessell,T.M., and Stern,C.D. (1998). Chordin regulates primitive streak development and the stability of induced neural cells, but is not sufficient for neural induction in the chick embryo. *Development* **125,** 507-519.

Strunk,K.E., Amann,V., and Threadgill,D.W. (2004). Phenotypic Variation Resulting From a Deficiency of Epidermal Growth Factor Receptor in Mice Is Caused by Extensive Genetic Heterogeneity That Can Be Genetically and Molecularly Partitioned. *Genetics* **167,** 1821-1832.

Sullivan,K.E. (2004). The clinical, immunological, and molecular spectrum of chromosome 22q11.2 deletion syndrome and DiGeorge syndrome. *Current Opinion in Allergy and Clinical Immunology* **4,** 505-512.

Sumazaki,R., Shiojiri,N., Isoyama,S., Masu,M., Keino-Masu,K., Osawa,M., Nakauchi,H., Kageyama,R., and Matsui,A. (2004). Conversion of biliary system to pancreatic tissue in Hes1-deficient mice. *Nat Genet* **36,** 83-87.

Summerbell,D. (1983). The effect of local application of retinoic acid to the anterior margin of the developing chick limb. *Journal of Embryology and Experimental Morphology* **78,** 269-289.

Suster,M.L., Abe,G., Schouw,A., and Kawakami,K. (2011). Transposon-mediated BAC transgenesis in zebrafish. *Nat. Protocols* **6,** 1998-2021.

Swillen,A., Vogels,A., Devriendt,K., and Fryns,J.P. (2000). Chromosome 22q11 deletion syndrome: Update and review of the clinical features, cognitive-behavioral spectrum, and psychiatric complications. *Am. J. Med. Genet.* **97,** 128-135.

Swindell,E.C., Thaller,C., Sockanathan,S., Petkovich,M., Jessell,T.M., and Eichele,G. (1999). Complementary Domains of Retinoic Acid Production and Degradation in the Early Chick Embryo. *Developmental Biology* **216,** 282-296.

Tada,M. and Smith,J.C. (2001). T-targets:Clues to understanding the functions of T-box proteins. *Develop. Growth Differ.* **43,** 1-11.

Taddei,I., Morishima,M., Huynh,T., and Lindsay,E.A. (2001). Genetic factors are major determinants of phenotypic variability in a mouse model of the DiGeorge/del22q11 syndromes. *PNAS* **98,** 11428-11431.

Tahayato,A., Dolle,P., and Petkovich,M. (2003). Cyp26C1 encodes a novel retinoic acid-metabolizing enzyme expressed in the hindbrain, inner ear, first branchial arch and tooth buds during murine development. *Gene Expression Patterns* **3,** 449-454.

Takada,S., Stark,K.L., Shea,M.J., Vassileva,G., McMahon,J.A., and McMahon,A.P. (1994). Wnt-3a regulates somite and tailbud formation in the mouse embryo. *Genes & Development* **8,** 174-189.

Takebayashi,K., Sasai,Y., Sakai,Y., Watanabe,T., Nakanishi,S., and Kageyama,R. (1994). Structure, chromosomal locus, and promoter analysis of the gene encoding the mouse helix-loop-helix factor HES-1. Negative autoregulation through the multiple N box elements. *J. Biol. Chem.* **269,** 5150-5156.

Takeuchi,J.K. and Bruneau,B.G. (2009). Directed transdifferentiation of mouse mesoderm to heart tissue by defined factors. *Nature* **459,** 708-711.

Takeuchi,J.K., Mileikovskaia,M., Koshiba-Takeuchi,K., Heidt,A.B., Mori,A.D., Arruda,E.P., Gertsenstein,M., Georges,R., Davidson,L., Mo,R. et al. (2005). Tbx20 dose-dependently regulates transcription factor networks required for mouse heart and motoneuron development. *Development* **132,** 2463-2464.

Takeuchi,J.K., Ohgi,M., Koshiba-Takeuchi,K., Shiratori,H., Sakaki,I., Ogura,K., Saijoh,Y., and Ogura,T. (2003). Tbx5 specifies the left/right ventricles and ventricular septum position during cardiogenesis. *Development* **130,** 5953-5964.

Tanibe,M., Michuie.T., Yukita,Y., Danno,H., Ikuzawa,M., and Ishiura,S.A.A. (2008). Retinoic metabolizing factor *xCyp26c* is specifically expressed in neuroectoderm and regulated anterior neural patterning in *Xenopus laevis*. *International Journal of Developmental Biology* **52,** 893-901.

Tanigaki,K., Nogaki,F., Takahashi,J., Tashiro,K., Kurooka,H., and Honjo,T. (2001). Notch1 and Notch3 Instructively Restrict bFGF-Responsive Multipotent Neural Progenitor Cells to an Astroglial Fate. *Neuron* **29,** 45-55.

Tateya,T., Imayoshi,I., Tateya,I., Ito,J., and Kageyama,R. (2011). Cooperative functions of Hes/Hey genes in auditory hair cell and supporting cell development. *Developmental Biology* **352,** 329-340.

Tavares,A.L.P., Garcia,E.L., Kuhn,K., Woods,C.M., Williams,T., and Clouthier,D.E. (2012). Ectodermal-derived Endothelin1 is required for patterning the distal and intermediate domains of the mouse mandibular arch. *Developmental Biology* **371,** 47-56.

Tazumi,S., Yabe,S., and Uchiyama,H. (2010). Paraxial T-box genes, Tbx6 and Tbx1, are required for cranial chondrogenesis and myogenesis. *Developmental Biology* **346,** 170-180.

Thisse,B., Pflumio,F., Furthauer,M., Loppin,B., Heyer,V., Degrave,A., Woehl,R., Lux,A., Steffan,T., Charbonnier,X.Q. et al. (2001). Expression of the zebrafish genome during embryogenesis (NIH R01 RR15402). *ZFIN Direct Data Submission zfin. org*.

Thisse,B. and Thisse,C. (2004). Fast Release Clones: A High Throughput Expression Analysis. *ZFIN Direct Data Submission zfin. org*.

Thisse,C. and Thisse,B. (2005). High Throughput Expression Analysis of ZF-Models Consortium Clones. *ZFIN Direct Data Submission zfin. org*.

Thomas,P.S., Sridurongrit,S., Ruiz-Lozano,P., and Kaartinen,V. (2012). Deficient Signaling via Alk2 (Acvr1) Leads to Bicuspid Aortic Valve Development. *PLoS ONE* **7,** e35539.

Timmerman,L.A., Grego-Bessa,J., Raya,A., Bertran,E., Perez-Pomares,J.M., Diez,J., Aranda,S., Palomo,S., McCormick,F., Izpisua-Belmonte,J.C. et al. (2004). Notch promotes epithelial-mesenchymal transition during cardiac development and oncogenic transformation. *Genes Dev.* **18,** 99-115.

Tirosh-Finkel,L., Elhanany,H., Rinon,A., and Tzahor,E. (2006). Mesoderm progenitor cells of common origin contribute to the head musculature and the cardiac outflow tract. *Development* **133,** 1943-1953.

Tomita,K., Hattori,M., Nakamura,E., Nakanishi,S., Minato,N., and Kageyama,R. (1999). The bHLH gene Hes1 is essential for expansion of early T cell precursors. *Genes Dev.* **13,** 1203-1210.

Tomita,K., Ishibashi,M., Nakahara,K., Ang,S.L., Nakanishi,S., Guillemot,F., and Kageyama,R. (1996). Mammalian hairy and Enhancer of Split Homolog 1 Regulates Differentiation of Retinal Neurons and Is Essential for Eye Morphogenesis. *Neuron* **16,** 723-734.

Torres,J., Prieto,J., Durupt,F.C., Broad,S., and Watt,F.M. (2012). Efficient Differentiation of Embryonic Stem Cells into Mesodermal Precursors by BMP, Retinoic Acid and Notch Signalling. *PLoS ONE* **7,** e36405.

Towbin,J., and, and Belmont,J. (2000). Molecular Determinants of Left and Right Outflow Tract Obstruction. *American Journal of Medical Genetics* **97,** 297-303.

Tucker,A.S. and Lumsden,A. (2004). Neural crest cells provide species-specific patterning information in the developing branchial skeleton. *Evolution & Development* **6,** 32-40.

Tumer,Z. and Bach-Holm,D. (2009). Axenfeld-Rieger syndrome and spectrum of PITX2 and FOXC1 mutations. *Eur J Hum Genet* **17,** 1527-1539.

Tzahor E. and Evans S.M. (2011). Pharyngeal mesoderm development during embryogenesis: implications for both heart and head myogenesis. *Cardiovasc Res.* **91(2),** 196-202.

Uehara,M., Yashiro,K., Mamiya,S., Nishino,J., Chambon,P., Dolle,P., and Sakai,Y. (2007). CYP26A1 and CYP26C1 cooperatively regulate anterior-posterior patterning of the developing brain and the production of migratory cranial neural crest cells in the mouse. *Developmental Biology* **302,** 399-411.

Uehara,M., Yashiro,K., Takaoka,K., Yamamoto,M., and Hamada,H. (2009). Removal of maternal retinoic acid by embryonic CYP26 is required for correct Nodal expression during early embryonic patterning. *Genes & Development* **23,** 1689-1698.

Ueo,T., Imayoshi,I., Kobayashi,T., Ohtsuka,T., Seno,H., Nakase,H., Chiba,T., and Kageyama,R. (2012). The role of Hes genes in intestinal development, homeostasis and tumor formation. *Development* **139,** 1071-1082.

van Bueren,K.L., Papangeli,I., Rochais,F., Pearce,K., Roberts,C., Calmont,A., Szumska,D., Kelly,R.G., Bhattacharya,S., and Scambler,P.J. (2010). Hes1 expression is reduced in Tbx1 null cells and is required for the development of structures affected in 22q11 deletion syndrome. *Developmental Biology* **340,** 369-380.

Vermot,J., Llamas,J.G., Fraulob,V., Niederreither,K., Chambon,P., and Dolle,P. (2005). Retinoic Acid Controls the Bilateral Symmetry of Somite Formation in the Mouse Embryo. *Science* **308,** 563-566.

Vermot,J., Niederreither,K., Garnier,J.M., Chambon,P., and Dollé,P. (2003). Decreased embryonic retinoic acid synthesis results in a DiGeorge syndrome phenotype in newborn mice. *PNAS* **100,** 1763-1768.

Vincent,S.D. and Buckingham,M.E. (2010). How to Make a Heart: The Origin and Regulation of Cardiac Progenitor Cells. In *Current Topics in Developmental Biology; Organogenesis in Development*. (ed. Peter,K.), pp. 1-41. Academic Press.

Vitelli,F., Morishima,M., Taddei,I., Lindsay,E.A., and Baldini,A. (2002a). Tbx1 mutation causes multiple cardiovascular defects and disrupts neural crest and cranial nerve migratory pathways. *Hum. Mol. Genet.* **11,** 915-922.

Vitelli,F., Taddei,I., Morishima,M., Meyers,E.N., Lindsay,E.A., and Baldini,A. (2002b). A genetic link between Tbx1 and fibroblast growth factor signaling. *Development* **129,** 4605-4611.

Vitelli,F., Viola,A., Morishima,M., Pramparo,T., Baldini,A., and Lindsay,E. (2003). TBX1 is required for inner ear morphogenesis. *Hum. Mol. Genet.* **12,** 2041-2048.

Vitelli,F., Huynh,T., and Baldini,A. (2009). Gain of function of Tbx1 affects pharyngeal and heart development in the mouse. *Genesis* **47,** 188-195.

Vitelli,F., Lania,G., Huynh,T., and Baldini,A. (2010). Partial rescue of the Tbx1 mutant heart phenotype by Fgf8: Genetic evidence of impaired tissue response to Fgf8. *Journal of Molecular and Cellular Cardiology* **49,** 836-840.

Vitelli,F., Zhang,Z., Huynh,T., Sobotka,A., Mupo,A., and Baldini,A. (2006). Fgf8 expression in the Tbx1 domain causes skeletal abnormalities and modifies the aortic arch but not the outflow tract phenotype of Tbx1 mutants. *Developmental Biology* **295,** 559-570.

von Gise,A., Zhou,B., Honor,L.B., Ma,Q., Petryk,A., and Pu,W.T. (2011). WT1 regulates epicardial epithelial to mesenchymal transition through +¦-catenin and retinoic acid signaling pathways. *Developmental Biology* **356,** 421-431.

Voss,A., Vanyai,H., Collin,C., Dixon,M., McLennan,T., Sheikh,B., Scambler,P., and Thomas,T. (2012). MOZ Regulates the Tbx1 Locus, and Moz Mutation Partially Phenocopies DiGeorge Syndrome. *Developmental Cell*.

Vrijens,K., Thys,S., De Jeu,M.T., Postnov,A.A., Pfister,M., Cox,L., Zwijsen,A., Van Hoof,V., Mueller,M., De Clerck,N.M. et al. (2006). Ozzy, a Jag1 vestibular mouse mutant, displays characteristics of Alagille syndrome. *Neurobiology of Disease* **24,** 28-40.

Wagner,E., McCaffery,P., and Drager,U.C. (2000). Retinoic Acid in the Formation of the Dorsoventral Retina and Its Central Projections. *Developmental Biology* **222,** 460-470.

Waldo,K., Miyagawa-Tomita,S., Kumiski,D., and Kirby,M.L. (1998). Cardiac Neural Crest Cells Provide New Insight into Septation of the Cardiac Outflow Tract: Aortic Sac to Ventricular Septal Closure. *Developmental Biology* **196,** 129-144.

Waldo,K.L., Hutson,M.R., Stadt,H.A., Zdanowicz,M., Zdanowicz,J., and Kirby,M.L. (2005a). Cardiac neural crest is necessary for normal addition of the myocardium to the arterial pole from the secondary heart field. *Developmental Biology* **281,** 66-77.

Waldo,K.L., Hutson,M.R., Ward,C.C., Zdanowicz,M., Stadt,H.A., Kumiski,D., Abu-Issa,R., and Kirby,M.L. (2005b). Secondary heart field contributes myocardium and smooth muscle to the arterial pole of the developing heart. *Developmental Biology* **281,** 78-90.

Wall,D., Wang,Y., and Wallace,V. (2005). Interaction Between the Shh and Notch Signaling Pathways in Retinal Development. *Invest. Ophthalmol. Vis. Sci.* **46,** 586.

Wall,D.S., Mears,A.J., McNeill,B., Mazerolle,C., Thurig,S., Wang,Y., Kageyama,R., and Wallace,V.A. (2009). Progenitor cell proliferation in the retina is dependent on Notch-independent Sonic hedgehog/Hes1 activity. *J. Cell Biol.* **184,** 101-112.

Walshe,J. and Mason,I. (2003). Fgf signalling is required for formation of cartilage in the head. *Developmental Biology* **264,** 522-536.

Wang,D.Z., Chang,P.S., Wang,Z., Sutherland,L., Richardson,J.A., Small,E., Krieg,P.A., and Olson,E.N. (2001). Activation of Cardiac Gene Expression by Myocardin, a Transcriptional Cofactor for Serum Response Factor. *Cell* **105,** 851-862.

Wang,J., Greene,S.B., Bonilla-Claudio,M., Tao,Y., Zhang,J., Bai,Y., Huang,Z., Black,B.L., Wang,F., and Martin,J.F. (2010). Bmp Signaling Regulates Myocardial Differentiation from Cardiac Progenitors Through a MicroRNA-Mediated Mechanism. *Developmental Cell* **19,** 903-912.

Wang,M.M. (2011). Notch signaling and Notch signaling modifiers. *The International Journal of Biochemistry & Cell Biology* **43,** 1550-1562.

Wang,Y., Wu,L., Wang,P., Lv,C., Yang,Z., and Tang,X. (2012). Manipulation of gene expression in zebrafish using caged circular morpholino oligomers. *Nucleic Acids Research* **40,** 11155-11162.

Ward,C., Stadt,H., Hutson,M., and Kirby,M.L. (2005). Ablation of the secondary heart field leads to tetralogy of Fallot and pulmonary atresia. *Developmental Biology* **284,** 72-83.

Washington Smoak,I., Byrd,N.A., Abu-Issa,R., Goddeeris,M.M., Anderson,R., Morris,J., Yamamura,K., Klingensmith,J., and Meyers,E.N. (2005). Sonic hedgehog is required for cardiac outflow tract and neural crest cell development. *Developmental Biology* **283,** 357-372.

Watanabe,T., Koibuchi,N., and Chin,M.T. (2010). Transcription factor CHF1/Hey2 regulates coronary vascular maturation. *Mechanisms of Development* **127,** 418-427.

Watanabe,Y., Kokubo,H., Miyagawa-Tomita,S., Endo,M., Igarashi,K., Aisaki,K.i., Kanno,J., and Saga,Y. (2006). Activation of Notch1 signaling in cardiogenic mesoderm induces abnormal heart morphogenesis in mouse. *Development* **133,** 1625-1634.

Watanabe,Y., Zaffran,S.p., Kuroiwa,A., Higuchi,H., Ogura,T., Harvey,R.P., Kelly,R.G., and Buckingham,M. (2012). Fibroblast growth factor 10 gene regulation in the second heart field by Tbx1, Nkx2-5, and Islet1 reveals a genetic switch for down-regulation in the myocardium. *PNAS* **109,** 18273-18280.

Webb,S., Qayyum,S., Anderson,R., Lamers,W., and Richardson,M. (2003). Septation and separation within the outflow tract of the developing heart. *J. Anat.* **202,** 327-342.

Weinberg,E.S., Allende,M.L., Kelly,C.S., Abdelhamid,A., Murakami,T., Andermann,P., Doerre,O.G., Grunwald,D.J., and Riggleman,B. (1996). Developmental regulation of zebrafish MyoD in wild-type, no tail and spadetail embryos. *Development* **122,** 271-280.

Weinstein,B.M., Stemple,D.L., Driever,W., and Fishman,M.C. (1995). gridlock, a localized heritable vascular patterning defect in the zebrafish. *Nat Med* **1,** 1143-1147.

Wendling,O., Dennefeld,C., Chambon,P., and Mark,M. (2000). Retinoid signaling is essential for patterning the endoderm of the third and fourth pharyngeal arches. *Development* **127,** 1553-1562.

Wendling,O., Ghyselinck,N.B., Chambon,P., and Mark,M. (2001). Roles of retinoic acid receptors in early embryonic morphogenesis and hindbrain patterning. *Development* **128,** 2031-2038.

Wendorff,A.A., Koch,U., Wunderlich,F.T., Wirth,S., Dubey,C., Br^{3}ning,J.C., MacDonald,H.R., and Radtke,F. (2010). Hes1 Is a Critical but Context-Dependent Mediator of a Canonical Notch Signaling in Lymphocyte Development and Transformation. *Immunity* **33,** 671-684.

White,J.A., Guo,Y.D., Baetz,K., Beckett-Jones,B., Bonasoro,J., Hsu,K.E., Dilworth,F.J., Jones,G., and Petkovich,M. (1996). Identification of the Retinoic Acid-inducible All-trans-retinoic Acid 4-Hydroxylase. *J. Biol. Chem.* **271,** 29922-29927.

White,J.A., Ramshaw,H., Taimi,M., Stangle,W., Zhang,A., Everingham,S., Creighton,S., Tam,S.P., Jones,G., and Petkovich,M. (2000a). Identification of the human cytochrome P450, P450RAI-2, which is predominantly expressed in the adult cerebellum and is responsible for all-trans-retinoic acid metabolism. *PNAS* **97,** 6403-6408.

White,J.C., Highland,M., Kaiser,M., and Clagett-Dame,M. (2000b). Vitamin A Deficiency Results in the Dose-Dependent Acquisition of Anterior Character and Shortening of the Caudal Hindbrain of the Rat Embryo. *Developmental Biology* **220,** 263-284.

Whitfield,T.T., Granato,M., van Eeden,F.J., Schach,U., Brand,M., Furutani-Seiki,M., Haffter,P., Hammerschmidt,M., Heisenberg,C.P., Jiang,Y.J. et al. (1996). Mutations affecting development of the zebrafish inner ear and lateral line. *Development* **123,** 241-254.

Wiese,C., Grieskamp,T., Airik,R., Mommersteeg,M.T.M., Gardiwal,A., de Gier-de Vries,C., Schuster-Gossler,K., Moorman,A.F.M., Kispert,A., and Christoffels,V.M. (2007). Formation of the Sinus Node Head and Differentiation of Sinus Node Myocardium Are Independently Regulated by Tbx18 and Tbx3. *Circ Res* **104,** 388-397.

Wiese,C., Heisig,J., and Gessler,M. (2010). Hey bHLH Factors in Cardiovascular Development. *Pediatric Cardiology* **31,** 363-370.

Wilkinson D (1992). Whole mount *in situ* hybridization of vertebrate embryos. In *In situ hybridization: a practical approach*. (ed. Wilkinson D), pp. 75-84. Oxford, England: IRL Press.

Wilkinson,D.G., Bhatt,S., and Herrmann,B.G. (1990). Expression pattern of the mouse T gene and its role in mesoderm formation. *Nature* **343,** 657-659.

Wilson,D.I., Goodship,J.A., Burn,J., Cross,I.E., and Scambler,P.J. (1992). Deletions within chromosome 22q11 in familial congenital heart disease. *The Lancet* **340,** 573-575.

Wilson,V. and and Conlon,F.L. (2002). The T-box family. *Genome Biology* **3,** reviews30008.1-reviews3008.7.

Winkler,C., Elmasri,H., Klamt,B., Volff,K., and Gessler,M. (2003). Characterization of hey bHLH genes in teleost fish. *Development Genes and Evolution* **213,** 541-543.

Wurdak,H., Ittner,L.M., Lang,K.S., Leveen,P., Suter,U., Fischer,J.A., Karlsson,S., Born,W., and Sommer,L. (2005). Inactivation of TGFβ signaling in neural crest stem cells leads to multiple defects reminiscent of DiGeorge syndrome. *Genes Dev.* **19,** 530-535.

Xi,J. and Yang,Z. (2008). Expression of RALDHs (ALDH1As) and CYP26s in human tissues and during the neural differentiation of P19 embryonal carcinoma stem cell. *Gene Expression Patterns* **8,** 438-442.

Xiang,F., Sakata,Y., Cui,L., Youngblood,J.M., Nakagami,H., Liao,J.K., Liao,R., and Chin,M.T. (2006). Transcription factor CHF1/Hey2 suppresses cardiac hypertrophy through an inhibitory interaction with GATA4. *American Journal of Physiology - Heart and Circulatory Physiology* **290,** H1997-H2006.

Xu,H., Cerrato,F., and Baldini,A. (2005). Timed mutation and cell-fate mapping reveal reiterated roles of Tbx1 during embryogenesis, and a crucial function during segmentation of the pharyngeal system via regulation of endoderm expansion. *Development* **132,** 4387-4395.

Xu,H., Chen,L., and Baldini,A. (2007a). In vivo genetic ablation of the periotic mesoderm affects cell proliferation survival and differentiation in the cochlea. *Developmental Biology* **310,** 329-340.

Xu,H., Morishima,M., Wylie,J.N., Schwartz,R.J., Bruneau,B.G., Lindsay,E.A., and Baldini,A. (2004). Tbx1 has a dual role in the morphogenesis of the cardiac outflow tract. *Development* **131,** 3217-3227.

Xu,H., Viola,A., Zhang,Z., Gerken,C.P., Lindsay-Illingworth,E.A., and Baldini,A. (2007b). Tbx1 regulates population, proliferation and cell fate determination of otic epithelial cells. *Developmental Biology* **302,** 670-682.

Xu,Q., Holder,N., Patient,R., and Wilson,S.W. (1994). Spatially regulated expression of three receptor tyrosine kinase genes during gastrulation in the zebrafish. *Development* **120,** 287-299.

Xue,Y., Gao,X., Lindsell,C.E., Norton,C.R., Chang,B., Hicks,C., Gendron-Maguire,M., Rand,E.B., Weinmaster,G., and Gridley,T. (1999). Embryonic Lethality and Vascular Defects in Mice Lacking the Notch Ligand Jagged1. *Hum. Mol. Genet.* **8,** 723-730.

Yagi,H., Furutani,Y., Hamada,H., Sasaki,T., Asakawa,S., Minoshima,S., Ichida,F., Joo,K., Kimura,M., and Imamura,S.i. (2003). Role of TBX1 in human del22q11.2 syndrome. *The Lancet* **362,** 1366-1373.

Yamagishi,H. (2003). Tbx1 is regulated by tissue-specific forkhead proteins through a common Sonic hedgehog-responsive enhancer. *Genes Dev.* **7,** 269-281.

Yamagishi,H., Maeda,J., Hu,T., McAnally,J., Conway,S.J., Kume,T., Meyers,E.N., Yamagishi,C., and Srivastava,D. (2003). Tbx1 is regulated by tissue-specific forkhead proteins through a common Sonic hedgehog-responsive enhancer. *Genes Dev.* **17,** 269-281.

Yamagishi,H. and Srivastava,D. (2003). Unraveling the genetic and developmental mysteries of 22q11 deletion syndrome. *Trends in Molecular Medicine* **9,** 383-389.

Yamaguchi,T.P., Takada,S., Yoshikawa,Y., Wu,N., and McMahon,A.P. (1999). T (Brachyury) is a direct target of Wnt3a during paraxial mesoderm specification. *Genes & Development* **13,** 3185-3190.

Yamamoto,Y., Zolfaghari,R., and Ross,A.C. (2000). Regulation of CYP26 (cytochrome P450RAI) mRNA expression and retinoic acid metabolism by retinoids and dietary vitamin A in liver of mice and rats. *FASEB J.* **14,** 2119-2127.

Yang,J., Bucker,S., Jungblut,B., Bottger,T., Cinnamon,Y., Tchorz,J., M++ller,M., Bettler,B., Harvey,R., Sun,Q.Y. et al. (2012). Inhibition of Notch2 by Numb/Numblike controls myocardial compaction in the heart. *Cardiovascular Research* **96,** 276-285.

Yashiro,K., Zhao,X., Uehara,M., Yamashita,K., Nishijima,M., Nishino,J., Saijoh,Y., Sakai,Y., and Hamada,H. (2004). Regulation of Retinoic Acid Distribution Is Required for Proximodistal Patterning and Outgrowth of the Developing Mouse Limb. *Developmental Cell* **6,** 411-422.

Yasuhiko,Y., Haraguchi,S., Kitajima,S., Takahashi,Y., Kanno,J., and Saga,Y. (2006). Tbx6-mediated Notch signaling controls somite-specific Mesp2 expression. *Proceedings of the National Academy of Sciences of the United States of America* **103,** 3651-3656.

Yasuhiko,Y., Kitajima,S., Takahashi,Y., Oginuma,M., Kagiwada,H., Kanno,J., and Saga,Y. (2008). Functional importance of evolutionally conserved Tbx6 binding sites in the presomitic mesoderm-specific enhancer of Mesp2. *Development* **135,** 3511-3519.

Yelbuz,T.M., Waldo,K.L., Kumiski,D.H., Stadt,H.A., Wolfe,R.R., Leatherbury,L., and Kirby,M.L. (2002). Shortened Outflow Tract Leads to Altered Cardiac Looping After Neural Crest Ablation. *Circulation* **106,** 504-510.

Yen,H.Y., Ting,M.C., and Maxson,R.E. (2010). Jagged1 functions downstream of Twist1 in the specification of the coronal suture and the formation of a boundary between osteogenic and non-osteogenic cells. *Developmental Biology* **347,** 258-270.

Yoshikawa,Y., Fujimori,T., McMahon,A.P., and Takada,S. (1997). Evidence That Absence ofWnt-3aSignaling Promotes Neuralization Instead of Paraxial Mesoderm Development in the Mouse. *Developmental Biology* **183,** 234-242.

Zaffran,S. and Kelly,R.G. (2012). New developments in the second heart field. *Differentiation* **84,** 17-24.

Zhang,L., Zhong,T., Wang,Y., Jiang,Q., Song,H., and Gui Y. (2006a). TBX1, a DiGeorge syndrome candidate gene, is inhibited by retinoic acid. *Int. J. Dev. Biol.* **50,** 55-61.

Zhang,Z. and Baldini,A. (2008). In vivo response to high-resolution variation of Tbx1 mRNA dosage. *Hum. Mol. Genet.* **17,** 150-157.

Zhang,Z. and Baldini,A. (2010). Manipulation of endogenous regulatory elements and transgenic analyses of the Tbx1 gene. *Mamm Genome* **21,** 556-564.

Zhang,Z., Cerrato,F., Xu,H., Vitelli,F., Morishima,M., Vincentz,J., Furuta,Y., Ma,L., Martin,J.F., Baldini,A. et al. (2005). Tbx1 expression in pharyngeal epithelia is necessary for pharyngeal arch artery development. *Development* **132,** 5307-5315.

Zhang,Z., Huynh,T., and Baldini,A. (2006b). Mesodermal expression of Tbx1 is necessary and sufficient for pharyngeal arch and cardiac outflow tract development. *Development* **133,** 3587-3595.

Zhao,D., McCaffery,P., Ivins,KJ., Neve,RL., Hogan,P., Chin,WW., and Drager,UC. (1996). Molecular identification of a major retinoic-acid-synthesizing enzyme, a retinaldehyde-specific dehydrogenase. *Eur J Biochem* **240,** 15-22.

Zheng,J.L., Shou,J., Guillemot,F., Kageyama,R., and Gao,W.Q. (2000). Hes1 is a negative regulator of inner ear hair cell differentiation. *Development* **127,** 4551-4560.

Zhong,T.P., Childs,S., Leu,J.P., and Fishman,M.C. (2001). Gridlock signalling pathway fashions the first embryonic artery. *Nature* **414,** 216-220.

Zhong,T.P., Rosenberg,M., Mohideen,M.A., Weinstein,B., and Fishman,M.C. (2000). gridlock, an HLH Gene Required for Assembly of the Aorta in Zebrafish. *Science* **287,** 1820-1824.

Zhou,Y., Cashman,T.J., Nevis,K.R., Obregon,P., Carney,S.A., Liu,Y., Gu,A., Mosimann,C., Sondalle,S., Peterson,R.E. et al. (2011). Latent TGF-[bgr] binding protein 3 identifies a second heart field in zebrafish. *Nature* **advance online publication**.

Zile,M.H. (2004). Vitamin A Requirement for Early Cardiovascular Morphogenesis Specification in the Vertebrate Embryo: Insights from the Avian Embryo. *Experimental Biology and Medicine* **229,** 598-606.

Zine,A., Aubert,A., Qiu,J., Therianos,S., Guillemot,F., Kageyama,R., and de Ribaupierre,F. (2001). Hes1 and Hes5 Activities Are Required for the Normal Development of the Hair Cells in the Mammalian Inner Ear. *J. Neurosci.* **21,** 4712-4720.

Zuniga,E., Stellabotte,F., and Crump,J.G. (2010). Jagged-Notch signaling ensures dorsal skeletal identity in the vertebrate face. *Development* **137,** 1843-1852.